Genetic analyses of sensory and motoneuron physiology in Drosophila melanogaster

Dissertation zur Erlangung des
naturwissenschaftlichen Doktorgrades
der Julius-Maximilians-Universität Würzburg

vorgelegt von

Nicole Scholz

aus Mühlhausen (Thür.)

Würzburg, 2015

Genetic analyses of sensory and motoneuron physiology in Drosophila melanogaster

Dissertation zur Erlangung des
naturwissenschaftlichen Doktorgrades
der Julius-Maximilians-Universität Würzburg

vorgelegt von

Nicole Scholz

aus Mühlhausen (Thür.)

Julius-Maximilians-Universität Würzburg
Physiologisches Institut – Lehrstuhl für Physiologie
Neurophysiologie

Würzburg, 2015

Eingereicht am:…….

Mitglieder der Promotionskommission:

Vorsitzender:…….

Gutachter: PD Dr. med. Tobias Langenhan, MSc DPhil (Oxon)

Gutachter: Prof. Dr. Christian Stigloher

Tag des Promotionskolloquiums:……..

Doktorurkunde ausgehändigt am:……..

Erklärungen nach §4 Abs. 3 Satz 3, 5, 8 der Promotionsordnung der Fakultät für Biologie

Affidavit

I hereby declare that my thesis entitled: „**Genetic analyses of sensory and motoneuron physiology in *Drosophila melanogaster***" is the result of my own work.

I did not receive any help or support from commercial consultants. All sources and / or materials applied are listed and specified in the thesis.

Furthermore I verify that the thesis has not been submitted as part of another examination process neither in identical nor in similar form.

Eidesstattliche Erklärung

Hiermit erkläre ich an Eides statt, die Dissertation: „**Genetic analyses of sensory and motoneuron physiology in *Drosophila melanogaster***", eigenständig, d. h. insbesondere selbständig und ohne Hilfe eines kommerziellen Promotionsberaters, angefertigt und keine anderen, als die von mir angegebenen Quellen und Hilfsmittel verwendet zu haben.

Ich erkläre außerdem, dass die Dissertation weder in gleicher noch in ähnlicher Form bereits in einem anderen Prüfungsverfahren vorgelegen hat.

_____, den _____

_____
Unterschrift

Acknowledgements

First, I would like to thank my supervisors Tobias Langenhan and Robert Kittel for the opportunity to conduct these studies in their research groups. Their scientific brilliance, guidance and patience were priceless. I would like to extend my gratitude to Tobias for his continuous support, fruitful and inspiring discussions, and the scientific liberty that he has granted me throughout my studies.

I would like to thank Christian Stigloher for being a member of my thesis committee and his collaboration on the BRP project. Further, I thank Brigitte Trost for her amazing efforts on the *Drosophila* EM. In this context I would like to mention Carolin Wichmann and thank her for her kind advice.

I also wish to thank Manfred Heckmann for providing my workspace and also for his kind advice on the BRP project.

Further, I am thankful to all my colleagues for creating a pleasant atmosphere. Special thanks go to: Jenny, Nadine, Dimi, Matze, Mila and Martin for exciting kicker matches and a very joyful office- and lab life. Maria, Uta, and Claudia for excellent technical assistance, reliability and kindness.

I would like to express my gratitude to my parents, Kersten and Rudolf, and my sister for their never-ending support and encouragement.

Finally, I am incredibly grateful to my beloved husband Martin for being my rock, my most important critic and my sanctuary. I am sincerely thankful for your understanding, enduring and kind support, and patience during my thesis.

Parts of this thesis are published in the following articles:

Nicole Scholz[*], Jennifer Gehring[*], Chonglin Guan[*], Dmitrij Ljaschenko, Robin Fischer, Vetrivel Lakshmanan, Robert J. Kittel, Tobias Langenhan, (2015). The Adhesion-GPCR Latrophilin/CIRL shapes mechanosensation. *Cell Reports 11,* 1-9*;* doi:10.1016/j.celrep.2015.04.008.

Nicole Scholz[*], Nadine Ehmann[*], Christian Stigloher, Tobias Langenhan, Robert J. Kittel. Bruchpilot and Complexin interact to regulate synaptic vesicle tethering to the active zone cytomatrix. *In preparation*.

The postsynaptic architecture of the *Drosophila* neuromuscular junction is regulated through the Adhesion-GPCR Latrophilin/CIRL. *In preparation*. Author list not final.

[*] Equal contribution

Contents

Genetic analyses of sensory and motoneuron physiology in Drosophila melanogaster

1. Summary

During my PhD I studied two principal biological aspects employing *Drosophila melanogaster*. Therefore, this study is divided into *Part I* and *II*, whereby *Part I* addresses the identification of binding partners of the active zone component Bruchpilot (BRP) *in vivo* and *Part II* shows the functional characterization of the Adhesion-GPCR Latrophilin/CIRL.

1.1. *Part I*

Bruchpilot and Complexin interact to regulate synaptic vesicle tethering to the active zone cytomatrix

At the presynaptic active zone (AZ) synaptic vesicles (SVs) are often physically linked to an electron-dense cytomatrix – a process referred to as "SV tethering". This process serves to concentrate SVs in close proximity to their release sites before contacting the SNARE complex for subsequent fusion (Hallermann and Silver, 2013). In *Drosophila*, the AZ protein Bruchpilot (BRP) is part of the proteinous cytomatrix at which SVs accumulate (Kittel et al., 2006b; Wagh et al., 2006; Fouquet et al., 2009). Intriguingly, truncation of only 1% of the C-terminal region of BRP results in a severe defect in SV tethering to this AZ scaffold (hence named brp^{nude}; Hallermann et al., 2010b).

Consistent with these findings, cell-specific overexpression of a C-terminal BRP fragment, named $mBRP^{C\text{-}tip}$ (corresponds to 1% absent in brp^{nude}; m = mobile) phenocopied the brp^{nude} mutant in behavioral and functional experiments. These data indicate that $mBRP^{C\text{-}tip}$ suffices to saturate putative SV binding sites, which induced a functional tethering deficit at motoneuronal AZs. However, the molecular identity of the BRP complement to tether SVs to the presynaptic AZ scaffold remains unknown. Moreover, within larval motoneurons membrane-attached C-terminal portions of BRP were sufficient to tether SVs to sites outside of the AZ. Based on this finding a genetic screen was designed to identify BRP interactors *in vivo*. This screen identified Complexin (CPX), which is known to inhibit spontaneous SV fusion and to enhance stimulus evoked SV release (Huntwork and Littleton, 2007; Cho et al., 2010; Martin et al., 2011). However, so far CPX has not been associated with a function upstream of priming/docking and release of SVs. This work provides morphological and functional evidence, which suggests that CPX promotes recruitment of SVs to the AZ and thereby curtails synaptic short-term depression. Together, the presented findings indicate a functional interaction between BRP and CPX at *Drosophila* AZs.

1.2. *Part II*

The Adhesion-GPCR Latrophilin/CIRL shapes mechanosensation

The calcium independent receptor of α-latrotoxin (CIRL), also named Latrophilin, represents a prototypic Adhesion class G-protein coupled-receptor (aGPCR). Initially, Latrophilin was identified based on its capacity to bind the α-component of latrotoxin (α-LTX; Davletov et al., 1996; Krasnoperov et al., 1996), which triggers massive exocytotic activity from neurons of the peripheral nervous system (Scheer et al., 1984; Umbach et al., 1998; Orlova et al., 2000). As a result Latrophilin is considered to play a role in synaptic transmission. Later on, Latrophilins have been associated with other biological processes including tissue polarity (Langenhan et al., 2009), fertility (Prömel et al., 2012) and synaptogenesis (Silva et al., 2011). However, thus far its subcellular localization and the identity of endogenous ligands, two aspects crucial for the comprehension of Latrophilin's *in vivo* function, remain enigmatic.

Drosophila contains only one latrophilin homolog, named *dCirl,* whose function has not been investigated thus far.

This study demonstrates abundant *dCirl* expression throughout the nervous system of *Drosophila* larvae. $dCirl^{KO}$ animals are viable and display no defects in development and neuronal differentiation. However, *dCirl* appears to influence the dimension of the postsynaptic subsynaptic reticulum (SSR), which was accompanied by an increase in the postsynaptic Discs-large abundance (DLG). In contrast, morphological and functional properties of presynaptic motoneurons were not compromised by the removal of *dCirl*. Instead, *dCirl* is required for the perception of mechanical challenges (acoustic-, tactile- and proprioceptive stimuli) through specialized mechanosensory devices, chordotonal organs (Eberl, 1999). The data indicate that *dCirl* modulates the sensitivity of chordotonal neurons towards mechanical stimulation and thereby adjusts their input-output relation. Genetic interaction analyses suggest that adaption of the molecular mechanotransduction machinery by *dCirl* may underlie this process. Together, these results uncover an unexpected function of Latrophilin/dCIRL in mechanosensation and imply general modulatory roles of aGPCR in mechanoception.

2. Zusammenfassung

2.1. *Teil I*

Die Interaktion von Bruchpilot und Complexin vermittelt die Anbindung von synaptischen Vesikeln an die Zytomatrix der aktiven Zone

Oft findet man an aktiven Zonen (AZ) von Präsynapsen elektronendichte Matrices, welche meist in physischem Kontakt mit synaptischen Vesikeln (SV) stehen. Dieser als „SV Tethering“ bezeichnete Prozess dient der Anreicherung SV in der unmittelbaren Nähe ihrer Freisetzungszonen, noch bevor diese mit dem SNARE Komplex interagieren, um mit der präsynaptischen Plasmamembran zu fusionieren (Hallermann und Silver, 2013). In der Taufliege *Drosophila melanogaster* bildet das AZ Protein Bruchpilot (BRP) Protrusionen, um welche SV akkumulieren (Kittel et al., 2006b; Wagh et al., 2006; Fouquet et al., 2009). Interessanterweise resultiert bereits eine minimale Verkürzung von BRP (1% der Gesamtlänge) am C-terminalen Ende in einem schwerwiegenden Anbindedefekt von SV, der mit einem Funktionsverlust dieser Synapsen einhergeht (brp^{nude}; Hallermann et al., 2010b).

Entsprechend diesem Vorbefund resultierte die gewebespezifische Überexpression eines C-terminalen BRP Fragments - $mBRP^{C\text{-}tip}$ (entspricht dem fehlenden Fragment der brp^{nude} Mutante; m = mobil) - sowohl in Verhaltens- als auch funktionellen Analysen in einer Phänokopie der brp^{nude} Mutante. Dies deutet daraufhin, dass $mBRP^{C\text{-}tip}$ vermeintliche vesikuläre Interaktionspartner blockiert und so die Anreicherung von SV an motoneuronalen AZ verhindert, was ähnlich wie in brp^{nude} Mutanten zu einem funktionellen Tethering-Defekt führt. Die molekulare Identität eines BRP Partners zur Anreicherung von SV an der Zytomatrix der AZ wurde bisher nicht beschrieben.

Weiterhin zeigt diese Arbeit, dass membrangebundene C-terminale BRP Anteile genügen, um SV an Positionen außerhalb von AZ zu binden. Basierend auf diesem Befund wurde ein genetischer *in vivo* Screen zur Identifikation von BRP Interaktoren entwickelt. Dieser Screen identifizierte Complexin (CPX), ein Protein, dessen hemmende beziehungsweise fördernde Wirkung auf die spontane und reizinduzierte Vesikelfusion bekannt ist (Huntwork und Littleton, 2007; Cho et al., 2010; Martin et al., 2011). CPX wurde bisher nicht mit einer Funktion oberhalb von Vesikelpriming und -fusion in Verbindung gebracht. Diese Studie dokumentiert strukturelle und funktionelle Hinweise, die darauf hindeuten, dass CPX mit BRP interagiert, um Vesikelakkumulation an AZ zu fördern und dadurch synaptischer Kurzzeit-Depression entgegen zu wirken.

2.2. *Teil II*

Adhäsions-GPCR Latrophilin/CIRL moduliert die Wahrnehmung mechanischer Reize

Der Kalzium-unabhängige Rezeptor für α-Latrotoxin (CIRL), oder Latrophilin, ist ein prototypischer Rezeptor der Adhäsions G-Protein gekoppelten Klasse (aGPCR). Identifiziert wurde Latrophilin ursprünglich aufgrund seiner Fähigkeit die α-Komponente von Latrotoxin (α-LTX) zu binden (Davletov et al., 1996; Krasnoperov et al., 1996), welches seine Wirkung am peripheren Nervensystem entfaltet und dort übermäßige Transmitterausschüttung an neuronalen Endigungen induziert (Scheer et al., 1984; Umbach et al., 1998; Orlova et al., 2000). Basierend auf diesem Effekt wurde Latrophilin eine Rolle bei der synaptischen Transmission zugesprochen. Später wurden Latrophiline mit weiteren biologischen Prozessen in Zusammenhang gebracht, darunter Gewebepolarität (Langenhan et al., 2009), Fertilität (Prömel et al., 2012) und Synaptogenese (Silva et al., 2011). Allerdings blieb sowohl die subzelluläre Lokalisation als auch die Identität endogener Liganden, zwei Schlüsselaspekte im Verständnis der *in vivo* Funktion von Latrophilinen bisher rätselhaft.
Drosophila besitzt lediglich ein latrophilin Homolog, *dCirl*, dessen Funktion bisher nicht untersucht wurde.
Diese Arbeit zeigt, dass *dCirl* in weiten Teilen des larvalen Nervensystems von *Drosophila* exprimiert ist. *dCirl* knock-out Mutanten sind lebensfähig und weisen keine Störungen in der Entwicklung und neuronalen Differenzierung auf. Allerdings schien *dCirl* Einfluss auf die Ausdehnung des postsynaptischen subsynaptischen Retikulums (SSR) zu nehmen, was mit einer erhöhten Menge an Discs-large (DLG) assoziiert war. Die morphologischen und funktionellen Eigenschaften präsynaptischer Motoneurone der Fliegenlarve hingegen, waren durch den Verlust von *dCirl* funktionell weitestgehend unbeeinträchtigt. Vielmehr ist *dCirl* notwendig für die Wahrnehmung mechanischer Reize (akustische-, taktile und propriozeptive) durch spezialisierte Vorrichtungen - Chordotonalorgane (Eberl, 1999). Die Befunde deuten daraufhin, dass *dCirl* die Sensitivität der Chordotonalneurone gegenüber mechanischen Reizen moduliert und dadurch das Input-Output Verhältnis einstellt. Adaptation der molekularen Mechanotransduktionsmaschinerie durch *dCirl* könnte die molekulare Grundlage für diesen Prozess darstellen, eine Hypothese die durch genetische Interaktionsanalysen gestützt wird. Schlussfolglich enthüllen die experimentellen Befunde dieser These eine unerwartete Funktion von Latrophilin/*dCirl* bei der Mechanoperzeption und implizieren eine generelle modulatorische Rolle für aGPCR bei der Wahrnehmung mechanischer Reize.

3. Background

The common fruit fly, *Drosophila melanogaster*, is a versatile organism, which has been used productively for over 100 years to study a variety of biological processes. In fact, *Drosophila* has developed to become one of the most powerful and influential model organisms in experimental research.

Initially, the fly was chosen as a model organism for practical reasons: body size, simplicity of their diet, easy and robust handling and a short life cycle (Fig. 1A; 10 days at room temperature), thus inexpensive and easy to cultivate in large numbers.

The *Drosophila* genome is ~ 180 Mbp in size, with 120 Mbp of euchromatin allocated over four chromosome pairs and predicts a number of ~ 14000 genes (Adams et al., 2000). Most of these genes are remarkably conserved over large phylogenetic distances including vertebrates (Adams et al., 2000; Rubin, 2000). Accordingly, a wide range of fundamental mechanisms and pathways are conserved over these species (Jennings, 2011). Therefore, knowledge achieved in the fly may essentially be applicable to more highly evolved species. Importantly, relative to vertebrate models genetic redundancy can be neglected in *Drosophila*, which simplifies genetic approaches, and generation of mutants can be achieved comparatively rapidly.

Drosophila is genetically highly manipulable. A tremendous number of technologies has become available to create mutants [e.g. ends-out targeting (Gong and Golic, 2003; Huang et al., 2008), CRISPR (Gratz et al., 2013)]. In addition, well established binary expression systems such as UAS/GAL4, LexA/LexAop and Q/QF allow spatio-temporally controlled transcriptional activation of a gene of interest (Fig. 1B; Brand and Perrimon, 1993; Pfeiffer et al., 2010; Potter et al., 2010). Moreover, binary expression systems in conjunction with RNA-mediated interference (RNAi) are frequently used for tissue-specific knock-down of a target gene [Fig. 1B; (Fire et al., 1998; Dietzl et al., 2007)].

Additionally, using *Drosophila* the precision of electrophysiological measurements can be combined with the powerful genetic toolbox available for this organism. In particular the neuromuscular junction (NMJ) of the large third instar larva has become a popular model to study the cellular and molecular mechanisms that govern synaptogenesis and basic neurotransmission (Ruiz-Cañada and Budnik, 2006).

Moreover, *Drosophila* proved useful to study the function of sensory neurons that innervate mechanosensory organs. The peripheral sensory system is optically accessible, but due to its structural layout its functional analysis has presented more challenging. Nevertheless, in recent years protocols have been developed to enable detailed insights into sensory neuron function (Göpfert and Robert, 2003; Chalfie, 2009; Zhang et al., 2013).
Last but not least, *Drosophila* is suitable to study simple behavior.

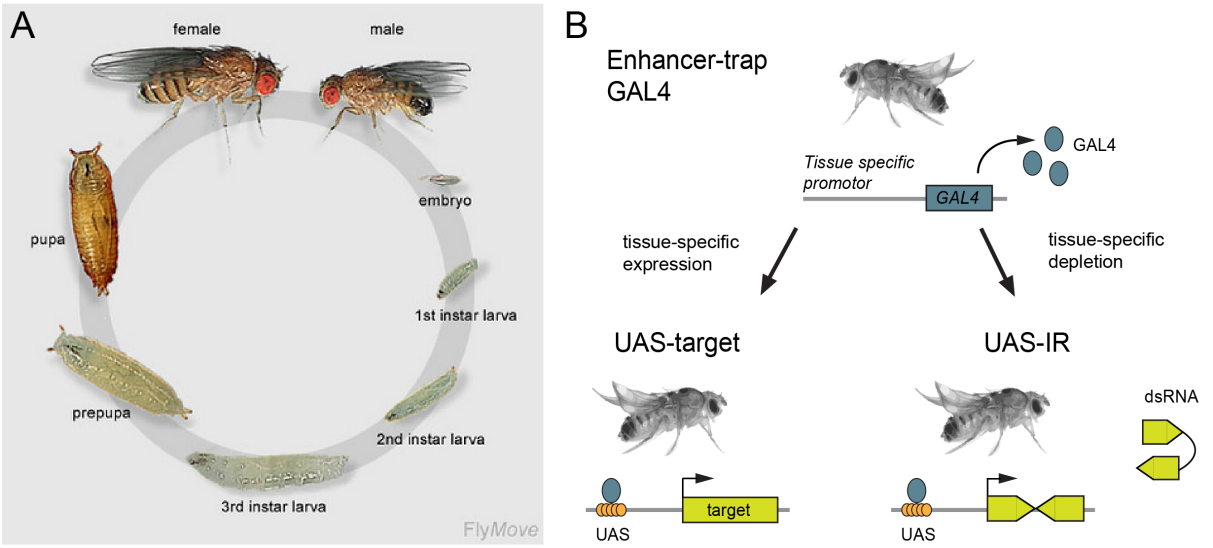

Figure 1. *Drosophila melanogaster*. A) *Drosophila* life cycle. The fly's egg is ~ 0.5 mm long. Cultivated at 25 °C the embryo hatches approximately 24 h after the egg was laid. The resulting larva grows for about four days moulting twice (24 h and 48 h after hatching) during that time. Next, the larva encapsulates in the puparium. For the next four days the larva undergoes metamorphosis. Finally, after ~10 days the adult fly encloses from the puparium (Weigmann et al., 2003). B) The fly is genetically highly amenable. The UAS/GAL4 binary expression system allows tissue-restricted transcriptional activation of a gene of interest (UAS-target) (Brand and Perrimon, 1993). In contrast, RNAi-based approaches are utilized for tissue-specific knock-down of a gene of interest [UAS-inverted-repeat (IR); Fire et al., 1998].

Taken together, *Drosophila* is due to its assessable peripheral motoneuronal and sensory layout, as well as the above listed reasons, a suitable organism for the genetic analyses of motoneuron (*Part I*) and sensory neuron physiology (*Part II*).

Part I

Bruchpilot and Complexin interact to regulate synaptic vesicle tethering to the active zone cytomatrix

4. Introduction

4.1. The concept of neurotransmission at chemical synapses

The decisive neuro-anatomical work by Santiago Ramón y Cajal provided the basis for the idea, that the nervous system is build up of discrete individual cells, which represent basic functional and structural units - an idea known as the neuron doctrine (López-Muñoz et al., 2006). Later on the German anatomist Heinrich Waldeyer-Hartz, who among others presented this concept, popularized the term "neuron" as a possibility to refer to the cells in question. Today we know that neurons act as distinct metabolic units, which not only transmit information through electrochemical signals onto their target cells, but are also equipped to modify and filter incoming signals.

Communication between nerve cells occurs at synapses, specialized intercellular junctions located at the interface between presynaptic neurons and postsynaptic target cells. Depending on their functional requirements, neurons are provided with electrical or chemical synapses or both. At electrical synapses pre-and postsynaptic membranes are connected by gap junctions allowing rapid transmission of information by the flow of electrical current from the pre- to the postsynaptic cell. In contrast, at chemical synapses the pre- and postsynapse are spatially separated by ~ 30 nm wide synaptic cleft (Landis, 1988) bridged by the discharge of physiologically active messenger molecules – the neurotransmitters. These transmitters are packed into transport organelles - synaptic vesicles (SVs). Under resting conditions SVs are mostly stored in the cytoplasm of the presynaptic terminal. Neuronal activity translocates SVs to release sites, where they dock to the neuronal membrane and are primed for subsequent release. Finally, depolarization-triggered Ca^{2+} influx into the presynapse leads to fusion of SV membrane with the plasma membrane. Subsequently, released neurotransmitters activate postsynaptic receptors, inducing current flow, thereby mediating signal transduction. Chemical synaptic communication is highly adaptable (Magleby, 1987), but is characterized by a synaptic delay of < 1 ms (Geiger and Jonas, 2000).

Complex neuronal processes such as learning, memory, cognition and behavior require an intricate network of neurons forming an extensive neuronal circuit. The prerequisite for such neuronal circuits to operate properly is based on tight spatial-temporal precision of synaptic transmission at individual synapses. Thus, physiological properties and the interplay of single

synaptic computational units constitute the basis required for higher brain function.

4.2. Synaptic Vesicles

At a chemical presynapse a large number of cellular functions and processes are aligned on efficient synaptic transmitter release. Classical neurotransmitters (e.g. glutamate, acetylcholine) are stored and transported in uniformly sized SVs (~ 20 - 40 nm, Fig. 2) from which they are released into the synaptic cleft. However, many neurons possess the capacity to release both classical and peptidergic transmitters with the latter being stored in large dense-core vesicles (LDCV; Hökfelt et al., 1991; Karhunen et al., 2001).

SV fusion is preceded by neurotransmitter uptake, translocation of SVs to release sites, docking and priming events and is followed by endocytosis and recycling of SV components. Each step involves an organized and sequential employment of proteins from the cytoplasm, orchestrated by an extensive set of integral and membrane-associated SV proteins. Therefore, the SV surface is densely bestowed with, in some cases more than 400 different proteins (Takamori et al., 2006). In recent years, many of them have been identified (DiAntonio et al., 1993; Bonifacino and Glick, 2004; Takamori et al., 2006). SV proteins can be divided into two groups: transport proteins involved in transmitter uptake and trafficking proteins that participate in the endo-exocytosis cycle. Due to the frequent association and dissociation of cytoplasmic factors SVs are considered “dirty” nanostructures (Takamori et al., 2006), which rendered quantification of protein complement of an entire SV difficult. After all, Jahn and coworkers were able to quantify the molecular composition of a prototypic SV using purified SV fractions from rat brain. They found several proteins, hitherto described as central exocytotic components, to be expressed most abundantly on SVs [Synatobrevin (SYB) 69.8 copies/SV; Synaptotagmin (SYT) 15.2 copies/SV; VGLUT 14.4 copies/SV; RAB-3A 10.3 copies/SV]. This might reflect their functional necessity in exocytosis. In addition, constituents of the SV release machinery [VAMP/SYB, Syntaxin (SYX) and soluble *N*-ethylmaleimide-sensitive factor attachment (SNAP-25)] appear highly diverse, indicating that SVs are equipped not only for exocytosis but also other fusion events of the SV cycle (Takamori et al., 2006).

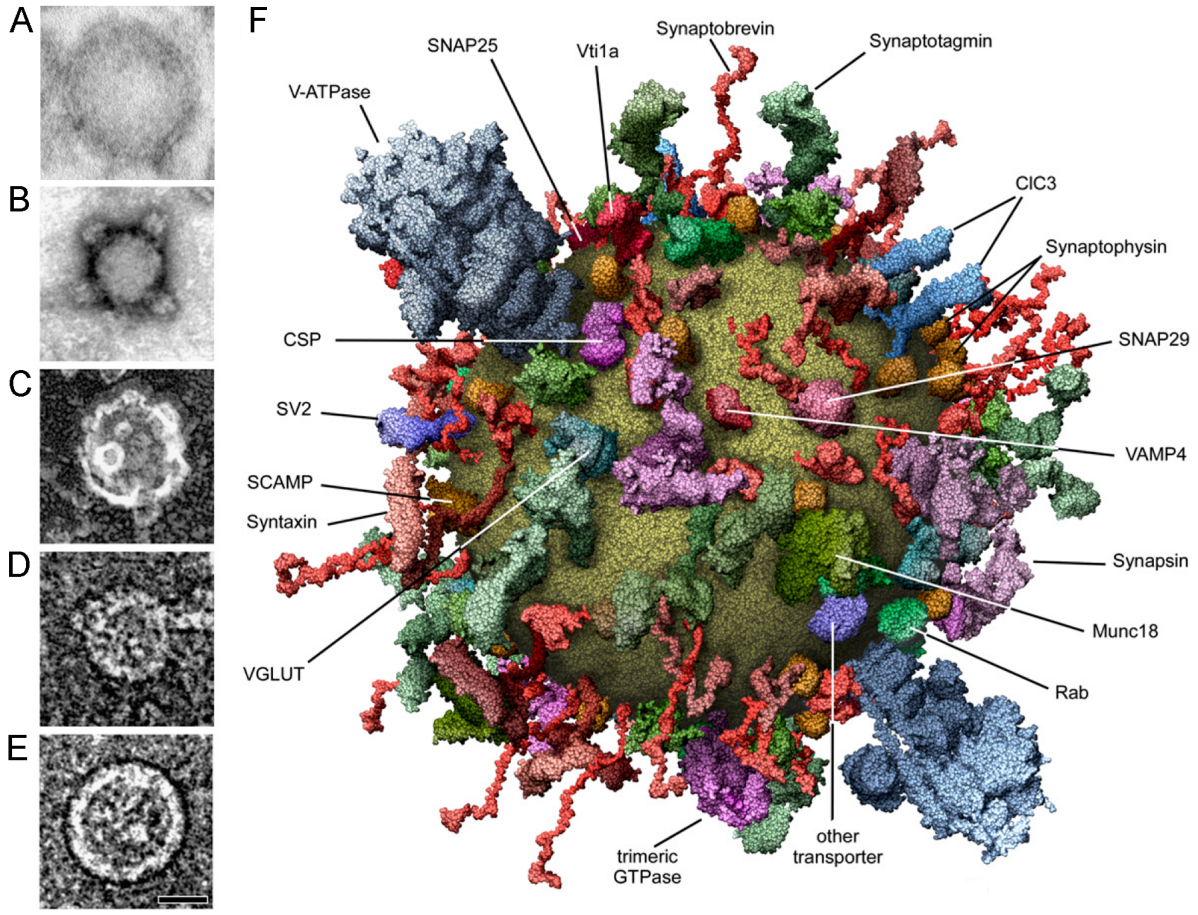

Figure 2. Architecture of an average synaptic vesicle. A) Chemically fixed from *Drosophila* larva. B) Negatively stained by uranyl acetat and subsequently imaged using STEM (scanning transmission electron microscope). C) Shadowed by platinum after quick-freeze/deep etching. D) Native cryopreparation. E) Native cryopreparation followed by digestion of surface protein by pronase. Scale bar 20 nm. F) Schematic view of a SV from rat brain. Adapted from (Takamori et al., 2006).

The SV proteome is evolutionarily highly conserved from vertebrates all the way through to invertebrates. The high degree of protein conservation is not exclusive to the SV proteome, but extends to the majority of proteins involved in the exo-endocytosis cycle. Astonishingly, for more than 90 % of vertebrate gene homologs have been identified in the fly genome. On average these are 60 % identical and 74 % similar to their vertebrate homologs (Lloyd et al., 2000). Thus, this indicates that in the evolution of synaptic transmission fundamental principles have been retained.

4.2.1. SV pools

Sustained and reliable release of neurotransmitters depends on continuous SV supply maintained through SV recycling and refilling of functionally specified SV depots. Beside the differences in spatial residences, no other morphological or biochemical feature is presently at hand to distinguish SVs within neuron terminals (Rizzoli and Betz, 2005; Alabi and Tsien, 2012). However, at multiple synapses, including the *Drosophila* NMJ, three major SV pools with different functions have been suggested: i) the readily releasable pool (RRP), ii) the recycling pool (RP) and iii) the reserve pool (Fig. 3A; Zucker and Regehr, 2002; Rizzoli and Betz, 2005; Hallermann et al., 2010a). Note that at the larval *Drosophila* NMJ the RRP and RP are located in the periphery of each bouton, while the reserve pool resides in the center (Delgado et al., 2000).

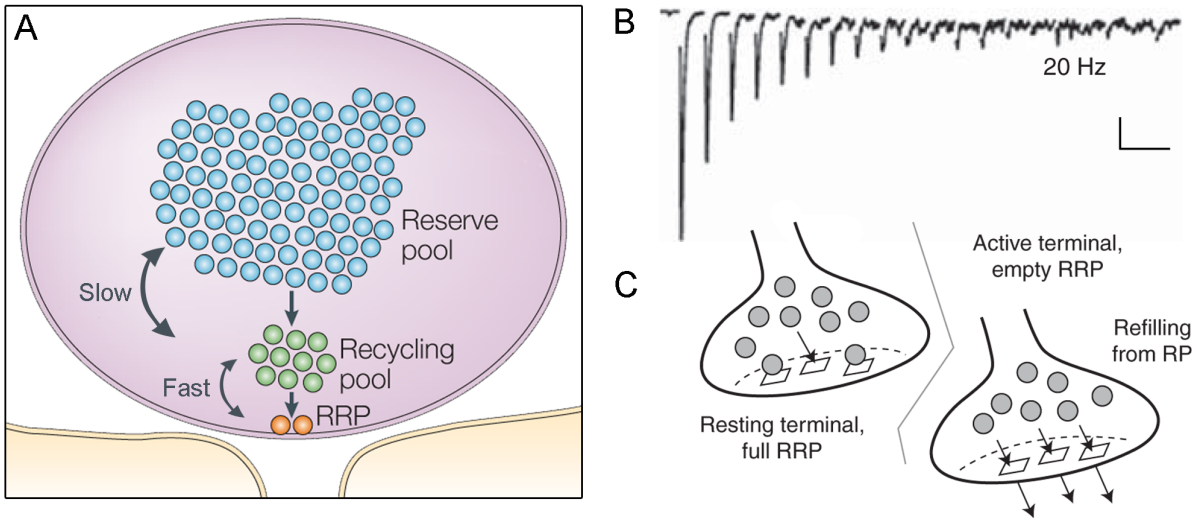

Figure 3. SV pools. A) The reserve pool holds the majority (~ 80-90 %) of SVs. The recycling pool harbors ~10 - 15 % of all SVs. The RRP contains only a few SVs (~ 1%), which appear to be docked/tethered and fusion competent. B) Representative trace of synaptic depression recorded during high-frequency stimulation (20 Hz; Figure adapted from (Stevens and Williams, 2007). Scale bar B = 500 ms and 100 pA. C) Scheme illustrating a model in which synaptic depression results from step-wise recruitment of functionally distinct SV pools (from Alabi and Tsien, 2012). Depletion of the RRP induces rate-limiting replenishment from a recycling pool.

The RRP contains only a few SVs, which are generally thought to be docked/tethered and ready for release (Fig. 3A; Imig et al., 2014). Hence, these SVs are immediately available upon stimulation contributing to phasic neuronal responses (Elmqvist and Quastel, 1965; Schneggenburger et al., 1999; Delgado et al., 2000).

During prolonged stimulation SVs are recruited from the RP to maintain release. With respect to RRP, the RP hosts a larger number of SVs (~ 5-20 % of all presynaptic SVs; Fig. 3A; Rizzoli and Betz, 2005).
The reserve pool harbors the vast majority of SVs within the terminal and constitutes a SV depository accessed only during intense stimulation that exceeds the physiological range. For example, at the *Drosophila* NMJ, 30 Hz stimulation is required to mobilize SVs from the reserve pool (Kuromi and Kidokoro, 2000). Therefore, recycling of SVs from the RP is largely responsible for continuous release after the RRP has been depleted (Fig. 3B), with only a minor contribution from the reserve pool (Heuser and Reese, 1973; Delgado et al., 2000; Zucker and Regehr, 2002).

Synapses are able to filter, modify and integrate information through activity-dependent reversible short-term changes in transmission strength. During short-term plasticity the postsynaptic response to repetitive presynaptic activity can increase (facilitation) or decline (depression) over time. The final state of a given presynapse is primarily shaped by two antagonistic mechanisms. Synaptic-short term depression, which can be induced by depletion of the limited RRP, when quantal release rates from the RRP exceed the rates at which the RRP is replenished through SV mobilization from other pools (Fig. 3B; del Castillo and Katz, 1954a; Birks and MacIntosh, 1961; Elmqvist and Quastel, 1965). By contrast, short-term facilitation can be caused by an elevated release probability brought about by build-up of residual Ca^{2+} in the nerve terminal (del Castillo and Katz, 1954b). Hence, the quantity of release-ready SVs and the exocytotic probability of a single SV define the number of SVs released at a synapse (del Castillo and Katz, 1954b; Murthy et al., 1997). Frequently, synapses which tend to exhibit facilitation are characterized by low release probability, whereas synaptic depression often occurs at high probability synapses (Zucker and Regehr, 2002).

Before SVs contact the SNARE complex, they have frequently been found associated with presynaptic specializations through filaments also referred to as SV tethers. Advanced EM techniques enabled visualization of a range of tethering structures at ribbon-, central- and NMJ synapses (Fouquet et al., 2009; Siksou et al., 2011; Stigloher et al., 2011; Fernández-Busnadiego et al., 2011). Detailed analysis of SV tethering has been obtained at ribbon synapses, where tethers appear to be important for temporal dynamics of SV delivery to release sites (Lenzi and Gersdorff, 2001). Synaptic activity reduced the quantity of SVs that tethered at the base of the ribbon (Jackman et al., 2009; Lenzi and Gersdorff, 2001; Pangršič et al.,

2010), a phenomenon not exclusive to ribbon synapses (Fernández-Busnadiego et al., 2010; Szule et al., 2012). Lately, SV tethering has been causally linked to synaptic short-term plasticity and establishment of a SV supply pool (Hallermann et al., 2010a; 2010b). Three mechanistic models have been proposed to explain the coherence between SV tethering and formation of a supply pool (Hallermann and Silver, 2013). First, tethering provides a pool of SVs at the AZ, drawn from during activity (Zhai, 2004). Second, tethers restrain and locate SVs in Ca^{2+} channel vicinity (positional priming; Snellman et al., 2011). Third, tethers support rapid SV fusion through molecular interactions of the tether with SV proteins and cytoplasmically distributed priming factors (molecular priming) to allow priming of SVs as they encounter the AZ membrane (Jiao et al, 2010; Lee et al., 2013).
Thus, tethering may be considered the initial step to prime SVs for the subsequent fusion event.

4.2.2. SV transport

The major fraction of SVs and other transport organelles of the neuron originate from the neuron soma and are shuttled to the axon terminal (Goldstein et al., 2008). Catalyzed by motor proteins [e.g. kinesin superfamily protein (KIFs), kinesins] SVs are anterogradly transported along the axon guided through an organized array of polar microtubules (Hall and Hedgecock, 1991; Okada et al., 1995; Hurd and Saxton, 1996; Pack-Chung et al., 2007), which comprise a molecular navigation system. The numerous microtubules in the axon are regularly spaced and encircle a bundle of neurofilaments. The bundled neurofilaments are often located in the center of the axon (Yamada et al., 1971).
Visualized using an electron microscope molecular motors appear as short cross-bridged structures between microtubules and the organelle (e.g. SVs or mitochondria; Hirokawa, 1982; Morris and Hollenbeck, 1995). The size of molecular motors varies from ~ 25 to 100 nm (Hirokawa, 1998). In mammals, neuronally expressed KIF1A was demonstrated to specifically associate with SV precursors and mediates, with 1.2 µm/s, one of the fastest anterograde motor activity (Okada et al., 1995). In *Drosophila*, transport of SV precursors is mediated by the kinesin-3 family member *imac* (immaculate connections). Genetic removal of *imac* results in the arrest of motoneuronal synaptogenesis (Pack-Chung et al., 2007). In summary, the neuronal transport machinery mediates proper targeting of SV precursors to their sites of action – the presynapse, a process crucial throughout the lifetime of any neuron.

4.2.3. The SV marker Synaptotagmin

Initially SYT was named p65, a 65-kDa SV protein identified in a monoclonal antibody screen (Matthew et al., 1981). Neuronal SYTs are composed of short N-terminal intravesicular sequences, two cytoplasmic C_2 domains (C_2A and C_2B domain) and a single transmembrane spanning region that occupies the vesicular membrane (Fig. 5; Perin et al., 1991; Geppert et al., 1991).

SYT is one of the most abundant SV proteins and is expressed on precursor- and mature SVs (Littleton et al., 1993a; Takamori et al., 2006). During neurogenesis, SYT-positive SVs locate to axons only prior to synapse formation and are relocated to the bouton after the synapse has matured. Accordingly, in *Drosophila* larvae SYT localizes most prominently to the longitudinal tracts of the VNC, brain neuropil and to synaptic boutons of the NMJ (Littleton et al., 1993a).

Compelling evidence from synapses of various model organisms demonstrated that stimulus evoked Ca^{2+} elevations are sensed by SYT, which subsequently triggers fast exocytosis (Bommert et al., 1993; DiAntonio et al., 1993; Littleton et al., 1993b; Nonet et al., 1993; Geppert et al., 1994; Littleton et al., 1994; Mikoshiba et al., 1995). Besides, SYT was proposed to modulate spontaneous SV release whilst acting as a fusion clamp. In support of this, several studies documented that *Drosophila* SYT knock-out larvae exhibit an increase in the spontaneous release event frequency at larval NMJs (Littleton et al., 1994; DiAntonio and Schwarz, 1994; Mackler et al., 2002). In this context the interaction of SYT with mature- and premature SNARE complexes seems to further substantiate this finding (Söllner et al., 1993; Vrljic et al., 2010). Taken together, SV location of SYT together with its Ca^{2+} sensing properties enables efficient stimulus-secretion coupling in evoked neurotransmitter release. Moreover, SYT's engagement with SNAREs and phosopholipids regulates speed and precision of SV release (Paddock et al., 2008; 2011; Lee and Littleton, 2015). However, it is still incompletely understood as to how Ca^{2+} influx results in such extraordinarily precise, fast and cooperative exocytosis.

4.3. The presynaptic active zone

4.3.1. Ultrastructure

Morphologically, electron-dense material localized to opposing pre-and postsynaptic plasma membranes indicates a synapse (Gray and Young, 1964), a term coined in 1897 by the neurophysiologist Charles Scott Sherrington (syn- 'together' and hapsis- 'joining'). Fusion of SVs is restricted to only a small area of the synapse, which is referred to as the "active zone" (AZ; Couteaux and Pécot-Dechavassine, 1970; Landis, 1988). Ultrastructurally, AZs are characterized by electron-dense membrane, associated with macromolecular cytomatrices, which are frequently identified as distinctly shaped protrusions. These protrusions frequently jut out into the presynaptic cytoplasm and tether neurotransmitter-laden SVs (Bloom and Aghajanian, 1968; Pfenninger et al., 1972; Feeney et al., 1998; Fouquet et al., 2009; Stigloher et al., 2011). Depolarization-dependent Ca^{2+} influx through voltage gated Ca^{2+} channels takes place in the immediate SV vicinity to rapidly trigger exocytosis (Neher and Sakaba, 2008). Therefore, AZ scaffolds are considered prime structures to couple SVs to Ca^{2+} channels – a process also referred to as positional priming. By contrast, SVs that are primed more distantly from Ca^{2+}-channels are believed to be more slowly released (Neher and Sakaba, 2008).

The first three-dimensional view of AZ scaffolds emerged from the frog NMJ (Harlow et al., 2001). Electron tomography unraveled a ribcage-like arrangement of "ribs" and "beams" that provides SV "slots" in the vicinity of Ca^{2+} channels ("pegs"; Fig 4A, B; Harlow et al., 2001). This tight spatial coupling is consistent with the short delay (0.2 ms) of SV fusion after Ca^{2+} entry (Stanley, 1996).

At mammalian central nervous system (CNS) synapses pyramid shaped particles interconnected by evenly spaced fibrils form a "particle" web, which is analogous to "ribcage", providing "slots" for SV docking and fusion (Fig. 4C, D; Stanley, 1996; Phillips et al., 2001; Wang et al., 2002). Previously, biochemical purification and molecular characterization revealed that these presynaptic specializations include Synapsin (SYN) and RIM (Wang et al., 1997; Hilfiker et al., 1999; Phillips et al., 2001). Some mammalian sensory neurons form conspicuous ribbon synapses, which tether numerous SVs conferring the capacity for sustained, graded release (von Gersdorff, 2001). The ribbons with their SV "halo" are positioned perpendicularly to the plane of the plasma membrane and reach ~ 200 nm into the cytoplasm, but can vary in length ranging from 200-1000 nm (Fig. 4E, F; Sterling and Matthews, 2005; tom Dieck and Brandstätter, 2006; Matthews and Fuchs, 2010).

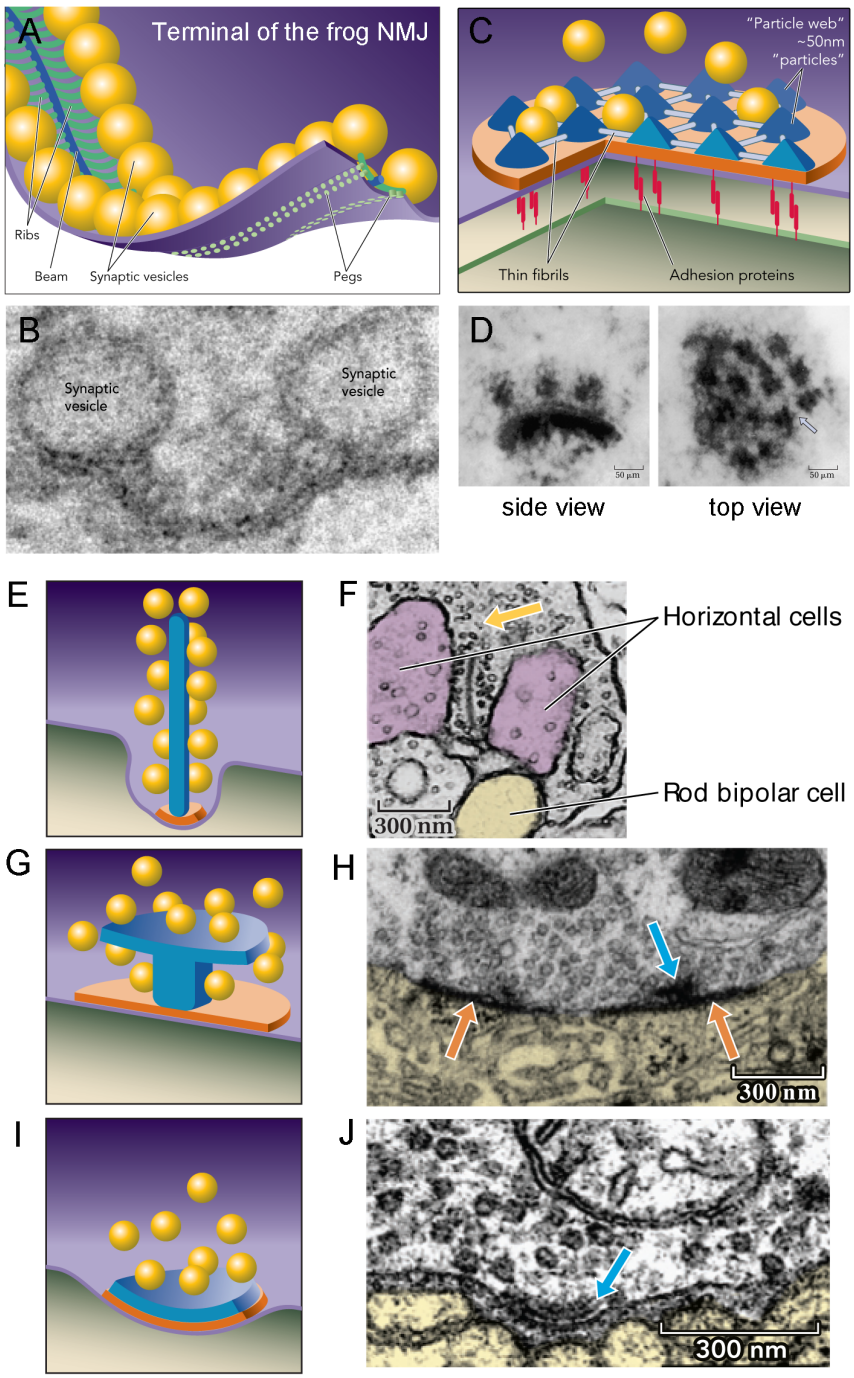

Figure 4. Ultrastructure of synaptic AZs from different organisms. A, B) Model of the AZ structure at the frog NMJ with ribs, beams, pegs and SVs. An array of ribs, oriented perpendicular to a central beam localize SVs in parallel rows at the AZ and thereby in close range to pegs [putative Ca^{2+} channels, (Harlow et al., 2001; Zhai & Bellen, 2004)]. B) EM micrograph of the frog NMJ shows SVs docked to the plasma membrane through dense projections (Harlow et al., 2001). C, D) AZ layout of a mammalian central synapse. Evenly spaced fibrils (~ 50 - 100 nm) interconnect pyramidally shaped (~ 50 nm) particles forming a "particle web" (Phillips et al., 2001), which provides slots for SVs to tether/dock. D) Electron micrograph of purified AZs according to C) from side view (left panel) and top view (right panel). E, F) AZ structure of a ribbon synapse. E) Scheme of the AZ specialization of ribbon synapses. F) Ultrastructure of a triadic photoreceptor ribbon synapse between rod photoreceptor and horizontal cell and a rod bipolar cell in rat (Dick et al., 2003). G, H) AZ specialization of a synapse from *C. elegans* NMJ (Hallam et al., 2002). G) Schematic representation of the plaque formed AZ material to which SVs tether/dock. H) EM micrograph according to G). I, J) Schematic (I) and ultrastructural (J) of *Drosophila* NMJ synapse. SVs accumulate around a T-shaped AZ specialization (Meinertzhagen et al., 1998). Scale bar D = 50 µm; F, H, J = 300 nm. Figure adapted from Zhai & Bellen, 2004.

Electron-dense specializations are not exclusive to vertebrate synapses. For example, T- [T-bar; ~ 70 nm long; extent ~ 110 - 150 nm into the cytoplasm; (Atwood et al., 1993; Fouquet et al., 2009)] and plaque-shaped protrusions formed at *Drosophila* and *C. elegans* synapses, respectively, tether SVs (*Drosophila* Fig. 4G, H, 6, 7; *C. elegans* Fig. 4I, J; Atwood et al., 1993; Hallam et al., 2002).

Thus, presynaptic specializations come in a wide range of geometric "flavors" but with a common physiological function: to aid in tethering or accumulating SVs. Presumably, this function serves two purposes. First, SVs are concentrated at synapses and can be rapidly mobilized to the AZ membrane in times of need. Second, SVs are restrained in a defined range to presynaptic Ca^{2+} channels. The heterogeneity in AZ cytomatrices across different synapses, however, may be nature's solution to synaptic size restrictions: a bigger cytomatrix tantamount to an increased number of available SV docking/tethering slots. Thus, the physiological demand of a particular synapse may be imprinted in the morphology of its AZ scaffold.

4.3.2. Molecular layout

Intercellular communication through synapses is an exceedingly fast biological process, which relies on rapid Ca^{2+}-triggered fusion of SVs (Rosenmund, 2003). SYT serves to detect the rise in Ca^{2+} levels and stimulates fusion (Fig. 5; Littleton et al., 1993b; Geppert et al., 1994; Koh and Bellen, 2003). Other putative Ca^{2+} sensor proteins have been identified, which may substitute and/or complement SYT function (Groffen et al., 2010; Walter et al., 2011; Yao et al., 2011). Subsequently, fusion is catalyzed through the SNARE machinery, which constitutes a 4-α-helix bundle (Sutton et al., 1998), composed of vesicular SYB, presynaptic SYX and soluble *N*-ethylmaleimide-sensitive factor attachment protein 25 (SNAP-25; Fig. 5). On contact, the SNAREs associate in *trans* and progressively zipper up thus pulling the membranes into close proximity (Jahn and Fasshauer, 2012; Südhof, 2013). This process features sequential SNARE folding events including a intermediate SNARE complex, which is only partly-zippered (Krishnakumar et al., 2011). The basic, SNARE complex driven, fusion event is supplemented by a number of regulatory components, i.e. MUNC-18, SYT and Complexin (CPX), which are vital for regulated SV release during stimulus-triggered synaptic transmission (Fig. 5; Südhof and Rothman, 2009; Jahn and Fasshauer, 2012; Südhof, 2013). After fusion, the *cis*-configurated SNARE complex resides in the plasma membrane and is subsequently disassembled by the ATPase *N*-ethylmaleimide-sensitive fusion protein (NSF; Jahn et al., 2003; Südhof, 2004).

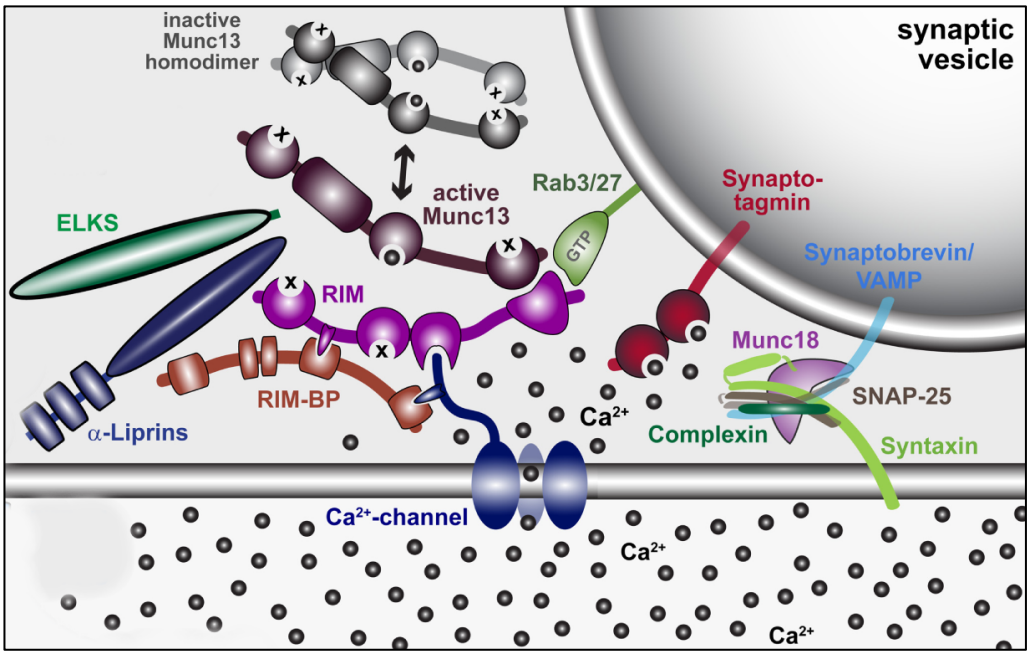

Figure 5. Model of the molecular protein décor at the AZ. Several conserved proteins build up the AZ complex that orchestrates the organization of SVs, presynaptic Ca^{2+} channels and the SV fusion machinery. Adapted from (Südhof, 2012).

While the synapse-specific protein composition imparts structural individualization of AZ scaffolds, distinct evolutionarily conserved proteins appear to establish a core that associates SNARE machinery, Ca^{2+} channels and SVs with each other and the plasma membrane and thus control the precise spatiotemporal regulation that characterizes synaptic exocytosis. Thus far, a number of proteins have been reported in this virtue: Rab-3-interacting molecule (RIM; Wang et al., 1997)], MUNC-13 (Brose et al., 1995), RIM-binding protein (RIM-BP; Wang et al., 2000), α-LIPRIN (Schoch et al., 2002) and cytomatrix of the active zone-associated structural proteins (CAST/ELKS; Ohtsuka, 2002; Wang et al., 2002).

From an organizational and biochemical point of view RIMs are central AZ elements, because they interconnect many other known AZ components (Ohtsuka, 2002; Wang et al., 2002; Takao-Rikitsu, 2004). RIM forms a tripartite complex with MUNC-13 and with the small vesicle-attached GTPase RAB-3 (Fig. 5; Wang et al., 1997; 2000; Betz et al., 2001). This complex appears to promote SV docking to the AZ to increase RRP size and facilitate SV priming (Dulubova et al., 2005). Accordingly, RIM deficient neurons display aberrant RRP size and altered SV priming (Schoch et al., 2002; Müller et al., 2012). In the absence of RIM

the C_2A domains of MUNC-13 form tight homodimers. However, in the presence of RIM this "inactive" state can be converted to form "active" RIM/MUNC-13 heterodimers (Dulubova et al., 2005; Lu et al., 2006). Other studies suggest that RIMs switch on MUNC-13's priming function by interfering with its autoinhibitory homodimerization (Deng et al., 2011). In addition, through its regulatory influence on SV priming MUNC-13 also influences synaptic short-term plasticity (Rosenmund et al., 2002; Lipstein et al., 2013).
Furthermore, RIM plays a role in Ca^{2+} channel targeting at AZs (Han et al., 2011; Graf et al., 2012). Hence, the RIM/MUNC-13/RAB-3 complex provides tight spatial configuration between docked SVs and Ca^{2+} channels and thus ensures short diffusional distances between Ca^{2+} channels and the Ca^{2+} sensor(s).

RIM-BP binds Ca^{2+} channels and RIM to recruit Ca^{2+} channels to the AZ (Fig. 5; Wang et al., 2000; Hibino et al., 2002; Kaeser, 2011). The recruitment of synapse specific Ca^{2+} channels (N- and P/Q-type) is mediated by its PDZ domain (Kaeser, 2011), whereas RIM binding occurs at a C-terminal SH3 domain (Wang et al., 2000). Consistently, loss of *drbp* in *Drosophila* disrupted Ca^{2+} channel clustering, alongside changes in AZ ultrastructure (Liu et al., 2011). However, information about the exact function of RIM-BP is still at large.

The Liprin-α family of scaffolding proteins comprise proteins with coiled coil (CC) rich N-termini through which they associate with themselves to form homodimers (Taru and Jin, 2011), and with RIM (Schoch et al., 2002) and ELKS/CAST (Ko et al., 2003), aiding interactions necessary for proper exocytosis (Ohtsuka, 2002; Schoch et al., 2002; Ko et al., 2003). Furthermore, Liprin-α constitutes crucial regulators of synapse formation in both immature and mature neurons. The first clue on α-Liprin function at the AZs derived from a loss-of function mutation in *C. elegans*, which revealed an enlargement of the presynaptic scaffold and defective SV accumulation (Zhen and Jin, 1999; Patel et al., 2006). *Drosophila* α-Liprin performs similar functions (Kaufmann et al., 2002). Interestingly, Liprin not only interacts with RIM, CAST but also with LAR-type receptor phosphotyrosine phosphatases (PTPRF; Serra-Pagès et al., 1995). Thus, Liprin may relate transsynaptic cell adhesion to presynaptic AZ assembly. However, thus far data on Liprin function from vertebrate terminals is not at hand and it will be interesting if this function is conserved all the way through to mammals.

The mammalian genome encodes two CAST homologs (ELKS1 and ELKS2), which are structurally similar. However, the *cast* loci possess different promotors and alternatively

spliced C-termini resulting in CAST variants, which are differentially distributed throughout the nervous system (Wang et al., 2002). CAST, which was originally purified from rat brain, is a CC rich protein with roughly ~180 kDa and a unique terminal IWA-motif through which it interacts with RIM and α-Liprin (Ohtsuka, 2002; Wang et al., 2002; Ko et al., 2003). Moreover, similar to RIM, CAST interacts with the majority of the known AZ proteins. This indicates a central function in organizing the complex proteinous cytomatrix observed at the AZ (Takao-Rikitsu, 2004; Hida and Ohtsuka, 2010). Recent work showed that deletion of CAST/ELKS2 in mice did not affect SV release, but instead induced an increase in SV quantity within the RRP (Kaeser et al., 2009). The authors advocate a interesting model in which CAST/ELKS2 possesses a regulatory function in gating access to the release machinery rather than providing an essential building block, which enhances SV release (Kaeser et al., 2009).

At mouse ribbon synapses CAST localizes, similar to RIM and Bassoon, at the base of the ribbon (Deguchi-Tawarada et al., 2006). At ribbon synapses of rod photoreceptors the disruption of CAST function results in smaller yet seemingly intact AZs. However, these animals suffer from impaired visual acuity, dendritic sprouting of bipolar and horizontal cells and show altered responses in electroretinogram (ERG; tom Dieck et al., 2012). Thus, at this synapse CAST appears to contribute to AZ stability and is required for proper vision.

Unlike mammals, the genomes of *Drosophila* and *C. elegans* each encode only one CAST homolog namely Bruchpilot (*brp*) and *ceCast/elks*, respectively (Wagh et al., 2006; Deken et al., 2005). In line with the above proposed function of mammalian CAST, *C. elegans* ELKS appears dispensable for SV release (Deken et al., 2005). In contrast, BRP represents a key player in AZ establishment, SV accumulation and Ca^{2+} channel clustering and thus has profound impact on SV release rates of the synapse (Kittel et al., 2006a; 2006b Wagh et al., 2006; Hallermann et al., 2010b).

4.3.3. Bruchpilot

Utilization of the monoclonal antibody Nc82 (Hofbauer, 1991) enabled the identification of the CAST/ELKS homolog BRP in *Drosophila* (Fig. 6B, C). BRP is present at most synapses, is roughly 200 kDa in size and contains CC rich regions (Wagh et al., 2006). Structurally BRP represents a fusion protein uniting a CAST/ELKS component, which corresponds to BRP's N-terminal region, and a C-terminal portion that resembles cytoskeletal molecules that may

constitute an interaction interface (Wagh et al., 2006). Therefore, BRP was proposed to combine functions of vertebrate CAST/ELKS and cytoskeletal structural protein in a single polypeptide that is highly conserved among insects (Wagh et al., 2006). Later on, BRP was demonstrated to constitute an integral component of the AZ cytomatrix that forms T-shaped bodies in chemically fixed specimen (Wagh et al., 2006; Kittel et al., 2006b; Fouquet et al., 2009). Recently, localization microscopy (*d*STORM short for *direct* stochastic optical reconstruction microscopy) enabled single molecule quantification of BRP and revealed that the AZ cytomatrix is composed of units containing ~ 137 BRP proteins, from which three quarters are organized into 15 heptameric clusters (Ehmann et al., 2014).

Investigation of the AZ ultrastructure of high pressure frozen larval NMJs revealed the filamentous structure of BPR molecules (Fouquet et al., 2009), which are arranged in a circular manner, comparable to flowers in a bouquet (Fig. 6B). In fact, detailed biochemical analysis identified two BRP isoforms ($BRP^{\Delta 170}$ corresponds to C-terminal truncated protein and $BRP^{\Delta 190}$ corresponds to full length protein), which alternate to build up the T-bar structure (Matkovic et al., 2013). The N-terminus of BRP faces the presynaptic plasma membrane and physically interacts with the intracellular C-terminus of Ca^{2+} channel Cacophony (CAC; Fouquet et al., 2009). In contrast, the C-terminus elongates into the presynaptic terminal, where SVs tether (Fig. 6B; Fouquet et al., 2009).

Functional analysis of *brp*-depleted synapses of adult compound eyes and larval NMJs disclosed a specific defect in evoked transmission (Wagh et al., 2006). Later on, electrophysiological recordings from *brp* null mutant (brp^{69}) synapses uncovered that the residual evoked transmission was asynchronous and that repetitive stimulation induced prominent synaptic short-term facilitation. This change in short-term plasticity was shown to be associated to Ca^{2+} channel clustering defect. These findings link BRP directly to a function in efficient stimulus-secretion coupling and presynaptic plasticity (Kittel et al., 2006b).

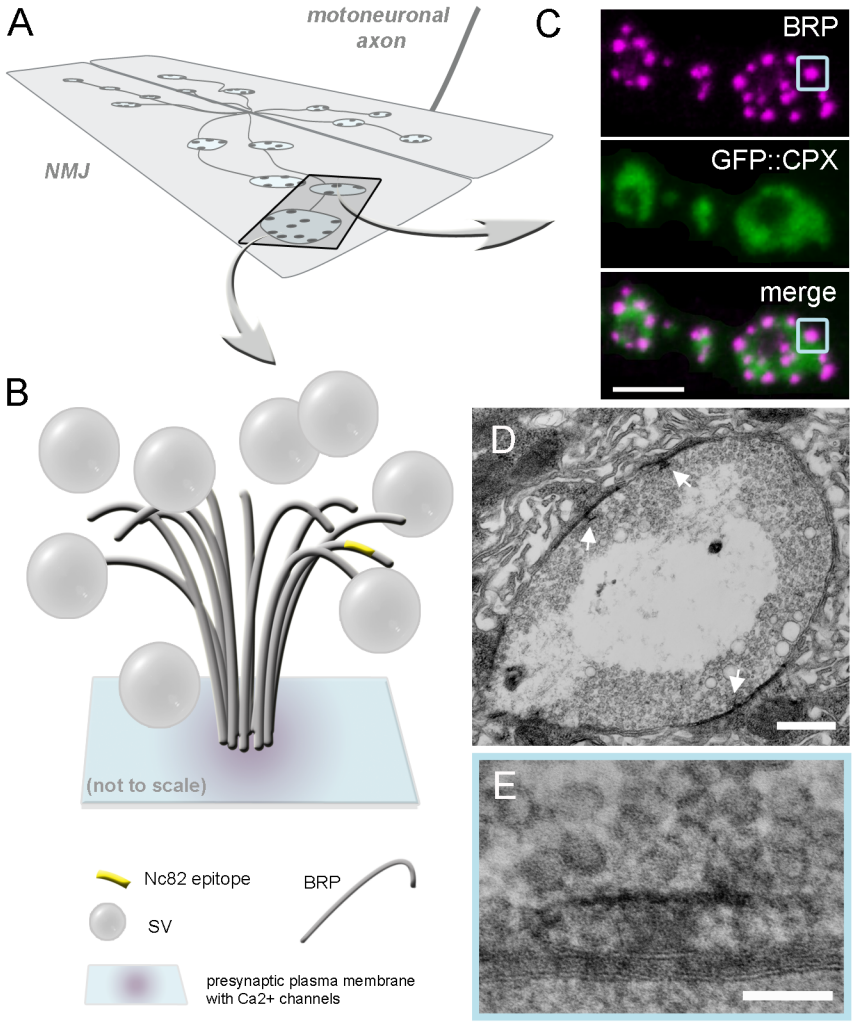

Figure 6. BRP - a central component of presynaptic AZs in *Drosophila*. A) Scheme of larval *Drosophila* NMJ. Grey dots indicate AZs. B) Close-up view of an AZ with circularly arranged BRP filaments, which tether a "cloud" of SVs. Ca^{2+} channels, which are indicated by magenta shade, are embedded in the presynaptic plasma membrane at the base of the BRP N-termini. Approximate position of the Nc82 epitope is highlighted in yellow. C) Confocal image of boutons of the NMJ at muscle pair 6/7 shows BRP puncta recognized using Nc82 antibody. D) EM micrograph of chemically fixed Ib bouton of the NMJ at muscle 6/7. Arrows indicate AZs. E) Magnified view of a T-bar shaped electron-dense material characteristic for *Drosophila* synapses (see also Fig. 4). Scale bar C = 3µm; D = 600 nm; E = 100 nm.

Isoform specific knock-out of *brp* ($brp^{\Delta 170}$ or $brp^{\Delta 190}$) results in miniaturized cytomatrix, which ultimately lead to a reduction in RRP size. As a consequence these synapses displayed diminished basal synaptic transmission (Matkovic et al., 2013). In both mutants no Ca^{2+} channel declustering was observed, which is consistent with CAC binding at BRP's N-terminal region (Matkovic et al., 2013). The authors proposed that the macromolecular architecture established by the alternating arrangement of $BRP^{\Delta 170}$ and $BRP^{\Delta 190}$ isoforms sets the stage for the available number of Ca^{2+} nanodomain-coupled SV release slots per AZ and thereby speci-

fies the RRP size (Matkovic et al., 2013). Therefore, it is likely that complete loss of BRP from AZs represents a disastrous scenario characterized by collapse of the AZ integrity, which is accompanied by defective SV release (Matkovic et al., 2013).

Plasticity of a given synapse is vital for efficient synaptic transmission at any given moment. Therefore, pre- and postsynapse are coordinated to homeostatically maintain appropriate postsynaptic excitation. In *Drosophila*, as in vertebrates, the NMJ comprises several hundreds of individual release sites (Atwood et al., 1993), each located precisely apposed to postsynaptic glutamate receptor (GluIIR) fields (Petersen et al., 1997). Loss of postsynaptic glutamate receptor subunit *glurIIA* lead to an increase in T-bar size as well as gain in SV release as a compensatory consequence (DiAntonio et al., 1999; Weyhersmüller et al., 2011). Consequently, the abundance of BRP per release site is not fixed but dynamic, which results in T-bar heterogeneity across synapses (Marrus and DiAntonio, 2004).
Recently, RAB-3 has been suggested to dynamically configure the AZ layout. Light microscopy of *Drosophila rab3*^{rup} (running unopposed; null or strong hypomorphic allele) synapses revealed fewer but significantly enlarged T-bars (also referred to as "super sites"), with corresponding amounts of BRP and Ca^{2+} channels (Graf et al., 2009). Strikingly, late introduction of RAB-3 reversed this phenotype, demonstrating that RAB-3 rapidly recruits BRP to AZs. Hence, RAB-3 contributes in setting up proper AZ protein complement at individual release sites and thereby takes part in regulating site specific release probability (Graf et al., 2009). Interestingly, BRP levels also cycle according to circadian rhythm, which adds another layer of exocytotic control (Gilestro et al., 2009; Górska-Andrzejak et al., 2013; Sugie et al., 2015).

Beside dynamic BRP abundance, post-translational modifications of BRP were shown to have an impact on AZ complexity. Reduced levels of *elp3*, an acetyltransferase that neutralizes positive charges at the C-terminal end of BRP, induced an extension of the AZ cytomatrix and thus increased surface area to tether SVs (Miskiewicz et al., 2011). HDAC6, a cytoplasmically expressed deacetylase, was demonstrated to be necessary and sufficient to execute the reverse reaction, thereby "shrinking" AZs (Miskiewicz et al., 2014). Finally, sophisticated work from Peled and co-workers provided *in vivo* data of synaptic transmission with quantal resolution suggesting that basal synaptic transmission as well as short-term synaptic plasticity is modulated at the level of release probability at individual AZs (Peled and Isacoff, 2011).

In summary, the size of the AZ cytomatrix scales the release of SVs and might be an evolutionarily conserved feature of synapses, as a possibility to fine-tune synaptic transmission at any given moment.

As described above when viewed by EM presynaptic specializations across different species and synapse types are characterized by a surrounding "cloud" of SVs (Zhai, 2004). In *Drosophila*, SVs are concentrated at T-bars establishing a RRP through the interaction with the last C-terminal 17 aa of BRP (Hallermann et al., 2010b). This finding is based on the characterization of hypomorphic *brp* allele (brp^{nude}), which lacks 1% of its C-terminus due to the introduction of a premature stop codon (Fig. 7A, B).

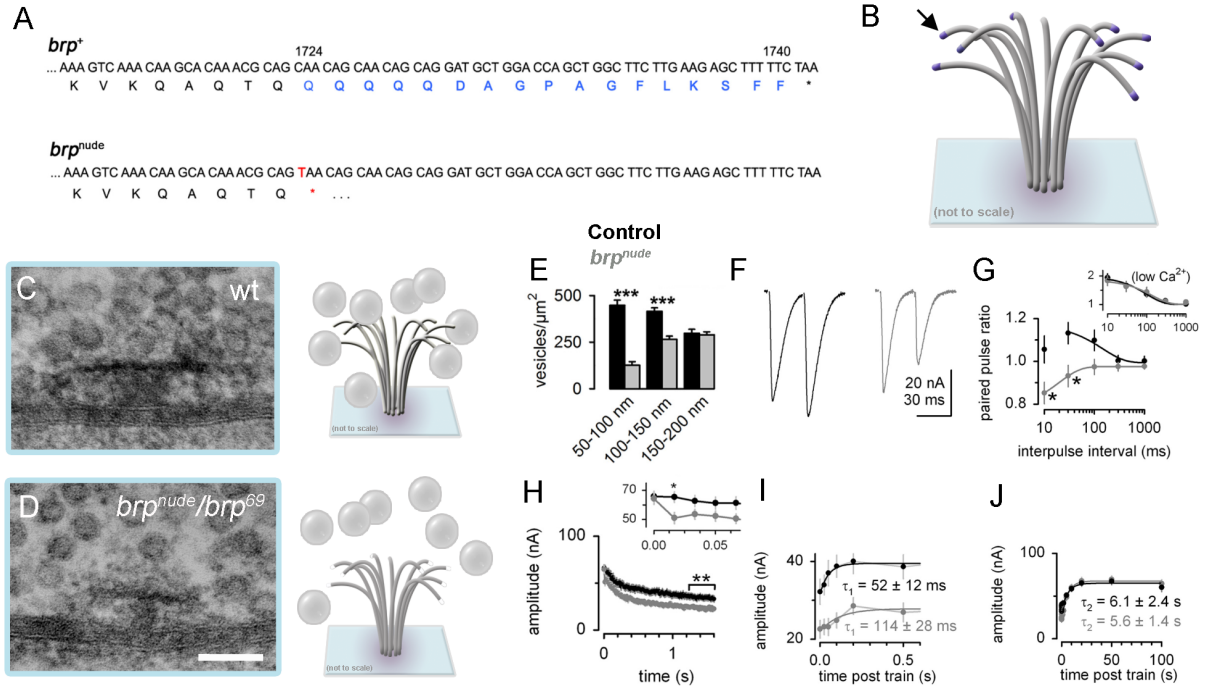

Figure 7. Characterization of the *brp*^{nude} allele. A, B) Introduction of premature stop (1724 aa) codon through chemical mutagenesis resulted in expression of a truncated BRP variant, which lacks 1% of its C-terminus (corresponds to 17 aa). B) Illustration of BRP protein. The purple colored fragment at the far C-terminal end is deleted in brp^{nude} animals. C, D) EM micrographs of wild-type and brp^{nude} AZs. Loss of last C-terminal 17 aa impaired tethering of SVs to the AZ scaffold. E-J) Control is depicted in black and brp^{nude} in grey. E) Quantification of SV tethering deficit. The SV number in 50 nm thick shells surrounding the AZ showed defined reduction in SV number in vicinity to the T-bar structure of brp^{nude} compared to control. F) Example traces of eEPSCs during paired pulse stimulation (30 ms interpulse interval) in control and brp^{nude}. Average paired pulse ratio of control and brp^{nude} as a function of interpulse interval in 1.0 mM Ca^{2+} superimposed with exponential fits. H) Peak amplitudes (average) elicited by 60 Hz train. Inset depicts the average amplitudes of the first five eEPSCs. The brackets indicate significant differences in steady-state amplitude between control and brp^{nude}. I, J) Average peak amplitudes of EPSCs during the first (I) and second (J) recovery component after the stimulus train ($\tau_{1 \text{ and }} \tau_{2,}$ respectively). Fig. A, E-J are from Hallermann et al., 2010b.

Brp^{nude} flies display drastic reduction in life expectancy and impaired motor output (Hallermann et al., 2010b). According to high-resolution microscopy and EM analysis *brp*^{nude} synapses are unaltered with respect to dimension of the AZ cytomatrix and T-bar (Hallermann et al., 2010b; Ehmann et al., 2014). Strikingly, however, at these synapses a diminished number of SVs tethered to the T-bar, particularly within the vicinity of 50-150 nm around the AZ (Fig. 7D, E). This structural alteration did not affect basal synaptic transmission. However, recordings of synaptic transmission during paired-pulse stimulation uncovered a pronounced synaptic depression at short interstimulus intervals (10- and 30 ms; Fig. 7F, G). Also, compared to control, *brp*^{nude} synapses showed stronger depression during a train of 100 stimuli at 60 Hz (Fig. 7I). In addition, *brp*^{nude} synapses exhibit altered recovery kinetics upon sustained high-frequent stimulation. In principle, during recovery two components can be measured at the *Drosophila* NMJ: The first component describes the synapses' ability to tether SVs over time in order to refill the RRP. The second component, however, indicates a slower Ca^{2+}-dependent reload of the supply pool (Hallermann et al., 2010a; 2010b). *Brp*^{nude} synapses specifically showed a slowed first component of recovery (Fig. 7I, J; Hallermann et al., 2010b), which suggests that the change in synaptic short-term plasticity originates from a reduced SV tethering capacity rather than a decrease of the overall RRP size or defective Ca^{2+} clustering.
Thus, morphological and functional data indicate the necessity of the C-terminal 1% of BRP for proper SV tethering and synaptic transmission. Finally, these findings causally relate SV tethering at a synapse to synaptic plasticity (Hallermann et al., 2010b). However, thus far the molecular identity of the BRP complement(s) to physically link SVs to the AZ scaffold has not been reported.

4.3.4. Complexin

Complexin (CPX), also known as synaphin, is predominantly expressed in the nervous system and was initially identified based on its affinity to the presynaptic SNARE machinery (Ishizuka et al., 1995; McMahon et al., 1995). Ever since CPX has been investigated in various species. However, conflicting results from different experimental setups and preparations led to contradictory hypotheses of CPX function (Brose, 2008). Recently, a more differentiated view of CPX's physiological role has emerged in which it exerts domain-specific effects on different modes of synaptic transmission thus constituting a multi-task component of the synapse (Huntwork and Littleton, 2007; Xue et al., 2007; Xue et al., 2009 Martin et al., 2011; Jorquera et al., 2012; Dhara et al., 2014; Martin et al., 2011).

CPXs are small proteins rich in glutamic acid and lysine residues (Ishizuka et al., 1995; McMahon et al., 1995). CPXs are evolutionarily highly conserved and comprise 134 to 160 aa long α-helical proteins [(Fig. 8A, B); *Mus musculus*: 134-160 aa, *C. elegans* and *Drosophila*: 143 aa; www.uniprot.com)]. In mammals four genes encode CPX proteins - CPXI/II/III/ and IV. CPXI and II transcripts are highly enriched in the brain, and their protein products are found in overlapping yet distinct subdomains (McMahon et al., 1995). In contrast, CpxIII and -IV are found abundantly at ribbon synapses of photoreceptor and bipolar cells (Reim, 2005). Judged from systematic sequence analysis, on an evolutionary scale CPXI-IV originate from a common ancestor that contained a farnesylation CAAX-motif, which was lost in CPXI and –II after separation from CPXIII and –IV subfamily. Therefore, CPXIII and –IV form a sub-family separate from CPXI and –II (Brose, 2008) implying a distinction on a functional level (Fig. 8B). *Drosophila* contains only one *cpx* gene (Fig. 8A), from which multiple splice variants are generated. For example, alternative splice events from exon 7 results in two isoforms (Fig. 8D; Buhl et al., 2013; Iyer et al., 2013). The *C. elegans* genome predicts two *cpx* loci – *cpx-1* and *cpx-2* (also *cpx-A* and *cpx-B*; Fig. 8A; Hobson et al., 2011). *Cpx*-promotor directed expression of GFP revealed broad *cpx-1* distribution throughout the entire nervous system. To the contrary, *cpx-2* expression is confined to a small number of neurons with little or no overlap with *cpx-1* (Martin et al., 2011).

CPXs are divided into four subdomains. The central α-helical portion of CPX, which consists of a central- and an accessory subdomain. This portion of CPX is flanked by short, presumably unstructured N- and C-termini (Fig. 8D; Pabst et al., 2002).

Central α-helix (CH)

Combined NMR and X-ray crystallography showed that the central α-helix of CPX binds in an anti-parallel orientation to the groove formed by SYB and SYX helices of the SNARE complex (Fig. 8C; Bracher et al., 2002; Chen et al., 2002). It lies along the interface between vesicle- and target SNAREs, positioning CPX roughly halfway along this complex (Fig. 8C). Interestingly, this interaction appears necessary for several CPX functions including inhibition of spontaneous SV fusion as well as facilitation of evoked release (Cho et al., 2010; Xue et al., 2010; Cho et al., 2014). However, CPX alone is not sufficient to mediate these effects (Maximov et al., 2009).

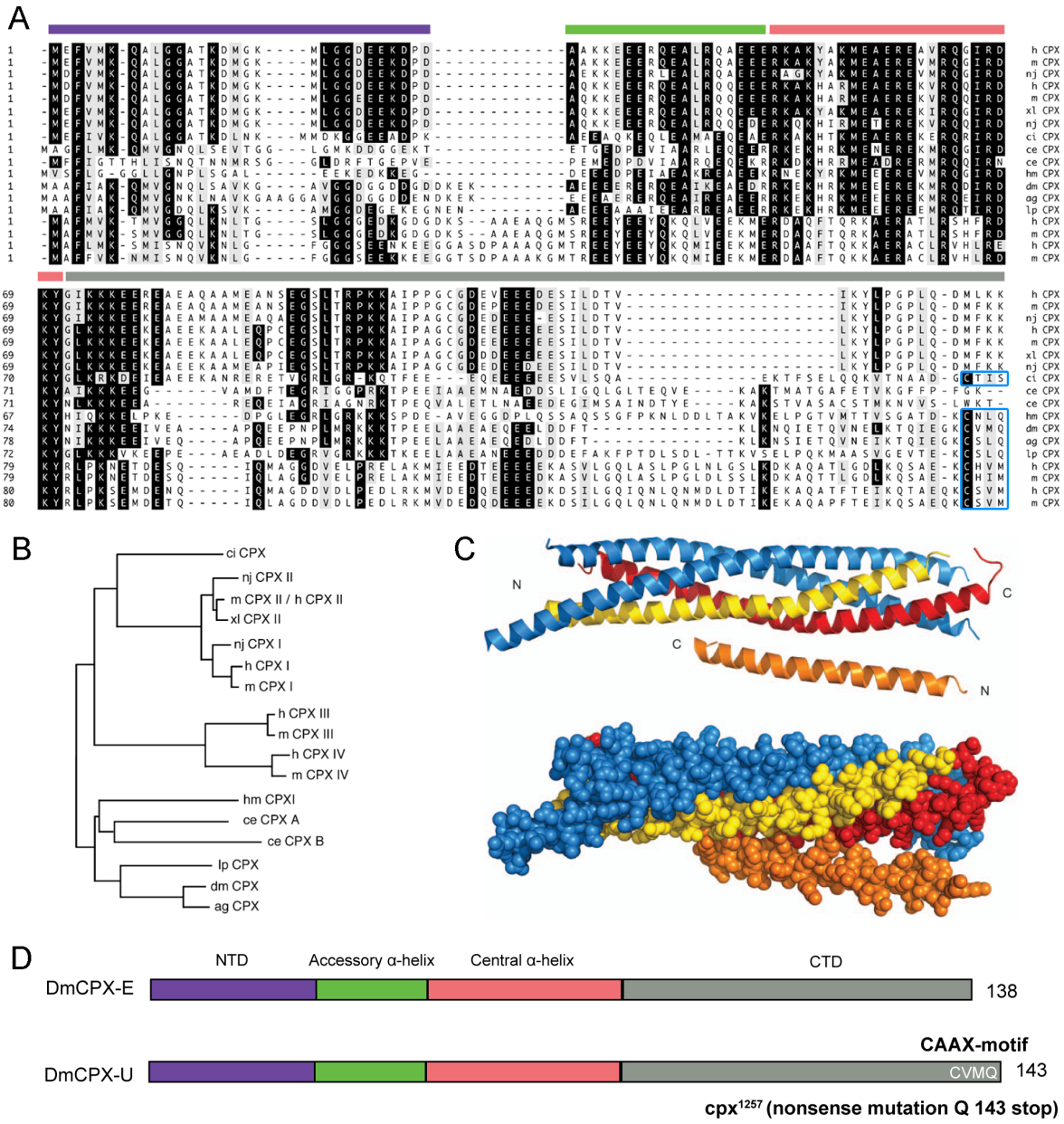

Figure 8. CPX is a highly conserved regulator of exocytosis. Alignment of aa sequences of CPX proteins of different species (single letter code; maximal homology). AA's on black background are identical in the bulk of sequences. Similar residues are shaded in grey (similarity groups: F, Y, W; I, L, V, M; H, R, K; D, E; G, A; T, S; N, Q). The four subdomains are indicated according to annotation of mouse homolog CPXI: NTD (residues 1-29, magenta), AH (residues 30-47), CH (residues 48-70, pink), CTD (71-134, grey). Farnesylating CAAX-motifs are shown in blue boxes. B) Phylogenetic tree shows the long evolutionary history of CPXs. Note that CPXIII/IV form a separate subfamily. Abbreviations for A and B: ag, *A. gambia*; ce, *C. elegans*; ci, *C. intestinalis*; dm, *D. melanogaster*; h, *human*; hm, *H. medicinalis*; lp, *L. pealei*; m, mouse; nj, *Narke japonica*; xl, *X. laevis*. Adapted from Reim, 2005; Brose, 2008. C) Top: ribbon diagram; bottom: space-filling model of the CPX/SNARE bundle (Chen et al., 2002). SNAP-25 in blue, SYX in yellow, SYN in red and CPX in orange. C- and N-termini are indicated. CPX binds in an anti-parallel orientation to the groove formed by the SYB and SYX helices (Bracher et al., 2002; Chen et al., 2002). D) Schematic of CPX isoforms generated by alternative splicing from exon 7 of *cpx* locus (dmCPX-E and –U; adapted from Iyer et al., 2013).

Accessory helix (AH)

The accessory helix (Fig. 8A, D) of CPX was advocated to block the assembly of trans-SNARE complexes to prevent premature vesicle fusion (Xue et al., 2007; Giraudo et al., 2009; Maximov et al., 2009; Xue et al., 2009). Molecular-dynamics simulations suggest that the AH of CPX exerts this function by binding to the C-terminal stretch of trans-SNARE complexes, which destabilized the four-helix SNARE bundle, thus favoring its partial-zipped prefusion state (Giraudo et al., 2009; Bykhovskaia et al., 2013). Alternatively, CPX holds the SNARE complex in the trans-configuration to prevent unzippering of the SNARE bundle and unpriming of SVs (Chen et al., 2002; Pabst et al., 2002), a possibility supported by *in vitro* docking assays (Yoon et al., 2008). More recent studies proposed an "open-closed switch" model. According to this model, in the clamped state the AH of CPX tilts away from the ternary complex ("open state") to bridge a second SNARE bundle forming a cross-linked zig-zag array, which prevents full zippering of SNARE complexes (Kümmel et al., 2011). In contrast, in the fully zippered postfusion complex the AH precedes nearly parallel to the SNARE bundle ("closed state"; Giraudo et al., 2009; Krishnakumar et al., 2011; Kümmel et al., 2011). The authors argue that this way CPX enables the inhibition of release, which can be rapidly disabled to induce fast and efficient SV fusion. Recently, this model has been extended by *in vivo* data from *Drosophila*, which indicated that intermolecular trans-SNARE cross-linking through CPX is indeed conserved for spontaneous fusion but dispensable for evoked SV release (Cho et al., 2014).

N-terminal domain (NTD)

In mammals, the N-terminal domain (NTD; Fig. 8A, D) was shown to promote spontaneous and evoked release efficacy, while being expandable for the clamping function of CPX (Xue et al., 2007; 2009; 2010). Accordingly, the facilitating function of CPX's NTD does not involve SNARE complex binding (Xue et al., 2007). The NTD's promoting role on evoked transmission has been validated by other groups, however its precise function in spontaneous fusion remains incompletely understood (Maximov et al., 2009). In mice the methionine and lysine residues at position five and six are believed to be responsible for the promoting effect of the NTD (Xue et al., 2010). Although these residues are conserved between mice and *C. elegans* their N-termini exhibit opposite effects on both transmission modes (Hobson et al., 2011). Also, recent work from *Drosophila* reported absolute requirement of the NTD to clamp fusion *in vivo* with no effect on evoked release (Cho et al., 2014).

The function of CPX was suggested to be linked to SYT (Tang et al., 2006). Indeed CPX and SYT contain similar functional profile in that both enhance Ca^{2+}-dependent release putatively through the engagement with the SNARE complex (Littleton et al., 1993b; Geppert et al., 1994; Reim et al., 2001). Furthermore, it was proposed that SYT relieves the CPX-SNARE clamp upon Ca^{2+} entry (Giraudo et al., 2006; Schaub et al., 2006; Tang et al., 2006). Genetic experiments support a functional interaction of these proteins, however they also indicate that CPX promotes evoked release in the absence of SYT indicative of cooperativity rather than a requirement (Xue et al., 2010). Recently, interdependency of CPX and SYT has been studied at the *Drosophila* NMJ. This work suggested that CPX influences both transmission modes through the regulation of timing and features of SYT activity (Jorquera et al., 2012).

C-terminal domain (CTD)

The C-terminal domain of CPX (CTD, Fig. 8A, D), initially reported to be expendable (Xue et al., 2007), has later on been implicated to hinder spontaneous SV release (Xue et al., 2009; Cho et al., 2010; Martin et al., 2011; Kaeser-Woo et al., 2012). Similar to other SV-associated proteins, e.g. RAB-3A (Clarke, 1992), several CPX isoforms in different organisms are attached to membranes through a CAAX-motif (C: cysteine, A: aliphatic residue, X: any amino acid) positioned at the far C-terminal end (Xue et al., 2009; Cho et al., 2010; Buhl et al., 2013; Iyer et al., 2013; Wragg et al., 2013). In general, this motif is known to provide the consensus sequence for post-translational farnesylation of proteins at cysteine residues (Marshall, 1993; Zhang and Casey, 1996). This process is catalyzed by farnesyl transferases and increases protein hydrophobicity alleviating membrane interactions (Zhang and Casey, 1996). This post-translational modification appears also crucial for protein-protein interactions (Marshall, 1993).

Genetic disruption of CAAX-motif specifically abolishes the inhibitory function of CPX on spontaneous release, which indicates that membrane association of CPX might be a general feature required for this particular release mode (Xue et al., 2009; Cho et al., 2010; Buhl et al., 2013; Iyer et al., 2013; Wragg et al., 2013). However, not all CPXs contain CAAX-motifs for membrane attachment. For example, in mammals CPXI and -II lack this motif, while CPXIII and IV, exclusively expressed at ribbon synapses containing neurons, possess CAAX-motifs (Reim, 2005). Similarly, two isoforms are generated from exon 7 of the *cpx* locus, which encodes the final 24 and 20 residues in *Drosophila* (Dm-CPX-RE and Dm-CPX-RU). Only Dm-CPX-RU contains the farnesylation motif and was proposed to constitute the predominant brain isoform (Iyer et al., 2013). Mammalian and *C. elegans* CPX-1, although de-

void of CAAX-motif, associate with phospholipids enabled via amphipathic regions near their C-termini (Seiler et al., 2009; Wragg et al., 2013). A recent study reported that amphipathic regions are present in all CPX sequences across different phyla, in some cases together with CAAX-motif (Wragg et al., 2013). This finding is consistent with the idea that membrane-association is a general property of CPXs.

Mutation experiments showed that the CTD, presumably through CAAX motifs, determines the subcellular localization of CPX, which specifically affects spontaneous release (Buhl et al., 2013; Iyer et al., 2013). While CTD truncated CPX protein is constantly found in clusters, reports on the localization of these clusters with respect to AZs differ. Apparently, at the larval NMJ CPX clusters are spread throughout the boutons and do not co-localize with BRP (Buhl et al., 2013). In contrast, at adult Dorsal Longitudinal Muscle (DLM) NMJs mutation of the very C-terminal aa, the X position in the CAAX motif, reorganized CPX within the bouton from a SV-alike to AZ-associated pattern (Iyer et al., 2013). These conflicting results may arise from neuron type and difference in developmental stage of *Drosophila*.

In sum, CPX function at the synapse appears diverse. Although mechanistic details are still controversially discussed CPX's regulatory role in spontaneous release through components of the SNARE complex is well established. To the contrary, much less is known about how CPX contributes to evoked release even though the state of evidence of CPX's promoting function is comparatively consistent.

4.4. Scope of this study

This study aimed to reveal the molecular identity of vesicular and/or cytoplasmic binding partner(s) of BRP. Characterization of the molecular protein décor responsible for synaptic transmission has been and is a central focus in neuroscience. In *Drosophila*, BRP is known to constitute an integral component of the AZ that is required for proper synaptic transmission, Ca^{2+} channel clustering and short-term plasticity of the synapse (Kittel et al., 2006b; Wagh et al., 2006; Fouquet et al., 2009). In particular, a 17 aa long fragment of its C-terminus is required for the association of SVs to the AZ scaffold, a process crucial for efficient sustained SV release (Hallermann et al., 2010b).

This study used immunohistochemistry, larval behavior and electrophysiology to demonstrate that a short 17 aa long C-terminal BRP peptide suffices to bind putative vesicular binding

partners. As a consequence, the pool of SVs accessed during sustained release appeared affected as these exhibit pronounced synaptic short-term depression. However, the molecular identity of the BRP complement to mediate this process remained unknown. To this end, an optical *in vivo* screen was developed, which uses C-terminal BRP fragments to identify putative BRP interactors. This screen uncovered CPX, a known regulator of exocytosis, as an interactor at the peptide. Genetic, behavioral, structural and functional data support this finding and thus uncover a novel role for CPX in BRP-dependent tethering of SVs at *Drosophila* AZs. Finally, this finding may help to further dissect the molecular mechanisms that shape the allocation and recruitment of SVs during continuous release.

5. Results

5.1. Expression pattern of membrane-attached GFP at the NMJ

The fusion protein mCD8::GFP is frequently used to visualize neuronal plasma membranes (Lee and Luo, 1999). Cluster of differentiation (CD8) is a transmembrane spanning protein natively expressed on mammalian T-lymphocytes. The CD8 utilized in this study is from *Mus musculus* (hence, mCD8).

Panneuronal and motoneuronal overexpression of *mCD8::GFP* was performed using *elav(X)*- and *ok6-GAL4*, respectively (Yao and White, 1994; Sanyal, 2009). The localization of mCD8::GFP protein within motoneurons differed prominently depending on the promotor element employed. The *Drosophila* body wall neuromuscular system consists of stereotyped pattern of 30 muscle cells per abdominal hemisegment (Bate, 1990; Hoang and Chiba, 2001). Muscle 6 is innervated by the SNb/SNd, which harbors two types of processes: Large Ib bouton and smaller Is boutons, which are 3-6 µm and 2-4 µm in diameter, respectively (Hoang and Chiba, 2001). *ok6-GAL4* driven *mCD8::GFP* expression was predominantly detectable in Is projections of the larval NMJ (Fig. 9A). In contrast, *elav-GAL4* specific expression resulted in a more uniform distribution of mCD8::GFP in type I and type II processes (Fig. 9B).

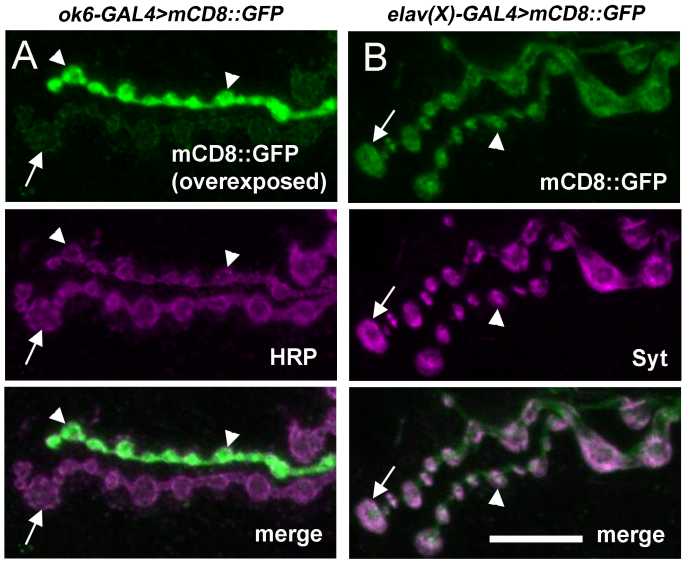

Figure 9. Promotor-specific localization of mCD8::GFP at the larval NMJ. A, B) *ok6-GAL4* (A) and *elav(x)-GAL4* (B) driven mCD8::GFP (A, digitally overexposed). *Ok6-GAL4* specific expression was predominantly found in Is fibers, but only weakly in Ib boutons. Employment of *elav(X)-GAL4* results in a more uniform distribution of fusion protein throughout the NMJ. Arrows indicate Ib projections whereas arrowhead indicates Is projections. Scale bar 10 µm.

5.2. mBRP$^{C\text{-}tip}$ co-localizes with SVs

Previous findings demonstrated the requirement of the far C-terminus of BRP, which comprises the last 17 aa, in SV tethering to AZs (Hallermann et al., 2010b). Based on this finding, it was reasoned that cytoplasmic expression of this terminal peptide (mBRP$^{C\text{-}tip}$) might suffice to bind and occupy putative vesicular interactors and consequently hinder their interaction with wild-type BRP (Fig. 10A), a situation reminiscent of *brp^{nude}*.

To test this conjecture a *3xflag-tag::cfp::mbrp$^{C\text{-}tip}$* (henceforth referred to as *mbrp$^{C\text{-}tip}$ = mobile brp$^{C\text{-}tip}$*) fusion gene was engineered, motoneuronally expressed using *ok6-GAL4* and larval filet preparations were co-immunostained against Flag and the SV marker Vglut (Takamori et al., 2000; Daniels et al., 2008). The addition of CFP served to visualize endogenous fusion protein and to increase mRNA size to prevent degradation through non-sense mediated mRNA decay (NMD; Baker and Parker, 2004). Confocal microscopy of NMJs revealed cortical distribution of mBRP$^{C\text{-}tip}$ within boutons and colocalization with Vglut (Fig. 10C). In addition, *gmr-GAL4* and *ok107-GAL4* driven *mbrp$^{C\text{-}tip}$* co-localized with vesicular SYT in photoreceptor and kenyon cells, respectively (data not shown; Connolly et al., 1996; Freeman, 1996). This data implies that mBRP$^{C\text{-}tip}$ associates with SVs.

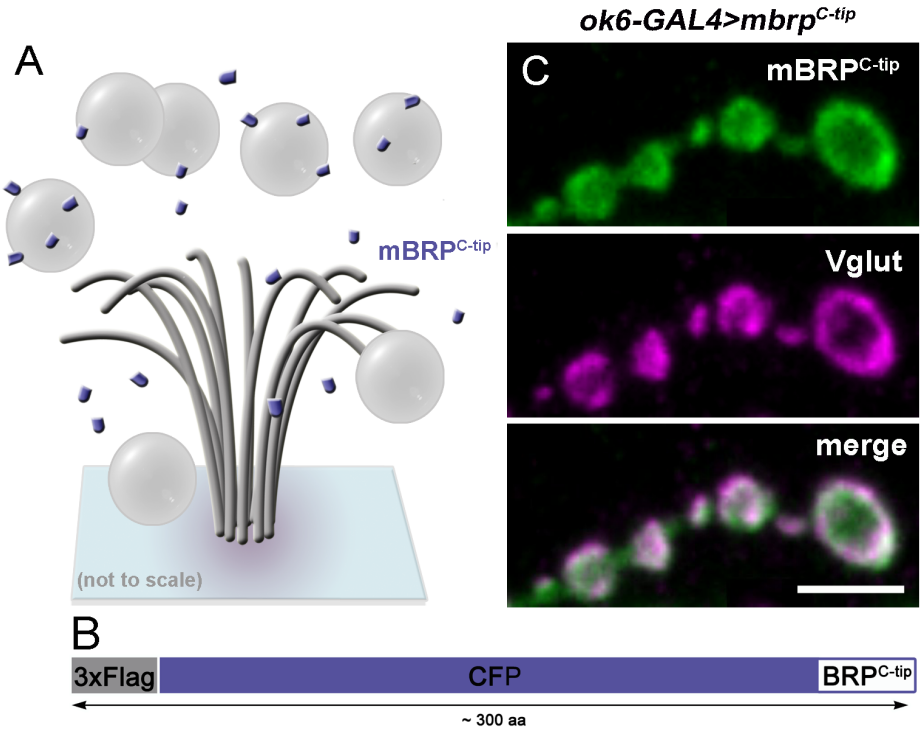

Figure 10. mBRP$^{C\text{-}tip}$ co-localizes with SVs. A) Illustration of AZ with BRP and mBRP$^{C\text{-}tip}$ saturating SVs to inhibit SV tethering to the AZ scaffold. The number of SVs and mBRP$^{C\text{-}tip}$ molecules is exemplary. B) Scheme of the mBRP$^{C\text{-}tip}$ makeup. C) Confocal image of boutons from NMJ of *ok6-GAL4 > UAS-mbrp$^{C\text{-}tip}$* larva. Antibody against the glutamate transporter Vglut was used to detect SVs (Takamori et al., 2000; Daniels et al., 2004). Scale bar 5µm.

5.3. Expression of mobile BRP$^{C\text{-}tip}$ in motoneurons impairs synaptic function

Brp^{nude} mutant flies suffered from severe defects in motor output, which resulted in a significant decrease in their walking distance compared to controls (Hallermann et al., 2010b). First, it was tested if this is true for *brp*^{nude} larvae as well. Hence, the net crawling distance of *brp*^{nude} larvae was scored using a locomotion assay. Indeed, over a period of two minutes *brp*^{nude} larvae covered significantly less distance compared to control (Fig. 11A, B; Suppl. Table 2). This locomotor defect provided a suitable read-out to investigate the effect of mBRP$^{C\text{-}tip}$ expression on motor function. Interestingly, animals with *mbrp*$^{C\text{-}tip}$ expression, but not control larvae, in which the *mbrp*$^{C\text{-}tip}$ moiety was omitted from the transgene, displayed a locomotor defect, similar to *brp*^{nude}. This finding confirmed the potency and specificity of the mBRP$^{C\text{-}tip}$-mediated effect on crawling distance (Fig. 11A, B; Suppl. Table 2).

Electrophysiological analysis of *mbrp*$^{C\text{-}tip}$-positive motoneurons was performed to corroborate peptide function (by N. Ehmann). Strikingly, this experiment uncovered a pronounced short-term depression in *UAS-mbrp*$^{C\text{-}tip}$ expressing animals, reminiscent of *brp*^{nude} mutants (Fig. 11C; Suppl. Table 3).

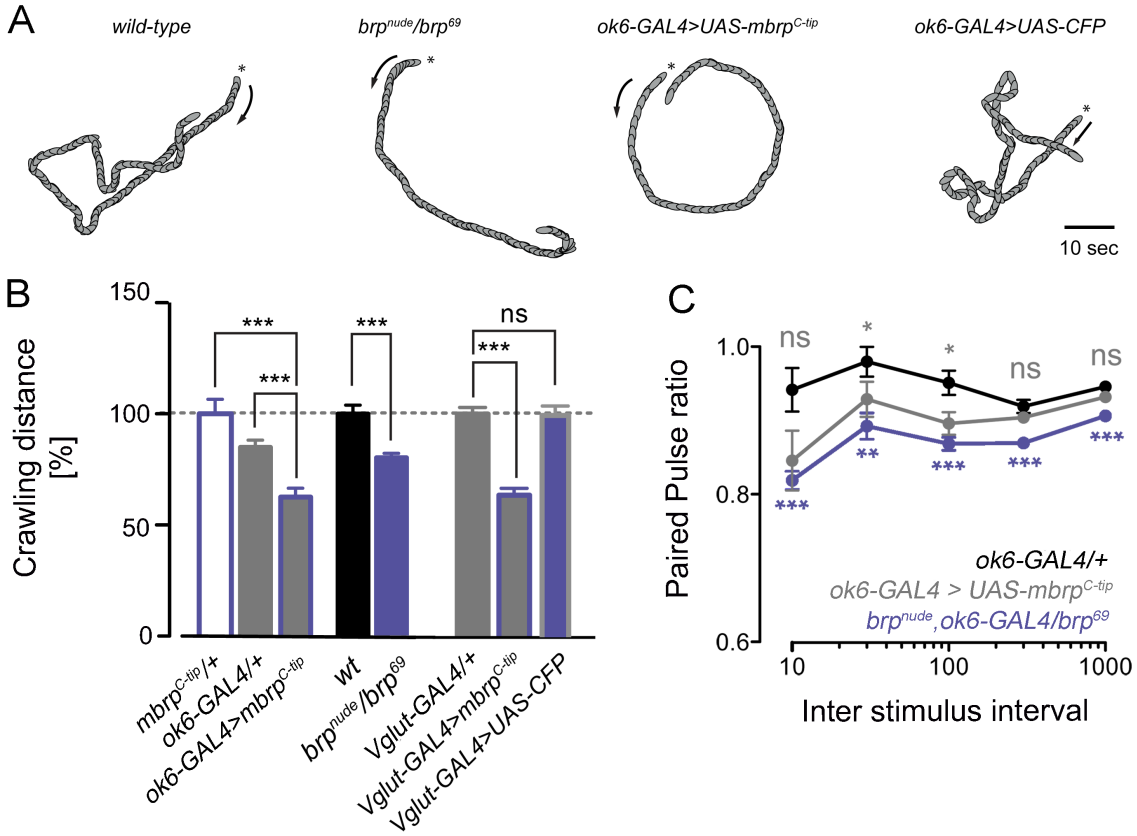

Figure 11. Motoneuronal mBRP$^{C\text{-}tip}$ expression impairs synaptic function and larval crawling behavior. A) Representative trajectories of crawling paths of wild-type, *brp^{nude}/brp^{69}* and *ok6-GAL4* driven *UAS-mbrp$^{C\text{-}tip}$* and *UAS-CFP* larvae. Stars indicate start und arrows indicate initial direction. B) Quantification of crawling distances. Values measured for *ok6-GAL4>UAS-brp$^{C\text{-}tip}$* and *brp^{nude}/brp^{69}* are comparable. Sole expression of CFP does not result in impaired locomotion, excluding functional impact of CFP. Scores were normalized to *mbrp$^{C\text{-}tip}$/+, wt* or *Vglut-GAL4/+*. C) Quantification of two-electrode voltage clamp recordings from larval NMJs show similar synaptic short-term depression of *ok6-GAL4>UAS-brp$^{C\text{-}tip}$* and *brp^{nude}* eEPSCs during paired-pulse stimulation (1,5 mM $CaCl_2$). *ok6-GAL4/+,* (black), *brp^{nude}, ok6-GAL4 /brp^{69,}* (magenta) and *ok6-GAL4>UAS-brp$^{C\text{-}tip}$* (grey). Expression of *mbrp$^{C\text{-}tip}$* induces synaptic short-term depression. Data are presented as mean ± S.E.M. * $P \leq 0.05$, ** $P \leq 0.01$, *** $P \leq 0.001$. Electrophysiological recording performed by N. Ehmann.

Next, I asked if the C-terminal portion of BRP is required for the concentration of SVs to AZs exclusively in glutamatergic motoneurons or if this is a general phenomenon across synapses of different neuron types. To this end the larval crawling paradigm was used to assess the impact of *UAS-mbrp$^{C\text{-}tip}$* expression on SV tethering at different synapses. Consistently, expression of *UAS-brp$^{C\text{-}tip}$* in glutamatergic motoneurons resulted in a severe locomotion defect, independent from the driver strain used (Fig. 12, Suppl. Table 2; *vglut-GAL4*; Daniels et al., 2008*;* see also Fig. 11B, *ok6-GAL4*). A similar defect was observed in animals, which expressed transgene under control of choline acetyltransferase promotor (Fig. 12, Suppl. Table 2; *cha-GAL4;* Salvaterra and Kitamoto, 2001).

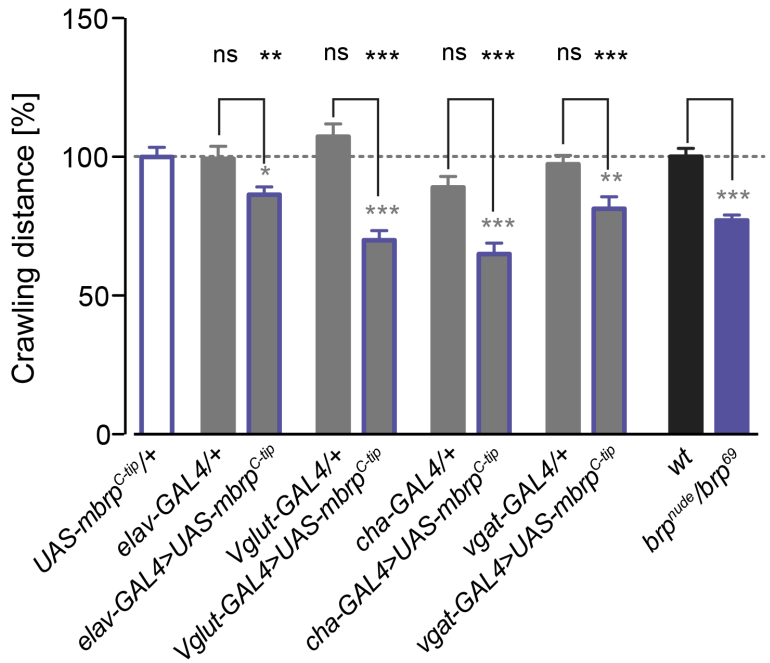

Figure 12. Several neuron types rely on BRP to tether SVs to their AZs. Larval crawling paradigm was used to score the involvement of mBRP$^{C\text{-}tip}$ in SV tethering at AZs of different neuron types. *elav-GAL4*, *vglut-GAL4*, *cha-GAL4* and *vgat-GAL4* driver strains were used to induce expression of *UAS-mbrp*$^{C\text{-}tip}$. BRP$^{C\text{-}tip}$ effect is not restricted to glutamatergic synapses, but can be induced in several neuron types.

In the CNS the vesicular transporter *vgat* is responsible for uptake and storage of γ-aminobutyric acid (GABA) and glycine into SVs (McIntire et al., 1997; Chaudhry et al., 1998). Unexpectedly, confined expression of *UAS-brp*$^{C\text{-}tip}$ in inhibitory neurons using *vgat-GAL4* (Fei et al., 2010) also disrupted motor output (Fig. 12).

Collectively, this set of data suggests that the far end of BRP is required for the accumulation of SVs at the AZ not only at glutamatergic synapses of the motoneuron, but may also act similarly at other excitatory and possibly inhibitory synapses.

In sum, morphological and functional evidence suggests that motoneuronal expression of mBRP$^{C\text{-}tip}$ phenocopies *brp*^{nude} and thus impairs synaptic function through a functional tethering defect. Moreover, in conjunction with binary expression systems mBRP$^{C\text{-}tip}$ may serve as a tool to induce synaptic depression in single neurons or subpopulations of interest.

5.4. BRP$^{C\text{-}term}$ is sufficient to tether SVs to ectopic sites of the motoneuron

Next, based on these observations an optical two-step assay - named KURZSCHLUSS - was designed to identify BRP interactors *in vivo* (Fig. 13). This assay utilizes membrane-attached C-terminal fragments of BRP as bait to tether and stably link fluorophore-marked SVs through its natural binding partner(s) to ectopic sites of larval motoneurons, e.g. in the axon (Fig. 13B).

In a second step, genes of putative BRP interactors were knocked-down using RNA interference (RNAi; Dietzl et al., 2007) to release the BRP-SV interaction and detach SVs from axonal membranes (Fig. 13C).

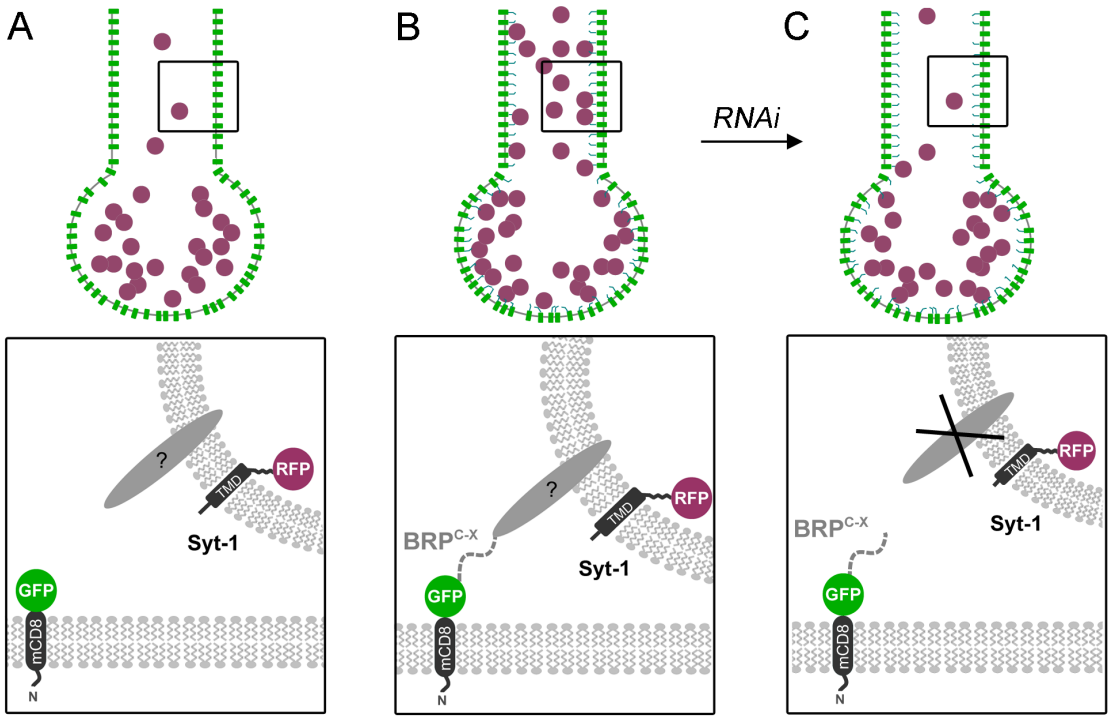

Figure 13. Concept of the KURZSCHLUSS assay. A) In motoneurons, SVs localize predominantly to the soma and terminals. B) Artificial attachment of C-terminal BRP fragments (BRP^{C-X}) to motoneuronal membrane is hypothesized to tether SVs to sites outside of AZs – the axon. C) RNAi-mediated depletion of single genes is thought to identify potential BRP binding partners through reversion of SV attachment to axonal membranes.

The following section provides information on the components engineered to build the KURZSCHUSS assay.

Membrane-attached BRP bait variants (BRP^{C-X})

Full-length BRP is roughly 200 kDa and comprises 1740 residues (Fig. 14D; Wagh et al., 2006). Three different BRP bait variants that differed only in BRP fragment size were generated to increase the probability of SVs to encounter the BRP bait expressed in motoneuronal axons [Fig. 14B-D; $BRP^{C\text{-}long}$ (862 aa) > $BRP^{C\text{-}medium}$ (294 aa) > $BRP^{C\text{-}tip}$ (17 aa)]. The longest BRP fragment ($BRP^{C\text{-}long}$) corresponds to approximately the C-terminal half of BRP (Fig. 14B-D). $BRP^{C\text{-}medium}$ contains the last 294 C-terminal aa (Fig. 14B-D) and has been chosen

because of its striking number of glutamine residues (polyQ; Suppl. Fig. 2), which are known to induce protein aggregation (Dobson, 2001). However, the role of polyQ motifs in BRP oligomerization or AZ nucleation remains elusive. Finally, $BRP^{C\text{-}tip}$ corresponds to 17 C-terminal aa of BRP truncated in *brp*^{nude} mutants. All $BRP^{C\text{-}X}$ versions were C-terminally fused to mCD8::EGFP, which mediates membrane attachment of the BRP bait and visibility of the fusion protein (Fig. 14C).

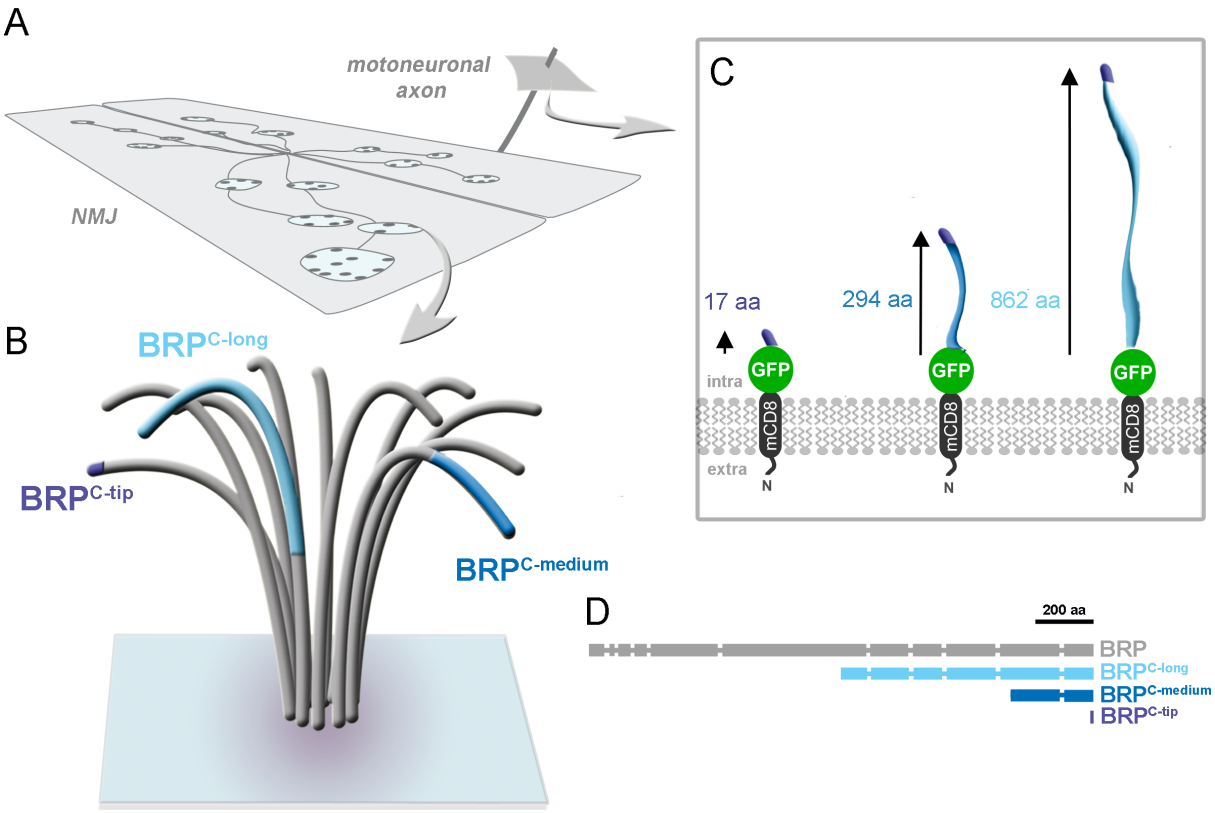

Figure 14. BRP bait variants of the KURZSCHLUSS assay. A) Illustration of NMJ from muscle pair 6/7. This muscle is innervated by glutamatergic Is and Ib processes. BRP puncta are drawn as dots. B) Magnified view of an AZ with circular arranged BRP filaments. BRP bait variants are indicated. C) Schematic illustration of BRP bait fusion proteins and their predicted axonal elongation distances: $BRP^{C\text{-}long}$ (862 aa, ~ 310 nm), $BRP^{C\text{-}medium}$ (294 aa, ~ 105 nm), $BRP^{C\text{-}tip}$ (17 aa; ~ 6 nm). D) Size of BRP fragment according to B). Color code B-D) Full-length BRP (grey), $BRP^{C\text{-}long}$ (light blue), $BRP^{C\text{-}medium}$ (blue), $BRP^{C\text{-}tip}$ (purple).

In principle, when fully extended the distance between two aa is 3,6 Å (= 0,36 nm; O'Sullivan et al., 2014). Therefore, the size of the BRP bait variants in an unstructured confirmation was predicted ~ 310 nm for $BRP^{C\text{-}long}$ (862 aa), ~ 105 nm for $BRP^{C\text{-}medium}$ (294 aa) and ~ 6 nm for $BRP^{C\text{-}tip}$ (17 aa). However, as native BRP is known to form CCs (Wagh et al., 2006) the re-

maining BRP portion included in BRP$^{C\text{-}medium}$ and BRP$^{C\text{-}long}$ bait variants may possess the capacity to fold α-helices. Hence, the dimension of fusion protein may decrease and thus the actual elongation of BRP bait into the axoplasm would be below this value. Note that each bait variant is fused to a GFP, which measures ~ 2 nm from N- to C-terminus (Ormö et al., 1996) and thus elevates each bait variant roughly 2 nm into the axoplasm.

ok6-GAL4 was used to drive expression in VNC and at the NMJ of third instar larvae to assay the motoneuronal distribution of the different BRP bait variants (BRP$^{C\text{-}X}$) with respect to control (mCD8::EGFP). Confocal microscopy revealed uniform distribution of mCD8::EGFP and BRP$^{C\text{-}tip}$ within the VNC and at the NMJ, while BRP$^{C\text{-}medium}$ and BRP$^{C\text{-}long}$ formed conspicuous clusters (Fig. 15E-H). Clustering appeared most severe in *brp$^{C\text{-}long}$* expressing animals (Fig. 15G, H). Note, BRP agglomerates are most prominent in Is fibers of larval NMJs, which may reflect *ok6-GAL4*-specific increase in fusion protein abundance in Is fibers (Fig. 15F, H). Conclusively, overexpression of membrane-tethered BRP accumulates in a Brp$^{C\text{-}X}$-size dependent manner.

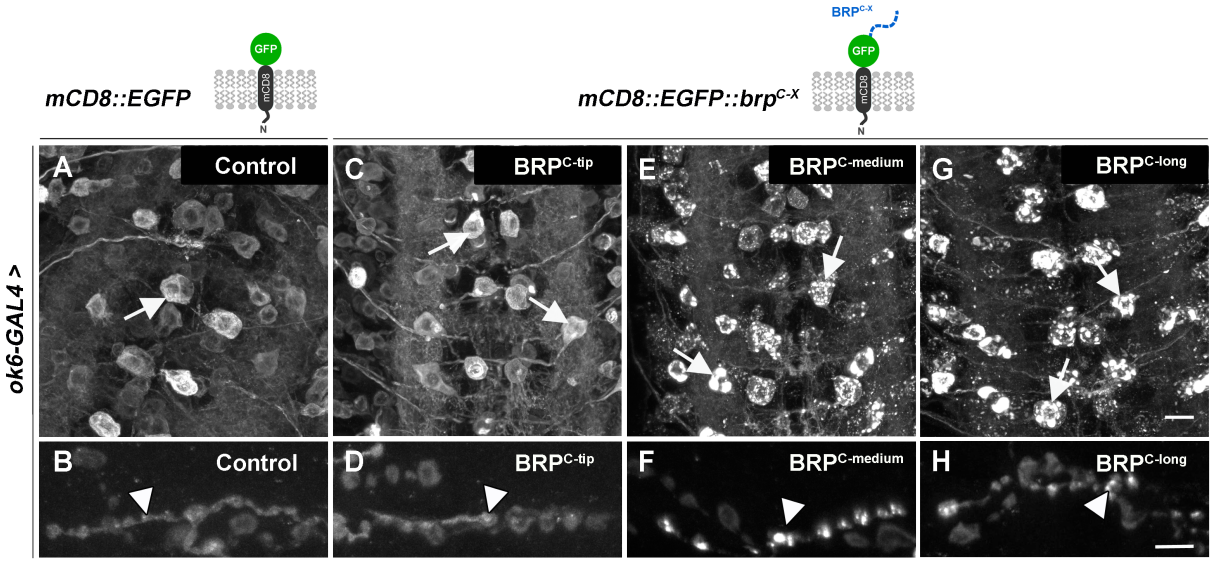

Figure 15. Immunodetection of BRP$^{C\text{-}X}$ bait in VNC and at the NMJ of third instar larvae. A-H) Confocal images of VNCs and NMJs of *mCD8::EGFP* (Control) or *brp$^{C\text{-}X}$* variant expressing larvae. Monoclonal GFP antibody was used to enhance endogenous signals. A, B) mCD8::EGFP in VNC (A) and NMJ (B). C, D) BRP$^{C\text{-}tip}$. E, F) BRP$^{C\text{-}medium}$. G, H) BRP$^{C\text{-}long}$. Arrows indicate motoneuronal somata and arrow heads indicate Is boutons. Strikingly, agglomeration of transgenic BRP seems to depend on BRP fragment length. This becomes most evident in Is boutons, which might be due to stronger Is expression characteristic for *ok6-GAL4*. Scale bar A, C, G, E = 10 µm; Scale bar B, D, F, H = 5 µm.

Visualization of SVs

The KURZSCHLUSS assay relies on the visibility of SVs within larval axons. To simplify the screening procedure we sought to generate a fusion protein between a SV marker and a fluorophore, which enables the identification of SV location without immunohistochemistry.
In order to successfully conduct the KURZSCHLUSS assay the SV marker must meet the following criteria. First, the marker should be an integral vesicular protein to exclude detachment of fusion protein from the SV. Second, the putative protein must be integrated into vesicular membranes prior to anterograde transport of SVs. Finally, at the larval stage SV marker should preferentially localize to terminals and/or somata of motoneurons.

Previous work suggests that SYT complies with these criteria. SYT constitutes an abundant, integral SV protein (Takamori et al., 2006). SYT is expressed on precursor and mature SVs throughout the development of the fly (Littleton et al., 1993a). Finally in *Drosophila* larvae the vast majority of SYT is located in motoneuronal somata in the VNC and at the NMJ in the periphery (Littleton et al., 1993a).
SYT possesses C2 domain (C_2A and C_2B) -containing extravesicular C-terminus and a short intravesicular N-terminus (Fig. 16 A; Geppert et al., 1991; Perin et al., 1991). Monomeric RFP (mRFP) was fused to the N-terminus of SYT (henceforth, mRFP::SYT) to prevent steric hindrance of vesicular and cytoplasmic factors through the fluorophore. Fig. 16B-D depicts the residence of mRFP::SYT in axons, VNC and NMJ when expressed under control of *ok6*-promotor. Location pattern is reminiscent of that characteristic for endogenous SYT protein. Somata of the VNC are densely packed with SYT (Fig. 16C). Similar to NMJs of *ok6-GAL4* driven *mCD8::EGFP* animals, mRFP::SYT is predominantly located to Is fibers with weak yet detectable signals from Ib fibers (Fig. 16D). Importantly, mRFP::SYT is largely omitted from the axons (Fig. 16B) and thus appears a suitable component for the KURZSCHLUSS assay.

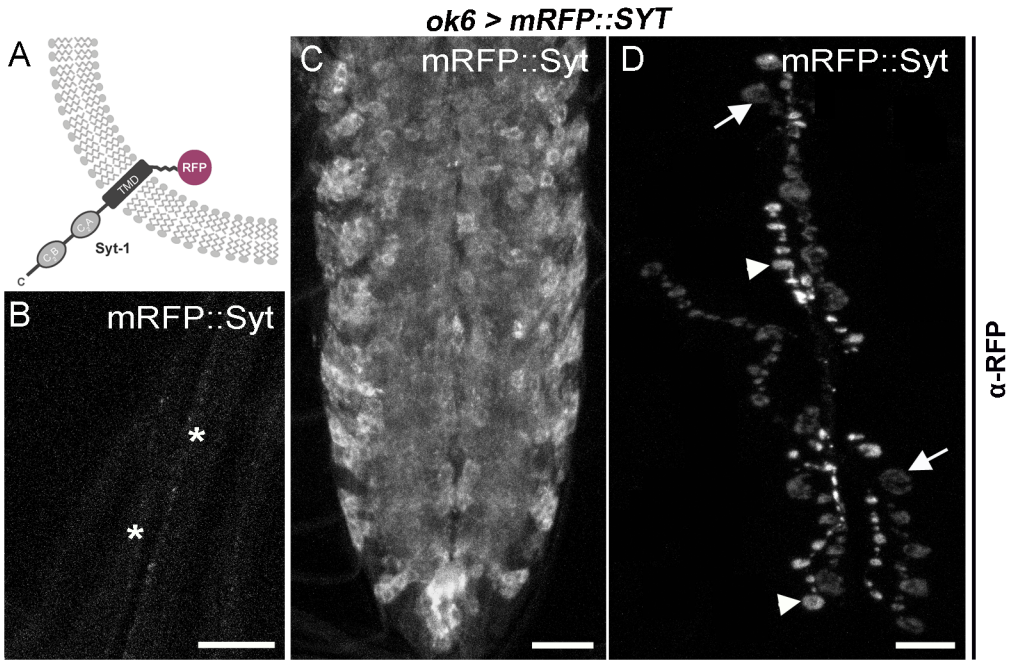

Figure 16. Expression pattern of mRFP::SYT fusion protein in larval motoneurons. A) Illustration of mRFP::SYT transgenic protein. B-D) Example of anti-RFP stained axons (B), VNC (C), and NMJ at muscle pair 6/7 (D) of third instar larvae that express mRFP::SYT under transcriptional control of *ok6-GAL4*. Importantly, N-terminal tagged SYT localizes to somata and terminals of motoneurons, while axons are sparsely labeled. As demonstrated for other UAS-reporters *ok6-GAL4* directs a major fraction of fusion protein expression to Is fibers. Arrow indicate Ib and arrowhead Is processes. Scale bars C =30 μm; B, D = 10 μm.

To investigate whether any of the BRP bait variants are sufficient to tether SVs to axonal membranes of motoneurons, $BRP^{C\text{-}X}$ variants and mRFP::SYT were co-expressed under transcriptional control of *ok6* promotor and axons of the motoneurons were examined.

Both SVs and BRP bait were stained using RFP and GFP antisera, respectively. The abundance of SVs in axons of $BRP^{C\text{-}tip}$ larvae were indistinguishable from controls (Fig. 17 A, *1*, B). Whether $BRP^{C\text{-}tip}$ simply failed or does not engage with SVs due to its small size is not clear. Strikingly, membrane-attachment of $BRP^{C\text{-}medium}$ and $BRP^{C\text{-}long}$ efficiently tethered SVs to axonal membranes (Fig. 17C, D, *2*). Hence, $BRP^{C\text{-}medium}$ with its 294 C-terminal residues of BRP comprises the necessary components and/or structural layout sufficient to attract and stably bind SVs. However, $BRP^{C\text{-}long}$ appeared to recruit SVs most efficiently (Fig. 17D, *2*), which may be attributable to its size or additional sequences that promote SV tethering. In sum, $BRP^{C\text{-}medium}$ and $BRP^{C\text{-}long}$ are sufficient to attract SVs to sites other than AZs.

To ensure specifity of the $BRP^{C\text{-}long}$-SV interaction, cytoplasmic $mBRP^{C\text{-}tip}$ and membrane-attached $BRP^{C\text{-}long}$ were co-expressed in an attempt to compete for putative BRP interactors

rendering SVs incompetent to interact with BRP$^{C\text{-}long}$ (Fig. 17E, *3*). Indeed, the fraction of SVs that coupled to BRP$^{C\text{-}long}$ and thereby remained within the axon declined in the presence of BRP$^{C\text{-}tip}$ (Fig. 17E) demonstrating the specifity of the SV tethering effect mediated through the C-terminal portion of BRP.

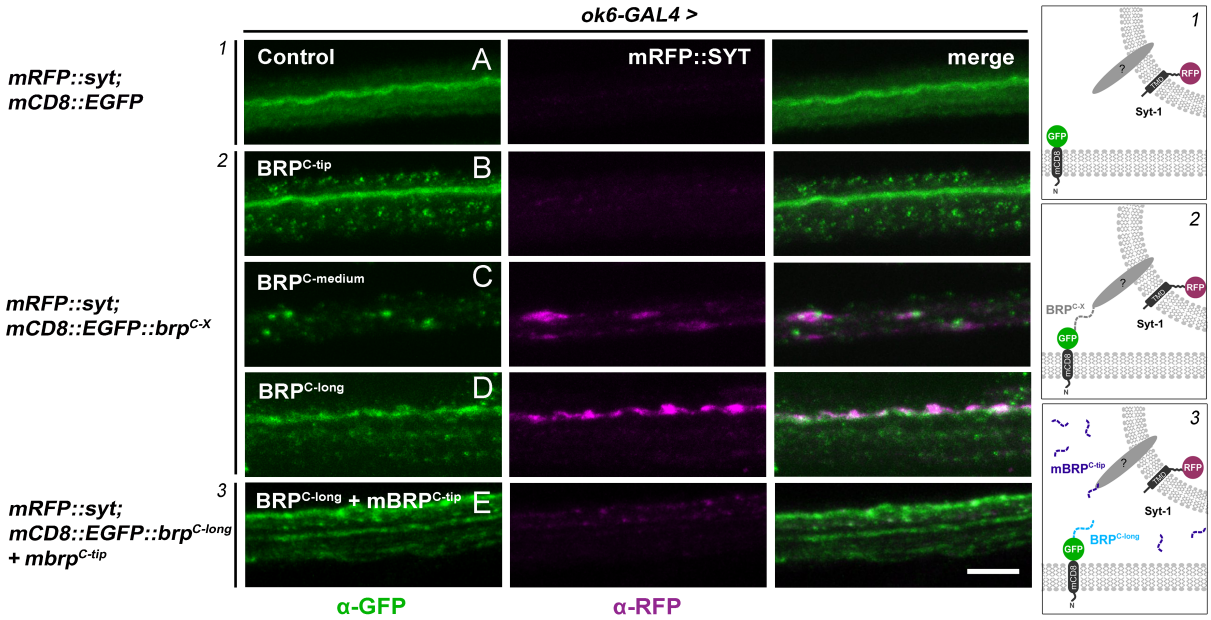

Figure 17. The C-terminal portion of BRP is sufficient to attach SV to sides outside of AZs. A-E) Concurrent motoneuron expression of BRP bait variants and mRFP::SYT ensued by GFP and RFP, respectively. A) Axons of control, B) BRP$^{C\text{-}tip}$, C) BRP$^{C\text{-}medium}$, D) BRP$^{C\text{-}long}$ and E) BRP$^{C\text{-}long}$ + mBRP$^{C\text{-}tip}$. Only BRP$^{C\text{-}medium}$ and BRP$^{C\text{-}long}$ possess the capacity to bind SVs to axons. Scale bar 10 µm. *1-3*) Graphic abstract of control situation (*1*), experimental situation in which differentially sized BRP fragments are used to tether SVs (*2*) and competitive situation with co-expression of BRP$^{C\text{-}long}$ and mBRP$^{C\text{-}tip}$ (*3*).

These data suggest that BRP$^{C\text{-}long}$ is the most efficient SV tethering fusion protein candidate for the KURZSCHLUSS assay. Thus, this BRP bait variant was used for the following experiments.

To corroborate the functionality of the KURZSCHLUSS assay, ratios of mRFP::SYT signals of axons and corresponding NMJs immunolabeled against RFP were quantified [henceforth termed SYT ratio (axon/NMJ), Fig. 19A, B; Suppl. Table 5]. SYT ratios in *brp*$^{C\text{-}long}$ expressing animals were significantly increased compared to controls (Fig. 19B). This increase could be suppressed through the additional expression of mBRP$^{C\text{-}tip}$ (Fig. 19B), a finding that is in line with the reduced SV density within the axon of these larvae (Fig. 17E).

Collectively, this data suggested that the C-terminal end of BRP suffices to induce robust SV attachment to axonal membranes. Thus, the KURZSCHLUSS system constitutes an adequate tool to screen for BRP interactors *in vivo*.

5.5. Screen for BRP interactors

Next, it was reasoned that depletion of putative BRP interactor(s) results in the disengagement and release of SVs from $BRP^{C\text{-}long}$ abolishing their axonal localization (Fig. 18A). To this end, RNAi-mediated knock-down of candidate genes in larvae expressing mRFP::SYT and $BRP^{C\text{-}long}$ was performed to screen for binding partners (Fig. 18A; Dietzl et al., 2007). Vesicular and cytoplasmic factors involved in the exo-endocytosis cycle were tested (Suppl. Fig. 1). The selection of vesicular proteins was based on previously published protein composition of SVs (Lloyd et al., 2000; Takamori et al., 2006). Additional cytoplasmic factors were chosen based on their involvement in exocytosis.

For each gene tested, larval axons of the experimental genotype were screened for SV clusters. Confocal microscopy laser settings were adjusted to optimally visualize these axonal SV clusters and were subsequently used to obtain images of the corresponding control genotypes. Thus, laser settings varied between different RNAi experiments, but were constant among experimental and control recordings within the same RNAi experiment.

From 28 genes tested by RNAi knock-down employing the KURZSCHLUSS assay (Suppl. Table 1), 4 genes showed no difference between experimental and control settings, 21 exhibited increased and 3 experiments decreased SYT signals in larval axons when compared to the respective control (Suppl. Fig.1).
Exemplary, knock-down of *syn* and *dysb,* both of which are known components vital for proper synaptic transmission at glutamatergic synapses (Ferreira and Rapoport, 2002; Shao et al., 2011), did not abolish axonal SV clustering mediated through $BRP^{C\text{-}long}$ (Fig. 18B). In contrast, axons of *cpx*-depleted animals no longer contained SV accumulations (Fig. 18B), which indicated CPX's capacity to mediate SV-$BRP^{C\text{-}long}$ attachment at axonal membranes. Thus, CPX may constitute a putative binding partner of active zone protein BRP.

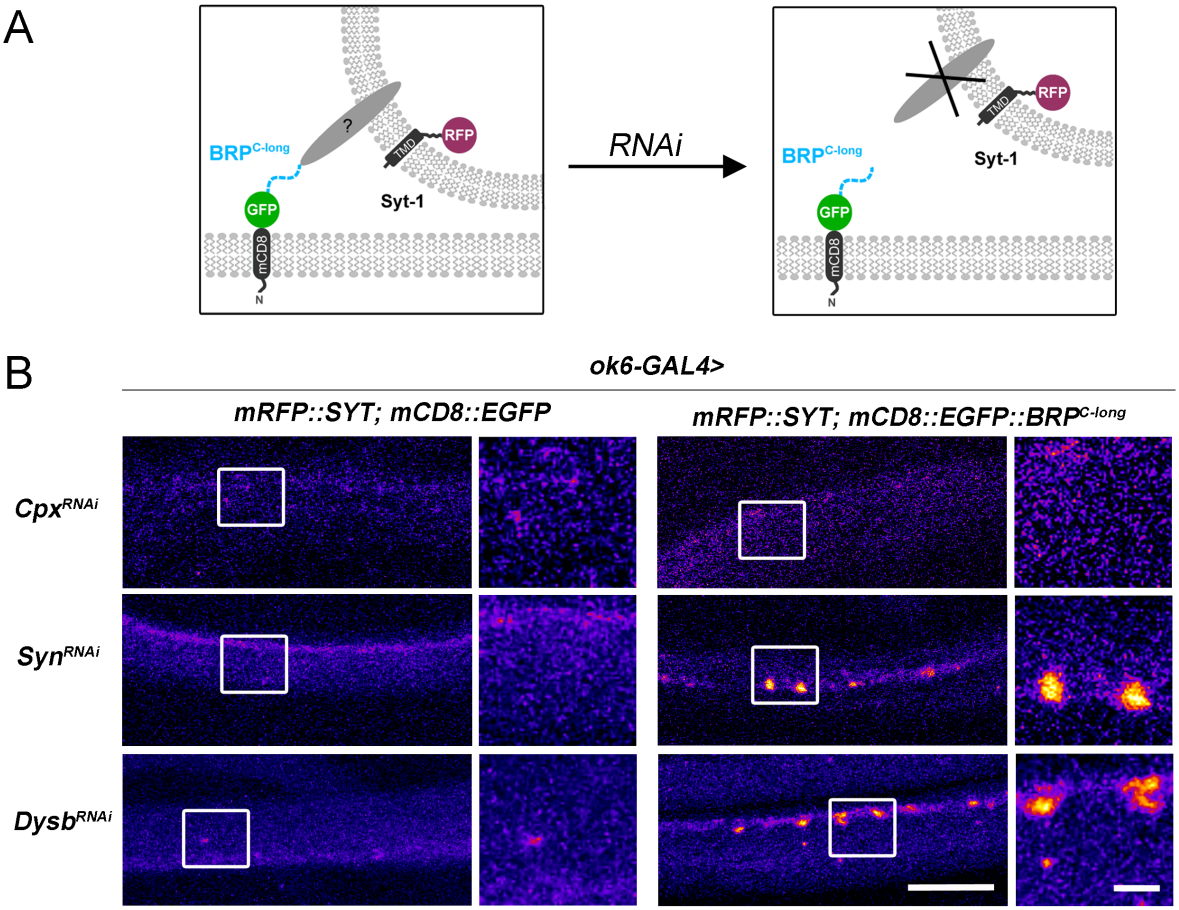

Figure 18. Knock-down of *cpx* results in BRP$^{C\text{-}long}$-SV disengagement. A) Graphic abstract shows concept of the BRP$^{C\text{-}long}$ based KURZSCHLUSS screen. B) Images of larval axons of control (left panel) and *brp*$^{C\text{-}long}$ (right panel) expressing animals. Knock-down of *cpx* resulted in release of SVs from BRP$^{C\text{-}long}$, hence SVs largely omit larval axons, similar to control. In contrast, depletion of other genes did not abolish SV clustering exemplified for *syn* and *dysb*. Full table of results is shown in Suppl. Fig. 1. Scale bar = 10 µm, insets = 2 µm.

5.6. CPX mediates SV tethering to BRP

To substantiate this finding, SYT ratios were quantified in *cpx*-depleted animals that expressed *brp*$^{C\text{-}long}$ or *mCD8::EGFP* (control). Intriguingly, in contrast to larvae that expressed *brp*$^{C\text{-}long}$ in wild-type background, SYT ratios were not elevated when *brp*$^{C\text{-}long}$ was expressed in *cpx*^{RNAi} background (Fig. 19B, Suppl. Table 5). Hence, reduced levels of CPX suppressed the interaction of SVs with BRP$^{C\text{-}long}$, which is consistent with the notion that CPX participates in BRP-dependent SV tethering.

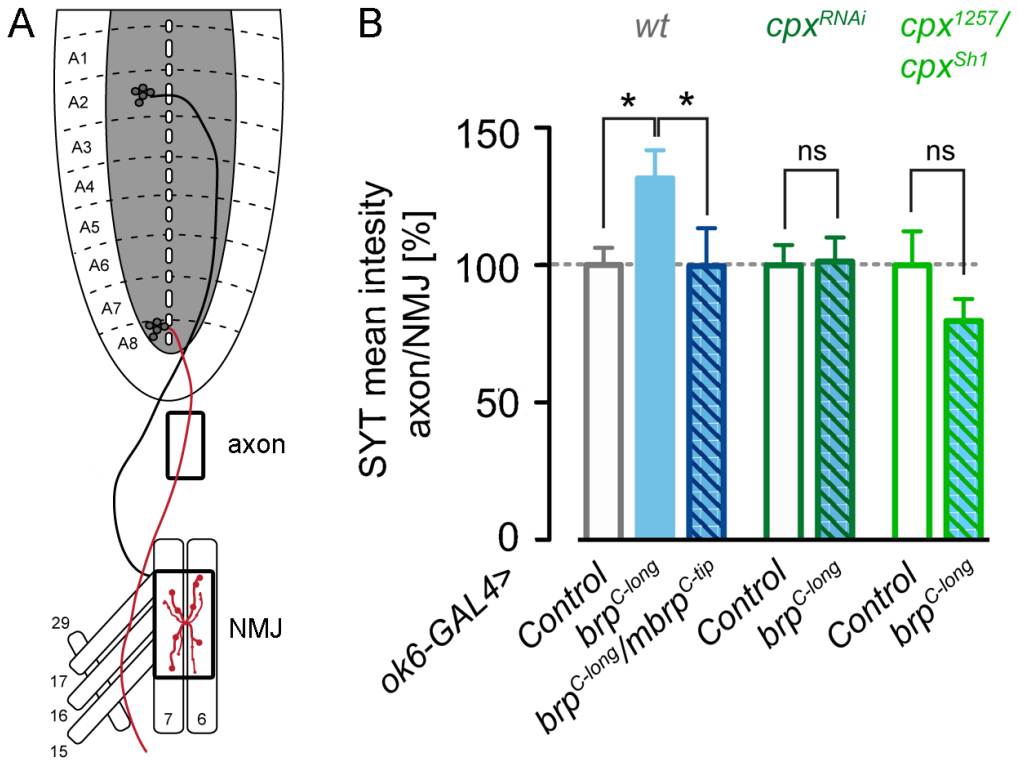

Figure 19. CPX promotes SV tethering to BRP$^{C\text{-}long}$. A) Schematic representation of the larval VNC with axons originating from somata located in segment A2 and A8. Average mRFP::SYT intensity was measured in axons and NMJs at muscle pair 6/7 to calculate SYT ratios. B) Quantification of SYT ratios in control and *brp*$^{C\text{-}tip}$ expressing animals in wild-type (grey), *cpx*^{RNAi} (dark green) and *cpx*^{1257} (light green) background. Introduction of *brp*$^{C\text{-}long}$ in wild-types led to elevated SYT ratios. In contrast, both knock-down of *cpx* and absence of CPX from SVs (*cpx*^{1257} mutant background) resulted in comparable SYT ratios between controls and *brp*$^{C\text{-}long}$. Data are presented as mean ± S.E.M. * $P \leq 0.05$, ** $P \leq 0.01$, *** $P \leq 0.001$.

Although CPX was identified as a cytosolic protein (McMahon et al., 1995), recent studies obtained in *Drosophila* and *C. elegans* indicate the importance of CPX's SV association. Loss of vesicular residence of CPX alters its targeting to synapses and selectively impairs spontaneous release (Buhl et al., 2013; Iyer et al., 2013; Wragg et al., 2013). Membrane-association through the farnesylation CAAX-motif appeared particularly important (Zhang and Casey, 1996; Cho et al., 2010; Buhl et al., 2013; Iyer et al., 2013; Wragg et al., 2013). In *Drosophila*, only one of two transcripts generated from exon 7 contains this motif (Dm-CPX-RU). Genetic removal of C-terminal X-position appeared to abolish membrane-coupling (*cpx*^{1257} mutant) and resulted in accumulation of CPX protein distant from SVs (Suppl. Fig. 3; Iyer et al., 2013).

Therefore, in a next step, *cpx*^{1257} mutant was utilized to test if CPX-deficient SVs possess the capacity to recognize BRP$^{C\text{-}long}$. Interestingly, judged from quantification of SYT ratios axon-

al SV clustering was not observed in these animals (Fig. 19B), demonstrating that vesicular residence of CPX is required for the attachment of SVs to $BRP^{C\text{-}long}$. This finding supports the notion that CPX interacts with BRP. Note, SYT ratios measured in cpx^{1257} background were comparable to those in *cpx* knock-down indicating the specifity of cpx^{RNAi} effect (Fig. 19B, Suppl. Table 5).

Together, this set of experiments showed that CPX promotes SV tethering to BRP-bestowed axonal membranes, a finding that implies a physiological role for CPX in SV concentration at the AZ scaffold established among others by BRP.

5.6.1. *cpx* and *brp* interact genetically

In order to verify that BRP and CPX are components of a common signaling pathway their genetic interaction was evaluated. First, individual and compound effects of hypomorphic alleles of either locus on larval locomotion were assessed. Homozygous brp^{nude} and cpx^{1257} mutant flies exhibit severe defects in their motor output (Hallermann et al., 2010b; Iyer et al., 2013). Similarly, brp^{nude} and cpx^{1257} larvae displayed reduced locomotion (Fig. 20A, Suppl. Table 2). Importantly, the motility defect of brp^{nude}; cpx^{1257} double mutants was not additive, but was comparable to those of cpx^{1257}/cpx^{Sh1} mutants (Fig. 20A; Suppl. Table 2). These data support the assumption that BRP and CPX function in a common signaling pathway.

The relationship of BRP and CPX was further examined employing a second behavioral paradigm, in which the mortality rate of adult flies after eclosion from the pupae was scored. Brp^{nude} animals die within five to six days (Fig. 20B, C; Hallermann et al., 2010b). Similarly, cpx^{1257} animals exhibit survival rates that are significantly reduced compared to controls, but live longer than brp^{nude} mutants (Fig. 20B, C, Suppl. Table 4). In contrast, cpx^{Sh1} null mutants are semilethal with escaper animals that die within a few days (Huntwork and Littleton, 2007). The reduction in life expectancy of brp^{nude}; cpx^{1257} double mutants was not significantly exacerbated compared to brp^{nude} (Fig. 20B, C; Suppl. Table 4), which supports functions for BRP and CPX in the same signaling pathway.

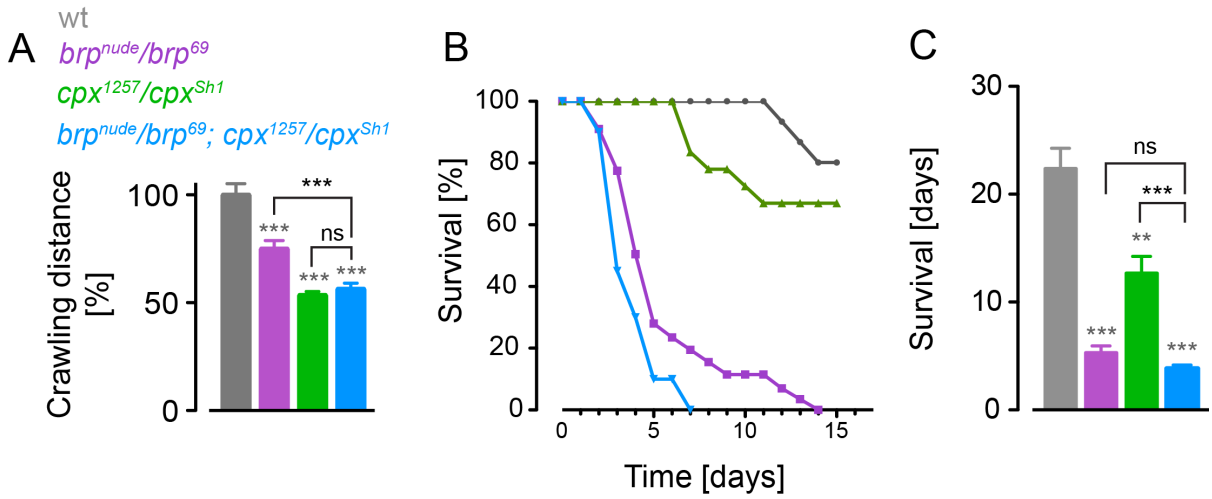

Figure 20. BRP genetically interacts with CPX. A) Examination of epistatic relationship of BRP and CPX employing the larval crawling paradigm. Loss-of-function of *brp* or *cpx* leads to an impairment of motor function. brp^{nude}/brp^{69}; cpx^{1257}/cpx^{Sh1} double mutants displayed motor function defect comparable to *cpx* single mutants. This suggests a genetic interaction between BRP and CPX and their roles in a common signaling pathway. B) Kaplan-Meier-Curve depicting survival rates of single and double mutants. C) Quantification of survival rates. Reduced life expectancy is not additive in brp^{nude}/brp^{69}; cpx^{1257}/cpx^{Sh1} double mutants. Data are presented as mean ± S.E.M. * $P \leq 0.05$, ** $P \leq 0.01$, *** $P \leq 0.001$.

Next, the genetic interaction between *brp* and *cpx* was independently verified by investigating the complementation capacity of *brp* and *cpx* alleles, a genetic method well established (Yook et al., 2001). The phenomenon when two recessive alleles of different gene loci fail to complement one another is referred to as non-allelic non-complementation. Interestingly, this genetic particularity has been frequently observed when two genes encode proteins that physically interact, but this appears not to be a requirement (Hays et al., 1989; Yook et al., 2001). Non-allelic non-complementation has been explained by two models: the dosage model and the poison model (Stearns and Botstein, 1988; Fuller et al., 1989). In the dosage model, gene dose reduction at one locus does not affect protein function, however additional reduction of the gene dose at second locus leads to loss of function and mutant phenotype. In contrast, the poison model describes a scenario in which the function of one mutated gene product is disturbed (poisened) by the function of another mutated gene product. While the first mutation is harmless on its own, introduction of the second mutation may have detrimental consequences.

The function of BRP and CPX appears to affect larval motility (Fig. 20A). Therefore, larval crawling distances of double heterozygous *brp; cpx* larvae were scored as a measure of their allelic complementation faculty. The combination of either null and hypomorphic *brp* and *cpx* allele ($brp^{nude}/+$; $cpx^{Sh1}/+$ and $brp^{69}/+$; $cpx^{1257}/+$) resulted in non-allelic non-

complementation, i.e. a reduction in crawling path length (Fig. 21, Suppl. Table 2). This finding is consistent with a genetic interaction that requires a poisonous gene product that impairs the protein complex with which it normally associates. This sensitizes the genetic background for the second mutation, which induces a functional deficit of the relevant protein complex.

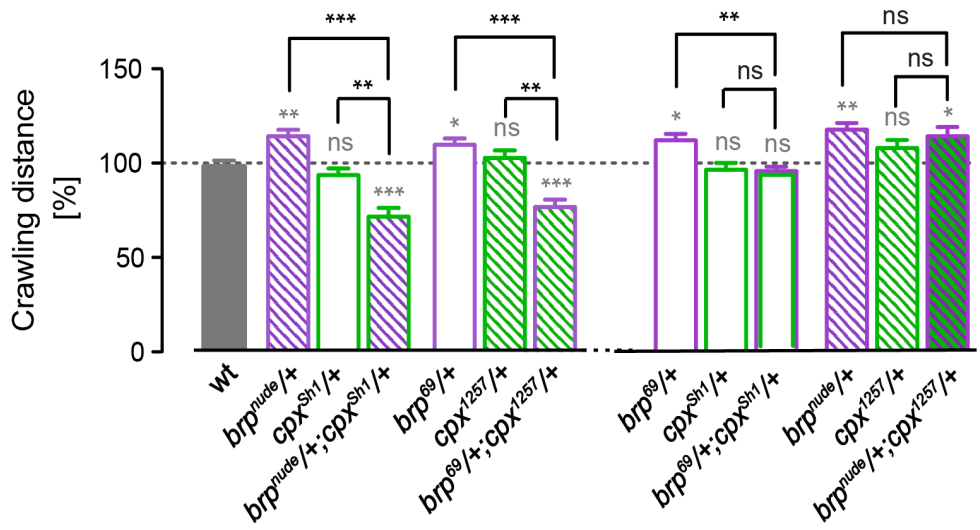

Figure 21. *brp* and *cpx* alleles display non-allelic non-complementation. Quantification of larval crawling paths lengths to investigate allelic complementation capacity of heterozygous *brp; cpx* animals. Partial loss of function of either gene product resulted in non-allelic non-complementation, consistent with a genetic interaction between *cpx* and *brp* (left). In contrast, brp^{69} and cpx^{Sh1} null alleles and brp^{nude} and cpx^{1257} hypomorphs complemented each other. Data are presented as mean ± S.E.M. * $P \leq 0.05$, ** $P \leq 0.01$, *** $P \leq 0.001$.

Interestingly, brp^{69} and cpx^{Sh1} null alleles complemented one another (Fig. 21, Suppl. Table 2). Hence, simple dosage reduction at these two loci did not result in non-allelelic non-complementation. Complementation was also observed for brp^{nude} and cpx^{1257} alleles (Fig. 21, Suppl. Table 2), which demonstrated that the combined effects of partial loss of BRP and CPX function can be compensated to exert wild-type behavior.

In conclusion, this set of experiments confirms the genetic interaction between BRP and CPX and supports the finding that these genes act in a common signaling cascade.

5.6.2. BRP and CPX tether SVs to the AZ scaffold

BRP exerts a vital function in SV tethering at the AZ (Hallermann et al., 2010b). Therefore, it was examined whether BRP and CPX interact to concentrate and constrain SVs at the AZ cytomatrix. To this end, morphological analysis of cpx^{1257} synapses was conducted. Transmis-

sion electromicrographs of single *cpx*^{1257} and *brp*^{nude}*; cpx*^{1257} double mutant synapses were assessed and the number of SVs within 50 nm thick shells surrounding the AZ were quantified (Fig. 22A, B, Suppl. Table 6). First, the reduction in SV number that tethered to *brp*^{nude} AZs was confirmed (Fig. 22B, C; Suppl. Table 6; Hallermann et al., 2010b).

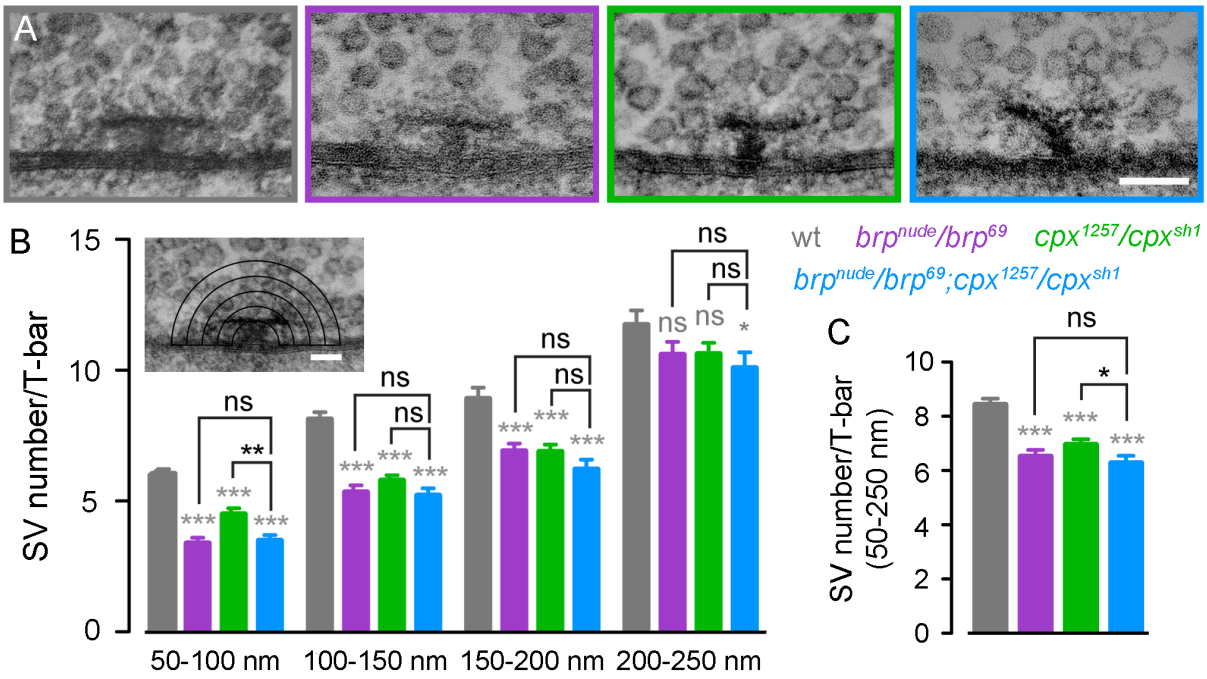

Figure 22. BRP and CPX promote SV tethering to the AZ cytomatrix. A) Electron micrographs of chemically fixed wild-type, *brp*^{nude}*/brp*^{69}, *cpx*^{1257}*/cpx*^{Sh1} and *brp*^{nude}*/brp*^{69}; *cpx*^{1257}*/cpx*^{Sh1} (displayed from left to right in this order) synapses of third instar larvae. B) Quantification of SV numbers found in 50 nm thick shells that surround the T-bar structure. Inset: The grid used to count SVs was aligned with the presynaptic plasma membrane with the T-bar in its center [according to (Hallermann et al., 2010b)]. As expected at *brp*^{nude} synapses SVs that tethered to the AZ were reduced within the radius of 50 – 200 nm (Hallermann et al., 2010b). Similarly, less SVs tethered to AZs of *cpx*^{1257} larvae, however the deficit was less severe. Strikingly, *brp*^{nude}*/brp*^{69}; *cpx*^{1257}*/cpx*^{Sh1} synapses host SV numbers comparable to either single mutant. No gross morphological changes were observed within the 200-250 nm shell. C) Total number of SVs within a 50-250 nm shell. Scale bars A = 100 nm; Inset = 100 nm. Data are presented as mean ± S.E.M. * $P \leq 0.05$, ** $P \leq 0.01$, *** $P \leq 0.001$.

Intriguingly, at *cpx*^{1257} synapses the average number of SVs within the inner shells was significantly reduced compared to controls (Fig. 22B). However, the decrease in SV number was less severe than in *brp*^{nude} (Fig. 22 B, C), which may suggest that CPX is note the sole binding partner of BRP to mediate this function. Importantly, the defect was not enhanced in *brp*^{nude}*; cpx*^{1257} double mutants supporting the notion that BRP and CPX interact to generate SV pool at AZs (Fig. 22A-C).

5.6.3. BRP and CPX function to prevent synaptic depression

In principle, SV tethering enables continuous release during high-frequency transmission by providing a reservoir of SVs in striking distance to the Ca^{2+} influx at their release sites (Neher, 1998; Hallermann et al., 2010a; 2010b; Hallermann and Silver, 2013). In brp^{nude} mutants disruption of this process induces pronounced synaptic short-term depression (Hallermann et al., 2010). Based our current model, it was assumed that the absence of vesicular CPX abolishes BRP-mediated SV recruitment/tethering reflected in changes in synaptic plasticity, similar to that observed in brp^{nude} mutants (Hallermann et al., 2010b). To this end, cpx^{1257} synapses were functionally characterized (recordings performed by N. Ehmann). Indeed, paired-pulse recordings of cpx^{1257} mutants unveiled pronounced synaptic short-term depression, indistinguishable from brp^{nude} mutants (Fig. 23A, B; Suppl. Table 7). As expected, cpx^{1257} mutants displayed extensive spontaneous release with no change in evoked release efficacy (Fig. 23C-E; Suppl. Table 7; Iyer et al., 2013). The evidence indicated that the C-terminal residues of CPX shape synaptic plasticity and support the notion that CPX and BRP interact to tether SVs to AZs.

To further examine the interdependency of *brp* and *cpx* loci brp^{nude}*;* cpx^{1257} double mutants were analyzed. Interestingly, these animals exhibit a milder defect in spontaneous SV release compared to cpx^{1257} single mutants even though brp^{nude} animals display unaltered spontaneous release (Fig. 23D, E; Suppl. Table 7). Hence, the C-terminal region of BRP is required to mediate high-frequency evoked- and spontaneous SV release. Further, this finding implicates a causal link between SV tethering and spontaneous release. Also, eEPSC amplitudes of brp^{nude}*;* cpx^{1257} double mutants were significantly increased compared to either single mutants (Fig. 23C). Furthermore, the combination of brp^{nude} and cpx^{1257} resulted in a more pronounced synaptic short-term depression (Fig. 23A, B).

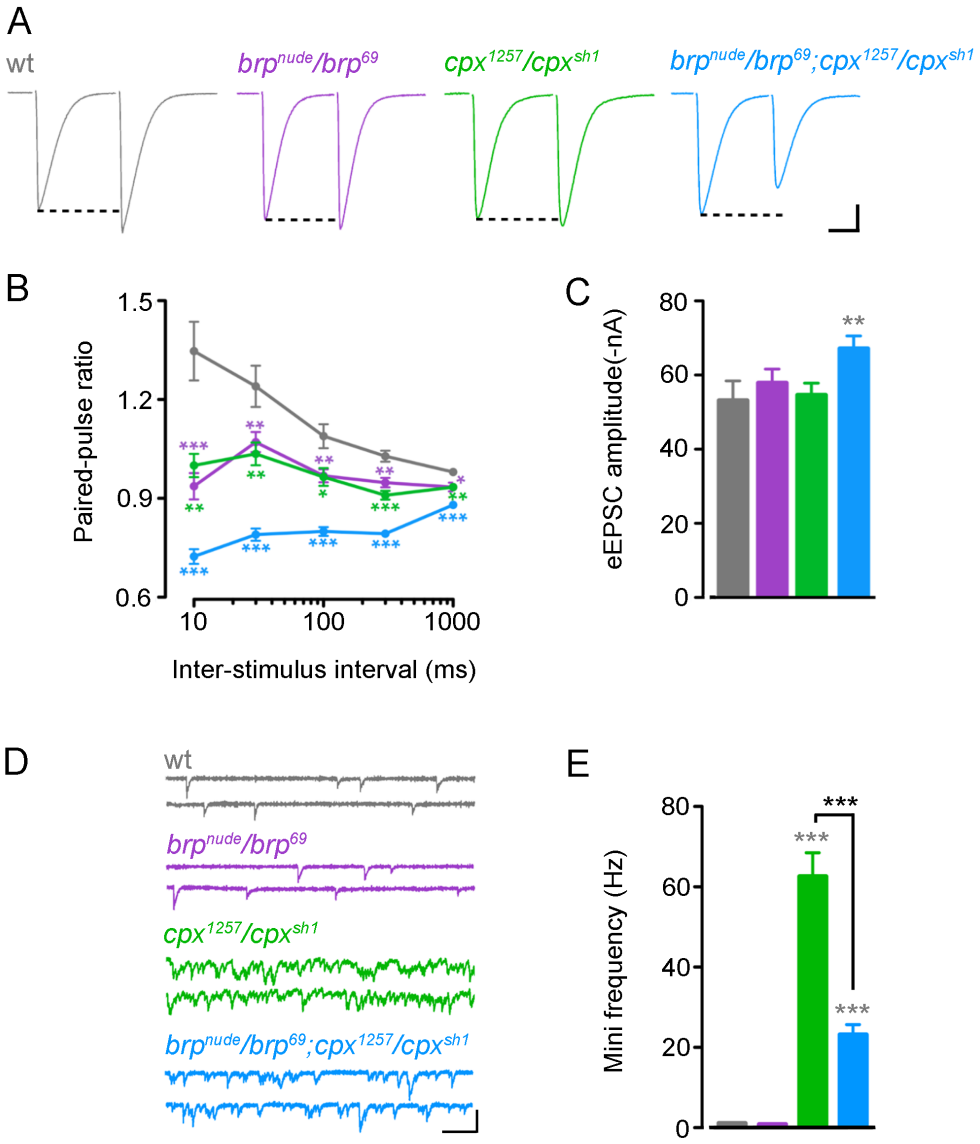

Figure 23. **CPX and BRP interact to tether SVs to AZs**. A, B) Representative traces (A) and quantification of two-electrode voltage clamp recordings (B) from larval NMJs. *brp*^{nude} and *cpx*^{sh1} animals show similar synaptic short-term depression. Double mutants exhibit more pronounced synaptic short-term depression compared to single mutants. C) The average eEPSC amplitude was significantly increased in *brp*^{nude}*; cpx*^{1257} double mutants. D, E) Example traces of minis (D) and quantification of mini frequencies (E) showed marked increase in *cpx*^{sh1} and *brp*^{nude}*; cpx*^{1257}. Note double mutants exhibit a milder defect compared to *cpx*^{1257} single mutants. Scale bar (**a**) 100 nm, (**c**) 10 nA, 10 ms, (**e**) 2 nA, 100 ms. Data are presented as mean ± S.E.M. * $P \leq 0.05$, ** $P \leq 0.01$, *** $P \leq 0.001$.

Collectively, the findings cannot be explained by simple additivity of the defects. Instead, the data suggests an involvement of CPX in several processes, which shape the physiology of the synapse. This interpretation is consistent with previous work, which highlights the functional significance of CPX in different modes of synaptic transmission (Martin et al., 2011; Jorquera et al., 2012; Buhl et al., 2013).

6. Discussion

In accord with previous work this study demonstrates that the last C-terminal 17 aa of BRP recognize and bind to an heretofore unknown molecular factor, which promotes SV tethering and thereby prevents short-term depression at synapses of *Drosophila* larvae.
This work provides several lines of evidence to support that CPX constitutes such a binding partner of BRP in order to fulfil this task.
First, depletion of *cpx* abolished SV tethering to the C-terminus of BRP outside of AZs in motoneurons. Similarly, ectopic BRP was no longer recognized by SVs that lacked CPX.
Second, several independent genetic experiments suggested a function for BRP and CPX in a common signaling cascade.
Third, morphological analysis revealed that brp^{nude} and cpx^{1257} single as well as double mutant synapses harbored reduced numbers of tethered SVs.
Fourth, the lack in SV tethering of cpx^{1257} synapses is, similar to brp^{nude}, accompanied by pronounced synaptic short-term depression.

6.1. Accumulation of BRP bait variants

Motoneuronally expressed $BRP^{C\text{-}medium}$ and $BRP^{C\text{-}long}$ formed clusters in the VNC and at the NMJ of *Drosophila* larvae (Fig. 15). This is consistent with previous data, which showed that N-terminally tagged BRP forms clusters in larval motoneurons and brains when panneuronally expressed (Wagh et al., 2006). However, expression of a N-terminally truncated version of BRP (BRPΔ1-267) localized frequently to the AZ membrane, although in small electron-dense aggregates rather than T-bars, but was not reported to form membrane-detached clusters (Fouquet et al., 2009). The same study provided evidence for a physical interaction of BRP's N-terminus with Ca^{2+} channels (Fouquet et al., 2009). Thus, this portion appears to be required for the association of BRP with the AZ membrane and its loss may result in altered AZ nucleation.

Alternatively, the observed agglomeration of BRP may be mediated through its C-terminus. This portion of BRP is rich in CC structures, α-helical supersecondary structures, which mediate a number of processes including oligomerization and interaction between proteins (Parry et al., 2008). These CC regions promote oligomerization of BRP to form elongated, polarized filaments (Fouquet et al., 2009). Therefore, it appears reasonable to assume that overexpres-

sion of BRP protein disrupts this well regulated process due to a non-physiological overload of oligomerizing C-termini. Interestingly, a similar BRP clustering phenotype was found in *srpk79D* kinase mutants (Nieratschker et al., 2009; Johnson et al., 2009). SRPKs phosphorylate serine-arginine rich splicing factors (SR proteins; Giannakouros et al., 2011), which are involved in constitutive and alternative splicing (Zahler et al., 1992). Although BRP co-localizes with a particular SRPK isoform it lacks serine-arginine rich regions and therefore constitutes unlikely a substrate (Nieratschker et al., 2009). Furthermore, BRP expression levels are unaltered in *srpk79D* mutants (Nieratschker et al., 2009; Johnson et al., 2009). Thus, an additional yet unknown factor may be present in a specific stoichiometric ratio to prevent BRP agglomeration within the axon. The fact that the removal of the C-terminal end of BRP impairs T-bar formation, even though it locates to presynaptic sites (Fouquet et al., 2009), supports this hypothesis.

BRP is considered to perform dual functions at *Drosophila* synapses, which in vertebrates are separately conducted by two AZ components, CAST/ELKS and Piccolo/BASSOON (BSN). Functionally, the N-terminus of BRP corresponds to CAST/ELKS, and its C-terminus is similar to BSN/piccolo. Accordingly, the CC domains of BRP and BSN/piccolo were proposed to convey interactions with cytoskeletal factors (Wagh et al., 2006).
Sequence analysis of BRP uncovered a large number of glutamines in the last C-terminal 294 aa of BRP, hence present in $BRP^{C\text{-}medium}$ and $BRP^{C\text{-}long}$ (Suppl. Fig 2). The C-terminal stretch of BSN (but not piccolo) contains a conspicuous number of glutamine residues as well (Winter et al., 1999). PolyQ motifs are known to induce protein aggregation in several neurodegenerative conditions (e.g. Alzheimer, Parkinson, Huntington; Dobson, 2001). Interestingly, polyQ-containing proteins commonly possess CC domains in close proximity to the polyQ domain. This appears also be the case in BRP (Suppl. Fig 2). In fact, it has been proposed that stable CC formation acts to inhibit polyQ aggregation and thus determines the polyglutamine aggregation potential (Thakur et al., 2009; Fiumara et al., 2010; Wetzel, 2012; Kokona et al., 2014).
Hence, the formation of BRP molecules into functional T-bar structures may be regulated on several levels and may be not set by default.

6.2. A BRP peptide induces synaptic short-term depression and alters larval locomotion

Previous work revealed the requirement of the C-terminal end of BRP to tether SVs to the AZ (Hallermann et al., 2010b). Here, expression of this C-terminal portion (mBRP$^{C\text{-}tip}$) in glutamatergic motoneurons, phenocopied the behavior and electrophysiology of *brp^{nude}* larvae (Fig. 11A, B). Interestingly, distribution of mBRP$^{C\text{-}tip}$ in other neuron types was sufficient to alter larval locomotion as well (Fig. 12). This implies that BRP tethers SVs through a putative binding partner common across synapses of different neuron species. The present study identified CPX as a vesicular or cytoplasmic partner of BRP required for the interaction with SV. Interestingly, CPX mRNA expression, although distinctly distributed in certain cell populations, appears not to be confined to a particular neurotransmitter system (Freeman and Morton, 2004). For example, mammalian CPX-2 was reported to be selectively concentrated in axo-spinal and axo-dendritic glutamatergic terminals, whereas CPX-1 was predominantly localized in axo-somatic GABAergic terminals (Takahashi et al., 1995; Yamada et al., 1999). Furthermore, CPXIII and IV are enriched in glutamatergic ribbon synapses in the retina and inner ear (Reim et al., 2001; Glowatzki and Fuchs, 2002; Heidelberger et al., 2005; Reim, 2005). In *C. elegans*, CPX-1 has been reported to regulate SV release from cholinergic neurons (Fernandez and Dittman, 2009; Hobson et al., 2011; Martin et al., 2011).
Thus, mBRP$^{C\text{-}tip}$ may possess the capacity to recognize and block CPX to render SVs less capable to interact with BRP to become AZ tethered beyond glutamate releasing neurons.
This view is consistent with the finding that panneuronal expression of mBRP$^{C\text{-}tip}$ induces a less pronounced locomotion defect compared to animals with a more confined expression of mBRP$^{C\text{-}tip}$, i.e. the alteration of locomotor output may reflect mBRP$^{C\text{-}tip}$-mediated compound defects of excitatory and inhibitory synapses.

Interestingly, knock-down studies revealed the requirement of BRP for efficient synaptic transmission at histaminergic photoreceptor cells in the lamina (Wagh et al., 2006). Further, in mammals CAST/ELKS was demonstrated to support Ca^{2+} influx at nerve terminals of inhibitory neurons of the hippocampus (Liu et al., 2014). In line with these previous studies, *vgat-GAL4* specific expression of mBRP$^{C\text{-}tip}$ in inhibitory neurons reduced crawling distances significantly, which implies a function for BRP in these cells. However, this genetic configuration was suspected to induce phenotype that differed from mBRP$^{C\text{-}tip}$ expression in excitatory cells. Several factors may contribute to this result. First, *vgat-GAL4* activity may not be

exclusive to inhibitory neuron populations, which might result in compound effect of mBRP$^{C\text{-}tip}$ resembling the panneuronal expression situation. Indeed, *vgat*-promotor specific GFP expression was detected in motoneurons, known to release glutamate (data not shown). In mammals, the coexistence of vesicular transporters for both excitatory and inhibitory transmitters in the same synapse has been demonstrated (Gutiérrez and Heinemann, 2001; Walker et al., 2001; Zander et al., 2010). Alternatively, the driver strain used here may enhance UAS-transgene expression in an unspecific manner, as is often the case with promotor-GAL4 constructs. However, this study provides no direct evidence for this possibility.
Finally, proper locomotion requires a large number of cells, which exhibit complex and temporally precise activity pattern. Thus, efficient SV release from inhibitory neurons does not directly translate into enhanced motor activity. Therefore, the causal relationship of mBRP$^{C\text{-}tip}$ effect in inhibitory neurons on larval motility cannot be conclusively elucidated with this particular experiment.

6.3. Association of SVs with BRP bait variants

In contrast to BRP$^{C\text{-}long}$ and BRP$^{C\text{-}medium}$, membrane-attached BRP$^{C\text{-}tip}$ failed to tether SVs to ectopic neuronal sites (Fig. 17). Neuron-specific motor proteins translocate SVs intracellularly from the soma to their site of action – the synapse. As SVs pass through the axon they engage with BRP$^{C\text{-}long}$ and BRP$^{C\text{-}medium}$. However, BRP$^{C\text{-}long}$ appeared to recruit SVs more efficiently than BRP$^{C\text{-}medium}$. Organized arrays of microtubules reside in the neuronal cytoplasm and provide a railing system on which SVs are guided. The diameter of motor axons ranges from ~ 100 to 700 nm (Hurd and Saxton, 1996). Judged from the ultrastructure of motor axons microtubules are not located in the immediate membrane vicinity (Miller et al., 2005; Nieratschker et al., 2009).
BRP$^{C\text{-}long}$ and BRP$^{C\text{-}medium}$ extend differently far into the axoplasm (Fig. 14C). Merely the difference in size or the residues included in BRP$^{C\text{-}long}$ may explain the observed effect. At this point it is not clear whether the protein portions beside the last 17 aa simply act as spacer modules or if they enhance SV tethering in a residue-specific fashion. Investigation of the tethering capacity of BRP bait variants containing spacer sequences N-terminal to the last C-terminal 17 aa and the mere truncation of the last 17 aa would help to resolve this ambiguity.

Further, membrane-associated BRP$^{C\text{-}tip}$ was unable to tether SVs to axonal membranes. BRP$^{C\text{-}tip}$ reaches into the axoplasm no further than 6 nm and therefore may not extend into axoplasmatic regions occupied by microtubules and hence SVs (Fig. 14C).

However, cytoplasmatically expressed $BRP^{C\text{-}tip}$ ($mBRP^{C\text{-}tip}$) suppressed not only the interaction of SVs with native BRP, but also with $BRP^{C\text{-}long}$ (Fig. 17, 19B). Conclusively, $BRP^{C\text{-}tip}$ needs to be unleashed or from the membrane or deposited in closer vicinity to SVs to interact with CPX.

In sum, C-terminal portions of BRP are sufficient to attract and stably bind SVs to sites other than the AZ. Furthermore, cytoplasmatic distribution of $BRP^{C\text{-}tip}$ features in the recognition and interaction with CPX and putative other BRP interactors and constitutes a tool to re-route SVs within motoneurons.

6.4. Absence of CPX from SVs abolished association of SVs with $BRP^{C\text{-}long}$

Depletion of *cpx* in motoneurons abolished the association of SVs with $BRP^{C\text{-}long}$ (Fig. 19B). Furthermore, removal of *cpx* from SVs in cpx^{1257} mutants led to a similar deficit in SV tethering to $BRP^{C\text{-}long}$ bestowed axonal membranes (Fig. 19B). Together, this implies a novel function for CPX in SV tethering before SNARE complex-driven SV fusion occurs. Interestingly, CPX was initially identified as a cytoplasmic protein (McMahon et al., 1995). Recently, membrane coupling of CPX mediated through a C-terminal farnesylating CAAX motif was shown in various species including *Drosophila*, *C. elegans* and ribbon synapses of mammalian sensory neurons (Reim, 2005; Cho et al., 2010; Buhl et al., 2013; Iyer et al., 2013; Wragg et al., 2013).

Thus, CPXs may occur in soluble and membrane-attached configuration, similar to RAB proteins (Marshall, 1993; Zhang and Casey, 1996). Presynaptic specializations frequently occur at synapses that are capable to sustain high rates of SV release. They are believed to facilitate fast trafficking of SVs to their release sites (Hallermann et al., 2010a; Hallermann and Silver, 2013). Interestingly, most of these synapses express CAAX containing CPX's (Reim, 2005; Cho et al., 2010; Buhl et al., 2013; Iyer et al., 2013; Wragg et al., 2013). Thus, membrane-coupling of certain CPXs via CAAX-motifs seems particularly important at synapses characterized by presynaptic specializations (Reim, 2005; Cho et al., 2010; Buhl et al., 2013; Wragg et al., 2013).

6.5. SV detached CPX forms agglomerations distant from AZs

At the larval NMJ of *cpx*^{1257} mutants, the absence of CPX from SV membranes reduces CPX abundances and curtails its co-localization with the AZ component BRP (Suppl. Fig 3). This finding is in line with the expression profile of CPX in *cpx*^{572} mutants, which lack the C-terminal 25 residues (Buhl et al., 2013). One possibility is that SVs act as carriers to properly localize CPX, a scenario recently demonstrated for CPX-1 in *C. elegans* (Wragg et al., 2013). CPX binds the assembled SNARE complex, formed by SYB, SNAP-25 and SYX, in a 1:1 stoichiometry (Pabst, 2000; Pabst et al., 2002). As SYB constitutes a vesicular protein it is likely a cargo of SVs. However, how is CPX localized on SVs with respect to SYB? Maybe SVs are not simply couriers in this virtue, but deliver and position CPX in a specific spatial orientation to SYB, the SNARE complex and potentially other molecular factors to enable spontaneous SV release.

Furthermore, SV-detached CPX forms conspicuous clusters in the cytoplasm of motoneuron terminals, which did not co-localize with BRP (Suppl. Fig 3). Although the underlying mechanisms remain completely unresolved it seems conceivable that membrane association of CPX prevents unspecific intramolecular interactions. Interestingly, immunohistochemical analysis at DLM neuromuscular synapses of *cpx*^{1257} flies showed similar clustering of CPX, which in contrast coincided with AZs (Iyer et al., 2013). Morphological differences of these synapses and/or the developmental stage may account for the inconsistent localization pattern of CPX agglomerates.

6.6. CPX and BRP exert their functions in a common signaling cascade

CPX has frequently been shown to exert promoting and suppressing function on exocytosis (Huntwork and Littleton, 2007; Xue et al., 2007; 2009; Martin et al., 2011; Jorquera et al., 2012; Dhara et al., 2014). In this virtue it has been functionally associated with a number of proteins, foremost proteins of the SNARE complex and SYT (Jorquera et al., 2012; Cho et al., 2014). Here, the employment of independent genetic approaches revealed that CPX functions in a signaling pathway that includes BRP (Fig. 20, 21). However, classical epistasis experiments provided contradictory results in terms of sequence of events (Fig. 20). Considering that both larval locomotion and viability of the animal are shaped by complex neuronal circuits, which include tremendous amounts of cells, this was not surprising. Additionally, the functional contribution of BRP and CPX in different subsets of cells within these networks

may be diverse. Cell-specific cross rescue experiments have to be performed to provide more reliable information on the epistatic relationship of BRP and CPX.

Non-allelic non-complementation has been suggested to be quite general phenomenon among synaptic genes and is frequently considered to signify a direct physical interaction between the products of two gene loci (Yook et al., 2001). Non-allelic non-complementation was observed when either hypomorph was combined with null allele of the other locus (Fig. 21). By contrast, this effect was not observed when null alleles or hypomorphs were combined (Fig. 21). In the case for BRP and CPX the reduced complementation capacity followed the poison model, in which the alteration of either synaptic component was sufficient to sensitize the genetic background for the second mutation. This data is in agreement with a physical interaction between CPX and BRP.

However, non-allelic non-complementation is not limited to interacting proteins, but has been observed when two proteins are members of the same complex or act at distant positions within the same pathway (Fuller et al., 1989; Yook et al., 2001), thus the BRP-CPX interaction may be indirect.
Classical epistasis analysis is frequently employed to determine the sequence of action of certain genes within a regulatory hierarchy (Avery and Wasserman, 1992). Here, epistasis experiments provided inconclusive results in this virtue. As mentioned, cross rescue experiments may help to allocate sequence of events to the phenotypes observed. However, both BRP and CPX are known to mediate multiple functions at the presynapse. Hence, it appears highly likely that CPX mediates BRP-dependent and -independent functions.

Several experimental approaches are available to clarify the interaction status between BRP and CPX. Thus far, high-throughput biochemical approaches have proven unsuccessful for the identification of BRP binding partners, one of the reasons why this study used genetically encoded reporters in an optical screen. Nevertheless, co-immunoprecipitation assays or yeast-two hybrid-screen technology may help to confirm the direct physical contact between BRP and CPX. While biochemical evidence for direct BRP-CPX interaction would provide a useful platform to exactly map the respective interacting domains of CPX and BRP, absence of biochemical evidence may merely result from chemical reagents used during the procedure. Alternatively, protein-fragment complementation assays (e.g. split-GFP; Feinberg et al., 2008), bimolecular fluorescence complementation (BiFC; Hu et al., 2002), mass spectrometry

or fluorescence resonance energy transfer (FRET) could be useful to shed light on the relationship of BRP and CPX within the signaling pathway.

6.7. BRP and CPX prevent synaptic short-term depression

Functionally, loss of vesicular CPX residence specifically impairs spontaneous release, but left evoked release unchanged (Fig. 23C-E; Cho et al., 2010; Buhl et al., 2013; Iyer et al., 2013). The *in vivo* observations presented here matched those findings. In addition, these experiments uncovered that during paired pulse stimulation cpx^{1257} synapses showed synaptic short-term depression (Fig. 23A, B). Accordingly, both *cpx* null and cpx^{572} synapses exhibit similar defects in short-term plasticity (Jorquera et al., 2012; Buhl et al., 2013).
Collectively, these data indicate that CPX's C-terminus and potentially its membrane-associating function may be required for this particular release mode.
In principle, depression may be caused by both pre- and postsynaptic mechanisms (Heckmann and Dudel, 1997; Forsythe et al., 1998; Hosoi et al., 2009). However, previous work argues against a postsynaptic origin (Jorquera et al., 2012). Instead, based on foreknowledge of physiological properties of brp^{nude} synapses in combination with the mounting evidence of BRP-CPX interaction it was anticipated that synaptic depression resulted from presynaptic defect in SV recruitment/SV tethering.

On an ultrastructural level, cpx^{1257} synapses display a tethering deficit (Fig. 22), a morphological alteration that has been directly associated with impairment in continuous SV release (Hallermann et al., 2010b). The defect was less pronounced compared to brp^{nude} synapses and was not additive in brp^{nude}; cpx^{1257} double mutants (Fig. 22). Hence, BRP and CPX act in the same pathway to tether SVs to *Drosophila* T-bars. The difference in severity of tethering deficits implies that BRP interacts not only with CPX, but also with additional yet unknown molecules. Thus, BRP may constitute the bottleneck for the establishment of a SV pool at the AZ cytomatrix, an interpretation that goes hand-in-hand with its known function in SV tethering and establishment of the supply pool (Hallermann et al., 2010a; 2010b; Matkovic et al., 2013). Opposed to these findings, work on a *cpx* null allele reported no change in SV number at or around the T-bar at structural levels (Jorquera et al., 2012). At this point this discrepancy falls short of a detailed explanation, but may derive from differences in fixation procedure, in tissue thickness, orientation of sections, and/or muscles used for quantification.

To sustain a particular level of release the necessary amount of SVs reloaded relies on the dimension of the RRP (Hallermann and Silver, 2013). CPX is known to control the size of the RRP (Jorquera et al., 2012). In contrast, BRP mutant synapses contain a normally sized RRP, but tether less SVs (Hallermann et al., 2010a; 2010b). BRP was also reported to scale the number Ca^{2+}-coupled release slots per AZ (Hallermann et al., 2010a; 2010b; Matkovic et al., 2013). Heretofore, CPX was proposed to mediate molecular interactions necessary for the generation of SVs that are primed for release (Jorquera et al., 2012). An interesting study, carried out on hippocampal organic slice cultures, proposed that CPX is not required for docking and priming downstream of SV tethering (Imig et al., 2014). So how then, does CPX regulate the dimension of the supply pool? In light of the presented findings, it is conceivable that CPX mediates SV tethering to the AZ cytomatrix to establish a SV reservoir accessed during sustained SV release.

brp^{nude} synapses contain proper quantity of readily releasable SVs (Hallermann et al., 2010b). Synaptic short-term depression of *brp*^{nude} was accompanied by slowed first component of recovery, which reflected the synapses' inability to tether SVs (Hallermann et al., 2010b). To assess if the change in synaptic short-term plasticity found at *cpx*^{1257} synapses originates from the same defect, the kinetics of recovery of *cpx*^{1257} synapses from synaptic depression need to be analyzed.

In line with the multi-functionality of both BRP and CPX the double mutant situation appeared complex.

First, although evoked EPSC amplitudes were not affected in *brp*^{nude} nor *cpx*^{1257} animals, double mutants displayed a significant increase compared to control (Fig. 23C). Several presynaptic factors could contribute to this effect including enlarged Ca^{2+} channel clusters, increase in AZ number and size or change in the dimension of the RRP as putative compensatory consequences. The synthetic enhancement of short-term depression in *cpx*^{1257}*;brp*^{nude} double mutants (Fig. 23A, B) is most likely linked to the increase in eEPSC amplitudes. However, the enhancement in depression could be caused by several putative auxiliary and/or complementary mechanisms. For example, the BRP-CPX interaction may not only play a role in tethering, but also in active translocation of SVs to their release sites (Hallermann and Silver, 2013). The electron-dense matrix at ribbon synapses has been reported as a transport structure that delivers SVs to AZs (Lenzi and Gersdorff, 2001) and appeared to have also the capacity to restrain SV delivery (Jackman et al., 2009). Alternatively, interaction of CPX with BRP may alter its affinity to the SNARE complex, possibly through additional molecular fac-

tors [e.g. SYT (Jorquera et al., 2012; Paul et al., 2015)], which may directly determine exocytotic activity. In principle, BRP and CPX may be part of a protein complex, which involves additional molecules of yet unknown identity. Interestingly, biological tethers have been demonstrated to possess the capacity to support sustained release by binding to Ca^{2+} channels, thereby suppressing their inactivation (Kiyonaka et al., 2007). Thus, further data has to be obtained in order to gain more insights into mechanisms that shape synapse physiology during continuous neuronal activity.

Loss of CPX has a devastating impact on spontaneous release (Huntwork and Littleton, 2007). Compared to cpx^{1257}, brp^{nude} ; cpx^{1257} double mutants displayed considerable attenuation in their mini frequency (Fig. 23D, E). BRP's impact on evoked transmission has been demonstrated numerous times (Wagh et al., 2006; Kittel et al., 2006b; Peled et al., 2014). However, its role in spontaneous release is more controversial. A recent study reported that BRP functions to suppress spontaneous release and that diminished tethering capacity of BRP influences this release mode (Peled et al., 2014). Also, animals that express solely the short 170 kDa isoform of BRP release quanta more frequently compared to controls (Matkovic et al., 2013). These findings object work on *brp* and brp^{nude}, which shows that activity-independent release is largely unaltered in these mutants (Kittel et al., 2006b; Hallermann et al., 2010b), which is also demonstrated in the present study. The here presented data signifies BRP's role, and may it be indirect, in stimulus-independent SV release. Mechanistically, it is conceivable that insufficient tethering affects SV supply restricting the amounts of spontaneously released SVs in CPX mutants.
Further, this implies that different release modes draw their replenishment from a common SV source. Conventionally, evoked transmission is generated by the same quanta as spontaneous activity (del Castillo and Katz, 1954). Consistently, CPX acts as an enhancer of evoked release and inhibitor of spontaneous release, which would support the transmission-mode independent single-pool model. However, release of SVs drawn from distinct, transmission mode-dependent pools was proposed (Sara et al., 2005; Fredj and Burrone, 2009; Ramirez et al., 2012). A number of reports argue against this model (Groemer and Klingauf, 2007), leaving the question unresolved.

In conclusion, this work highlights the biological significance of CPX-BRP interaction-dependent establishment of a nanodomain-coupled SV pool, which can be rapidly recruited during synaptic activity. Furthermore, this molecular interaction may constitute an initial

priming event that facilitates continuous release by delivery of “fusion-ready” SVs to release sites. Thus, this work yields insights into the molecular nature of SV tethering at *Drosophila* AZs and provides a solid basis to further decipher its physiological relevance.

Part II

The Adhesion-GPCR Latrophilin/CIRL shapes mechanosensation

7. Introduction

7.1. Adhesion-class G-proteine coupled receptors

G-protein coupled receptors (GPCRs) constitute the largest and most diverse family of membrane receptors. Present on every eukaryotic cell GPCRs act as biological converters transmitting signals across the cell membrane, channeling information into signaling pathways thereby ultimately shaping cellular responses. Each GPCR can selectively be activated by specific ligand(s). However, considering the entire GPCR superfamily a wide spectrum of ligands including light sensitive-compounds, pheromones, hormones, calcium, odorants and neurotransmitters possess the capacity to trigger receptor activation (Bockaert and Pin, 1999). Therefore, GPCR are responsible for proper conduction of a multitude of physiological processes. Accordingly, mutations that occur within these receptors are associated with a broad spectrum of diseases providing one of the most fruitful sources for the pharmaceutical industry. Interestingly, GPCR are targets of almost one third of the drugs at the current pharmaceutical market (Zalewska et al., 2014).

GPCR contain seven hydrophobic transmembrane domains (7TM) and are therefore alternatively referred to as seven transmembrane receptors. Based on structural similarities of the 7TM regions GPCR can be grouped into five classes (GRAFS classification): Glutamate, Rhodopsin, Adhesion, Frizzled/Taste 2, and Secretin (Fig. 24A; Fredriksson et al., 2003; Lagerström and Schiöth, 2008). While long-lasting scientific focus on GPCR function lead to comprehensive pharmacological and physiological knowledge, the structurally unique aGPCR class, which contains more than 30 mammalian homologs and thus represents the second largest GPCR group, remains enigmatic on many levels.
However, evident from a broad spectrum of human conditions linked to mutations in aGPCR genes [e.g. Usher syndrome (Weston et al., 2004; Reiners, 2005), bilateral frontoparietal polymicrogyria (BFPP; Piao et al., 2004)] and their association with many forms of cancer (Aust, 2010; Lum et al., 2010; Yang and Xu, 2012), they occupy vulnerable positions in most if not all organ systems. Nonetheless, little is known about both signal input and output of aGPCR rendering their functions and signaling principles elusive.

The structural properties of aGPCR are comparatively well known. aGPCR share basic structural features with canonical GPCR including an extracellular domain (ECD), the seven

transmembrane helix domain (7TM) and an intracellular domain (ICD; Fig. 24A). However, unique structural features set aGPCR apart from other GPCR classes: First, the ECDs of many aGPCR are extraordinary in size and complexity and facilitate cell-cell and cell-matrix interactions (Fig. 24A, B; Hamann et al., 1996; Paavola et al., 2014). Second, aGPCR contain a highly conserved GPCR-proteolytic site (GPS) that is part of the much larger autoproteolysis inducing (GAIN) domain (Fig. 24B, C; Araç et al., 2012).

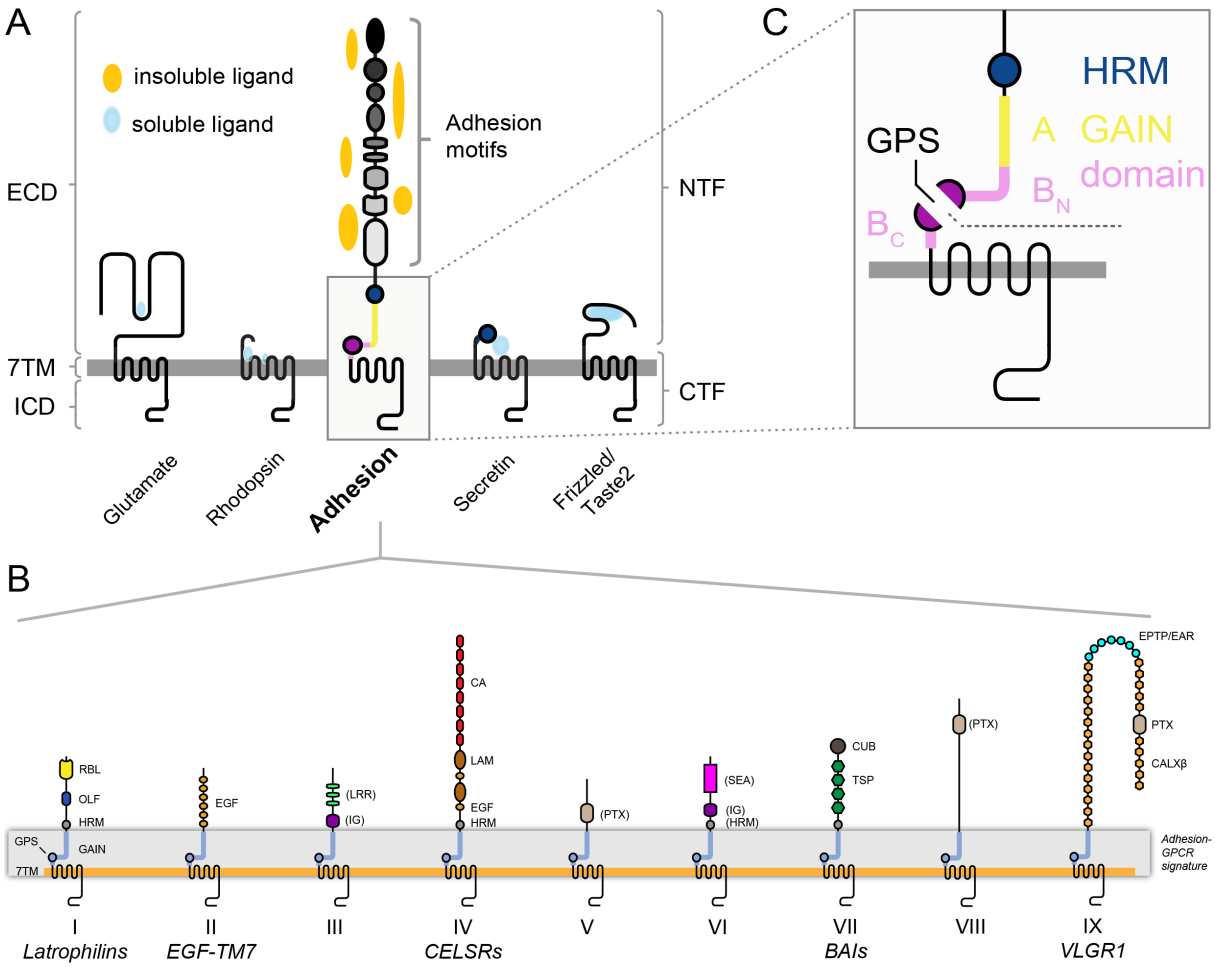

Figure 24. The Adhesion-GPCR class comprises structurally unique 7TM receptors. A, B) aGPCR class belongs to the GPCR superfamily. aGPCR can be set apart from other GPCR classes (Glutamate, Rhodopsin, Secretin and Frizzled/Taste 2) based on the presence of the GAIN domain (except for GPR123) and their remarkably long N-terminal regions. ECD, 7TM and ICD describe receptor topology based on protein compartmentation, while NTF and CTF describe cleavage-based compartmentation. Confirmed ligand interaction sites are indicated in yellow. Based on their extracellular folds and 7TM sequences aGPCR family can be further subdivided into nine distinct subfamilies (I-IX), all of which contain the GAIN domain. Also, the 7TM domains of different receptor families display sequence similarities, while the combinatorial NTF repertoire allows for structural and potentially functional diversity. Family I and IV include highly evolutionarily conserved receptors, which are found also in invertebrates, while all other receptor families are exclusive to vertebrates. A) Adapted from Prömel et al., 2012; B) from Langenhan et al., 2013. C) Structural blueprint of the aGPCR GAIN domain. The structurally complex GAIN domain mediates autoproteolysis and subsequently the re-attachment of the polypeptide chains (NTF and CTF) at the membrane surface. The GAIN domain can be divided in subdomains A and B, with B being cleaved at the GPS site resulting in N-terminal fragment containing the majority of the GAIN domain plus N-terminal part of the GPS site (A and B_N), while the CTF accommodates the other C-terminal half (B_C).

During protein maturation the GAIN domain mediates self-cleavage that results in the generation of a N-terminal and C-terminal fragment (NTF and CTF, respectively; Krasnoperov et al., 1997). Subsequently, NTF and CTF re-union through non-covalent binding by the GAIN domain generates natural receptor chimeras at the plasma membrane (Araç et al., 2012). Interestingly, the GAIN domain is recurrent in only one other molecule type, the polycystic kidney disease protein PKD-1 and its homologs (Ponting et al., 1999). While sufficiency and requirement of the GAIN domain for receptor autoproteolysis in post-translational processing has been demonstrated (Araç et al., 2012), the functional role for this process remains controversial.

Receptor cleavage at the GPS was shown to be required for membrane targeting of some but not all aGPCR. For example, cleavage-deficient Latrophilin and GPR56 show impaired receptor trafficking beyond the endoplasmic reticulum, the site where GPS cleavage occurs (Krasnoperov, 2002; Jin et al., 2007). In contrast, LAT-1 from *C. elegans* does not depend on cleavage for proper membrane localization (Prömel et al., 2012). Similarly, defective proteolysis of EMR2 at the GPS does not affect receptor trafficking (Chang et al., 2003; Lin et al., 2004). This indicates that autoproteolysis is not generally required for proper membrane trafficking of aGPCR (Langenhan et al., 2013).

The capacity of autoproteolytic cleavage of aGPCR at the GAIN/GPS domain raised an intriguing model in which NTF and CTF are available for re-association through hydrophobic interactions at the GAIN domain portions of the split fragments (Krasnoperov et al., 1997; Qian et al., 2002). In line with this notion is the "split personality" model proposed by Volynski and co-workers (Volynski et al., 2004). Their data suggests that the NTF and CTF, which result from GPS cleavage of Latrophilin 1 behave independent from each other. The dynamic re-association of aGPCR fragments at the cell surface may induce receptor signaling and thus may play pivotal role in aGPCR physiology (Volynski et al., 2004). The heterodimerization observed for EMR2 and the cross-complex formation of chimeric receptors (e.g. Latrophilin with GPR56 or EMR2) favors this model (Silva et al., 2009; Huang et al., 2012). To the contrary, functional analysis of cleavage-deficient LAT-1 and LAT-2 homologs from *C. elegans* revealed no functional loss- or gain-of-function phenotype (Prömel et al., 2012), which argues against the split personality model. Accordingly, structural analysis of the GAIN domain revealed that the cleavage site is interred within a rigid domain structure. This layout suggests that the split fragments cannot disengage and re-associate unless the protein is heavily denatured (Silva and Ushkaryov, 2010).

Further experimental data is necessary to test the "split receptor" hypothesis to conclusively elucidate the potential physiological role of heterogeneric aGPCR hybrids.

7.2. Latrophilin/*dCirl* a prototypic Adhesion-GPCR member

Evolutionarily very old and very young receptors co-exist in the Adhesion-class of GPCR. The sequence conservation of the 7TM domains of lectin-like latrophilins (LPHN; family I) - also known as lectomdin, CL or CIRL - and CELSRs (family IV, Flamingo/Starry night) suggest that they are the oldest receptor families among the entire aGPCR class. They appear conserved over a large phylogenetic distance ranging from invertebrates to humans (Nordström et al., 2009). Consequently, these receptors are considered prototype aGPCR and thus provide ideal targets to study aGPCR biology. The mammalian genome encodes three LPHN homologs (*LPHN1-3*), whereas *C. elegans* and *Drosophila* genomes encode only two (*lat-1, lat-2*) and one (*dCirl*) homolog, respectively (Fig. 25A).

This study focused on a detailed functional characterization of prototypic Latrophilin from *Drosophila* (*dCirl*) to gain insights into the specific function of *dCirl* and general signaling principles of aGPCR.

7.3. Structural features of Latrophilin

As characteristic for aGPCR Latrophilin consists of three major regions. The N-terminal region, which faces the extracellular space and comprises a variety of structural domains including a rhamnose binding lectin (RBL)-like domain (RBL), a hormone binding domain (HRM) and an olfactomedin-like domain (OLF; Fig. 25A). A heptahelical transmembrane region and an intracellular C-terminal region follow this multidomain stretch. The hallmark feature of aGPCR - the GAIN domain with the GPS motif (Fig. 24C, 25A, B; Bjarnadóttir et al., 2004; Araç et al., 2012) - mediates autoproteolytic cleavage of a precursor polypeptide resulting in 85 kDa (p85) and 120 kDa (p120) fragments, that correspond to the NTF and CTF, of Latrophilin, respectively (Krasnoperov et al., 1997).

RBL domain

The RBL domain was first described from sea urchin eggs (SUEL) in which it appeared as a cross-linked homodimer of small cysteine-rich subunits (Ozeki et al., 1991). The RBL domain structure of mouse Latrophilin-1 uncovered a unique α/β fold with two long structured loops that are essential for rhamnose binding (Vakonakis et al., 2008). Additionally, a RBL domain

was identified in PKD-1 (Li et al., 2003) and the Slit receptor EVA-1 (Fujisawa et al., 2007). The RBL domain preferably binds to rhamnose, a monosaccharide barely found in animals (Tymiak et al., 1993). In addition, amino acid sequence analysis of Latrophilin showed that the residues important for carbohydrate binding are substituted, leading to the hypothesis that RBL domains recognize non-carbohydrate ligands (Vakonakis et al., 2008). In accord with this assumption, *C. elegans* LAT-1 displayed no carbohydrate activity and RBL-deficient receptor variants were not sufficient to restore wild-type receptor function. Thus, the presence of the RBL domain is required for proper LAT-1 function (Prömel et al., 2012).

OLF domain

C-terminal to the RBL domain vertebrate Latrophilins possess an olfactomedin domain (Snyder et al., 1991), absent in invertebrate receptors (Fig. 25A). Less than a dozen olfactomedin-domain containing proteins have been identified in mammals. Some of them were characterized as secreted glycoproteins and others as membrane bound receptors (Tomarev and Nakaya, 2009). Detailed knowledge about their biological function remains scarce, although they have been associated with an array of processes such as cell-cell interaction, neurogenesis, cell cycle regulation, dorso-ventral patterning, tumorigenesis and they may take part in modulating certain signaling pathways (Tomarev and Nakaya, 2009; Boucard et al., 2012).

HRM domain

The N-terminal region includes a HRM domain that precedes a conserved "stalk" region (Fig. 25A) and represents the most frequently observed non-obligatory (= non GAIN or 7TM) domain within the aGPCR class (present in 12 out of 33 mammalian receptors). The HRM domain of FMI, the only other aGPCR expressed in *Drosophila*, was proposed to act as a putative secondary ligand binding site (Shima et al., 2004; Kimura et al., 2006). However, no hormones have been identified as ligands thus far and several lines of evidence support the dispensability of the HRM for receptor function. For example, molecular modeling data suggest that the HRM domain of GPCR are incapable of peptide hormone binding due to the lack of the ligand binding helix (Grace et al., 2004; Parthier et al., 2007). Accordingly, the HRM domain of LAT-1 was shown to be dispensable for receptor activation and no essential HRM domain mediated ligand-binding activity was reported (Prömel et al., 2012).

Structural data on LPHN-1 suggests that hormone binding presupposes a conformational change in LPHN-1 to expose the putative hormone binding site that is otherwise occupied by

the GAIN fold (Araç et al., 2012). This scenario does not exclude hormones as putative ligands, but rather suggests their requirement in an alternative receptor activating mechanism.

GAIN domain

The juxtamembrane region of the NTF is occupied by the highly conserved GAIN domain that holds the GPS at its C-terminal end (Fig. 24C, 25A, B; Araç et al., 2012). So far, the most striking feature of the GAIN domain/GPS motif is its capacity to promote self-cleavage of aGPCR and PKD-1 like proteins resulting in a two-subunit structure, non-covalently affixed at the cell surface. During this process the GAIN domain becomes unequally prorated between the NTF and CTF (Fig. 24C; Krasnoperov et al., 1997). The portion of the GAIN domain N-terminal to the GPS belongs to the NTF, whereas the C-terminal part pertains to the CTF. Mammalian Latrophilin-1 was one of the first aGPCR for which cleavage has been recognized. First, sequencing was used to pinpoint the cleavage site (Krasnoperov et al., 1997), which is embedded within a 40 amino acid stretch referred to as GPS motif (Krasnoperov et al., 1999). Recently, a sophisticated study provided the crystal structure of cleaved Latrophilin-1 and uncleaved BAI3 that allowed a more detailed view on the structure of this peculiar domain (Araç et al., 2012). The GAIN domain includes the GPS motif and is comprised of two subdomains (A and B; Fig. 25C) that extend across ~ 320 residues in mammalian aGPCR (Fig. 25C). The GPS motif resides within the C-terminal five β-strands of subdomain B and is surrounded by additional β strands, which administer association with six subdomain A-forming α-helices (Fig. 25B). Note that although the GPS motif is necessary for autoproteolysis (Chang et al., 2003), only the entire GAIN domain constitutes the structural entity sufficient for self-cleavage (Araç et al., 2012).

Removal of the NTF due to autoproteolytic cleavage at the GPS results in increased receptor activity, which led to the idea that the NTF accommodates an inverse agonist (Okajima et al., 2010; Paavola et al., 2011; Yang et al., 2011; Langenhan et al., 2013). Indeed, a short amino acid sequence within the N-terminal portion of the extracellular CTF - previously described as the linker sequence between NTF and the 7TM domain - was shown to act as a tethered agonist for aGPCR (Liebscher et al., 2014; Stoveken et al., 2015). Liebscher and co-workers propose that binding of an extracellular ligand or mechanical challenge triggers conformational changes of the N-terminus, resulting in the exposure of the "Stachel" peptide and binding to the 7TM, which subsequently triggers G-protein activation (Liebscher et al., 2014). Ligand-ECD interaction based dissociation or displacement represents an alternative mechanism to

relieve the tethered agonist from its GAIN domain envelope to induce metabotropic signaling (Stoveken et al., 2015). So far, tethered agonists have been reported for human GPR126, GPR133, GPR56 and GPR110 (Liebscher et al., 2014; Stoveken et al., 2015). However this activating mechanism may apply to other aGPCR members as well.

7TM region

The 7TM regions of aGPCR display a low percentage of conservation rendering the identification of extracellular ligand binding sites difficult. In contrast, structural diversity amongst 7TM domains potentially promotes interactions with various types of molecules (e.g. heterotrimeric G proteins, non-heterotrimeric G-proteins and transmembrane protein partners; Langenhan et al., 2013).

Intracellular C-terminal region

Finally, the intracellular C-terminus of Latrophilin/*dCirl* is unusually large and contains proline clusters. This proline signature seems to be confined to Latrophilin and proline rich proteins such as extensin and collagen (Krasnoperov et al., 1997). Among LPHNs the ICD is the least conserved domain (Silva and Ushkaryov, 2010), which might reflect the diverse functional requirement of Latrophilin in different biological contexts.

The structural layout of Latrophilin indicates an "outside-in" signaling mechanism (Langenhan et al., 2009) through interaction of the NTF with the 7TM region, which subsequently triggers proper response of the cell through an intracellular signaling cascade. Structure-function analysis of LAT-1 from *C. elegans* support this notion (Langenhan et al., 2009; Prömel et al., 2012). However, 7TM-independent LAT-1 activity was demonstrated as well (Prömel et al., 2012). This might indicate an additional "reverse signaling" mode/function similar to Notch-Delta (Bray, 2006). In this model the ECD serves as a ligand for a reciprocal receptor on an adjacent cell and thereby relays the signal in a non-cell-autonomous manner. The aGPCR FMI-1 (Flamingo/CELSR homolog), for example, employs this signaling mode to navigate axons in *C. elegans*. FMI-1 is expressed in both pioneer- and follower axons. Loss of *fmi-1* affects guidance in both axon classes. Remarkably, these guidance defects in follower axons can be rescued through re-expression of NTF-lacking FMI-1 variants. This indicates that the NTF of FMI-1 is required for the navigation of follower axons (Steimel et al., 2010).

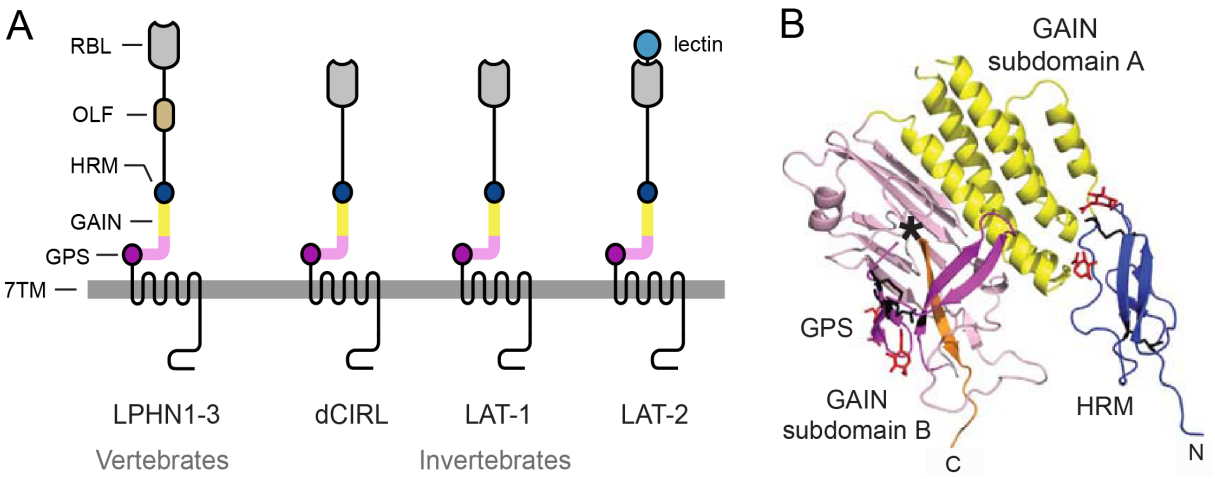

Figure 25. Structural layout of Latrophilin. A) Protein layout of Latrophilin: mammalian LPHN1-3, *C. elegans* LAT-1 and LAT-2, and *Drosophila* dCIRL. Domains N → C: RBL (rhamnose-binding lectin, grey), OLF (olfactomedin, brown), HRM (hormone-binding-motif, blue), GAIN (GPCR autoproteolysis inducing domain, yellow, pink), GPS (GPCR proteolysis site, dark pink), 7TM (seven-transmembrane domain). Adapted from Langenhan et al., 2009. B) Crystal structure of HRM and GAIN domain of LPHN1. The GPS motif comprises an integral part of the GAIN domain. The cleaved *β* strand is shown in orange. Disulfide bonds and carbohydrates are shown as red and black sticks, respectively. HRM blue, GAIN subdomain A: yellow, GAIN subdomain B: light pink, GPS motif: magenta (Araç et al., 2012).

7.4. Functional features of Latrophilin

Originally, mammalian LPHN1 was identified based on its ability to bind α-latrotoxin (α-LTX), a constituent of the venom cocktail secreted by the black widow spider (genus *Latrodectus*; Davletov et al., 1996; Krasnoperov et al., 1996). The Ca^{2+} independence of this interaction led to the alternative designation of LPHN - CIRL (Ca^{2+} independent receptor of latrotoxin; Krasnoperov et al., 1997).

At the NMJ, α-LTX elicits extensive exocytosis of SVs (Matteoli et al., 1988). In addition, release of large dense-core vesicles (LDCV) from sensory neurons and neuroendocrine cells has been reported (Barnett et al., 1996; De Potter et al., 1997; Lang et al., 1998). As a result of these findings Latrophilin was suggested to play regulatory role in synaptic transmission.

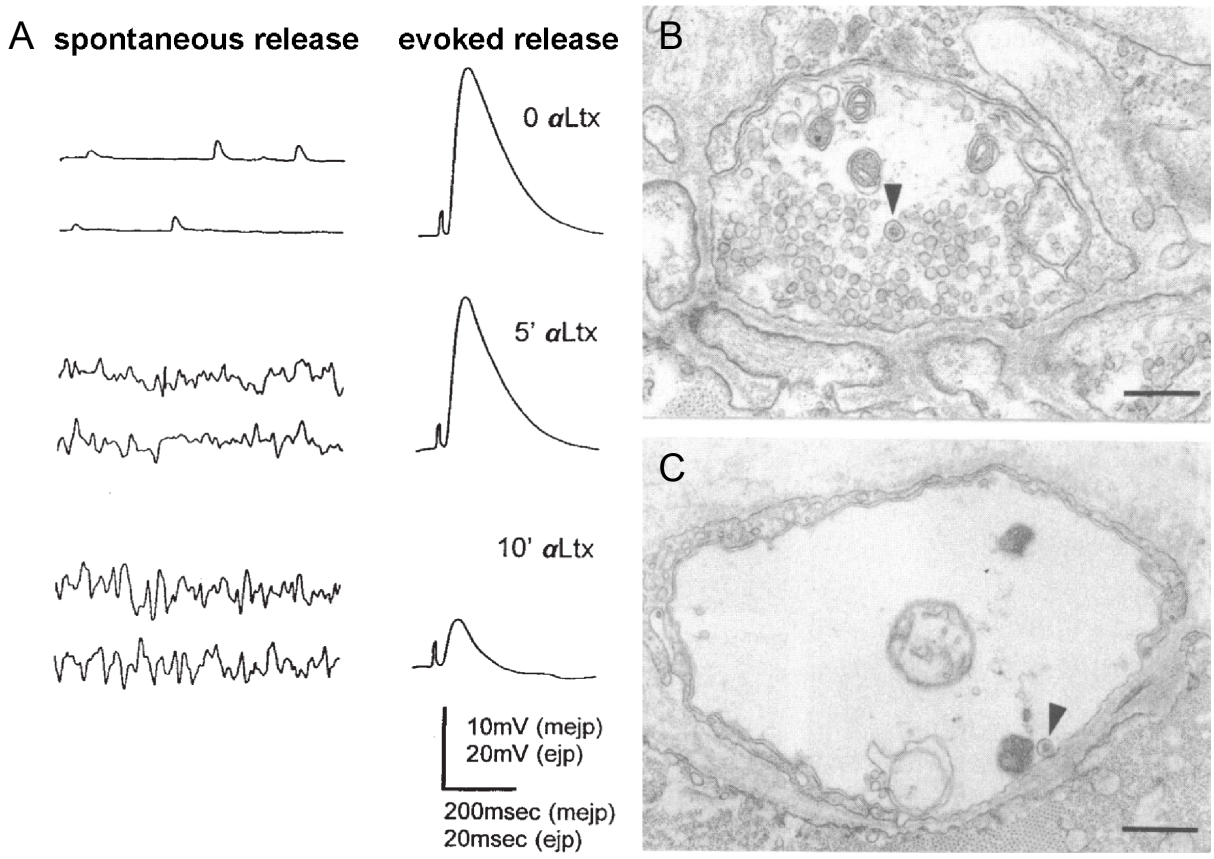

Figure 26. Effects of α-LTX. A) Electrophysiological recordings of miniature endplate potentials (minis) and AP evoked neurotransmitter release at the NMJ of muscle 6 of *Drosophila* larvae. Shown are the effects of 10 nM α-LTX on spontaneous and evoked release before application (upper panel), five (middle panel) and ten min (lower panel) after application. Mini frequencies are elevated after five minutes (5' α-LTX), but no change in evoked response was observed. Ten minutes after α-LTX application the mini frequency further increased and the evoked transmitter release declined (evoked release is abolished after 20min; data not shown). Adapted from Umbach et al., 1998. B and C) Electron micrographs of cross-sectioned boutons from the frog NMJ. B) Without α-LTX incubation the bouton is densely populated with SVs. C) α-LTX treated terminals appear swollen and completely depleted of SVs, while LCDVs are still present (indicated by black arrow). Scale bar A) 340 µm; B) 529 µm (Matteoli et al., 1988).

In the absence of Ca^{2+} α-LTX exists in a dimeric/inactive form. Addition of Ca^{2+} or Mg^{2+} leads to tetramerization of α-LTX dimers forming a pore at its center. This "active" conformation enables α-LTX to insert into the lipid layer, thereby increasing its secretory activity (Orlova et al., 2000). Later on, recombinant wild-type and non-pore forming α-LTX variants have been utilized to study Latrophilins endogenous activity, which failed to provide concordant results (Ichtchenko et al., 1998; Capogna et al., 2003). An additional challenge arises from α-LTX's affinity to additional receptors: neurexin and receptor-like protein-tyrosine phosphatase σ (PTP; Ushkaryov et al., 1992; Krasnoperov et al., 2002). Thus, the broad ac-

tion spectrum of α-LTX renders it unfit for the interrogation of Latrophilins physiological significance.

Moreover, in *Mus musculus* and *Danio rerio* Latrophilin was shown to play pivotal role in neuronal development (Lange et al., 2012; O'Sullivan et al., 2014). Finally, in *C. elegans,* the Latrophilin homolog LAT-1 is a key player in the establishment of tissue polarity and fertility (Langenhan et al., 2009; Prömel et al., 2012).

7.5. Latrophilins in mammals, *C. elegans* and *Drosophila*

The mammalian Latrophilin subfamily comprises three homologs (LPHN1-3), which display similar domain structures and a high degree of overall sequence identity (Ichtchenko et al., 1999; Matsushita et al., 1999). All three isoforms are recognized by α-LTX but with highly different affinities varying between 0.1 nM for LPHN1 and 10-fold lower affinity in the micromolar range for LPHN2 (Petrenko et al., 1990; Ichtchenko et al., 1999). LPHN1 and LPHN3 expression is largely restricted to the central nervous system (CNS), while LPHN2 is rather ubiquitously distributed (Sugita et al., 1998; Ichtchenko et al., 1999; Matsushita et al., 1999). *Lphn1* knock-out models revealed that LPHN1 is not essential for neuron function nor the viability or fertility of the mouse, clearly suggesting redundancy of LPHNs (Tobaben et al., 2002). As for several other aGPCR, generation of cellular and subcellular localization profiles proved difficult and remains fragmentary for Latrophilins.

Recently, *LPHN3* has been associated with attention deficit hyper-activity disorder (ADHD) a common psychiatric disorder with supposed inheritable background. Evidently, polymorphisms occurring in the *LPHN3* locus constitute risk factors for the development of this disease (Arcos-Burgos et al., 2010; Domené et al., 2010). Accordingly, loss of *lphn3.1* function in zebrafish disturbs the development of dopaminergic system and results in hyperactive and/or impulsive motor phenotype that may be linked to ADHD (Arcos-Burgos et al., 2010; Lange et al., 2012).

O'Sullivan and co-workers suggested a mechanistic model in which LPHN3 interacts trans-synaptically with identified ligands of the fibronectin leucine-rich transmembrane protein class (FLRTs) during synapse maturation (O'Sullivan et al., 2012). This interaction is suggested to determine synaptic terminal density of cortical pyramidal neurons (O'Sullivan et al., 2014).

Another line of evidence indicates that vertebrate LPHN1 forms heterophilic trans-synaptic complexes with Lasso (a splice variant of teneurin-2) capable of inducing presynaptic Ca^{2+} responses (Silva et al., 2011). Further examination of this trans-synaptic pair revealed LPHN1's capacity to induce postsynaptic specializations, while Lasso was suggested to be involved in axonal path finding and axon-target interaction (Silva et al., 2011). This data suggests a dual role for LPHN1 in synaptic function and synaptogenesis.

The *C. elegans* genome encodes two latrophilin homologs, *lat-1* and *lat-2*. However, α-LTX-triggered exocytosis seems mediated exclusively through LAT-1 (Mee et al., 2004). Later on, independent work demonstrated that Latrophilin is essential for development of *C. elegans* (Langenhan et al., 2009). While heterozygous hermaphrodites appear phenotypically inconspicuous the majority of homozygous *lat-1* mutants failed to develop beyond the first larval stage. However, a small fraction of homozygous hermaphrodites escape the L1 arrest. The offspring produced from these worms display embryonic lethality and variable morphogenetic defects in L1 larvae and adult stages. During the early stages of development maternal *lat-1* contributes to correct blastomere positioning (ABala; Fig. 27). Later embryonic development additionally requires zygotic *lat-1* to provide robust anterior-posterior alignment of cell division planes, which is delayed but not abolished in *lat-1* deficient animals. This evidence strongly favors a LAT-1-dependent pathway, that would provide a parallel "route" to known polarity and morphogenesis signaling pathways (Langenhan et al., 2009). The Flamingo ortholog FMI-1 controls the navigation of certain developing neurons, but was not associated with tissue polarity (Steimel et al., 2010), in contrast to its dipteran homolog *Flamingo/Starry night* (Usui et al., 1999). In addition, LAT-1 also plays a role in sperm function, a deficit reflected in reduced fertility of these mutants (Prömel et al., 2012).

The structural nature of Latrophilin suggests that the ECD contains various adhesive domains providing a protein interaction interface that presumably mediates intercellular engagement with predetermined "contact points" of an adjacent cell potentially providing reverse signaling function, similar to delta-notch signaling (Bray, 2006). This reverse signaling capacity was already demonstrated for CELSR/Flamingo homologs (Shima et al., 2004; Carreira-Barbosa et al., 2009; Steimel et al., 2010).

In fact, rescue experiments using *C. elegans* fertility and development as read-out showed that the RBL domain is indeed necessary for LAT-1 function (Fig. 27G). This was confirmed by the result that expression of RBL-deficient LAT-1 fails to rescue either defect. In contrast, loss of GPS proteolysis and deletion of the HRM domain did not affect the functionality of

the receptor in this assay (Fig. 27G, H). Strikingly, however, is the finding that selective deletion of the GPS site and destruction of the structural integrity of this domain abolishes rescuing activity (Fig. 27 H), which indicates functional importance of this domain independent from autoproteolytic cleavage. Moreover, expression of 7TM- or ICD-deficient rescue constructs sufficiently compensated the fertility defect, but did not rescue the tissue polarity defect (Fig. 27 G). This data uncovered distinct functions of LAT-1 domains and unraveled 7TM-dependent and 7TM-independent components of the Latrophilin phenotype (Prömel et al., 2012).

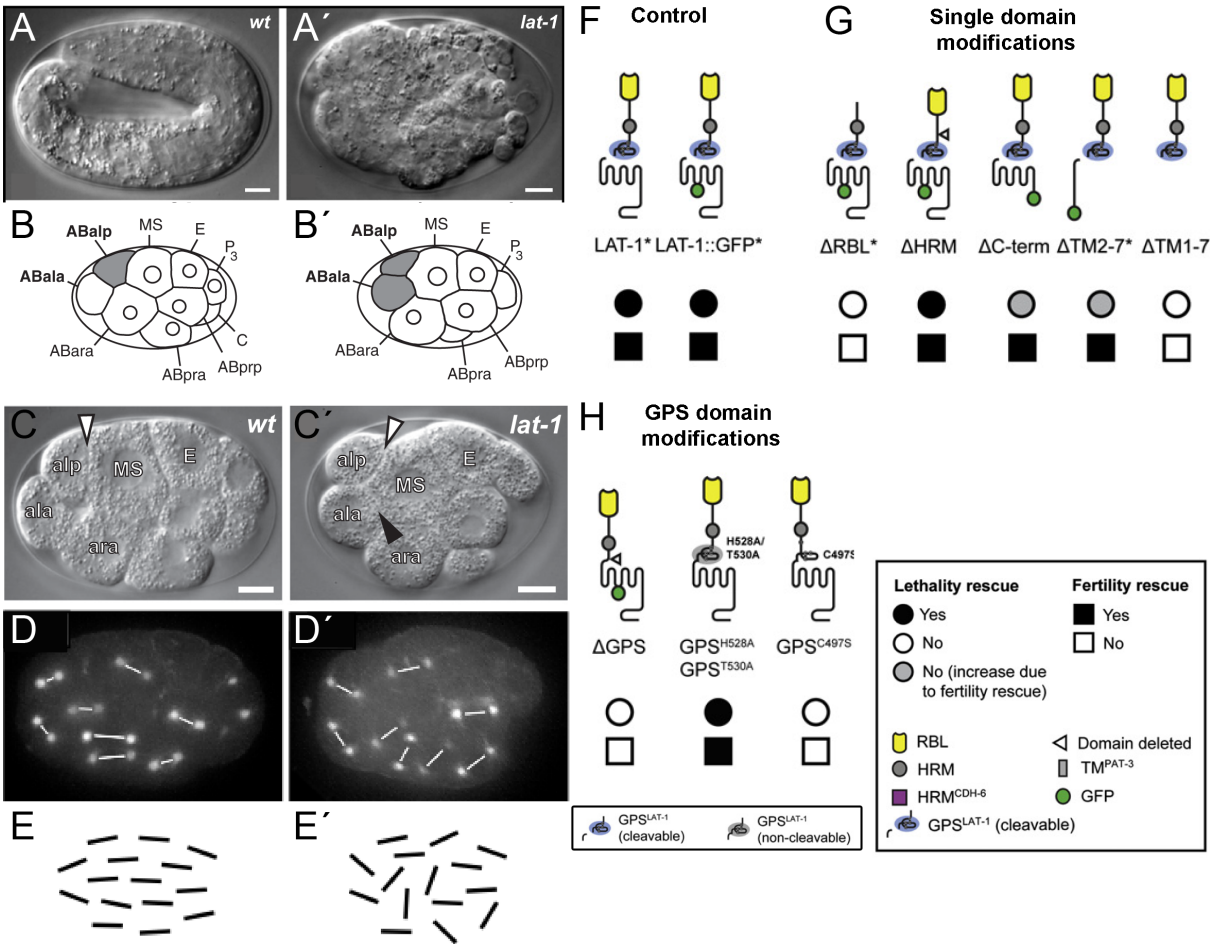

Figure 27. *In vivo* characterization of the *C. elegans* homolog LAT-1. A, A´) Wild-type and *lat-1* mutant embryos. A) Wild-type larva at Pretzel stage. A´) *lat-1* mutant lacking maternal and zygotic gene product. B-C´) Schematic and DIC microscopy of relative positions of blastomeres (ABala, ABalp, MS) from wild-type and *lat-1* embryos, respectively. The black arrow indicates membrane interface between ABala and MS. D, E) Fluorescence microscopy and illustration of a-p alignment of spindles in wild-type. D´, E´) Defective a-p alignment in *lat-1* embryos, which is delayed with respect to control (data not shown). Left: anterior, right: posterior, ventral: up: Scale bars 5 µm. F, G) Structural LAT-1 alterations possess varying capacities to rescue developmental and fertility phenotype of *lat-1* mutants. H) Truncation of the GPS motif abolishes rescuing activity. The same is true for introduction of missense mutation (C497S), which abrogates structural integrity of GPS. Note that GPS structure independent mutations do fully rescue both phenotypes. A-E adapted from Langenhan et al., 2009. F-H adapted from Prömel et al., 2012.

As in *C. elegans*, Latrophilin and Flamingo are the sole aGPCR representatives in *Drosophila*. FMI has been studied in intricate detail and has been shown to function instructively to mediate a Frizzled-VanGogh intercellular relay by recruiting these proteins to opposite cell boundaries. This establishes a molecular asymmetry that translates into planar cell polarity (PCP). Thus, in invertebrates at least one of the two aGPCR is essential for planar cell polarity (Usui et al., 1999; Langenhan et al., 2009).
As described above latrophilin orthologs from different species have been suggested to take part in various yet seemingly unrelated biological contexts such as synaptic activity, fertility and development. However, the physiological role for the latrophilin homolog in *Drosophila* - *dCirl* - has not been studied so far.

7.6. The onerous search for endogenous ligands of Latrophilin

Despite many efforts only a little more than a dozen aGPCR ligands have been identified so far. Note that the few ligands known correspond to nine aGPCR receptors from only four families (Langenhan et al., 2013; Paavola et al., 2014; Petersen et al., 2015). As a result, the vast majority of aGPCR remain orphans.

In 2011 a biochemical approach enabled the identification of a LPHN ligand from rat brain extracts – termed Lasso (LHN1-associated synaptic surface organizer; Silva et al., 2011). Lasso is a splice variant of teneurin-2 a large cell surface glycoprotein that possesses an EGF-like-rich and globular domain at its C-terminus, which precedes a single transmembrane region (Levine et al., 1994; Tucker and Chiquet-Ehrismann, 2006).
LPHN1 was reported to associate with the C-terminal globular domain of Lasso at multiple positions, which corresponds to provide a high-affinity interaction across intercellular junctions. Interestingly, the authors report that LPHN1 is expressed presynaptically, while Lasso appears mostly located postsynaptically. In hippocampal neurons this interaction was shown to induce substantial elevation of presynaptic Ca^{2+} concentration, which could be interpreted as putative mechanism to modulate transmitter release (Silva et al., 2011). Shortly after, LPHN1 was proposed to form intercellular transsynaptic adhesion complexes with specific splice variants of neurexin-1β (Boucard et al., 2012). Neurexin takes part in forming transsynaptic complexes with postsynaptically located neuroligin (Dean and Dresbach, 2006), which has evolved to one of the best studied trans-synaptic pairs (Lise and El-Husseini, 2006; Südhof, 2008). In this context, LPNH1 was demonstrated to compete with neuroligin-1 for neurexin-1β binding, with the olfactomedin domain of LPNH1 as the contact point (Boucard

et al., 2012). Strikingly, the fact that neurexin and Latrophilins are targeted by α-LTX prompted the hypothesis that the LPNH1-neurexin complex acts as the actual substrate for α-LTX action. This hypothesis remains to be elucidated and therefore the physiological importance of this interaction is still unclear. However, independent of the identity of the postsynaptic heterophilic interaction partner of LPHN1 the obtained data provide a convincing setting for LPNH1s involvement in the formation of junctional contacts.
Further, several biochemical assays suggest that FLRT3 (fibronectin-leucin-rich repeat transmembrane 3) strongly interacts with LPHN3 in *trans* (O'Sullivan et al., 2012). FLRT isoforms are genetically encoded by *flrt1-3* genes and are very distinctly expressed in hippocampal and cortical neurons among several other non-neuronal tissues (Allen Mouse Brain Atlas, 2009). Each isoform comprises a single-pass transmembrane domain, a leucine-rich extracellular domain, and a juxtamembraneous fibronectin type 3 domain (Lacy et al., 1999). *In vitro* and *in vivo* analyses demonstrate that shRNA mediated knock-down of either *lpnh3* or *flrt3* results in reduced synapse density alongside a reduction of glutamate release from these synapses (O'Sullivan et al., 2012; 2014).

Taken together, mounting evidence suggests that Latrophilins engage in transsynaptic complex with different partners to form intercellular adhesion complexes. The secondary effect of these arrangements appears to have several structural and physiological facets requiring further clarification. This will aid in comprehending Latrophilin and, as importantly, basic aGPCR biology.
It is striking, however, that all known Latrophilin ligands are insoluble. This suggests Latrophilins need for a mechanically fixed partner to exert its function, a finding that is in line with Latrophilins ECD mediating cell-cell and/or cell-matrix interactions.

7.7. Mechanosensation

All organisms rely on their senses (vision, taste, smell, hearing, touch, nociception, equilibrioception, nociception, temperature sensation) for survival. Mechanosensation underlies the perception of mechanical forces such as tactile, acoustic and proprioceptive stimuli, which are rapidly converted into high-fidelity electrical responses. Most unicellular organisms are able to detect membrane tension and other deformations of the cell caused by mechanical strain (Martinac, 2001). The somatosensory system of higher organisms comprises a set of special-

ized mechanosensitive cells and organs to perceive touch, sound and proprioception, mechanical qualities whose underlying molecular mechanisms are poorly understood.

In *Drosophila*, the peripheral nervous system (PNS) is composed of segmentally repeated mechanosensory neurons classified as type I and type II nerve cells (Fig. 28C). Type I sensory neurons are monodendritic, ciliated sensory processes surrounded by a set of support cells (Fig. 28D-F; Eberl et al., 2000). They are involved in the perception of touch, humidity, sound and proprioception (Eberl, 1999; Eberl et al., 2000; Liu et al., 2007; Cheng et al., 2010). Each individual sensory neuron with its surrounding cells is referred to as a scolopidial unit. Type I mechanoreceptors are subdivided in external sense organs (es) and chordotonal organs (chos) or pentascolopidial organs (Keil, 1997). Insertions of external sense organs such as sensory bristles allow to bypass the mechanically resistant exoskeleton, which is otherwise poorly conducive for touch and air flow. Chordotonal organs, however, are internal sense organs, functionally analogous to muscle spindles of mammals, providing awareness of the tension state and motion of muscles, a sensory quality called proprioception.

Type II sensory cells are individual, non-ciliated multidendritic neurons that lack accessory cells and are concerned with sensing nociception and proprioception (Tracey et al., 2003; Cheng et al., 2010; Kim et al., 2012). These multidendritic sensory cells (md) are further classified into tracheal dendrite (td) neurons, bipolar dendrite (bd) neurons and dendritic arborization (da) neurons (Bodmer and Jan, 1987).

Each chordotonal organ constitutes five identical scolopidial units organized in an array (hence pentascolopidial organ), internally suspended between cuticle and muscle through an attachment cell and ligament cell, respectively (Fig. 27E-F). A particularly large arrangement of 480 scolopidial units is located in the adult antenna (known as Johnston's organ) to perceive sound and wind flow through perception of vibration (Eberl, 1999; Kamikouchi et al., 2006).

The sensory input to each scolopidial unit is provided by the ciliated dendrite, which is immersed in characteristic high K^+, low Ca^{2+} endolymph secreted by the support cells (Grünert and Gnatzy, 1987). Each ciliary tip of the sensory processes is connected to an extracellular matrix, the dendritic cap, secreted by the scolopale cell (Chung et al., 2001). Upon flexion between two body segments the organ is stretched or relaxed leading to a displacement of the ciliated dendrite relative to the dendritic cap (Eberl, 1999). This presumably induces the opening of mechanosensitive ion channels such as transient receptor potential vanilloid (TRPV) channels at the outer dendritic segment (Gong et al., 2004). Subsequently, the sensory infor-

mation is conveyed to the CNS and integrated into central pattern generator (CPG) circuits (Fig. 28A, B). CPGs elicit locomotion independent from peripheral sensory input, however, delicate adjustments of the locomotor system, crucial for behaviorally relevant movements, require the integration of sensory information. Observation of larval locomotion of *cho* mutants suggests that these mechanosensory organs are pivotal for proprioception that underlies motor activity and rhythmic contraction by relaying sensory feedback to the locomotor CPG circuit (Caldwell et al., 2003; Hughes and Thomas, 2007).

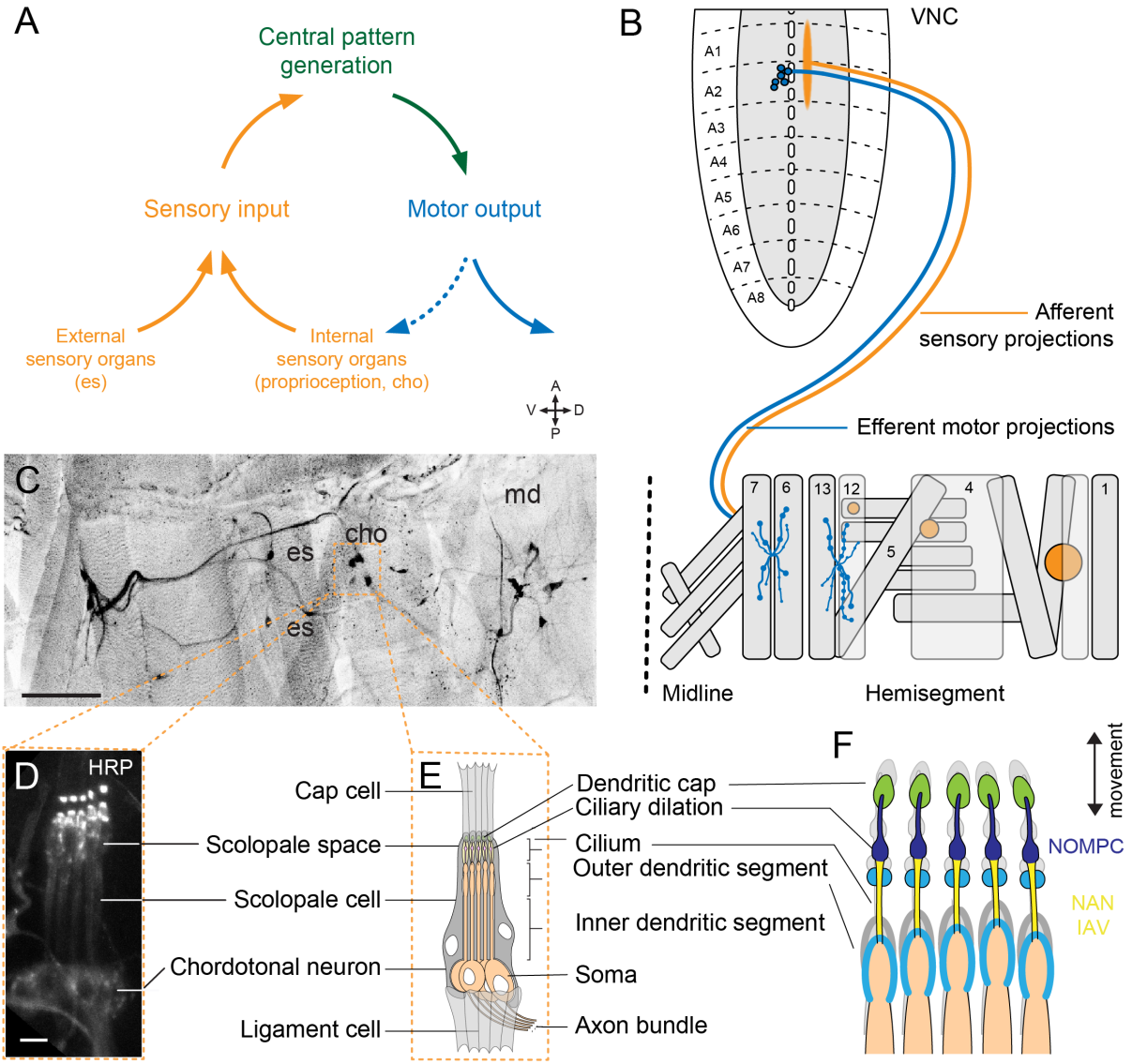

Figure 28. Peripheral sensory system of the *Drosophila* larva. A) Illustration of neuronal components involved in the generation of larval locomotion and their interdependences. B) Schematic portray of the anatomical layout of sensory afferents and motor efferents. C) Presentation of a larval hemisegment. es: external sensory neurons, cho: chordontonal sensory organ, md: multidendritic type II sensory neuron; Scale bar 100 µm. D) Confocal image of pentascolopidial organ of third instar larva visualized using conjugated HRP antibody; Scale bar 5 µm. E, F) Anatomical layout and components of a larval pentascolopidial organ from L3 larva after (Hartenstein, 1988). Figure adapted from Scholz et al., 2015.

One of the major challenges in investigating sensory systems is to unveil the molecular identity of transducers, which has proven to be particularly challenging for mechanotransduction. Strikingly, however, is the finding that mechanotransduction ensues extremely rapidly, with latencies on a sub-millisecond time scale, as demonstrated for various sensory cell types in different model organisms (Chalfie, 2009). Conclusively, it was hypothesized that mechanotransduction might be too fast for the signal transmission via chemical intermediates, and that electrical responses are more likely generated by direct force-dependent gating of a transduction channel (Howard and Hudspeth, 1988). Several efforts lead to the identification of putative mechanosensory channels among them TRP channel proteins. The first suggestion for TRP channel as transducer arose from genetic studies from *C. elegans*. In a screen for nose touch insensitivity, loss of *osm-9* resulted in mechanical hyposensation in addition to other defects (Colbert et al., 1997). A more specific characterization for TRP channels as mechanoreceptor molecules resulted from deletion of *nompC* (*no mechanoreceptor potential*) in zebrafish and *Drosophila* (Kernan et al., 1994; Sidi, 2003). Loss of NOMPC/TRPN1 in zebrafish results in deafness, loss of vestibular sense and microphonic potentials induced by mechanical stimulation of lateral line hair cells (Sidi, 2003). *NompC*-deficient multi-dendritic type II neurons of the body wall of *Drosophila* larvae lack elicitation of Ca^{2+} signals during locomotion (Cheng et al., 2010). Also, adult *nompC* mutants display partial loss of receptor potential peaks evoked by external sensilla of bristles, while sound induced receptor potentials measured from chos of Johnston's organ remain wild-typic (Kernan et al., 1994; Eberl et al., 2000; Walker et al., 2000). As NOMPC disruption results in residual responses of afferents, this channel may take part in transduction, but unlikely constitutes the sole transducer component in fly hearing. All in all the existing data suggest an evolutionarily conserved role for NOMPC/TRPN1 in mechanosensation. In this context it is important to mention that so far no *nompC* homolog has been identified in mammals (Sidi, 2003).

As in auditory hair cells of vertebrates, mechanosensory cells of the fly co-express NOMPC with other TRP channels: TRPV genes *nanchung* (*nan*) and *inactive (iav;* Kim et al., 2003; Sidi, 2003; Gong et al., 2004; Shin et al., 2005). NAN and IAV protein products most likely form Ca^{2+} permeable heteromultimeric channels and are mutually required for their targeting to proximal cilia of cho neurons (Kim et al., 2003; Gong et al., 2004; Göpfert et al., 2006). Similarly, both channels are required for hearing and the generation of electrical activity of chordotonal neurons in the Johnston's organ (Kim et al., 2003; Gong et al., 2004). Göpfert and co-workers provided an intriguing model for TRP channel interplay in mechanosensation.

Transduction of acoustic stimuli during hearing is coupled to non-linear amplification, a process in which mechanosensory cells actively generate motions to reinforce and amplify the minuscule sound-induced vibrations they sense (Fettiplace and Hackney, 2006). Genetic ablation of *Drosophila nompC* fully abolished non-linear amplification, resulting in linear feedback, which remained steady in sensitivity levels independent from stimulus strength (Göpfert et al., 2006). As opposed to this, removal of *nan* and *iav* induced excessive amplification that is the receivers response is non-linearly increased leading to drastic sensitivity boost. Hence, NOMPC subserves signal amplification and constitutes a candidate transducer channel, whereas IAV/NAN acts to control mechanical amplification and augment subthreshold signals to produce signals large enough to spark spike initiation. However, this process was suggested to depend on NOMPC function. Thus, according to this model NOMPC resides functionally downstream of NAN/IAV in the mechanotransduction pathway (Göpfert et al., 2006). Recently, this model has been challenged. Lehnert et al. agree with NOMPC's requirement in active amplification, but propose its dispensability for transduction in auditory receptor cells. Instead their data suggest that NOMPC sensitizes the transduction complex to mechanical strain and accurately regulates static force on the complex. Moreover, they find that response to sound relies on NAN and IAV. It follows that NAN/IAV may function as part of the transduction complex (Lehnert et al., 2013).

As mentioned above neurosensory signal transduction is astonishingly rapid, basically excluding signal transmission via second messenger cascades (Chalfie, 2009). Instead, transduction channel pore opening seems to occur by tensing elastic components, namely the gating springs, which directly apply force to the channel (Howard and Hudspeth, 1988; Albert et al., 2007; Tinevez et al., 2007). This forced activation is featured by non-linear gating compliance, which is a result of tension relief as the channel pore opens. Gating compliance has been documented for vertebrate hair cells (Howard and Hudspeth, 1988; Tinevez et al., 2007) and in *Drosophila* for Johnston's organ (Albert et al., 2007), in which NOMPC may act as the transduction channel and/or the gating spring (Effertz et al., 2012). Recent data from two independent groups underpin this observation in that NOMPC actually incorporates both the mechanically gated ion channel and the intracellular filament (gating spring) that tethers the channel to the cytoskeleton of the cilium (Liang et al., 2013; Yan et al., 2013). Ectopic expression of NOMPC in touch-insensitive cells converted these into touch-sensitive cells, electrophysiological analysis from heterologous expression of NOMPC in S2 cells revealed channel openings with very small latencies (1.5 ms), and selective mutation of pore region

confirmed that NOMPC is a pore forming subunit of mechanically gated ion channel (Yan et al., 2013). In addition, the exceptionally long intracellular domain of NOMPC comprises a number of 29 ankyrin repeats, which provide sufficient structural integrity and necessary compliance to act as molecular springs (Liang et al., 2013). Examination of the tertiary structure of ankyrin repeats showed that the crystallized 12 ankyrin repeats of the human ankyrinR protein form a spiral shape (Michaely et al., 2002). The 29 ankyrin repeats of TRPN1 were predicted to form an approximately 20 nm long helix enabling expansions and compressions of ~ 10 - 20 nm (Howard and Bechstedt, 2004). Interestingly, beside NOMPC/TRPN1, this structural motif is also present in other TRPN and TRPV channel subunits including NAN and IAV although in much lower repeat number (ranging from 3-5 repeats; 5 ankyrin repeats were predicted for IAV; Clapham et al., 2001; Gong et al., 2004).

Hence, the advanced yet divergent data on TRP channels provide a solid ground to further investigate mechanotransduction and coincidentally emphasize the necessity for further elucidation to completely understand the molecular nature of mechanosensation.

7.8. Scope of this study

This study set out to characterize the *in vivo* function of Latrophilin/*dCirl* employing *Drosophila melanogaster*. Latrophilin constitutes one of two highly conserved aGPCR homologs and thus serves to investigate basic signaling principles of these receptors, which are, so far, poorly understood.

Latrophilin has documented functions in different physiological processes: synaptic transmission (Scheer et al., 1984; Ichtchenko et al., 1998; Umbach et al., 1998; Südhof, 2001), development (Langenhan et al., 2009) and fertility (Prömel et al., 2012). However, the precise physiological role of *dCirl* within the nervous system remained largely undefined.

To this end, a genomic engineering technology was utilized to generate *dCirl* knock-out and knock-in animals (Scholz et al., 2015). First, the neuronal localization of *dCirl* on transcriptional and translational levels was studied during distinct developmental stages of *Drosophila* to identify cells that rely on *dCirl* function. Next, a combinatorial application of fly genetics, bioinformatics, fluorescence microscopy and behavioral paradigms was employed to relate *dCirl* receptor residence to function and to identify the stimulus modality perceived through this receptor and potentially other aGPCR. In the future, knowledge of this modality will help to unravel the context of physiologically adequate receptor activation and biochemical cellular responses mediated by aGPCR.

8. Results

8.1. Generation of *dCirl* null allele - $dCirl^{KO}$

The fly genome encodes a single latrophilin homolog named *dCirl/CG8639*. Cytologically, the *dCirl* locus maps to the 44D4-44D5 region on the second chromosome. Furthermore, the gene spans 10.7 kb and possesses 11 putative coding exons (Fig. 29).

To investigate *dCirl* function *in vivo* a homologous recombination based genomic engineering strategy was employed to produce a definite null allele (Huang et al., 2008). This set of experiments was performed by Robin Fischer and is documented in his diploma thesis (Fischer, 2011). Here, I will briefly lay out these results, which were the basis for several investigations that were subject of this thesis.

A recombination event enabled the replacement of *dCirl* open reading frame (ORF) together with 5' intergenetic putative promotor region and the 5'- and 3' UTRs by an *attP* site and a floxable *hsp70-white* cassette (Fig. 29; Scholz et al., 2015). The *attP* site subsequently allows for phiC31-mediated transgene insertion, while the *white* cassette serves as straightforward selection marker (Fig. 29; Groth et al., 2004).

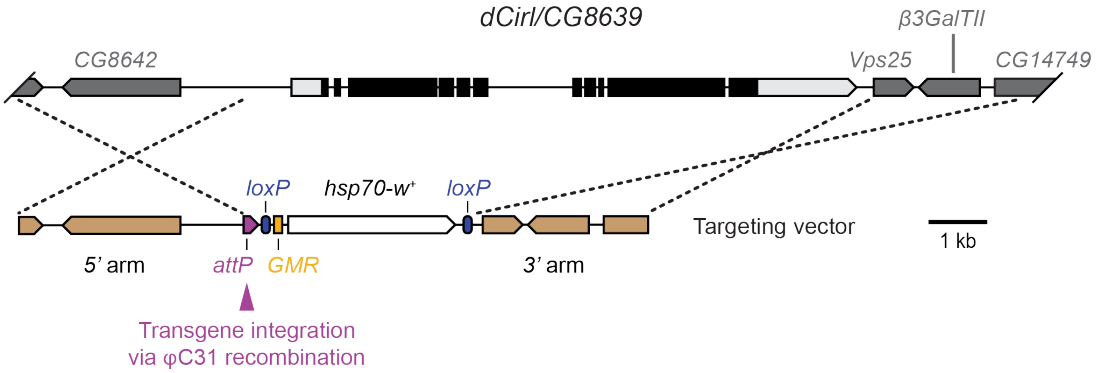

Figure 29. Generation of a *dCirl* null allele. Cartoon of genomic layout of the *dCirl* (*CG8639*) locus and homologous recombination based targeting strategy for its removal. 5'- and 3' targeting arms (light brown) specify DNA stretch (dashed lines) removed from the fly genome. Subsequently, the inserted cassette bears an *attP* site, which constitutes a landing pad for transgene insertion and white cassette flanked by *loxP* sites for subsequent removal of selection marker (Scholz et al., 2015).

Transcriptome and proteome analyses of the putative $dCirl^{KO}$ strain ascertained the absence of residual *dCirl* transcripts and protein, conclusively confirming that $dCirl^{KO}$ is a true null allele (Scholz et al., 2015).

In *C. elegans* removal of latrophilin homolog *lat-1* results in defective development (Langenhan et al., 2009). To investigate whether removal of *dCirl* from *Drosophila* leads to similar abnormalities in their development, lethal phase analysis was conducted (Scholz et al., 2015). Remarkably, development of $dCirl^{KO}$ animals remained unharmed, suggesting that *dCirl* is dispensable for development and viability of flies (Scholz et al., 2015).

8.2. Genomic engineering of *dCirl* toolkit

In scientific research *Drosophila melanogaster* has advanced to the status of a genetic all-rounder facilitating a tremendous repertoire of approaches.

Ends-out targeting technology was used to generate a $dCirl^{KO}$ knock-out allele specifically designed for subsequent *dCirl* locus-directed knock-in of wild-type and modified *dCirl* DNA fragments.

First, the endogenous *dCirl* locus was reconstituted through the re-integration of unmodified full-length genomic *dCirl* sequence. Accordingly, the resulting allele was named $dCirl^{Rescue}$.

In a second batch, transgenic *dCirl* fragments containing different biochemical tags - encoding a 3xFLAG tag (*flag* tag) or mRFP fluorophore - were generated to study the expression profile of dCIRL, since immunodetection of dCIRL using an antiserum against the native protein proved difficult (data not shown). The 3x*flag* tag sequence was inserted into the coding exon 8, which encodes the third intracellular loop of the 7TM domain of the dCIRL protein (Fig. 30A; Prömel et al., 2012). Henceforth the resulting allele is referred to as $dCirl^{Flag}$. In contrast, *mRFP* sequence was introduced into exon 3 partially encoding the intracellular domain of *dCirl*. The allele obtained through this insertion is hereinafter referred to as $dCirl^{RFP}$ (Fig. 30A).

Further, as an alternative to localize the dCIRL protein an allele was conceived that allowed surveillance of the transcriptional activity of the *dCirl* locus. For this purpose an optimized *gal4.2::p65* cassette was inserted before the translational start of the *dCirl* ORF leaving the endogenous locus completely intact ($dCirlp^{GAL4}$, Fig. 30B; Scholz et al., 2015). This modification leads to GAL4 production in a *dCirl*-dependent manner and enables, in conjunction with suitable UAS reporter transgenes, the visualization of *dCirl* transcription.

Importantly, genetic modifications of the *dCirl* locus seemed not to affect dCIRL receptor function as judged from the wild-type crawling behavior of these animals (Fig. 33B).

Finally, a genomic rescuing transgene was generated, in which the endogenous *dCirl* promotor was substituted with an optimized *20xUAS-IVS* promotor cassette to gain transcriptional control over *dCirl* expression (Fig. 30C; Scholz et al., 2015).

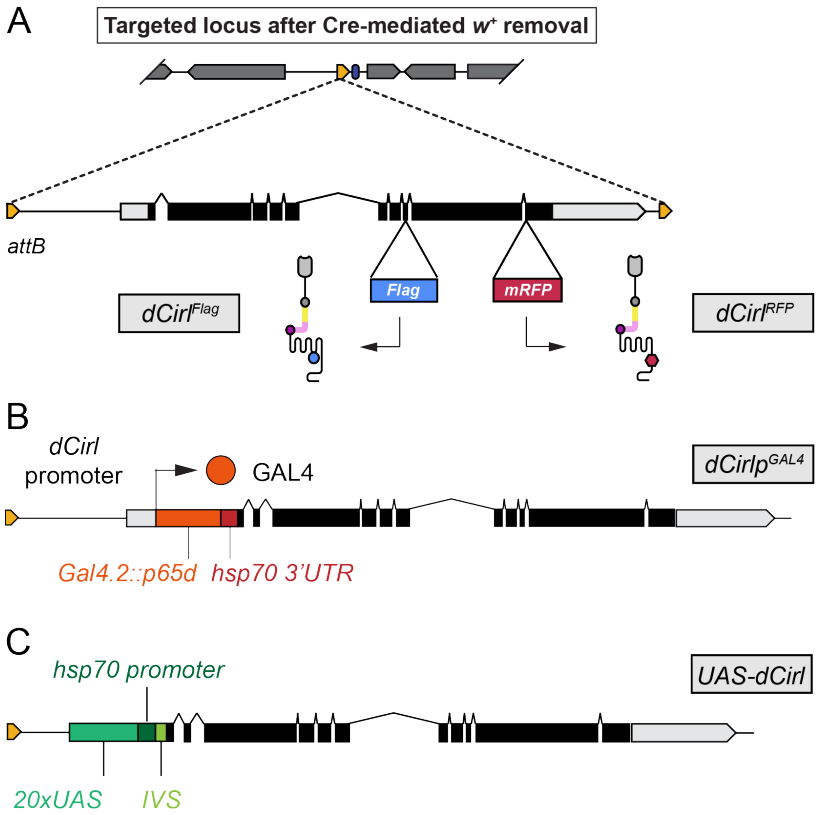

Figure 30. Establishment of a genetic *dCirl* toolkit. A) Schematic depiction of $dCirl^{Flag}$ and $dCirl^{RFP}$ fusion variants. *3xFlag* and *mRFP* were inserted in the third intracellular loop of the 7TM and the intracellular C-terminus, respectively. B, C) Illustration of *dCirl* promotor allele ($dCirlp^{GAL4}$) and genomic *dCirl* rescue construct (*UAS-dCirl*).

In summary, these alleles provided a versatile genetic toolkit for the examination of endogenous *dCirl* expression profile on transcriptional and translational levels, and offered an entry point for the functional characterization of *dCirl*.

8.3. Neuronal expression pattern of dCIRL in larval and adult stages

In order to resolve which cells within larvae depend on *dCirl* activity its endogenous localization pattern was observed.

Unfortunately, endogenous expression of dCIRL::RFP fusion proteins was not detectable using confocal microscopy, which might indicate low copy number similar to Latrophilin homolog LAT-1 in *C. elegans* (Langenhan et al., 2009). However, signal amplification achieved by antibody staining against 3xFLAG and mRFP epitopes disclosed the subcellular residence of dCIRL.

Immunostained brains from $dCirl^{Flag}$ and $dCirl^{RFP}$ homozygous larvae, respectively, revealed that dCIRL is broadly expressed throughout the VNC including the synapse-rich region (neuropile), which is prominently counterstained by the presynapse marker BRP (Kittel et al., 2006b; Wagh et al., 2006) and in the somata of dCIRL expressing cells (Gehring, 2014). Furthermore, co-localization of $dCirl^{Flag}$ with neuronal membrane marker HRP confirmed membrane targeting of dCIRL fusion protein (Gehring, 2014). This data suggested expression of dCIRL in the central nervous system of *Drosophila* larva. Note that no dCIRL signals were detected in the periphery of motoneurons of third instar larvae indicative for its absence or low copy number (data not shown).

The anatomy of the CNS of larvae differs considerably from that of adult flies (Hartenstein, 1993), which is why we set out to investigate dCIRL expression profile in the adult brain of the fly. Maximal projection of stained $dCirl^{RFP}$ whole-mount preparations displayed fluorescent signal in the mushroom body [Fig. 31A (arrow), B]. *Ok107-GAL4* (Connolly et al., 1996) driven *UAS-CD4::tdGFP* expression was used to outline the mushroom body structure in stainings. As judged from these maximal projections and single optical slices, dCIRL localized to medial γ-lobes but not or only faintly to the vertical α-and β-lobes of the mushroom body (Fig. 31B, B′, B′′), consistent with either γ-lobe specific dCIRL expression or lack of staining in interior parts of the preparation, e.g. through penetration errors of the immunostaining solutions.

Furthermore, dCIRL prominently localized to neuronal somata throughout the entire brain, but largely omitted synapse-rich neuropiles resulting in an inverse localization pattern with respect to BRP (Fig. 31A), which markedly differed from expression patterns obtained in larval brains (Gehring, 2014). Next, cell surface expression of dCIRL protein was validated through the alignment with ring neuron specific expression (*c232-GAL4*) of a membrane-

tethered GFP (*UAS-CD4::tdGFP*; Renn et al., 1999; Neuser et al., 2008). From an oblique perspective ring neurons comprise clusters of perikarya that provided a suitable readout for membrane location of dCIRL (Young and Armstrong, 2009).

Figure 31C depicts co-localization of dCIRL with CD4::tdGFP, which validates cell surface expression in the somata of ring neurons.

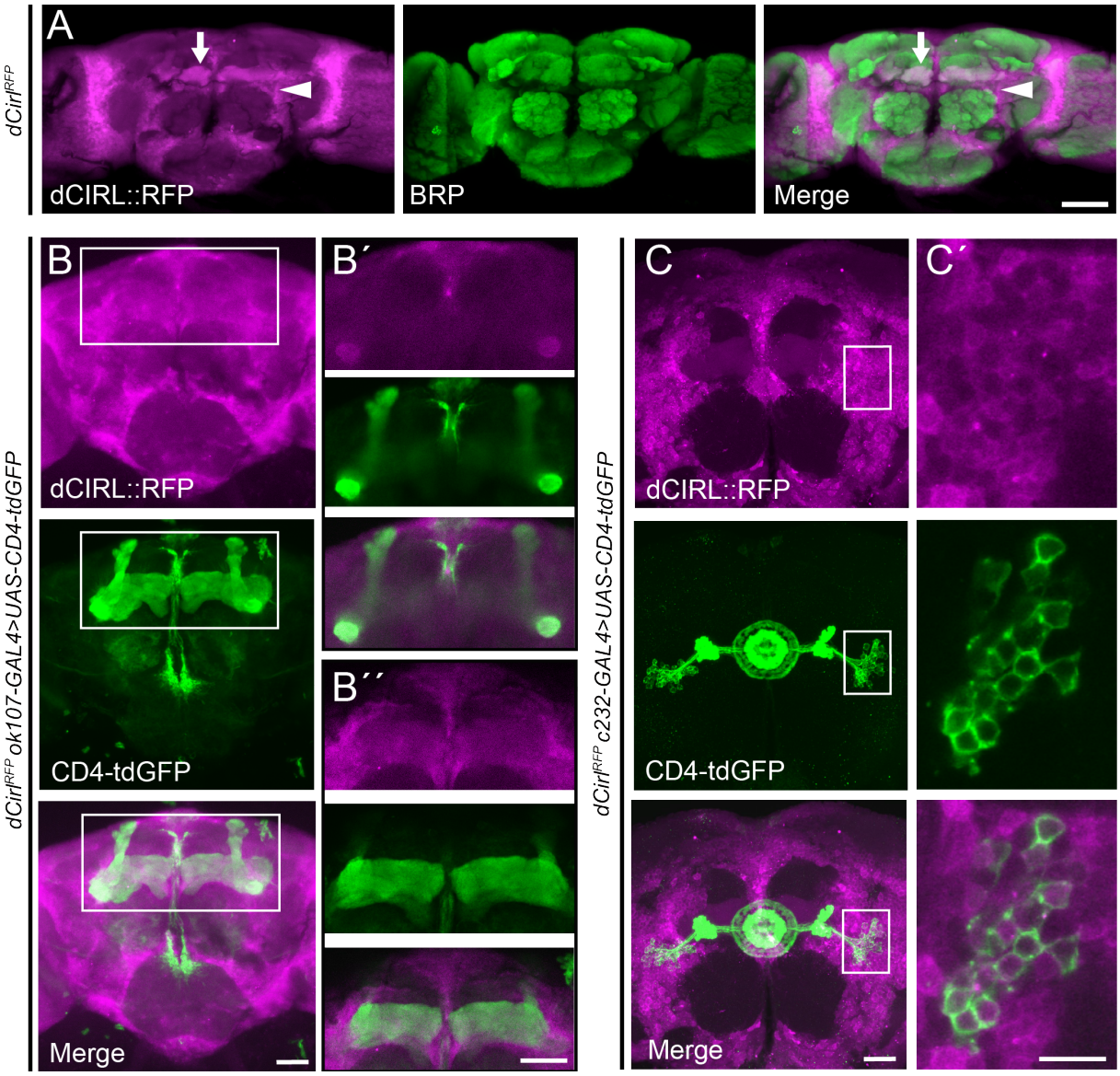

Figure 31. dCIRL is broadly expressed in the CNS of adult flies. A) Brains of adult *dCirl*^{RFP} animals displayed broad dCIRL expression with conspicuous signal in the mushroom body (arrow) and somata (arrowhead) throughout the entire brain (Gehring, 2014). With respect to BRP residence dCIRL expression does not coincide with larval expression data. B, B´, B´) Depicted is *ok107-GAL4* (Connolly et al., 1996) driven expression of GFP variant in *dCirl*^{RFP} background, which confirmed mushroom body localization assessed in A. C, C´) Observation of dCIRL cell surface targeting judged by counterstaining of membrane-attached GFP in ring neurons using *c232-GAL4* (Renn et al., 1999). Scale bar A, B´, B´´ = 50 µm, C = 30 µm, C´= 10 µm.

In addition, cryosections of adult brains revealed scarce yet detectable dCIRL expression in the fan shaped body (Fig. 32B, arrowhead), another structural component of the central complex. Neuropiles of the optical system were devoid of dCIRL signal (Fig. 32A). Interestingly, in insects the central complex has been linked to a myriad of biological processes, including coordination of motor behavior, spatial orientation and memory of spatial orientation (Heinze and Homberg, 2007; Poeck et al., 2007; Neuser et al., 2008).

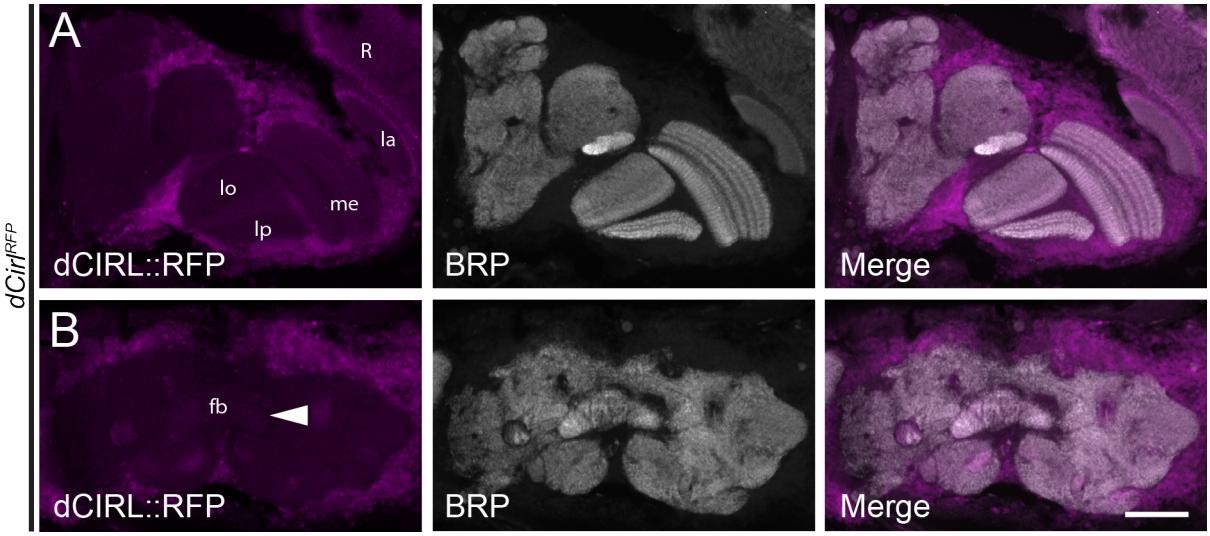

Figure 32. dCIRL largely omits synapse-rich regions. A, B) Projection of confocal images of cryosections of homozygous *dCirl*^{RFP} adults affirms perikaryal dCIRL expression in most if not all brain areas including optical system (A) and moreover enabled dCIRL detection in a distinct central complex component - the fan-shaped body (fb) (B). Scale bar = 50 µm.

In conclusion, the obtained data demonstrate broad dCIRL expression profile throughout the larval and adult CNS of *Drosophila,* however, with a shift to white matter distribution yet consistent membrane-specificity. Additionally, explicit dCIRL location to the mushroom body and central complex of adult flies might reflect dCIRLs involvement in biological process relayed through these brain structures.

8.4. *dCirl*^{KO} larvae display curtailed crawling distances

Wild-type larval crawling pattern is characterized by periods of linear movements occasionally intermitted by head swing periods that presumably reflect searching and decision making processes (Caldwell et al., 2003). Subsequently, larvae initiate linear locomotion in a new

direction (Wang et al., 1997). As experiments were carried out it seemed that *dCirl*^{KO} larvae exhibited aberrant locomotion patterns in that they lingered much longer in head swing periods, secondarily resulting in curtailed linear crawling phases (Fig. 33A). To quantify this behavior, net crawling distances were measured as a function of time (0, 5 - 2 min). Indeed, *dCirl*^{KO} larvae travelled significantly less distance compared to wild-type animals, an effect rescued by re-insertion of wild-type *dCirl* sequences (Fig. 33B, Suppl. Table 8). Similarly, *dCirl*^{KO} crossed over a deficiency (*Df(2R)Exel8047*) that uncovers the *dCirl* locus displayed diminished crawling path lengths, further validating that the phenotype is due to the loss of *dCirl* (Fig. 33B, Suppl. Table 8; Scholz et al., 2015).

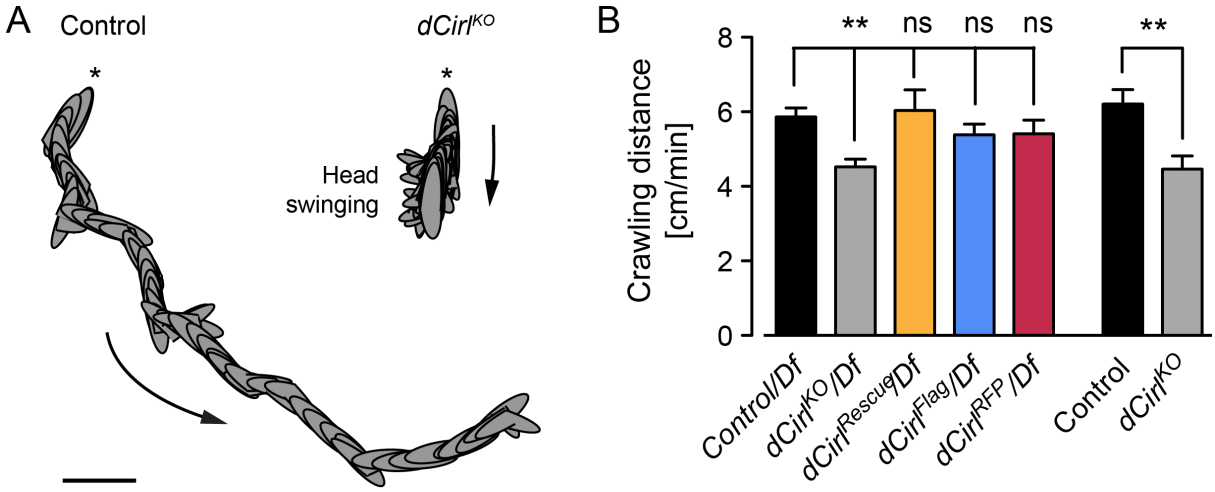

Figure 33. Loss of *dCirl* results in defective larval locomotion. A) Illustration of extensive head swing periods exhibited by *dCirl*^{KO} larvae. Reconstruction of 60 frames each genotype, which reflects a time period of 36 seconds. Arrows indicate the direction of movement; asterisks designate the locomotion start. Scale bar 5 mm. (Scholz et al., 2015) B) Quantification of crawling path lengths of homo- and hemizygous *dCirl* animals (Gehring, 2014). Error bars reflect standard errors of the mean. Data are presented as mean ± S.E.M. * $P \leq 0.05$, ** $P \leq 0.01$, *** $P \leq 0.001$.

This robust behavioral paradigm was further employed to test whether insertion of tags impacts dCIRL function. Both FLAG- and RFP tagged receptor variants sufficed to rescue the locomotion phenotype suggesting functionality of both for the generation of larval locomotion (Fig. 33B, Suppl. Table 8).

8.5. *dCirl* promotes elevation of postsynaptic Discs-large

Proper synaptic transmission relies on precise spatial arrangement of protein complexes at the NMJ. Hence, the overall NMJ structure was examined to test whether impaired locomotion displayed by $dCirl^{KO}$ larvae is associated with morphological alteration. For this purpose the distribution of synaptic proteins Futsch, Discs-large (DLG) and Fasciclin II (FasII), which are known to regulate different morphological aspects of the NMJ (Budnik et al., 1996; Stewart et al., 1996; Roos et al., 2000), were investigated. Comparative analysis of Futsch and FasII at mutant and control NMJs on muscle 6/7 disclosed that the cytoskeleton and periactive zones of motoneurons were unaltered, respectively (Fig. 34A-D). In contrast, DLG distribution differed between genotypes (Fig. 35).

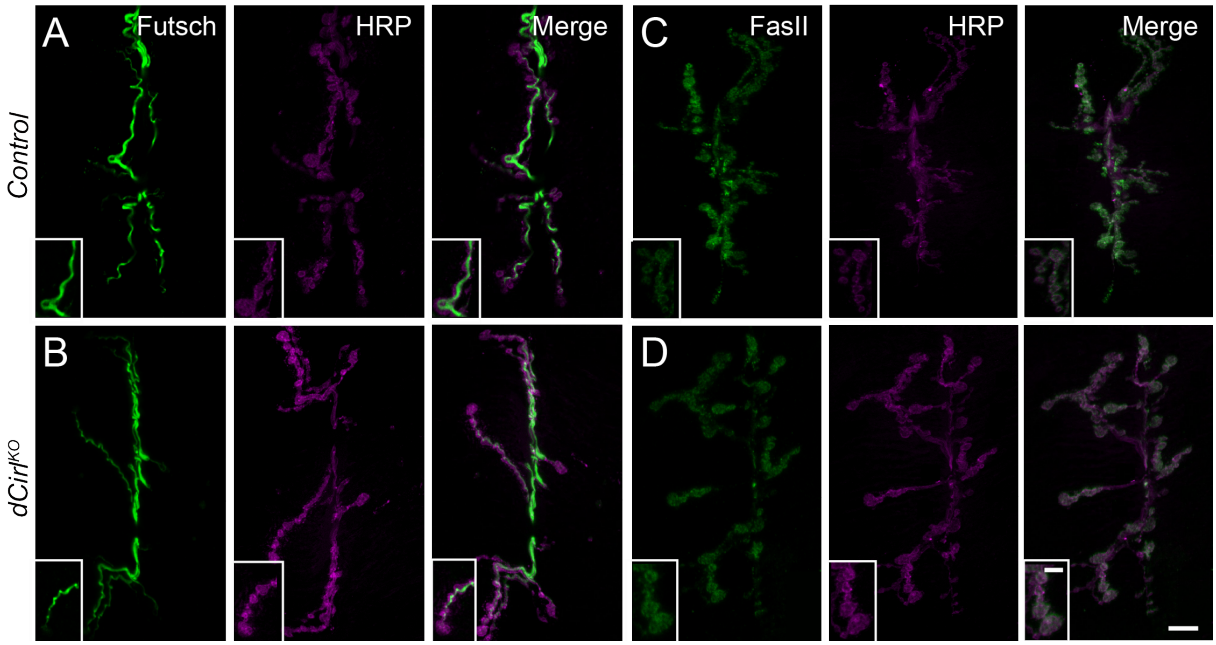

Figure 34. Morphology of the $dCirl^{KO}$ NMJ is largely preserved. A-D) Maximal projection of confocal images of muscle pair 6/7 of control (A, C) and $dCirl^{KO}$ larvae (B, D) stained for synaptic proteins. A, B) Anti-Futsch labeling is indistinguishable between genotypes. C, D) Loss of *dCirl* does not affect FasII distribution. Scale bar A-D 10µm, insets 5µm.

DLG is a member of the scaffolding protein family collectively referred to as MAGUKs (membrane-associated guanylate kinase homologs; Woods and Bryant, 1991; Hough et al., 1997). DLG is expressed both pre- and postsynaptically and is thought to play an essential role in the development and function of larval NMJs (Budnik et al., 1996; Thomas et al.,

1997). Hypomorphic mutations in *dlg* lead to poor development of the postsynaptic subsynaptic reticulum (SSR), a structure comprised of highly elaborated membranes specifically found in type I boutons (Thomas et al., 1997). Fluorescence analysis suggested that removal of *dCirl* causes larval NMJ specific elevation of DLG content (Fig. 35). Quantification of DLG protein done by western blot and subsequent densitometric measurements showed a near two-fold increase of DLG intensity in $dCirl^{KO}$ samples (Fig. 35E, F), although no statistical significance was achieved.

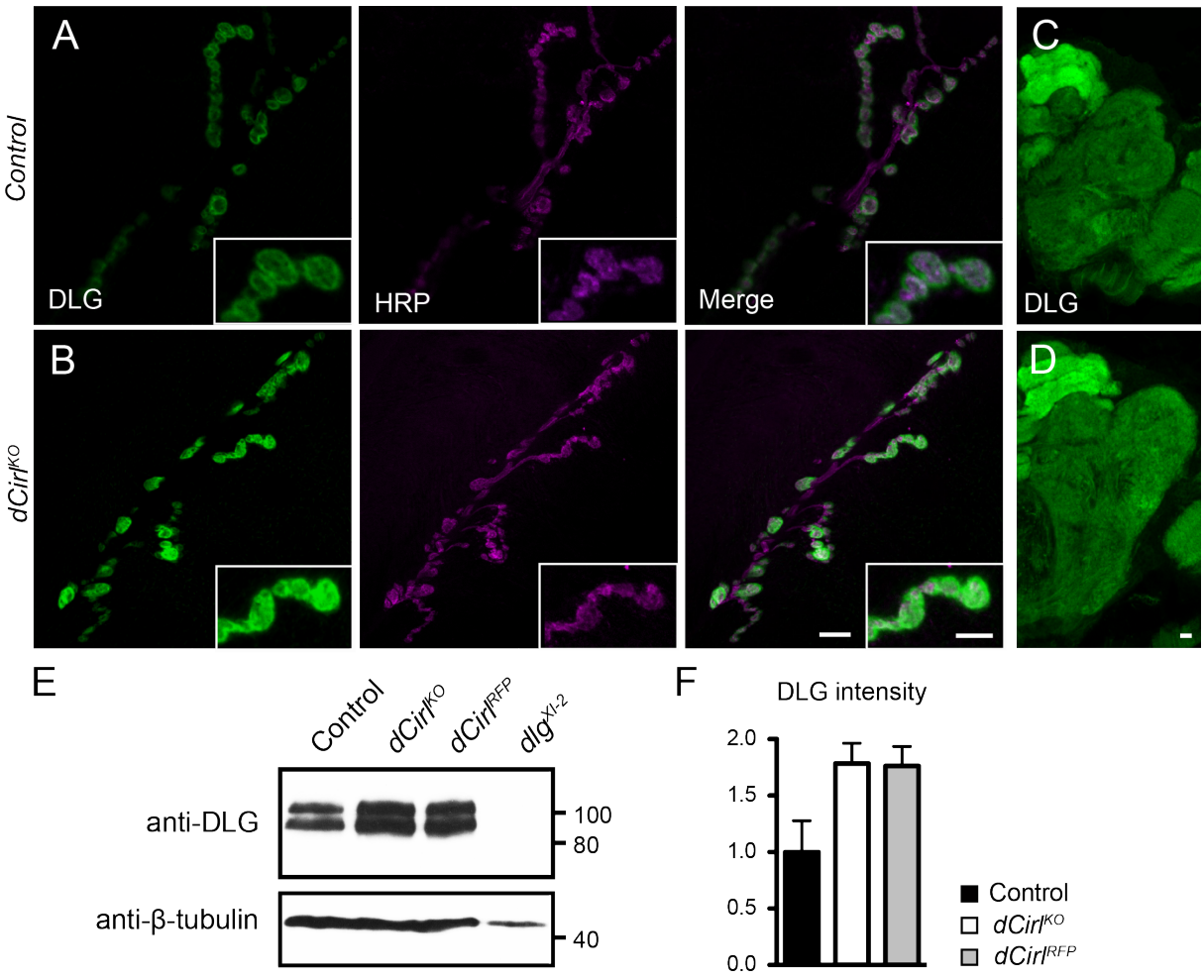

Figure 35. Removal of *dCirl* leads to NMJ specific increase in DLG abundance A, B) Localization of DLG proteins at the larval NMJ of control (A) and *dCirl* deficient animals (B). Loss of *dCirl* led to an increase in DLG expression. C, D) Adult brains of controls and mutants labeled with anti-DLG are indistinguishable. E) Western blot analysis of DLG contents from controls, $dCirl^{KO}$, $dCirl^{RFP}$ and dlg^{XI-2} hypomorphs. $dCirl^{KO}$ display a significant increase in DLG amounts, which were not rescued in $dCirl^{RFP}$ larvae. dlg^{XI-2} mutants exhibit severe loss of SSR size accompanied by the reduction in DLG protein. F) Densitometric measurement of DLG amounts detected via western blot demonstrates drastic rise in DLG in $dCirl^{KO}$ and $dCirl^{RFP}$ compared to control (Gehring, 2014). Note that no statistical significance between wild-type and mutant samples was achieved in this experimental data set. Scale bar A, B 10 µm, insets 5µm; C, D 10µm.

Hence, *dCirl* appears to enhance the expression of the scaffold protein DLG, an effect that may be linked to the extensive enlargement of postsynaptic SSR that is rescued in $dCirl^{Rescue}$ animals. However, in $dCirl^{RFP}$ animals, the tagged receptor is not sufficient to revert SSR extension to wild-type levels. Strikingly, previous work demonstrated that overexpression of *dlg* induces massive membrane formation resulting in increase in SSR size (Mendoza-Topaz et al., 2008), similar to postsynaptic SSR enlargement observed in $dCirl^{KO}$.

In conclusion, altered behavioral output of $dCirl^{KO}$ might be associated to SSR diversification, however the extent and causal relationship is unclear. For example, excessive head swinging and/or frequent directional changes may induce SSR extension. Alternatively, postsynaptic structural alteration of the NMJ may inflict deleterious larval locomotion of $dCirl^{KO}$ larvae.

8.6. *dCirl* has no impact on presynaptic components of the larval NMJ

To my knowledge defective locomotion in *Drosophila* larvae has not been associated with morphological changes of the postsynaptic reticulum. Hence, we sought to check whether crawling defect of $dCirl^{KO}$ larvae is determined by an alteration of presynaptic component.
This hypothesis was supported by former studies, which reported that α-LTX triggers massive neurotransmitter release from *Drosophila* NMJs (Umbach et al., 1998), likely through interaction with neuronal substrates including dCIRL. Although conclusive evidence is lacking, CIRL was suggested to be presynaptically expressed receptor with a function in synaptic transmission (Scheer et al., 1984; Südhof, 2001).
Unfortunately, labeling of tagged receptor variants did not produce reliable results at the NMJ, most probably due to expression levels below the detection threshold.
For this reason an alternative approach was employed. *UAS-myr::GFP* reporter was employed to assay the transcriptional regulation of *dCirl* promotor through the $dCirlp^{GAL4}$ allele (Fig. 36A, B), which enabled the surveillance of *dCirl* transcript production. Indeed, most if not all motoneuronal processes of each abdominal hemisegment showed a GFP signal (Fig. 36A, B; Gehring, 2014).
Thus, while the motoneuronal protein residence of dCIRL remains inconclusive, *dCirl* expression is clearly present.

Muscle innervation through type I motor endings is required for full motor response. Thus, functional defects of the neurons caused by *dCirl* removal might be responsible for the ob-

served motor defect. Changes in exocytotic activity are often accompanied by structural changes of the synapse in the relevant neurons. Morphometric analysis of presynaptic BRP (Kittel et al., 2006b; Wagh et al., 2006) from NMJs innervating muscle pair 6/7 of *dCirl*^{KO} and controls revealed no differences in presynaptic active zone size and number (Fig. 36C-D; Suppl. Table 9; Gehring, 2014). Similar, postsynaptic GluRIID subunit configuration were unaltered (Fig. 36C, D; Suppl. Table 9; Sepp et al., 2000; Qin, 2005). Additionally, the overall layout of the NMJ was indistinguishable between *dCirl*^{KO} and controls.

This data set provides one line of evidence contradictory to the hypothesis that *dCirl* influences exocytotic activity from motorneurons of *Drosophila*.

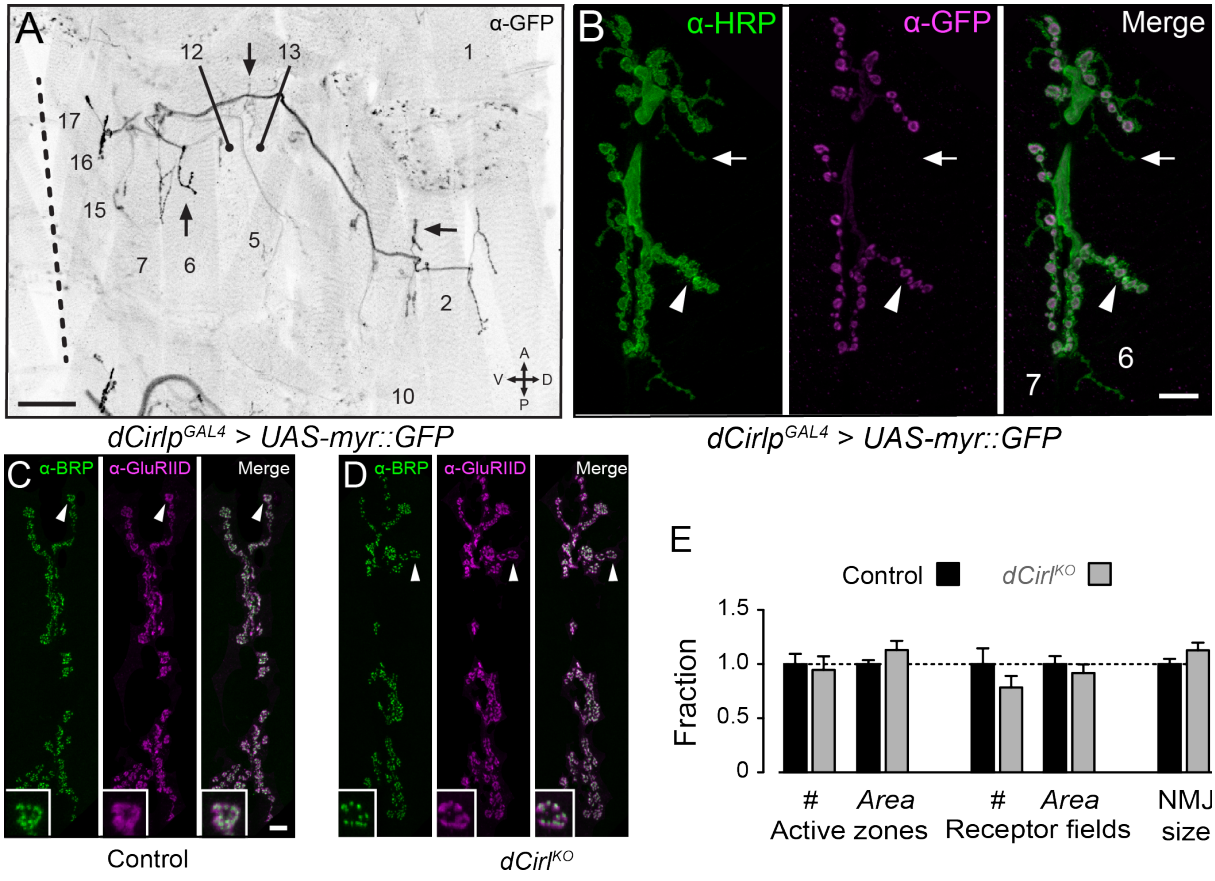

Figure 36. Loss of *dCirl* does not impair motor innervation. A) Helicopter view of larval *dCirl* expression pattern of abdominal hemisegment A3. *dCirl*-promotor driven GFP shows labeling of most motoneuronal processes that innervate body wall muscles (indicated by number) of the hemisegment. B) Close-up of NMJ at muscles 6/7 shows efficient *dCirl* localization to synaptic boutons, with more prominent labeling in Ib (arrowhead) than Is (arrow) processes. C, D) Confocal images of NMJ 6/7 in abdominal segments A2 and A3 of control (D) and mutant larvae (E) stained for active zone protein BRP and the glutamate receptor subunit GluRIID show no differences upon *dCirl* removal. Arrowheads indicate individual boutons magnified in the insets. E) Morphometric analysis of NMJ parameters (number and area, of active zones and glutamate receptor fields, NMJ size) are indistinguishable between *dCirl*^{KO} and controls (Gehring, 2014). Scale bar A - D = 10 μm.

Comparable to mammals, *Drosophila* neurons are ensheathed by glia cells, which are crucial regulators of nervous system development, function and health. The major classes of CNS glia in *Drosophila* are cortex, neuropile, surface and peripheral glia (Banerjee et al., 2006; Freeman and Doherty, 2006). CNS-derived peripheral glia enwraps motor axons (Auld et al., 1995) and constitutes to the speed of action potential conduction. Thus, I next asked whether the abnormal crawling behavior of $dCirl^{KO}$ larvae reflects alteration in glia ensheathing of motoneuronal processes.

To address this question glia cells of $dCirl^{KO}$ mutant and control animals were visualized by glia specific expression of a GFP reporter through *repo-GAL4* (Lai and Lee, 2006) in wild-type and mutant background. In contrast to vertebrate NMJs, where terminal Schwann cells entirely cover the NMJ (Feng et al., 2005), glutamatergic motoneurons of the fly are not completely "covered" by peripheral glia (Sepp et al., 2000; Banerjee et al., 2006). Instead, glia coverage terminates at the axon branch point where synaptic arbors contact the muscle surface (Sepp et al., 2000). Qualitative assessment of glia labeling from confocal images indicated that motoneuronal axon capping in $dCirl^{KO}$ does not differ from wild-type larvae (Fig. 37). Therefore, motoneuronal glia morphology appears not involved in the behavioral phenotype observed in the mutants.

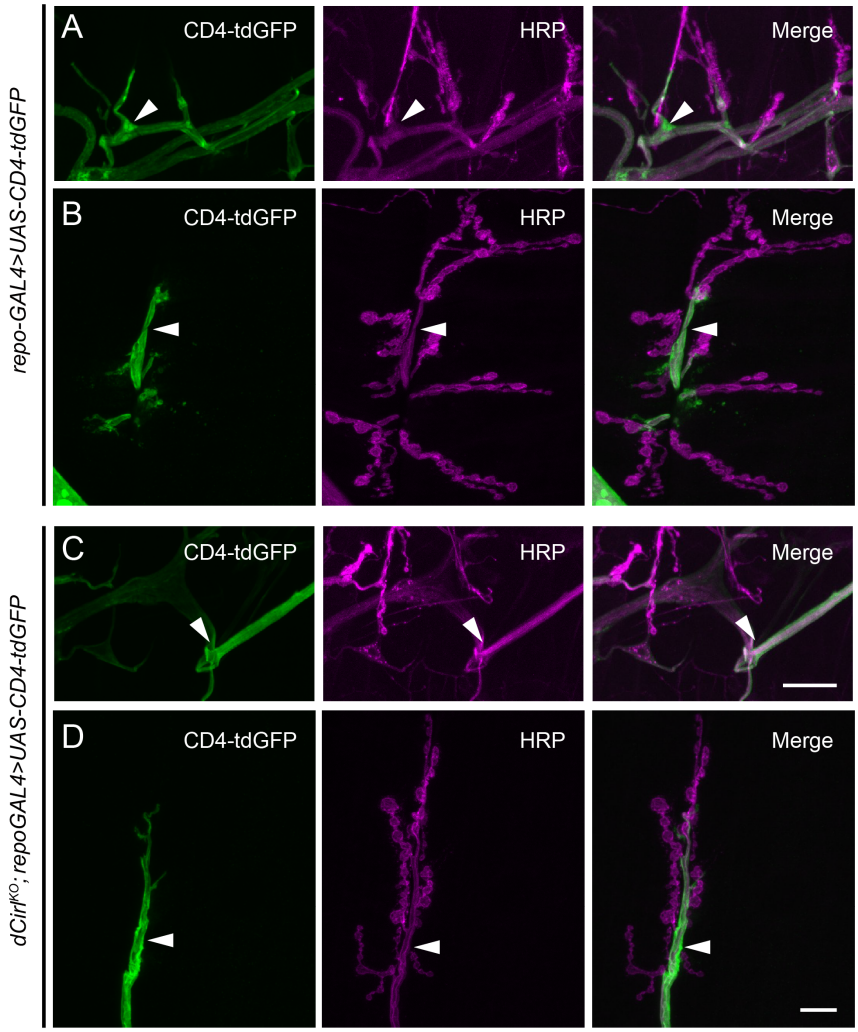

Figure 37. Glia ensheathment of motoneuronal axons of *dCirl-KO* appears unaltered. A-D) Confocal projection depicts segmental nerve tracts and NMJ with glia specific GFP expression. A, B) Depicted *are repo-GAL4* driven *CD4::tdGFP* in nerve tracts (A) and at the NMJ (B) of wild-type larvae. C, D) Representative nerve (C) and NMJ (D) of a mutant larva expressing *CD4::tdGFP* in peripheral glia cells. No obvious morphological changes were detected. Scale bar A, C = 30 µm; B, D = 10 µm.

Finally, to corroborate that motoneuron physiology does not rely on dCIRL function *dCirl*^{KO} mutants and controls were interrogated by a series of electrophysiological recordings (performed by D. Ljaschenko and C. Guan; data not shown). These analyses revealed that removal of *dCirl* has no impact on basal synaptic transmission or motoneuronal excitability of third instar larvae (unpublished results). This confirmed the morphological and expression analyses of *dCirl*^{KO} animals documented in this thesis.

In summary, no evidence was found to couple the locomotion defect of *dCirl*^{KO} to morphological or functional alterations of motorneurons or motorneuron-associated glial cells.

8.7. *dCirl* functions in peripheral sensory chordotonal neurons

Generation of rhythmic larval movement depends on central pattern generator and motor output but also sensory feedback to modify or regulate motor activity (Caldwell et al., 2003; Song et al., 2007). As shown above, motoneuronal efferents function independently of *dCirl*. In a next step, it was investigated whether *dCirl* plays a role in the function of peripheral sensory neurons that provide sensory feedback into the locomotion cycle.

First, *dCirl* promotor driven mCD8::GFP expression was monitored in sensory neurons. Indeed, strong GFP labeling in type I and II peripheral sensory somata was observed (Fig. 38A), suggesting that multiple sensory neurons express *dCirl* (Scholz et al., 2015). This suggested a requirement of *dCirl* function in these cells. Interestingly, transcription of *dCirl* was strongest in lateral chordotonal organs (lch1, lch5 or pentascolopidial organs; Fig. 38B; Scholz et al., 2015), which accommodate type I monodendritic sensory neurons that sense proprioceptive information used to generate muscle contractions, which drive rhythmic locomotions (Caldwell et al., 2003; Hughes and Thomas, 2007). Moreover, sensitivity to externally administered sound and gentle touch is conveyed through chordotonal organs (Kernan et al., 1994; Caldwell et al., 2003; Yan et al., 2013).

Deprivation of chordotonal neuron function frequently results in defective path morphology, (Caldwell et al., 2003; Hughes and Thomas, 2007) similar to crawling deficits discovered in $dCirl^{KO}$ larvae. However, as *dCirl* is expressed in a variety of sensory neurons we aimed to elucidate whether the larval crawling defect is specifically attributed to the loss of *dCirl* in chordotonal neurons. To this end *dCirl* expression was re-established in chordotonal neurons of $dCirl^{KO}$ (*iav-GAL4>20xUAS-dCirl*) mutants and crawling distances were scored.

Strikingly, extensive head swinging was ameliorated and the crawling path lengths improved nearly to wild-type values, indicative for function of *dCirl* in this sensory neuron type (Fig. 38C, Suppl. Table 8). Note that *20xUAS-dCirl* transgene did not facilitate crawling distances in the absence of *GAL4* driver and vice versa (Fig. 38C, Suppl. Table 8; Scholz et al., 2015).

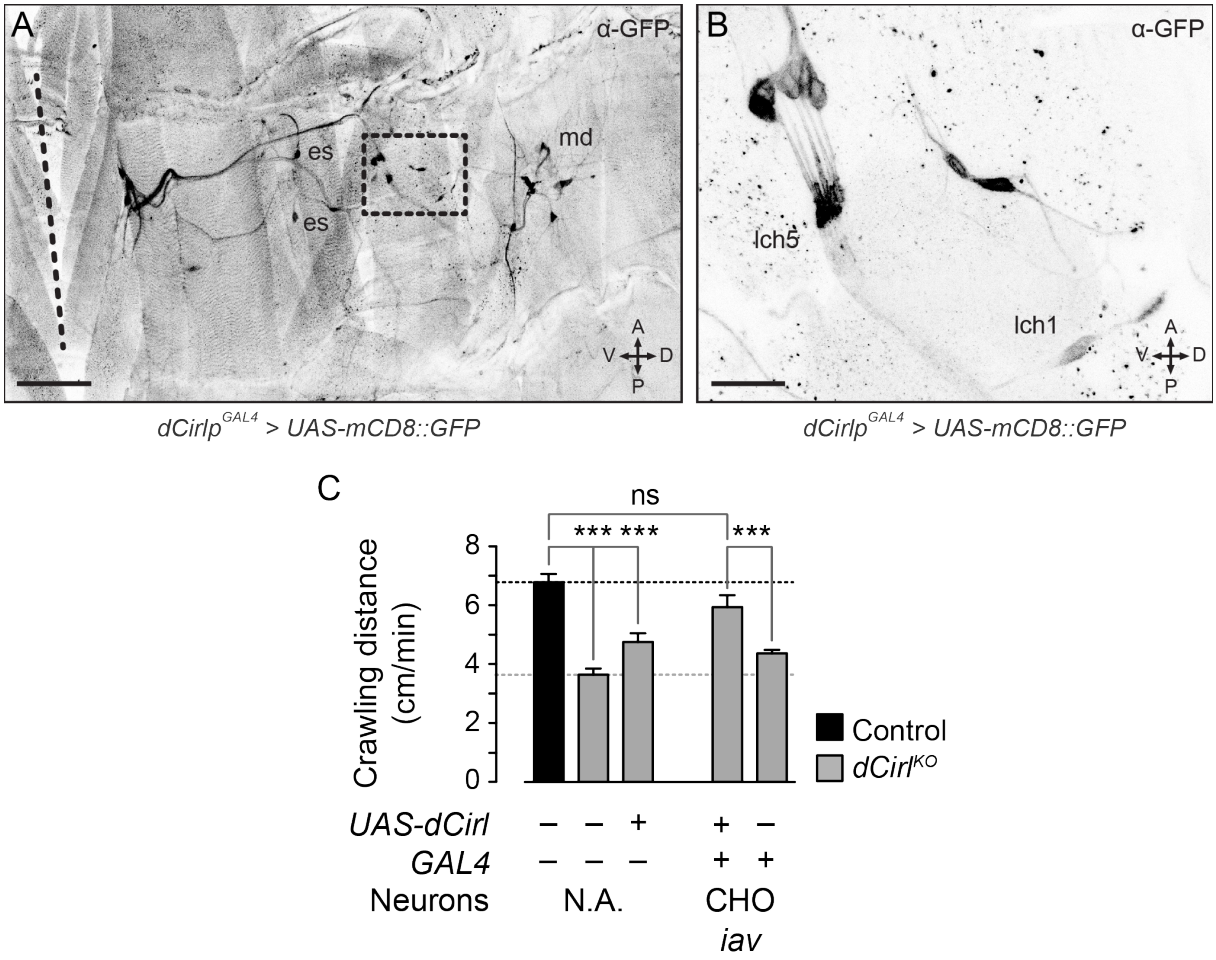

Figure 38. Peripheral chordotonal sensory neurons transcribe *dCirl* and require dCIRL for proper larval locomotion. A) Overview of *dCirl* expression in peripheral sensory neurons of larval a hemisegment visualized by *dCirlp*^{GAL4} specific anti-GFP expression (*UAS-mCD8::GFP*). *dCirl* was detected in type I external sensory neurons (es) and in lateral pentascolopidial and single chordotonal neurons (lch5 and lch1, respectively) as well as in type II multidendritic neurons (md). B) Prominent *dCirl* expression in lch5 and lch1 chordotonal organs. C) Confined re-expression of *dCirl* only in chordotonal organs partially rescued the crawling defect. Figure adapted from Scholz et al., 2015. Scale bar A = 100 µm, B = 20 µm. Data are presented as mean ± S.E.M. * $P \leq 0.05$, ** $P \leq 0.01$, *** $P \leq 0.001$. Scholz et al., 2015.

To independently investigate *dCirl* function in sensory neurons, touch sensitivity assay was performed, which robustly reported responsiveness of larvae towards gentle touch (Kernan et al., 1994; Caldwell et al., 2003). Consistent with a function of *dCirl* in chordotonal neuron, *dCirl* deficient larvae exerted decrease in touch sensitivity, a defect rescued upon reinsertion of *dCirl* (Scholz et al., 2015). In sum, these findings lead to the hypothesis that *dCirl* is necessary for the mechanoreceptive function of chordotonal neurons.

8.8. *dCirl* is expendable for protein décor and structural integrity of chordotonal organs

Mechanoreceptive properties of chordotonal organs are shaped by their distinct structural design. Nestled to a cylinder of scolopale cells, monodendritic chordotonal neurons are hooked to an apical cap cell through an extracellular matrix (aka dendritic cap) and a basal ligament cell thus constituting a sensory unit interlinked between muscle cells and the cuticle (Fig. 25D-F; Eberl, 1999). Each scolopidial unit is set up to mechanically couple the molecular machinery to muscle length changes, and isolate the neurons from their tissue environment. This presumably ensures constant conditions for the perception of mechanical stimuli through proper excitation of the bipolar neuron. In terms of chordotonal organ integrity and mechanosensory function several proteins have been identified. Consequently, their maldistribution or misregulation might underlie the examined mechanosensory defect of $dCirl^{KO}$ mutants.
To this end, expression and subcellular positioning of three well defined marker proteins were analyzed. All of them localize to the dendritic compartment that is responsible for sensing mechanical forces - the chordotonal cilium (Kernan, 2007). First, TRPN1 channel homolog NOMPC was visualized. NOMPC was proposed to act as a transducer channel that initiates receptor potentials through mechanical force-gated conduction of monovalent cations at the cilium (Walker et al., 2000; Cheng et al., 2010; Yan et al., 2013).

As in control samples, in $dCirl^{KO}$ specimen (and in $dCirl^{Flag}$ and $dCirl^{Rescue}$) NOMPC locates to the distal tip of each cilium within the pentascolopidial organ (Fig. 39A-G; Scholz et al., 2015).
In addition, the location of EYS/SPAM (*eyes shut/spacemaker*; Fig. 39B; Husain et al., 2006) a structural agrin/perlecan-related protein that encompasses the proximal cilium of chordotonal neurons and localizes to the membrane of the outer dendritic segment, did not differ between control and $dCirl^{KO}$ larvae (Fig. 39B-H; Scholz et al., 2015).

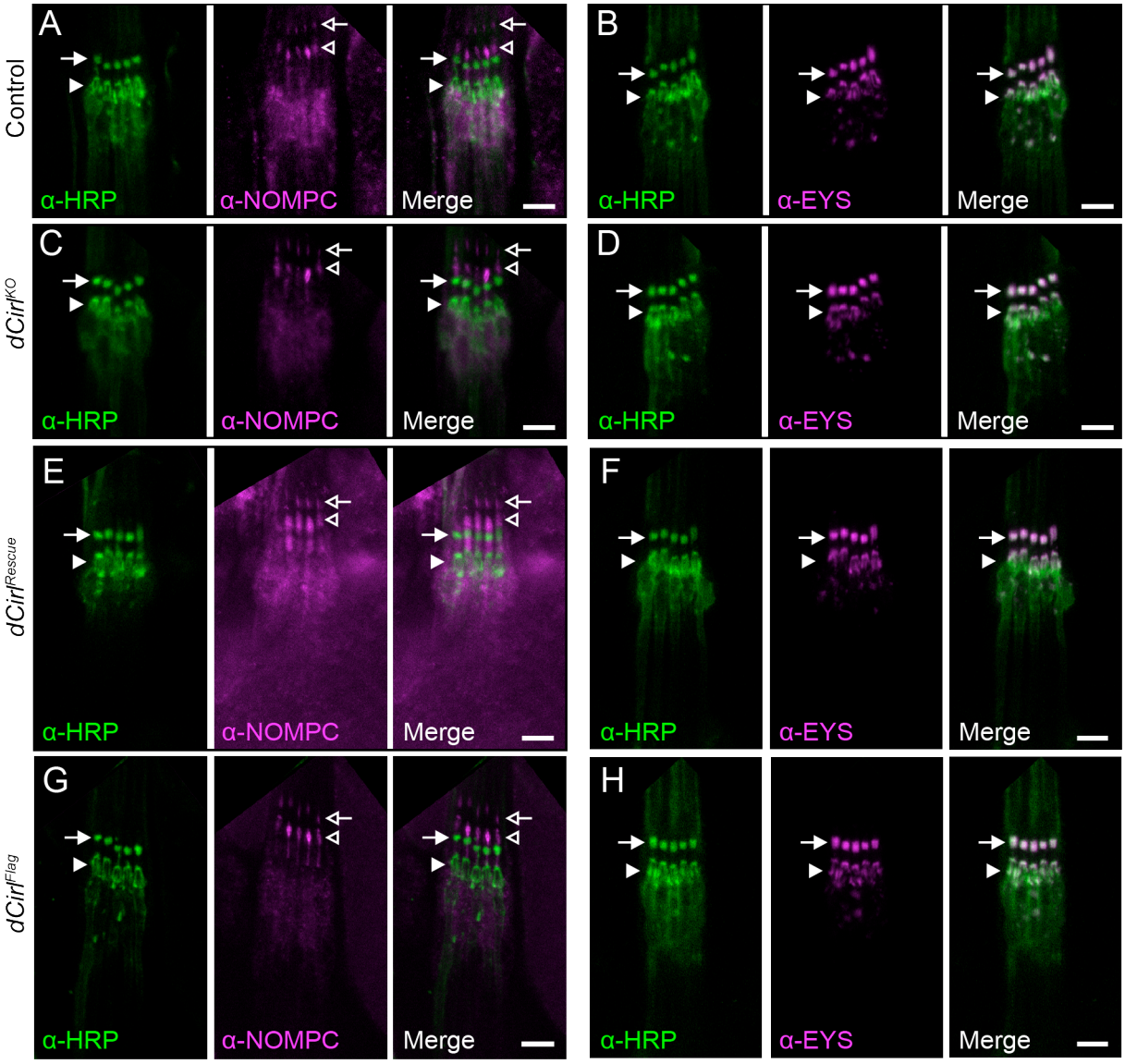

Figure 39. *dCirl* has no apparent impact on NOMPC and EYS distribution in chordotonal neurons. A-H) Localization of the markers HRP, NOMPC and EYS/SPAM in wild-type and *dCirl*^{KO} larval chordotonal neurons. C, D) NOMPC/TRPN1 is located in the distal portion of the cilium (open arrows) including the ciliary dilation (open arrowheads) and is indistinguishable between genotypes. E, F) EYS/SPAM form a collar around the cilium (closed arrows) beneath the ciliary dilation and mark the inner dendritic segment membrane (closed arrowheads). Figure adapted from Scholz et al., 2015. Scale bar = 5 µm.

Second, it was assessed whether the absence of *dCirl* impacts the structural integrity of chordotonal neurons. Expression of *20xUAS-IVS-mCD8::GFP* reporter under *iav-GAL4* control in either wild-type or *dCirl*^{KO} background was followed by immunostainings of GFP. This enabled inspection of the anatomy of the cells in question. FASII counter-labeling served to visualize longitudinal axon tracts that run through VNC and are innervated by chordotonal neuron afferents (Wu et al., 2011). No morphological changes could be observed in the somata and

dendrites of chordotonal neurons (Fig. 40A, B), and also the axonal processes of chordotonal neurons appeared comparable to controls (Fig. 40C, D; Scholz et al., 2015).

All in all, these findings expose that *dCirl* is not required for proper development and architecture of chordotonal sensory neurons.

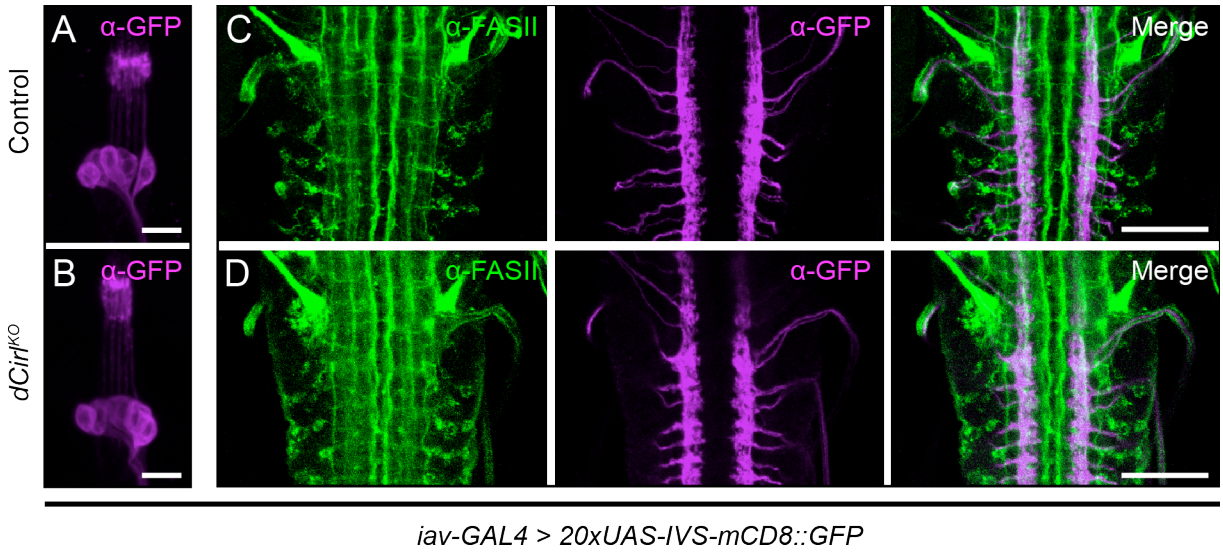

Figure 40. Gross chordotonal organ morphology is not affected by the loss of *dCirl*. A, B) Larval chordotonal neurons of the pentascolopidial organ are outlined by chordotonal neuron specific expression of GFP variant. No structural changes were observed between genotypes sampled. C, D) Afferent axonal projections of chordotonal neurons into the neuropile of the VNC and the internal structure of the VNC as visualized by α-FASII counter-immunostaining is not affected in $dCirl^{KO}$ larvae when compared with controls (Scholz et al., 2015). Scale bar A, B = 10 µm, C, D = 50 µm.

8.9. *dCirl* regulates responsiveness of chordotonal neurons to mechanical strain

Chordotonal organs are pivotal for detection of proprioceptive, tactile and acoustic stimuli. So far, we demonstrated that knock-out of *dCirl* influences chordotonal function in terms of altered proprioceptive and tactile perception that resulted in diminished locomotor activity and reduced sensitivity towards touch, respectively. To further corroborate that mechanical stimulation is the common sensory modality perceived by *dCirl* a third behavioral paradigm was employed that scored the response to the third mechanical quality detected by chordotonal organs – sound. Previously, this test was applied to *Drosophila* larvae to measure their response to natural occurring acoustic stimuli (Zhang et al., 2013). Here, a pure sine wave tone of 900 Hz, but with different amplitudes was applied to third instar larvae and subsequently

the elicited startle-freeze reaction was scored. Compared to controls *dCirl*^{KO} larvae displayed decreased startle response that was independent from sound pressure levels (SPL) applied (Fig. 41B; Suppl. Table 10). Importantly, this was also observed when the *dCirl* locus was uncovered using a deficiency (Fig. 41A; Suppl. Table 10). Importantly, rescue larvae recovered to wild-typic behavior in this paradigm (*dCirl*^{Rescue} and *dCirl*^{Flag}; Fig. 41A; Suppl. Table 10; Scholz et al., 2015).

Strikingly, at the lowest (50 dB) and highest (90 dB) sound intensities tested the responses of *dCirl*^{KO} and wild-type coincided, while this was not the case for lower volumes (60 dB and 70 dB) applied (Fig. 41A, B). Conclusively, in principal *dCirl*^{KO} mutants are able to perceive sound, which indicates that the mechanotransduction machinery is functionally intact. However, sensitivity of the transduction complex is reduced. This may indicate an increased gating threshold of chordotonal neurons in *dCirl*^{KO} larvae, which can be superseded by a higher SPL (Scholz et al., 2015).

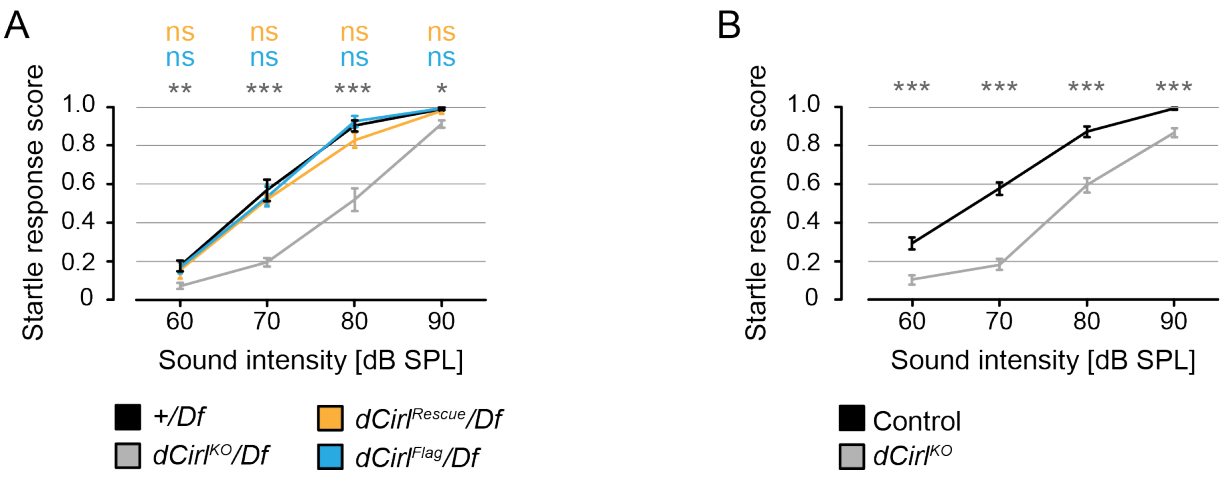

Figure 41. *dCirl* shapes the gating properties of the mechanotransduction machinery of chordotonal neurons. A, B) Larval sound-induces startle response of *+/Df, dCirl*^{KO}*/Df, dCirl*^{Rescue}*, dCirl*^{Flag} animals towards a 900 Hz sine tone with increasing amplitudes. Hemizygous (A) and homozygous (B) *dCirl*^{KO} animals display reduced responsiveness to sound, as judged by decrease in startle response. The defect is reversible by the reintroduction of either rescue allele. Data are presented as mean ± S.E.M. * $P \leq 0.05$, ** $P \leq 0.01$, *** $P \leq 0.001$. Scholz et al., 2015.

As the structure of chordotonal neurons of *dCirl*^{KO} mutants presented intact it was hypothesized that altered electrical activity in response to mechanical strain underlies the behavioral abnormalities observed. To address this conjecture C. Guan performed functional analysis of

chordotonal neurons and revealed several aspects. Cap cells of pentascolopidial organs were mechanically challenged at predetermined frequencies (100-1500 Hz) through piezoelectrically-actuated glass probe and electrical activity from the axon bundle was recorded simultaneously (Scholz et al., 2015). Previous work demonstrated that application of mechanical stimuli results in an increase in action current frequency (Zhang et al., 2013). In wild-type animals peak activity of neuronal responses was reached at stimulation frequencies around 900 Hz. In contrast, $dCirl^{KO}$ larvae exhibited significantly lower action current frequencies across the entire stimulation spectrum, although with a similarly shaped mechanical response curve peaking at 900 Hz as in control animals. $dCirl^{Rescue}$ larvae exhibited cho activity that was indistinguishable from controls (Scholz et al., 2015).
Sensory neurons depend on their ability to discriminate between spontaneous activity that occurs in the absence of stimulation and stimulus-evoked neuronal activity (discrimination ratio). Cell-specific re-expression of *dCirl* into chordotonal neurons of *dCirl* mutants did not rescue absolute firing frequencies, but only restored the relative action current ratio to wild-type levels (Scholz et al., 2015).

Altogether, the obtained data suggest a physiological role of *dCirl* at the level of the ionotropic mechanotransduction complex in chordotonal neurons. *dCirl* may thus shape the electrical response of chordotonal neurons upon application of mechanical force.

8.10. *dCirl* genetically interacts with constituents of the mechanotransduction complex

In order to corroborate this model genetic interactions of *dCirl* with components of the mechanical force sensing machinery were studied. For this purpose double mutants carrying hypomorphic alleles of TRPN1 ($nompC^{f00642}$; Sun et al., 2009), the TRPV channel subunit NANCHUNG (nan^{36a}; Kim et al., 2003) and EYS/SPAM ($eys^{BG02208}$; Husain et al., 2006) were combined with $dCirl^{KO}$ allele. NAN forms heteromeric complex with the IAV (inactive) subunit, which localizes to a proximal stretch of the cilium of chordotonal neurons (Gong et al., 2004). The precise role of either *nompC* and *nan* gene remains controversial, but both are undoubtedly involved in the transformation of mechanical stimuli into electrical impulses and in the fine-tuning of resting and generator currents in chordotonal cilia (Göpfert et al., 2006; Lehnert et al., 2013; Yan et al., 2013). EYS/SPAM, a protein which was shown to be required for the formation of the interrhabdomeral space (IRS) in *Drosophila* retina (Husain et al., 2006) also located to the proximal cilium of chordotonal neurons (Fig. 39B-H; Scholz et al.,

2015). However, knowledge about its exact function is still at large. To evaluate the epistatic relationship of these alleles with *dCirl*, crawling path lengths of single and double mutant larvae were measured.

Resembling $dCirl^{KO}$ behavior, $nompC^{f00642}$, nan^{36a} and $eys^{BG02208}$ mutant covered less distance with respect to control (control > $nompC^{f00642}$ > eys ^{BG02208} > $dCirl^{KO}$ > nan^{36a}; Fig. 42, Suppl. Table 9). This finding was prerequisite for examining the genetic interactions of *dCirl* with either hypomorphic allele. Importantly, crawling distances of all double mutants tested (i. $dCirl^{KO}$, $nompC^{f00642}$, ii. $dCirl^{KO}$; nan^{36a} *and* $dCirl^{KO}$, $eys^{BG02208}$), did not reveal simple additive effects (Fig. 42). This suggests that *nompC, nan* and *eys* act in series rather than in parallel to *dCirl*. However, the interdependency of *dCirl* with *trp* channels and *eys* diverge. The crawling distances of both $dCirl^{KO}$/*trp* channel double mutants matched those of $dCirl^{KO}$, hence $dCirl^{KO}$ behaved epistatically to $nompC^{f00642}$ and nan^{36a} implying that *dCirl* acts upstream of the *trp* subunits (Scholz et al., 2015). In contrast, distances covered by $dCirl^{KO}$, $eys^{BG02208}$ animals significantly exceeded those of $dCirl^{KO}$. Consequently, *eys* acts epistatically to *dCirl* indicating role upstream of *dCirl*.

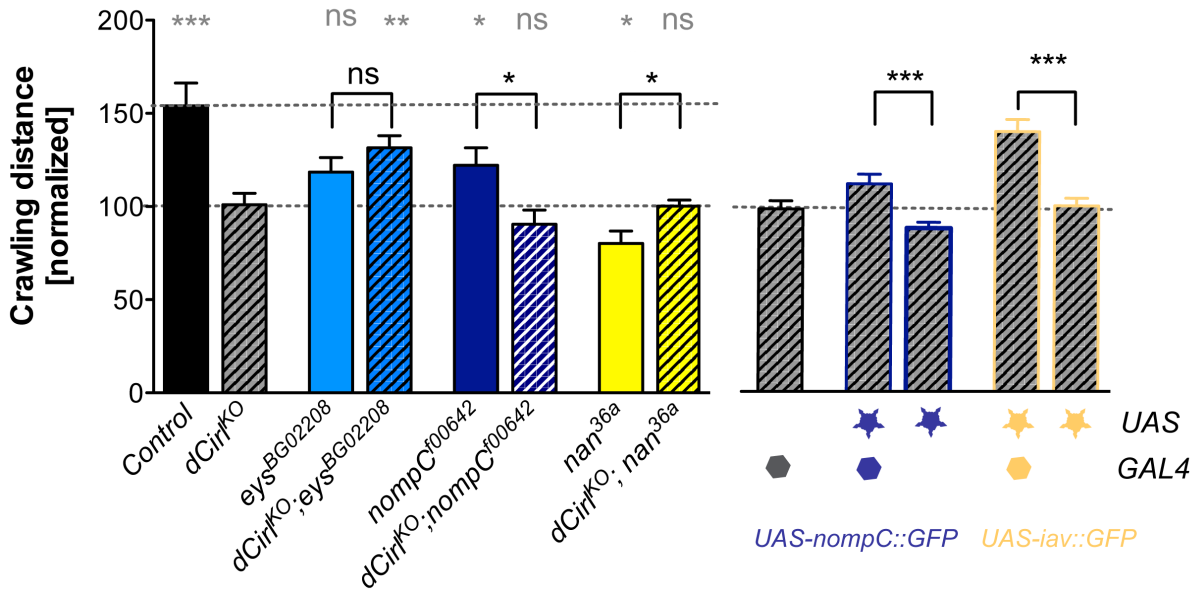

Figure 42. *dCirl* acts in one signaling pathway with elements of the mechanotransduction machinery. Left panel: Depicts investigation of genetic interaction of *dCirl* with cho-specific proteins. Grey dashed line indicates $dCirl^{KO}$ performance levels, to which the values of other genotypes were normalized. Oblique dashed columns depict genotypes with $dCirl^{KO}$ background. Right panel: *iav-GAL4* specific rescue of locomotion defect of $dCirl^{KO}$ through overexpression of *trp* channel subunits *nompC* (blue) and *iav* (orange). Values were each normalized to crawling distances of *iav-GAL4* in $dCirl^{KO}$ background (dashed grey line). Data are presented as mean ± S.E.M. * $P \leq 0.05$, ** $P \leq 0.01$, *** $P \leq 0.001$.

Next, *nompC::GFP* and *iaV::GFP* transgenes were overexpressed in chordotonal neurons of $dCirl^{KO}$ using *iav-GAL4* driver in order to test the notion that *dCirl* acts upstream of these components of the transduction machinery. Unfortunately, no *nan* transgene was available for *nan* overexpression. However, *nan* and *iav* are mutually required for channel targeting (Kim et al., 2003; Gong et al., 2004) and presumably for proper cilium function. Therefore, a *UAS-nan* allele was substituted with the *iav::GFP* reporter. This experiment revealed that increased levels of either *trp* subunit partially rescued the crawling impairment of $dCirl^{KO}$. This supports that overexpression of *trp* channel subunits circumvents the loss of *dCirl*. Thus, *dCirl* exerts its functions upstream of *nompC* and *iaV/nan* within the mechanosensory signaling cascade (Fig. 42). Excitingly, defects caused by loss of *dCirl* from $nompC^{f00642}$, nan^{36a} or eys^{BG0220} backgrounds differed substantially. As *dCirl* acts downstream of *eys*, removal of *dCirl* from $eys^{BG02208}$ background is not assayable, because $eys^{BG02208}$ might mask any phenotypes exhibited by *dCirl*. However, loss of *dCirl* minimized the net crawling distance of $dCirl^{KO}$, $nompC^{f00642}$ double mutant animals, whereas distances increased in $dCirl^{KO}$; nan^{36a} larvae displaying higher values than the respective single *trp* channel mutants (Fig. 42; Suppl.Table 9; Scholz et al., 2015).

This suggests that under physiological conditions *dCirl* adjusts the mechanotransduction complex. *dCirl* may facilitate *nompC* activity and reduce *nan* function. Further, *dCirl* function is potentially influenced by *eys*.

In sum, this series of experiments demonstrates that *dCirl* genetically interacts with pivotal elements of the mechanotransduction machinery in chordotonal cilia.

8.11. *Cis*-regulatory elements necessary for specialization of chordotonal cilia are present in the *dCirl* promotor

Based on the obtained genetic and functional data dCIRL most likely locates to chordotonal neurons, more specifically to the ciliated dendrites, where mechanosensitive TRP channels gate currents in response to mechanical strain (Gong et al., 2004; Yan et al., 2013). Because dCIRL location was not reliably detectable in immunostainings so far, alternative evidence for a putative ciliary abundance of dCIRL was obtained.

Recently, elegant work showed that transcriptional activators RFX and Fd3F often appear in context with genes involved in the ciliary specialization of mechanosensory neurons (Piasecki et al., 2010; Newton et al., 2012). RFX transcription factors comprise a characteristic winged helix DNA binding domain and recognize X-box promotor motifs of genes that regulate cilio-

genesis (Fig. 43; Swoboda et al., 2000) in sensory neurons including chordotonal neurons (Dubruille et al., 2002; Laurençon et al., 2007). The Forkhead box (Fox) transcription factor Fd3F, however, is a cell-specific transcriptional regulator that acts on a subset of chordotonal specific genes such as *nan* and *iav* (Fig. 43C). Interestingly, ciliated neurons specialized for mechanosensory stimuli detection, e.g. chordotonal cilia, are regulated by genes that contain closely spaced binding sites for both RFX and Fd3F in vicinity to their start sites (Newton et al., 2012).

To test whether *dCirl* possesses either RFX or Fd3F recognition sequence 2.2 kb intergentic region upstream of translational start site were analyzed (Emery et al., 1996; Laurençon et al., 2007). Intriguingly, the RFX and Fd3F tandem motif was identified in the region 200 bp upstream of *dCirls* translational initiation site (Fig. 43). Moreover, the RFX consensus sequence closely resembled that of other cilia-specific genes in *Drosophila*. Sequence alignments of both motifs in *dCirl* orthologs from 12 *Drosophila* species revealed an absolute conservation for Fd3F binding site, whereas RFX motif was present in the *melanogaster* subgroup of the *Sophophora* subgenus but not in the residual species (Fig. 43F). This finding suggests that *dCirl* function in cilia of chordotonal neurons is limited to *melanogaster* species (Scholz et al., 2015).

In conclusion, *dCirl* appears under transcriptional control of RFX and Fd3F. The presence of these *cis*-regulatory elements strongly implies dCIRL expression together with other genes, which functionalize ciliated chordotonal neurons for mechanosensation.

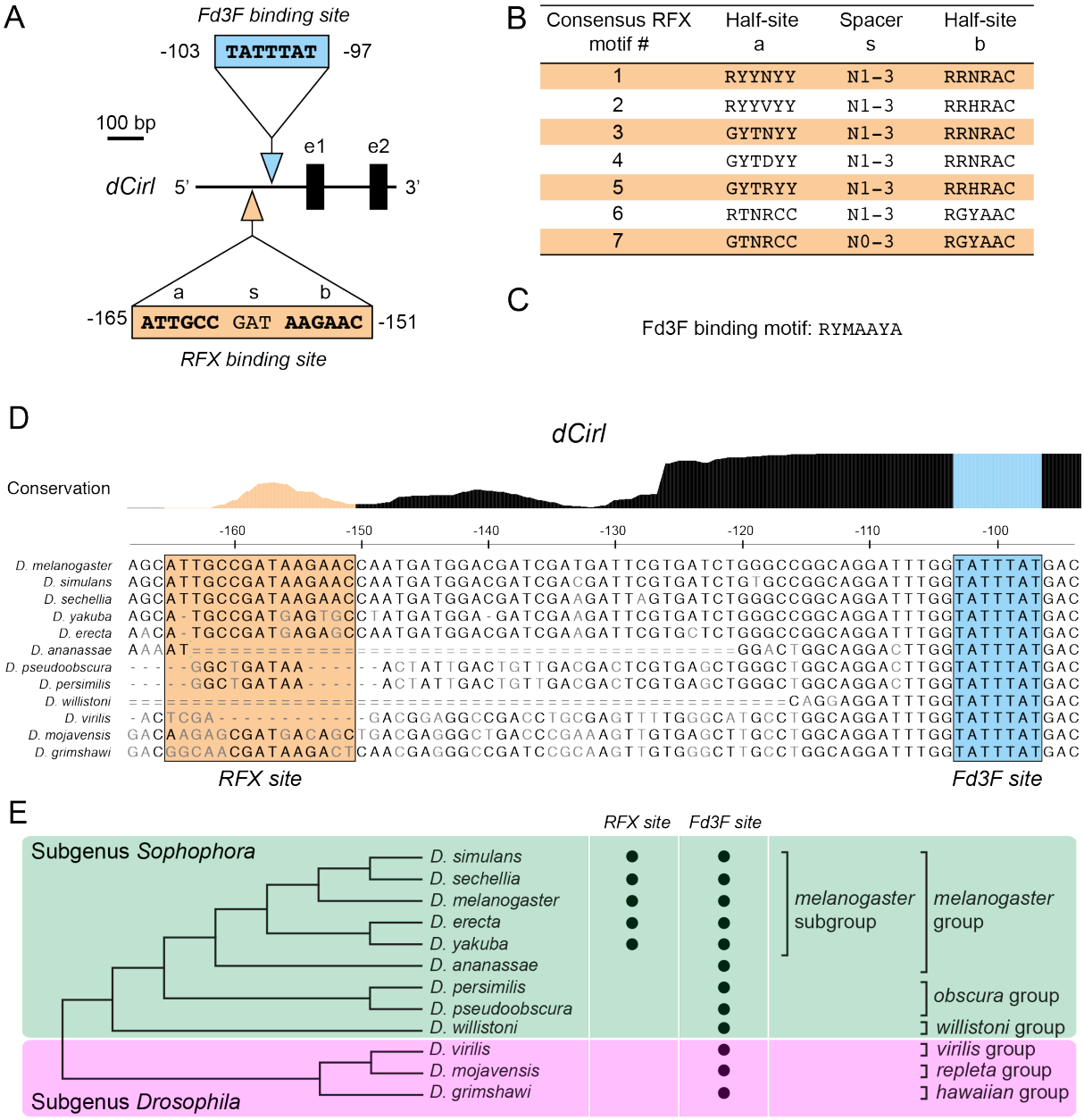

Figure 43. *dCirl* is part of a gene set that functionalizes chordotonal cilia for mechanoception. A) Sequence and position of putative RFX (orange arrowhead) and Fd3F binding sites exposed in the promotor region of *dCirl*. A and b half-sites of the X-box motif recognized by RFX activators (bold) are separated through a three-nucleotide spacer (s). e1 = exon 1, e2 = exon 2. B) Analysis if *dCirl* promotor region for RFX binding sites, which is constituted by X-box motif that consists of two half-sites recognized by the wings of the RFX DNA-binding domains. Nucleotide codes: D (A or G or T); H (A or C or T); M (A or C); N (any nucleotide); R (A or G); Y (C or T). C) Consensus sequence of Fd3F (Benayoun et al., 2008). D) Sequence alignment of genomic stretches from *Drosophila* orthologs to *dCirl* promotor that contains RFX and Fd3F sites. The latter is completely conserved, whereas RFX motif is only present in the *melanogaster* subgroup. Data exported from http://genome.ucsc.edu. Coordinates indicate relative position to the *dCirl* start codon in *D. melanogaster*. E) Depicts summary of RFX and Fd3F binding sites in promotor region of *dCirl* orthologs. Phylogram adapted from Clark et al., 2007. Figure A-D from Scholz et al., 2015.

9. Discussion

9.1. Investigation of *dCirl's in vivo* function

In contrast to the comprehensive pharmacological and physiological knowledge of other GPCR classes, aGPCR - although constituting the second largest group of the GPCR superfamily (Fredriksson et al., 2003) - have remained poorly defined both in signal input and output rendering their functions and signaling rationales elusive.

This study provides the first functional analysis of Latrophilin/*dCirl*, which is one of only two aGPCR expressed in *Drosophila*. Employing genetic analyses, bioinformatics, immunohistochemistry and behavioral paradigms it was demonstrated that *dCirl* is largely expendable for motoneuron function, but instead performs in mechanosensation of peripheral sensory neurons.

9.1.1. *dCirl*^{KO} animals develop normally and structural integrity of the nervous system is preserved

So far, the vast majority of aGPCR have remained orphaned with poorly defined *in vivo* functions. However, previously, mutations in members of the aGPCR class were associated with pathological conditions in humans (Langenhan et al., 2013). For instance, mammalian GPR56 is required for proper cortex development. Loss of *gpr56* results in a condition called bilateral frontoparietal polymicroglia (BFPP), which is characterized by abnormal gyral patterning and lamination, subsequently resulting in cerebral malformation (Piao et al., 2004; Bae et al., 2014). Also, development in the absence of *vlgr1* causes sensineural defects (McGee et al., 2006) that underlie a disease referred to as Usher syndrome (Weston et al., 2004). In zebrafish and mouse GPR126 was shown to be required in Schwann cells to initiate myelination (Monk et al., 2009; Patra et al., 2014). In addition, in mice GPR126 plays a role in heart development, a defect not observed in zebrafish (Waller-Evans et al., 2010). Follow-up studies argue that the CTF of GPR126 is not essential for cardiac development, while the NTF is sufficient to rescue both myelination and cardiovascular pathologies (Patra et al., 2014).

Beside *dCirl* the *Drosophila* genome encodes one other aGPCR – the invertebrate CELSR ortholog *flamingo/Starry night.* Flamingo (FMI) bridges adjacent cells through formation of intercellular homodimers and instructively recruits PCP core components (frizzled, Van

Gogh) across cell borders to propagate PCP signals from cell to cell. Accordingly, loss of FMI distorts planar cell polarity and leads to severe morphological defects (Usui et al., 1999; Curtin et al., 2003; Chen et al., 2008). Similarly, in *C. elegans* Latrophilin/LAT-1 governs tissue polarization during embryogenesis (Langenhan et al., 2009), whereas Flamingo/*fmi-1* controls the navigation of pioneer and follower axons (Steimel et al., 2010). Strikingly, a considerable number of aGPCR have been documented to be required for developmental aspects. Interestingly, and surprisingly we did not observe alterations in gross maturation of $dCirl^{KO}$ animals as they develop at normal pace and number. Furthermore, overt morphological integrity of the nervous system seemed not compromised by the removal of *dCirl*. Hence, *dCirl* is not required for normal development of the nervous system of *Drosophila melanogaster* (Scholz et al., 2015).

However, morphological alteration of the postsynaptic SSR was observed in $dCirl^{KO}$ animals, a defect rescued through re-expression of *dCirl*. The enlargement of the SSR was accompanied by increased levels of DLG, a scaffolding protein with known a function in the regulation of SSR dimension (Budnik et al., 1996; Mendoza-Topaz et al., 2008). So far, the causal link between dCIRL function and altered muscle morphology or DLG function is completely enigmatic and thus calls for further investigation.

9.1.2. Expression profile of dCIRL in larval and adult stage

The first step towards the comprehension of *dCirl* function was the identification of dCIRL positive neurons. An antibody raised against a peptide in the extracellular domain of dCIRL was insufficient for immunohistochemistry, but engineering of specific transgenes enabled the expression of dCIRL fusion proteins (dCIRL::RFP and dCIRL::FLAG) under endogenous transcriptional control (Fig. 30). Similarly, location of dCIRL::RFP and dCIRL::FLAG was not detectable by confocal microscopy consistent with low endogenous expression profile of dCIRL. Interestingly, visualization of other aGPCR appears problematic as well. Detection of several GPCR, such as LAT-1 in *C. elegans*, GPR126 in mouse and β2-adrenergic receptor in humans proved very challenging because of their low copy number (Khorana, 1992; Kobilka and Deupi, 2007; Langenhan et al., 2009; Waller-Evans et al., 2010). To avert constitutive signaling GPCR often undergo agonist-induced feedback desensitization, a mechanism that assures responsiveness of the receptor. Several mechanisms that contribute to this receptor attenuation have been reported and include receptor endocytosis and subsequent internaliza-

tion, down-regulation of relevant GPCR transcription and translation, and also post-translational modifications (e.g. phosphorylation; Ferguson, 2001; Gainetdinov et al., 2004). Moreover, desensitization is regulated by agonist affinity (Ferguson, 2001), a concept that enables the cell to distinguish between background activity (noise) and essential activity (signal), the latter being subsequently amplified to ensure efficient signal transduction.
Hence, scarce expression levels of GPCR may present a consequence of a single or multiple of the above listed mechanisms.

To amplify signal strength mono- and polyclonal antibodies were used to detect the FLAG- and mRFP tag, respectively. Application of both antibodies revealed strong dCIRL signal in larval VNCs, however with differences in intensity (Gehring, 2014). dCIRL::RFP labeling appeared stronger than dCIRL::FLAG, presumably caused through recognition of multiple epitopes by the polyclonal RFP antibody. Within the VNC, dCIRL co-localized with BRP, which highlights presynaptic AZs (Kittel et al., 2006b; Wagh et al., 2006). Importantly, judged from co-localization with HRP, which labels neuronal plasma membranes, dCIRL fusion protein was properly delivered to the cell surface.
Consistently, dCIRL was visualized at the membrane of perikarya in adult fly brains (Fig. 31C, C', C''). However, dCIRL no longer co-localized with BRP. Instead, dCIRL was present in somata-rich regions but absent from synapse-rich neuropils, constituting an inverse expression profile compared to larval VNC (data from larvae shown in Gehring, 2014). The fly CNS becomes drastically reorganized as the animal matures (Hartenstein, 1993). Considerable amounts of larval neurons persist throughout development, but they show pronounced remodeling. Moreover, a multitude of adult-specific neurons are added to the basic configuration of larvae (Truman, 1990), which might explain varied protein localization.

In addition to cell somata, dCIRL was found in the γ-lobes of the mushroom body and faintly yet detectably in the fan shaped body (Fig. 31A, B, B', B'', 32), both involved in a variety of biological processes. The mushroom body was identified to be required for memory formation, but also in the control of spontaneous motor activity (Ito et al., 1998; Zars et al., 2000). The fan shaped body is part of the central complex and has been implicated in coordination of motor behavior, spatial orientation and memory of spatial orientation (Heinze and Homberg, 2007; Poeck et al., 2007; Neuser et al., 2008). Both brain structures participate in different aspects of locomotion, which may represent common ground for *dCirl* function.

In sum, the evidence suggests that dCIRL is broadly expressed throughout the central nervous system of larval and adult flies.

Although location of LPHN1-3 has not been identified *in vivo* so far, previous northern blot experiments using rat tissue indicated that *LPHN1* and *LPHN3* are almost exclusively expressed in the brain. In contrast, *LPHN2* was ubiquitously detected, but with a prevalence beyond the nervous system (e.g. liver, lung, placenta, kidney, spleen and heart; Sugita et al., 1998; Ichtchenko et al., 1999). Immunoblotting experiments of LPNH1 and LPNH3 from brain and liver membranes, respectively, validated these findings and implicate that latrophilin transcript localization concurs with protein residence (Matsushita et al., 1999). Interestingly, however, mammalian latrophilin homologs possess a common structural layout yet their tissue distribution differs substantially (Matsushita et al., 1999), indicating distinct functional specificity between these homologs.

Latrophilin is one of 17 aGPCR receptors detected in the CNS, which accounts for more than half of the entire aGPCR class (Strokes and Piao, 2010). However, detailed cellular expression profiles are available for only a minority of these receptors.
VLGR1 (aGPCR family IX) expression is confined to the embryonic central nervous system, inner ear and the eye of the mouse (McMillan et al., 2002), residences consistent with its requirement in developing photoreceptor cells and cochlear hair cells (McGee et al., 2006; Maerker et al., 2007). Further, brain-specific angiogenesis inhibitors 1-3 (BAI1-3; aGPCR family VII) are involved in regulation of brain angiogenesis and myoblast fusion and are expressed most prominently in the brain (Park and Ravichandran, 2010; Cork and Van Meir, 2011; Hochreiter-Hufford et al., 2013). Transcription from the *BAI1* locus was detected in fetal and adult brains and is presumably inhibited by p53, whereas *BAI2* and *BAI3* are additionally found in skeletal muscles and in the heart (Shiratsuchi et al., 1997; Mori et al., 2002).
FMI and its vertebrate counterparts (CELSRs; aGPCR family IV) are widely expressed throughout embryonic brain tissues. However, during development each homolog was shown to be distinctly located within the CNS resulting in a characteristic expression pattern (Shima et al., 2002).
Several aGPCR are also expressed outside the nervous system indicating a high degree of tissue dependent functional specificity of receptor homologs. For example, CD97, one of the founding members of the EGF-7TM family, is expressed in a number of tissues including macrophages, dendritic cells and T cells (Jaspars et al., 2001). Further, GPR116, which was

recently associated with a function in the regulation of the pulmonary surfactant pool size is additionally expressed in heart and kidneys (Bjarnadóttir et al., 2007; Bridges et al., 2013). Moreover, several aGPCR [e.g. GPR56 (Liu et al., 1999), GPR126 (Waller-Evans et al., 2010; Paavola et al., 2011), BAI2 (Kee et al., 2002)] are expressed in and beyond the nervous system.

aGPCR have been noticed for their intense splicing activities (Bjarnadóttir et al., 2007), which offer an additional level of receptor function diversification. For example, GPR123 shows alternative splicing that differs between grey and white matter of the CNS, leading to the assumption that the resulting isoforms serve different functions in these brain compartments (Mills et al., 2013). Moreover, latrophilin homologs from mammals and insects display extensive splicing potential that may result in isoforms that differentially interact with ligands. This mechanism has been demonstrated for CD97 and EMR2 (Hamann et al., 1998; Stacey et al., 2003), which are massively modified at the 7TM or at the C-terminus (Matsushita et al., 1999; Langenhan et al., 2009). Interestingly, public sources of *Drosophila* cDNA and EST data sets indicate the existence of *dCirl* mRNA species with a 7TM and 1TM (Fig. 44), confirmed through RT-PCR from *Drosophila* cDNA libraries (Fig. 44B; unpublished data). However, it remains to be explored if isoforms are expressed in different organs and whether they mediate different activities.

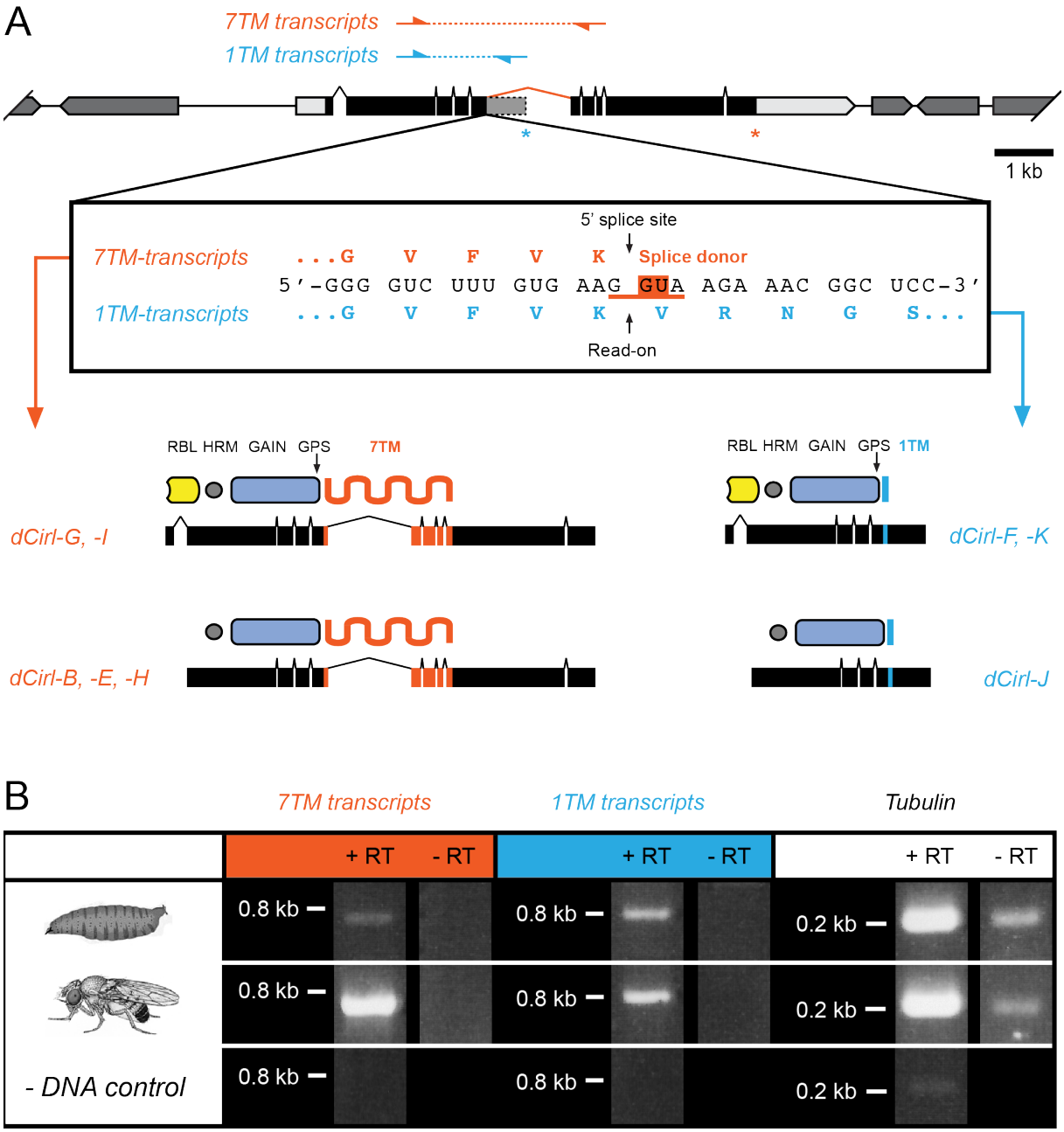

Figure 44. In *Drosophila* a single *dCirl* gene encodes at least two disparate receptor isoforms. A) Schematic of *dCirl* locus with putative splice isoforms predicted from cDNA sequence and EST data. *dCirl* transcripts with 7TM (orange) and 1TM domain (blue). 1TM receptor variant results from a read-on splicing event extending the reading frame into an intron (dashed white box). Both transcript categories possess individual mRNA species that encode either full RBL domain or truncated version that is unlikely to fold properly. Primer positions used to detect splice-specific fragments are indicated above with dashes lines; asterisks indicate the position of stop codons. B) 7TM and 1TM transcripts were detected by RT-PCR from cDNA libraries of larval and adult *Drosophila*. Absence of genomic DNA from RNA fractions was controlled for by omitting reverse transcriptase from the reaction (-RT control).

Finally, the presented data demonstrate the wide distribution of the invertebrate homolog of latrophilin - *dCirl* - within the central nervous system in different developmental stages of *Drosophila*.

9.1.3. Removal of *dCirl* disrupts larval locomotion

Crawling of foraging *Drosophila* larvae follows a stereotypic behavioral pattern consisting of linear forward locomotion phases interspersed by periods of pausing, which are defined as decision making phases (Wang et al., 1997). Observation of $dCirl^{KO}$ larvae revealed an altered locomotion pattern characterized by delayed onset of linear movement and prolonged decision-making periods with excessive head turning (Fig. 33; Scholz et al., 2015). A complex neuronal circuit comprised of CPG neurons, motoneurons and sensory neurons underlies this behavior (Caldwell et al., 2003; Song et al., 2007). Sensory afferents convey electrical signals from the periphery into the CNS, where they are implemented into the GPG network ensuring proper instruction of motoneuronal efferents, which subsequently transmit nerve impulses to the effector organs, the muscles (Suster and Bate, 2002; Caldwell et al., 2003; Cheng et al., 2010). Therefore, it was hypothesized that the movement of $dCirl^{KO}$ larvae is curtailed due to defective motoneuronal innervation. Alternatively larvae may move improperly due to the alteration in the perception of internal and/or external cues that ultimately lead to changes in the sensory input into the motor program.

Several lines of evidence suggest that motoneurons function largely independent of *dCirl.* First, in contrast to the broad dCIRL expression in larval VNCs detection at NMJs of either motoneuron type failed or was not reliably reproducible. This may result from scarce dCIRL expression. Alternatively, varying distribution of different dCIRL splice variants may contribute to inconsistency in staining experiments.
Second, another member of the aGPCR class - GPR126 - is required for development of Schwann cells in vertebrates (Monk et al., 2009). For this reason, glia-specific expression of GFP was employed to visualize peripheral glia that wraps the motoraxons in control and *dCirl* mutant larvae. Morphology of axon capping glia appeared indistinguishable between genotypes (Fig. 37) suggesting that motoneurons of $dCirl^{KO}$ larvae are properly supplied with nutrients and electrical insulation a prerequisite for proper function of these cells.
Third, synaptic and overall morphology of the NMJ was unaffected by the loss of *dCirl* (Fig. 36). Moreover, electrophysiological recordings largely exclude that synaptic release and

membrane excitability is affected by *dCirl* function (unpublished data). This data is consistent with previous findings, which indicated that knock-down of LPNH3 in mouse somatosensory cortex has no impact on synaptic release probability (O'Sullivan et al., 2014). It is noteworthy however, that the frequency of spontaneous vesicular release was slightly increased in $dCirl^{KO}$ larvae. Interestingly, a similar effect was observed in Synapsin null mutants (syn^{97}; unpublished data) coinciding with a slight reduction of SYN concentration at NMJ of $dCirl^{KO}$ mutants (data not shown), which may account for the slight decrease in spontaneous quantal release frequency.

In sum, the results suggest that motoneuron morphology and function is intact in $dCirl^{KO}$ mutants and thus does not cause crawling deficit observed in these animals.

However, the structural abnormality of the postsynaptic subsynaptic reticulum (SSR), an elaborate membrane system that underlies the membrane of the postsynapse of glutamatergic type I boutons (Lahey et al., 1994), was identified. This phenotype was initially detected by immunostainings against the scaffolding protein DLG (Thomas et al., 1997). This protein is associated with pre-and postsynaptic membranes. Stainings were not consistently reproducible. However, ultrastructural analysis of mutant and control NMJs (performed by N. Wagner) confirmed that a considerable fraction of animals displayed a SSR enlargement, which was rescued upon re-establishment of the wild-type *dCirl* sequence. This affirmed that the structural defect was associated to the loss of *dCirl* (data not shown). The finding was independently confirmed by western blots and subsequent analysis of DLG protein amounts. Previous studies showed that DLG is involved in neurotransmitter release and development of postsynaptic SSR structure at the NMJ (Budnik et al., 1996). Changes in synaptic transmission solely result from presynaptic loss of DLG (Budnik et al., 1996). In contrast, postsynaptic DLG determines the SSR size. *dlg* mutants display a downsized SSR, whereas *dlg* overexpression causes massive SSR extension (Lahey et al., 1994; Budnik et al., 1996). Hence, loss of *dCirl* may cause overproduction of postsynaptic DLG, which in turn may lead to SSR outgrowth. Importantly, presynaptic properties and postsynaptic glutamate receptor density were unchanged uncoupling dCirl's effect on DLG from synapse function. Also, note that DLG distribution and abundance was unchanged in adult brains of *dCirl* mutants, as was the morphology of the brain (Fig. 35C-F). The regulatory relationship between *dCirl* and *dlg* is enigmatic, but it is tempting to speculate that *dCirl* directly or indirectly inhibits *dlg* expression and thereby modifies postsynaptic NMJ morphology.

9.1.4. *dCirl* is required for the perception of mechanical stimuli through chordotonal sensory neurons

As removal of *dCirl* did not compromise the function of motor efferents, attention was directed to the peripheral sensory system. Strikingly, multiple lines of evidence suggest that *dCirl* is required for proper mechanosensation through specialized sensory cells accommodated in chordotonal organs. Elicited by sound/vibrations, mechanical deformation of body wall muscles during locomotion, or gentle touch as a tactile stimulus, chordotonal organs constitute mechanosensory devices essential for delivery of sensory feedback into the central nervous system (Caldwell et al., 2003; Hughes and Thomas, 2007).

Defined transcriptional recognition motifs (RFX and Fd3F) are frequently identified for proteins that determine the specialization of cilia of mechanosensory neurons (Newton et al., 2012). RFX transcription factor appears active in ciliated chordotonal neurons amongst others (Dubruille et al., 2002; Laurençon et al., 2007). In contrast, Fd3F activity is restricted to chordotonal neurons. A RFX/Fd3F recognition sequence tandem was identified in the *dCirl* promotor, not only in *D. melanogaster* but also in several other *Drosophila* species (Fig. 43D, E). This transcriptional fingerprint has been found for a number of genes that contribute to mechanosensitive specialization of chordotonal cilia, including *nan* and *iav* (Newton et al., 2012). This evidence suggests participation of *dCirl* in functional specialization of chordotonal cilium together with several other proteins.

Chordotonal organs possess an intricate structure that ultimately shapes their functional properties (Fig. 28; Eberl and Boekhoff-Falk, 2007). Based on the assessment of immunostainings against ciliary proteins [e.g. NOMPC (Walker et al., 2000), EYS/SPAM (Husain et al., 2006)] proper morphology of dendritic cilia was verified (Fig. 39). Furthermore, no structural abnormalities of chordotonal neuron somata, peripheral dendrites and sensory afferents were detected (Fig. 40). Therefore, *dCirl* is dispensable for chordotonal neuron development and morphology (Scholz et al., 2015). This finding further supports the conclusion that *dCirl* is not required for developmental aspects in *Drosophila*, but executes critical function beyond development.

Transcriptional activity from *dCirl* locus was located in multiple sensory neurons, but with the most prominent label in the lateral chordotonal organs. In accord with a function of *dCirl* in this mechanosensory cell type, perception of all mechanical qualities appeared disrupted as

judged from several independent behavioral paradigms. Importantly, wild-typic response to all mechanical stimuli were scored after reconstitution of the *dCirl* locus in the mutant background. However, restricted re-expression of *dCirl* only in chordotonal neurons suggests a more complex relation of *dCirl* function in these sensory cells.

Previous work demonstrated that sensitivity towards touch was inhibited only after silencing a combination of multidendritic and chordotonal neurons, but not by inhibiting any specific subset of neurons (Titlow et al., 2014). In particular, responsiveness of type II multidendritic arborization neurons towards gentle touch has been shown recently (Yan et al., 2013). However, despite its widespread distribution in peripheral sensory neurons application of gentle touch paradigm (Kernan et al., 1994) revealed that expression of *dCirl* solely in chordotonal neurons was sufficient to partially rescue touch sensitivity defect. Inversely, confined re-introduction of *dCirl* in multidendritic neurons did not alter the mutant phenotype, clearly indicating that *dCirl* acts exclusively in chordotonal organs to ensure proper touch sensation (Scholz et al., 2015). Cho-specific expression of *dCirl* in mutant background also resulted in partial rescue of the motility phenotype. Two hypotheses may explain this finding: First, larval crawling requires simultaneous function of *dCirl* in chordotonal sensory neurons and mutidendritic neurons as generation of larval locomotion depends on input from both sensory neuron types (Caldwell et al., 2003; Song et al., 2007). Second, *dCirl* exerts its function cell-autonomously and -non-autonomously (Chen et al., 2008; Steimel et al., 2010; Nishimura et al., 2012), and both modes are required for proper larval locomotion. Indeed, the overall aGPCR layout strongly implies receptor function with (Bohnekamp and Schöneberg, 2011) and also without G-protein coupling through the CTF. This cell non-autonomous signaling may be achieved via engagement of dCIRL's NTF with molecules on adjacent cells and/or alternatively with interactors at distant tissues via circulating soluble NTFs. This signaling mode was described for Latrophilin 1 (Krasnoperov et al., 2009) and LAT-1 from *C. elegans* (Prömel et al., 2012), but also for a vast number of other aGPCR members [e.g. CD97 (Gray et al., 1996), GPR126 (Patra et al., 2014) and BAI1/2 (Kaur et al., 2005; Okajima et al., 2010)].

Reflected in latencies on a submillisecond timescale (Corey and Hudspeth, 1979; Chalfie, 2009), electrical responses generated by the chordotonal neurons are presumably the result of direct force-dependent ion gating mediated by the mechanosensory machinery (Nadrowski et al., 2008; Zhang et al., 2013). Certainly, the structural properties of *dCirl* do not imply a function as an ionotropic transducer molecule. It is much more likely, that dCIRL acts in molecu-

lar signaling cascade, which allows the targeted modulation of effector molecules that generate action currents in response to mechanical challenge. Potential targets are DEG/ENaC (Degenerin/Epithelial Sodium Channel) subunit (Zhong et al., 2010), K^+ channels [*shaker* (Gu et al., 2001)*; TREK-1* (Dedman et al., 2009)] and TRP channels.

The analyses of the genetic interaction of *dCirl* with TRP channels provide an intriguing model, in which *dCirl* modulates gating properties of molecular components of the mechanotransduction complex (*nompC*, *nan*), while *dCirl* itself is potentially regulated by *eys/spam*. Interestingly, *nan* and *nompC* appeared inversely modulated by *dCirl* (Scholz et al., 2015), which may provide the functional versatility required for a dynamic regulation of action current generation upon mechanical challenge.

Interplay between GPCR and TRP channel function has been reported earlier. PKA and PKC kinase dependent control of TRP phosphorylation states appear to adjust the activation threshold and the open probability of the TRP channel complexes (Vay et al., 2011). Additionally, *in vitro* observations of mechanically activated GPCR signals suggest that metabotropic modulation of TRP channel gated ion fluxes are feasible (Schnitzler et al., 2008). Notwithstanding its attractive implications, this model requires further elucidation through the application of alternative behavioral paradigms and electrophysiological recordings from chordotonal sensory neurons of double mutants ($dCirl^{KO}$, $nompC^{f00642}$; $dCirl^{KO}$, nan^{36a}; and $dCirl^{KO}$, $eys^{BG02208}$). Furthermore, it remains to be resolved whether TRP channel subunits are directly modulated by *dCirl* or if additional steps are interposed. Identification and disruption of putative post-translational modification sites (e.g. phosphorylation sites) within TRP channel subunits should help to answer this question. While this study focused on *dCirl/trp* channel interplay, in the future it will be of interest if DEG/ENaC or K^+ channels are targeted by *dCirl* or other members of the aGPCR class.

In conclusion, here, I propose that the activity of *dCirl* is adjusted by mechanical force, which either leads to the modulation of the molecular mechanotransduction machinery or results in alteration of action current coding. Both scenarios ultimately converge on a change of sensorineural amplitudes and kinetics that may underlie graded regulation of *dCirl* positive sensory nerve cells as well as the extraction of essential mechanosensory information from background noise.

9.1.5. A novel role for Adhesion-GPCR as metabotropic mechanosensors

Canonical GPCR classically serve as the showpiece example for the cellular perception of external stimuli. In this model soluble ligands are recognized through externally exposed interaction interface of cognate receptor molecules. Instantaneous conformational changes result in an intracellular biochemical response carried out by heterotrimeric G-proteins, β-arrestin and receptor-associated kinases (Pierce et al., 2002). Due to the chemical nature of known activators, GPRC are commonly considered chemosensors. The idea that GPCR are suitable to detect and transduce physical modalities such as physical strain has been largely neglected thus far.

However, *in vitro* studies indicate that metabotropic activity of individual GPCR may be regulated through mechanical force. For example, the bradykinin 2 (B_2) receptor undergoes conformational changes in response to shear stress, changes in osmolarity and alteration of plasma membrane viscosity in endogenous ligand-independent fashion. Although, *in vivo* confirmation is not at hand, this force-dependent effect may contribute to the physiology of endothelial cells (Chachisvilis et al., 2006). Further, angiotensin II type 1 (AT_1) receptor responds to stretch with activity, and that is in the absence of its native ligand. This effect impacts the regulation of vascular myogenic tone (Schnitzler et al., 2008) and cardiac remodeling upon pressure overload (Zou et al., 2004). Importantly, both physiological processes rely on the cells' ability to constantly adapt to cyclic changes in mechanical load. Interestingly, beside integrins, cadherins and L-type voltage-sensitive Ca^{2+} channels GPCR were also suggested to be involved in mechanotransduction pathways of osteoblastic cells and therefore may play role in skeletal homeostasis and/or bone formation (Liedert et al., 2006). In sum, GPCRs may actually comprise a wider perception profile that is not limited to chemical activators, but is susceptible to mechanical stimulation as well. The physiological role of this receptivity was uncovered in Latrophilin*/dCirl* for the first time, but remains unknown for other aGPCR and GPCR.

The structural basis of an involvement of aGPCR in mechanotransduction is different from other GPCR. Physical contact of the receptor with the extracellular matrix is the linchpin of mechanical force application and may thus be a prerequisite to mechanically based signal transmission into cells (Ingber, 1991). In contrast to other GPCR classes, aGPCR interact with cellular and matricellular ligands (Hamann et al., 1996). Importantly, except for interaction between collagen type IV and GPR126 (Paavola et al., 2014) and laminin-211 and GPR126 (Petersen et al., 2015) ligand/aGPCR interactions proved inadequate to trigger intracellular

signaling cascades or were not examined in this virtue (Langenhan et al., 2013). Hence, receptor activation through soluble ligands is not feasible.

Based on the presented data, it was concluded that mechanical load is a co-requirement to elicit response of dCIRL, one of the oldest receptors among aGPCR. Strikingly, other aGPCR have been associated with mechanosensation. GPR56 was shown to be involved in a signaling pathway involved in the regulation of overload-induced muscle hypertrophy (White et al., 2014). In addition, recently GPR126, necessary for Schwann cell development and myelination in zebrafish and mouse, was demonstrated to induce cAMP elevation upon application of dynamic forces or vibration stimuli *in vitro* (Petersen et al., 2015).
Furthermore, *Celsr1* another prototypic receptor of this class, assures proper tissue polarity of neurons of the inner ear sensory epithelium (Curtin et al., 2003). VLGR1 forms connections between ankle regions of neighboring stereocilia at inner and outer hair cells of the cochlea (McGee et al., 2006). Furthermore, during photoreceptor development VLGR1 constitutes fibrous links that connect cilia to the apical inner segment membranes (Maerker et al., 2007). Loss of VLGR1 function in humans results in deafness and progressive retinis pigmentosa, collectively referred to type II Usher Syndrome (Weston et al., 2004). However, the putative biological role of CELSR1 and VLGR1 in a cellularly differentiated environment has not been studied so far.

Last but not least, the molecular blueprint of aGPCR further supports the putative predisposition for the perception of mechanical stimulation. All aGPCR are characterized by the juxtamembraneously located GAIN domain that appears to be vital in several ways: First, the GAIN domain holds the GPS motif, which imparts autoproteolytic enzymatic activity (Lin et al., 2004). Second, GAIN domain itself provides a ligand interaction interface and third, NTF and CTF are kept in assembly through clamping function of the GAIN domain (Araç et al., 2012; Wandel et al., 2012; Prömel et al., 2013). Interestingly, the only other molecule that contains this aGPCR hallmark is PKD-l (Ponting et al., 1999). PKD-1 is crucial for epithelial cilia function and is activated by fluid-evoked shear stress demonstrated for the mechanoreceptivity of this receptor (Nauli et al., 2008). However, the precise role of the GAIN domain in this process is not clear. Langenhan et al., 2013 suggested that NTF/CTF cleavage of aGPCR through autoproteolysis and subsequent re-attachment introduces a predetermined break point. This may possess a protective purpose, similar to the autoproteolytic sea urchin sperm protein-enterokinase-agrin (SEA) domain of mucins (Matsui et al., 1998; Macao et al., 2006).

Moreover, examination of other aGPCR such as EGF-TM7 and BAI homologs, as well as GPR56 revealed enhancement of metabotropic activity levels due to absence of NTF. Besides its stimulatory effect, mechanical strain exerted through receptor-ligand contact plays an essential role in aGPCR internalization (Karpus et al., 2013). Thus, aGPRC may constitute a receptors class tuned for mechanical challenges.

The current study documents multiple lines of evidence that show that *dCirl* primarily functions in mechanoception through sensory neurons. The identification of adequate physiological receptor stimulation is one key aspect towards an advanced understanding of aGPCR signaling. To shed light on the significance of aGPCR function, linkage of receptor stimulation with downstream pathways is crucially required to unravel general signaling mechanisms relevant for the entire aGPCR class.

10. General Material & Methods

10.1. Molecular biology

10.1.1. Materials

All reagents used in this study were, if not stated otherwise, purchased from Roth (Karlsruhe), Sigma (Diesenhofen) or Merck (Darmstadt). Most type II restriction endonucleases were purchased from New England Biolabs (Frankfurt). DNA polymerases were ordered from Eurogentec (AccuStar™, Cologne, Germany), Qiagen (*Taq* Polymerase Master Mix Kit, Hilden), and New England Biolabs (Q5® High Fidelity, Frankfurt). T4 ligase, Antarctic Phosphatase and T4 polynucleotide kinase were purchased from Roche (Mannheim). Furthermore, Gateway® enzyme mix was sourced from Invitrogen (Karlsruhe).
DNA extraction was performed using kits from either Macherey-Nagel (Düren) or Qiagen (Hilden). Amplification of DNA was established using chemically competent *E. coli* cells (Genotype *recA1 endA1 gyrA96 thi-1; hsdR17 supE44 relA1 lac [F′ proAB laqq ZΔM15 Tn10 (Tet′)]*. All PCR reactions were conducted using the Thermo cycler T3, T3000 or UNOII (Biometra, Göttingen).

10.1.2. Transgene engineering

In this study the Gateway® recombining cloning technology (Invitrogen, Karlsruhe) was used in conjunction with the *Drosophila* Gateway™ Vector collection, provided by the Murphy lab (Carnegie Institution of Washington, Baltimore), to engineer various DNA constructs.

Part I

pNH 28 (mBRP$^{C\text{-}tip}$)

AmCFP was amplified from pTL304 (Clontech Laboratories Inc., USA) using primer pair nh_56F/nh_57R and cloned into pENTR™3C (Invitrogen, Cat.No.: A10464) with *KpnI* and *XhoI* (pNH27). Nh_57R contained the last C-terminal 17 aa of BRP. LR-based recombination of pNH27 and expression plasmid TFW, which provided the 5'- prime 3xFlag-tag, led to pNH28.

pNH54 (CFP)

Primers nh_56F and nh_75R were used to amplify amCFP from pNH28. The resulting *XhoI*/*KpnI* fragment was cloned into pENTR^{TM}3C (pNH53). Subsequently, LR reaction with pTFW resulted in pNH54.

pNH42 (Control: mCD8::EGFP)

mCD8::EGFP was amplified from pTL231 using primers tl_330F and nh_02R. The resultant 1,4 kb fragment, which carried 3'-prime Kozak sequence was cloned into pENTR^{TM}3C using *DraI* and *XhoI* (pNH32). Next, the insert was cloned into pTW-attB using LR recombination reaction resulting in expression construct pNH42.

pNH39 (BRP$^{C\text{-}tip}$)

As before mCD8::EGFP was amplified from pTL231. Primers tl_330F and nh_03R were used to add 5'-prime Kozak sequence, 3'-prime 5x glycine linker and a sequence encoding the last C-terminal 17 aa of BRP. Amplicon insertion into pENTR^{TM}3C was done using *DraI* and *XhoI* (pNH33). LR recombination into pTW-attB led to expression construct pNH39.

pNH46 (BRP$^{C\text{-}medium}$)

0.9 kb fragment, encoding the C-terminal last 294 aa of BRP (BRP$^{C\text{-}medium}$), was amplified from pTL319 with primers nh_23F and nh_24R. The PCR fragment was subjected to a double digest with *DraI* and *XbaI* before subsequent ligation with pNH43. The resultant ENTRY clone (pNH38) was recombined with pTW-attB and led to pNH46.

pNH52 (BRP$^{C\text{-}long}$)

PCR amplification of BRP$^{C\text{-}long}$ from pTL319 was carried out using primers nh_25F and nh_24R. The following steps were identical to those of generation of BRP$^{C\text{-}medium}$. ENTRY clone pNH51; expression construct pNH52.

pNH60 (mRFP::SYT)

SYT amplification from pTL143 was performed using primers nh_94F and nh_95R. mRFP was amplified from pNH11 using nh_96F and nh_97R. Both PCR fragments were cloned into pTW-attB using *XhoI*, *NheI* and *AgeI* via triple liagtion (pNH60).

Part II

Generation of transgenes used in this thesis is elucidated in Scholz et al., 2015.

All custom designed oligonucleotides were manufactured by MWG-Biotech (Ebersberg, Germany) and were, except for primers used for annealing procedure (100 pmol/µl), used in 20 pmol/µl concentration. All PCR amplified DNA fragments were sequenced by MWG-Biotech (Ebersberg, Germany).

Primer	Sequence 5´- 3´orientation
tl_330F	TACACTTTTAAATATCAACATGGCCTCACCGTTGACCCGCT
nh_02R	CCGCTCGAGCTACTTGTACAGCTCGTCCATGCCGAGA
nh_03R	CCGCTCGAGCTAGAAAAAGCTCTTCAAGAAGCCAGCTGGTCCAGCA TCCTGCTGTTGCTGTTGCTGTCCGCCTCCGCCTCCGGGCTTGTAC
nh_23F	CCCAAGCTTATGCAGCAGCAGATGC
nh_24R	CTAGTCTAGACTAGAAAAAGCTCTTCAAGAAGCCAGCT
nh_25F	CCCAAGCTTGAGTTCGAAAAGATGCTGGAGAAGTAC
nh_27F	CGCCGGGATCACTCTCGGCATGGAC
nh_28R	CAGCTGGAGCTGTCGAAGGGCGAGG
nh_29F	GGCTGCAGCGGCGGCAGGAGCGAGT
nh_56F	CGGGGTACCATCAACATGGCCCTGTCCAACAAGTTCATCG
nh_57R	CGCGGATCCCCACGATCGCGAGTTCATACCCATT
nh_75R	CCGCTCGAGCTAGAAGGGCACCACGGAGGTGATGTGG
nh_90F	GCCCTCGAGATGGCCTCCTCCGAGGACGTCATCA
nh_92F	CAACTGCAACTACTGAAATCTGC
nh_93R	CCCGCCCACCAATGACGCTC
nh_94F	GCCCTCGAGATGCCGCCAAATGCAA
nh_95R	TCGGCTAGCTTACTTCATGTTCTTCAGGATCTCG
nh_96F	TAACCGGTCAACATGGCCTCCTCCGAGGACGTCATCA
nh_97R	CCGCTCGAGCGCAGCTGCAGCAGCGGCGCCGGTGGAGTGGCGGCCC TCG
nh_181R	CGCTCCCATCGAGCGTTGAAG
nh_182R	CGGAGGAGGCCATCTCGAG

10.2. *Drosophila melanogaster*

10.2.1. Fly cultivation

Drosophila stocks were generally raised at 18 °C on standard cornmeal food (1l H_20, 4,5 g Agar, 20 g beet syrup, 72,2 g malt, 9 g soy flour, 16,3 g yeast, 72,2 g corn flour, 1,45 g nipagine, 5,7 g propionic acid). Crosses were, if not stated otherwise, raised at 25 °C.

10.2.2. Transgenesis

Drosophila germ line transformation of transgenic DNA constructs was performed by Best-Gene Inc. (California, USA) either by conventional P-Element transformation (Rubin and Spradling, 1982), which occurs randomly or by site directed ΦC31 method (Groth et al., 2004). The site specific integrase from phage ΦC31 mediates recombination between bacterial attachment site (*att*B) and a phage attachment site (*att*P; Thorpe and Smith, 1998; Thorpe et al., 2000; Groth et al., 2004). Specific integration sites attP40 (second chromosome, cyto site 25C6; Markstein et al., 2008) and attP2 (BDSC Stock# 8622; third chromosome, cyto site 68A4; Groth et al., 2004) were used for transgene insertion on second or third chromosome, respectively.

10.2.3. Fly genetics

All fly strains used in this study are listed below. Stocks ordered from Bloomington Stock Center, CA, USA are indicated by *. All RNAi strains used were purchased from Vienna *Drosophila* Research Center (VDRC; Dietzl et al., 2007).

Name	Genetic background	Landing pad/ Expression	Reference
Transgenes			
RJK 181	w^{-};; Cpx^{1257}/TM6c Tb;		Iyer et al., 2013
RJK 187	w^{-};; Cpx^{Sh1}/TM6c Tb;		Huntwork, Littleton, 2007
BRP 38	w^{1118}; brp^{nude}/CyOact-GFPw^{+}		Hallermann et al., 2010b
BRP 34	w^{1118};brp^{69}/CyO act-GFPw^{+}		Kittel et al., 2006b
TAG 70	w^{1118};; UAS-mCD8::EGFP::$Brp^{C\text{-}tip}$ w^{+}/TM3 Sb;	attP2; 68A4	
TAG 77	w^{1118};; UAS-mCD8::EGFP w^{+}/TM3 Sb;	attP2; 68A4	
TAG 86	w^{1118};; UAS-mCD8::EGFP::$Brp^{C\text{-}medium}$ w^{+}/TM3 Sb;	attP2; 68A4	
TAG 118	w^{1118};; UAS-mCD8::EGFP::$Brp^{C\text{-}long}$ w^{+}/TM3 Sb;	attP2; 68A4	
TAG 151	w^{1118}; mRFP::Syt w^{+}/Cyo;;	attP40; 25C7	
TAG61	w^{1118}; UAS-3xFlag::amCFP::$mBrp^{C17}$ w^{+}/CyO;;		
TAG126	w^{1118}; P{UAS-3xFlag::amCFP w^{+}}/Cyo;;		
LAT 01	w^{1118};+;P{pTL161$^{Cirl\ targeting\ vector}$}$w^{+}$/TM3 Sb		
LAT 26	w^{1118};$Cirl^{108/11A}${attP+loxP}w^{-}/CyOGFPw^{-};		Scholz et al., 2015
LAT 54	w^{1118};$Cirl^{108/11A}$ {attP+ loxP-mW-loxP}w^{+}		

LAT 56	w^{1118};$Cirl^{108/11A}$ {attP+ loxP+}w^{-}, att{Cirl::mRFPw^{+}}^{attPLAT41};		
LAT 67	w^{1118};$Cirl^{108/11A}$ {attP+ loxP+} w^{-}, att{Cirl::Flag w^{+}}^{attPLAT};		
LAT 79	w^{1118};$Cirl^{108/11A}$ {attP+ loxP+}w^{-};att{Cirl w^{+}}[attPLAT];		Scholz et al., 2015
LAT 111	w^{1118};$Cirl^{108/11A}$ {attP+ loxP+}w^{-}/CyOGFPw-; 20xUAS-dCirl::Flag w^{+}/TM6B, Tb		
LAT 113	w^{1118};$Cirl^{108/11A}$ attP+ loxP+}w^{-}/CyOGFPw-; P{y[+t7.7] w[+mC]=20XUAS-IVS-mCD8::GFP}^{attP2}/TM6B, Tb		
LAT 118	w^{1118};;attP{5xUAS-dCirl::HA w^{+}} ^{attP2}/TM3, Sb		
GN 17	w^{1118};P{UAS-CD4::tdGFP}^{VK00033}		Han et al., 2011; BDSC #35836*
GN 67	w^{1118};PBac{WH}nompC^{f00642} w^{+}/CyO; TM6b/MKRS		Sun et al., 2003
GN 71	w^{1118};;nan^{36a}		Kim et al., 2003; BDSC #24902*
GN 74	w^{1118};P{w[+mGT]=GT1}$eys^{BG02208}$;		Zelhof et al., 2006; BDSC #12661*
GN 91	UAS-nompC::GFP/CyO;nompC-Gal4		Göpfert M.
GAL4			
cha	w^{1118}; cha-GAL4.7.4/CyO, P{ry[+t7.2]=sevRas1.V12}FK1;;	cholinergic	Salvaterra et al., 2001
elav	w^{-} elav-GAL4w^{+};;;	panneuronal	Yao et al., 1994
ok6	w^{-}; ok6-GAL4w^{+};;	motoneuronal	Sanyal et al., 2009
ok107	w^{-}; ok107-GAL4 w^{+};;	mushroom body	Connolly et al., 1996
iav	w^{-};; iaV-GAL4 w^{+};	cho neurons	Senthilan P.
c232	w^{-};; c232-GAL4 w^{+};	ring neurons	Renn et al., 1999
vGAT	w^{-} ;;vgat-GAL4;	gabaergic	Fei et al., 2010
Vglut	w^{-} vglut-GAL4;;;	glutamatergic	Daniels et al., 2008
RNAi			
dunc-13	w^{*}; P{GD9877}v33606;;		v33606
tomosyn	w^{*};; P{GD8641}v43629;		v43629
cpx	w^{*};; P{GD10482}v21477;		v21477
dCirl	w^{*}; P{GD14785}v29969;;		v29969
dCAPS	w^{*}; P{GD9502}v25291;;		v25291
csp	w^{*}; P{KK109431}v103201;;		v103201
syt-12	w^{*}; P{GD1171}v47506;;		v47506
syt-7	w^{*};; P{GD8644}v24988;		v24988

rim	*w**; P{GD15273}v39384;;	v39384
rab3-GAP	*w**;; P{GD12118}v27824/TM3;	v27824
gdi	*w**;; P{GD11312}v26537/TM3;	v26537
rph	*w**; P{GD7330}v52438;;	v52438
mutant	*w** *rab27*$^{GAL4\text{-}KO}$;;;	Chan et al., 2011
rab5	*w**;; P{GD10492}v34094;	v34094
rac-1	*w** P{GD7330}v52438;;;	v52438
sng-1	*w**; P{GD3785}v8784;;	v8784
syn	*w**;; P{KK108941}VIE-260B;	VIE-260B
annB9	*w**;; P{GD11750}v27493;	v27493
annB10	*w**;; P{GD14255}v36107;	v36107
twf	*w**;; P{GD10342}v25817;	v25817
dysb	*w**;; P{GD10754}v34354;	v34354
atg-1	*w**;; P{GD7149}v16133;	v16133
rsk	*w**; P{GD1254}v5702;;	v5702
sap47	*w**; P{GD12534}v35445;;	v35445
dsyd-1	*w**;; P{GD12383}v35346;	v35346
Vglut	*w**; P{GD834}v2574;;	v2574
Vti1A	*w**; P{GD2233}v45726;;	v45726

10.2.4. Isolation and purification of genomic DNA

Isolation of genomic DNA from *Drosophila* larvae and adult flies was done by mechanic shredding of the probe in 100 µl squishing buffer with proteinase K (200µg/ml). Incubation for 30 min at 37 °C was followed by inactivation of proteinase K at 95 °C for 3 min. Finally, the emulsion was centrifuged to solve the genomic DNA in the aqueous phase, which was collected separately.

10.3. Cell culture

Originally Schneider cells (S2 cells) were obtained from embryonal primary culture (Schneider, 1972). S2 cells were cultured sterile at 24 °C under CO_2 exclusion.

In this study S2 cells served as heterologous expression system to verify functionality of transgenes prior to germ line transformation. Expression vectors tested in S2 cells contained a GAL4 responsive UAS-promotor element (Brand and Perrimon, 1993). Therefore, reporter

and driver constructs (*Actin-GAL4*) were co-transfected using lipofectamine® (Invitrogen, Karlsruhe) to allowed reliable transgene verification.

10.4. Immunohistochemistry

10.4.1. Materials

Dissection of larval body wall muscles was performed in hemolymph-like saline solution (HL-3) without $CaCl_2$: NaCl 70 mM, KCl 5 mM, $MgCl_2$ 5 mM, $NaHCO_3$ 10 mM, trehalose 5 mM, sucrose 115 mM, HEPES 5 mM, ad 500 ml H_2O, pH 7,2 (Stewart et al., 1994).
Fixation of muscle filets was done using 4 % paraformaldehyde (PFA): 2 g PFA ad 18 ml H_2O (58 °C), 1 N NaOH, 25 ml 0,15 M KH_2PO_4, 6 ml 0,15 M $NaHPO_4$, pH 7.4.
Staining of larval NMJs was carried out in 1x PBS with 0.05 % Triton X-100 (10x PBS: 74 g NaCl, 12,46 g Na_2HPO_4 x 2 H_2O, 4,14 g NaH_2PO_4 x H_20, add 1 l H_2O, pH 7.4).

Larval whole brains were dissected in Ca^{2+}-free HL-3 and subsequently fixed in 1x PBS with 4 % PFA. Staining and washing steps were performed in 1x PBS containing 0.1 % Triton X-100 in ThinCert® Cell culture insets for 24-well plates (8 µm pore diameter; Greiner Bio-One, Kremsmünster, Austria). VNC's were embedded in 1 µl Vectashield (Vector Laboratories, California, USA) in double stacks of reinforcement washers.

Whole-mount adult brains were dissected in *Drosophila* Ringer's solution (Cold Spring Harb Protoc 2007): 3 mM $CaCl_2$ x 2 H_2O, 182 mM KCl, 46 mM NaCl, 10 mM Tris base, pH 7. Preparations were performed in 50 mm dishes filled with sylgard (SylGard 182 Silicone Elastomer Kit; Dow Corning).
Freshly prepared brains were fixed using 4 % PFA in 1x PBS with 0.3 % Triton X-100. Downstream washing steps were performed with 1x PBS with 0.3 % Triton X-100 or 1x PBS with 1% Triton X-100 depending on the antibody used. Similar as for larval brains, staining and washing procedures were realized using was 24-well plate insets.

10.4.2. Preparation of larval body wall muscles

Wandering third instar larvae (96 - 120 h post hatching at 25 °C) were placed in a drop of ice-cold Ca^{2+}-free HL-3 on a rubber pad and fixed with minutien pins (0.1 x 10 mm, FST, Heidelberg, Germany) at the anterior and posterior end. The larva was opened up making a fine incision at the posterior end, followed by dorsal cut along the midline towards the anterior end

using fine spring scissors (FST, Heidelberg, German). The cuticle was pinned down with two pins at each side exposing the larva's insides. With fine forceps (No5 and No5.5. FST, Heidelberg, Germany) the viscera were separated from the ventral body wall, which then openly displayed the nervous system and ventral body wall muscles.

10.4.3. Preparation of whole-mount brains from *Drosophila* larvae and adult flies

For the isolation of larval brain basically the same procedure as for muscle filet was executed. Additionally, motoneurons and surrounding tissue were carefully removed using spring scissors and forceps. Finally, the brain was transferred to 24-well plate inset.

For dissection of adult brains three-day-old female flies were anaesthetized on ice, placed on the sylgard-filled petri dish, affixed through the thorax and abdomen (ventral side upward) using minutien pins (0.1 x 10 mm) and covered with ice-cold *Drosophila* Ringer's solution. Through slight pulling the proboscis was forced to extend, the esophagus was severed using scissors. The large silvery tracheae were removed from the head capsule until the brain became visible. Next, very fine forceps (5.5 FST, Heidelberg, Germany) were used to "peel" of the head capsule. At best, the brain remained attached to the thorax, while removing residual tracheae. Before transferring the brain to 24-well plate inset for fixation, the brain was carefully separated from the head connective.

10.4.4. Fixation and staining procedures

10.4.4.1. Larval body wall muscles

Muscle filets were fixed for 10 min in 4 % PFA in 1x PBS, which was followed by 30 min blocking step using PBT containing 5 % normal goat serum (NGS). Subsequently, the samples were incubated with primary antibody/PBT/NGS solution over night at 4 °C. The following day the samples were rinsed twice and washed 3 x 20 min with PBT before secondary antibody/PBT/NGS mixture was applied and incubated for 2 h at 25 °C. Again, the specimens were rinsed and washed before application of Vectashield, which was left on over night at 4 °C to dehydrate the probes. Finally, filets were embedded using Vectashield, dorsal side facing upwards, covered with cover slip and sealed with nail polish.
Samples from different genotypes were marked and incubated together. Furthermore, all incubations, except for the Vectashield incubation, were performed while rotating the samples to ensure uniform antibody accessibility.

10.4.4.2. Larval pentascolopidial organ

Larvae were dissected and fixed as described in 10.4.2. The blocking step was carried out over night at 4 °C using 1 % PBT that contained 2 % BSA and 5 % NGS. Next, primary antibodies were added to fresh blocking solution and incubated for 24 h at 4 °C. Subsequently, samples were washed 4 x for 30 min with PBS containing 0.1 % Tween. Secondary antibodies were diluted in PBS (0.1 % Tween, 2 % BSA, 5 % NGS) and incubated over night at 4 °C. Samples were washed 4 x for 30 min with PBS containing 0.1 % Tween and stored in Vectashield over night before mounting.

10.4.4.3. Larval and adult brain specimen

Larval brains were fixed for 10 min in 4 % PFA. Adult brains were kept in 4 % PFA (1x PBS with 0.3 % Triton) for at least 30 min up to one hour. Subsequent to 90 min blocking (5 % NGS/PBT, 25 °C) the samples underwent over night incubation (4 °C) of primary antibody diluted in blocking solution. The next day the samples were washed four times for 30 min and incubated with secondary antibody over night (4 °C). The following day the probes were washed and subjected to Vectashield incubation (4 °C, over night) before mounting in Vectashield on cover slips prepared with reinforcement washers.
Brains of different genotypes were parallel incubated with mixture of antibody solutions to keep intra-experimental staining heterogeneity at a minimum.

10.4.5. Preparation and cryosectioning of adult *Drosophila* heads

Whole fly heads were fixed in 4% PFA for 3 hours at 25 °C and then washed once with 0.3 % PBT (PBS with 0.3% Triton-X). Next, they were transferred into 25 % sucrose-containing Ringer's solution and incubated over night at 4 °C. The following day, the samples were embedded in Cryo-Gel™ (for horizontal and/or vertical sections; Instrumedics Inc., St. Louis, USA), rapidly frozen using methyl butane and liquid nitrogen and incubated for 1 h at 20 °C to ensure proper Cryo-Gel™ texture. Subsequently, 20 µm brain sections were prepared using cryostat (Leica Microssystems CM3050) and picked up using superfrost object slides (Thermo Scientific, Braunschweig, Germany). Finally, the slices were air-dried for at least 30 min or at best over night. To keep staining solutions on the slices samples were encircled using PAP Pen – liquid blocker (Science Services).

10.4.6. Fixation and staining procedures of cryosections

Blocking solution (5 % NGS in 0.1-1 % PBT) was incubated for 90 min at 25 °C and carefully replaced by 0.1-1 % PBT containing 5 % NGS and primary antibodies, which was kept on over night at 4 °C. The following day samples were washed thoroughly (3x rinsed and 3 x 20 min) before applying secondary antibody solution (0.1-1 % PBT, 5 % NGS solution dosed with antibodies). After 2 h incubation period (25 °C) antibody solution was removed again, samples were washed (3x rinsed and 3 x 20 min) and mounted in Vectashield.

Antibody	Species/Dilution	Reference	Antigen
Primary			
Nc82	mouse/1:250	Prof. E. Buchner (Uni of Würzburg)	BRP
Anti-GFP	rabbit/1:500	Invitrogen (Karlsruhe)	GFP
Anti-GFP	mouse/1:500	Sigma-Aldrich (St. Louis, USA)	GFP
Anti-RFP	rabbit/1:500	Antikoerper-online.de (Aachen, Germany)	RFP
Anti-Flag	mouse/1:500	Sigma-Aldrich (St. Louis, USA)	FLAG
Anti-HA	rat/1:500	Roche (Mannheim, Germany)	HEMAGGLUTININ
Anti-Dlg	mouse/1:500	Developmental Studies Hybridoma Bank (Iowa, USA)	DLG
Anti-GluRIID	rabbit/1:500	Prof. Stefan Sigrist (FU Berlin)	GLURIID
Anti-Repo	mouse/1:20	Developmental Studies Hybridoma Bank (Iowa, USA)	REPO
Anti-NompC	mouse/1:200	Prof. Martin Göpfert (Göttingen)	NOMPC
Anti-Eys	mouse/1:20	Developmental Studies Hybridoma Bank (Iowa, USA)	EYS
Anti-Futsch	mouse/1:250	Developmental Studies Hybridoma Bank (Iowa, USA)	FUTSCH
Anti-FasciclinII	mouse/1:250	Developmental Studies Hybridoma Bank (Iowa, USA)	FASII
Anti-Spectrin	mouse/1:250	Developmental Studies Hybridoma Bank (Iowa, USA)	SPECTRIN
Anti-Syt	rabbit/1:3000	Mackler et al., 2002	SYT
Anti-dVglut$^{N\text{-}term}$	Rabbit/1:500	Prof. A. DiAntonio (Uni of St. Louis)	dVGLUT
Secondary			
Alexa 488	rabbit/1:250	Invitrogen (Karlsruhe)	-
Alexa 488	mouse/1:250	Invitrogen (Karlsruhe)	-
Alexa 488	rat/1:250		
Cy3	rabbit/1:250	Dianova (Hamburg)	-
Cy3	mouse/1:250	Dianova (Hamburg)	-
HRP-Cy3	goat/1:250	Dianova (Hamburg)	HRP

10.5. Imaging

10.5.1. Confocal microscopy

Confocal image acquisition was done using line scanning confocal LSM 5 system (Zeiss, Germany). Microscopy of NMJ stainings was performed utilizing Plan-Neofluar 63x/1.25 and 40x/1.30 oil immersion objectives. For acquisition of overview images of larval and adult brains EC Pan-Neofluar 10x/0.3 and 20x/0.5 air objective was used, while capture of close-up images of specific brain structures required the 63x/1.25 or 40x/1.30 oil immersion objective. All objectives were purchased from Zeiss, Germany. Selection of confocal settings was based on the proviso to obtain pixel size of 100 nm. To ensure appropriate resolution in Z-dimension a slice interval of 0.4 µm and depending on objective used 1 µm to 10 µm was set for NMJ and brain recordings, respectively. Depending on signal intensity the pinhole was tuned in a range between 1 and 2 airy units. Alexa 488 dye was excited at 488 nm using Argon laser. HeNe laser was used to excite Cy3 with a wavelength of 543 nm. Comparative analysis was performed using same laser settings for samples of different genotypes.

10.5.2. Image processing and quantification procedures

In principal, z-projections of confocal stacks, background subtraction and interpolation of images was processed by the use of MacBiophotonics ImageJ (http://macbiophotonics.ca/inagej/). Background subtraction and deletion of unspecific signals was manually executed, while quantification of molecule intensities was performed running ImageJ macros. Schematic illustrations, graphics and image designations were compiled using Adobe CS 5 package (adobe Illustrator and Photoshop, Adobe Systems, San Jose, USA).

10.5.3. Quantification of KURZSCHLUSS

Muscle filets of each genotype quantified were prepared and stained as described above. Subsequent to mRFP staining with rabbit-α-RFP, mRFP::SYT ratios were calculated from SV signals measured at the NMJ and nerve of a larva. In detail for each larva an image of NMJ (muscle 6/7, segment A2) and a defined area of the motor nerve that leaves the VNC at segment A8 (most caudal) was acquired. Laser settings were adjusted according to SV abundance at the NMJ of each larva and subsequently retained for the corresponding axon.
The background was manually subtracted from the maximal projections of all images. Procession and analysis of NMJ images was done as follows: first non-synaptic signals were manu-

ally removed and minimal threshold (adjusted for each batch of filets analyzed) was set to avoid analysis of unspecific signals. Second, a Gaussian blur (σ = 1 pixel) was applied. Third, average intensity of mRFP::SYT signal was measured by the "measure" command. Except for removal of unspecific signals and background subtraction all steps were automated. Procession and analysis of axon images was done as follows: The brightest area within the nerves that exit the VNC at segment A8 was identified through repeated measurement of SYT mean intensity over the area of 54.1 μm^2 using the "measure" command.

10.6. Electron microscopy

10.6.1. Fixation, contrasting and embedding procedure

Wandering third instar larvae were dissected as described in chapter 10.4.2. and fixed with glutaraldehyde solution (2.5 % glutaraldehyde, 50 mM cacodylate buffer, pH 7.2; 50 mM KCl, 2.5 mM $MgCl_2$, H_2O) for 45 min at 25 °C. Subsequently, samples were rinsed once and additionally washed 5 x 3 min with 50 mM cacodylate buffer. Tissue was additionally fixed with 2 % OsO_4 for 90 - 120 min, shifted to aqueous media and washed 5 x in short intervals in distilled water. Then specimens were contrasted over night in aqueous 10 % uranyl acetat. Next, after 5 washes with H_2O the samples were dehydrated in an ethanol array of 50 %, 70 %, 90 %, 96 % and 3 x 100 % for 15 min each. In preparation of tissue embedding samples were washed 2 x 20 min with propylene oxide. Thereafter, tissue was embedded in conventional Epon "hard", closed with gelatin cap and kept at 60 °C for 48 h.

10.6.2. Ultra-thin sectioning and contrasting

Upper part of gelatin capsule was removed to lay open Epon with tissue enclosed. An ultracut (Reichert Jung; Histo-diamont knife, Diatome) was used to prepare semi-thin sections, which were blotted onto objective slides and stained with methylene-blue azure-blue II solution. Once appropriate tissue depth was reached 70-100 nm ultra-thin sections were made and transferred onto EM grids (Plano, Wetzlar). Next, ultra-thin sections were contrasted by 20 min incubation with 2.5 % filtered uranyl acetate and 0.2 % lead citrate. In between and after incubation steps sections were dipped into 100 % ethanol, 50 % ethanol and H_2O. After careful drying the sections were again contrasted with lead citrate (7 min) and washed as described. After thorough drying the sections were ready for electron microscopy.

10.6.3. Image acquisition and image analysis

A Zeiss EM 900 (transmission electron microscope) was utilized to visualize the ultrastructure of AZs of larval NMJs. Images were registered on photo plates. The negatives were scanned (1200 dpi) to digitalize the images for subsequent analysis.

The number of SVs at particular synapse was quantified within four T-bar surrounding shells with a thickness of 50 nm and up to 250 nm (Hallermann et al., 2010b). All micrographs used to count SVs were acquired with 85000-fold magnification.

Contrasting, embedding, ultrasectioning and image acquisition was carried out by Brigitte Trost in collaboration with Prof. Christian Stigloher.

10.7. Behavioral assays

10.7.1. Sound-induced startle response paradigm

Startle response measurements were recorded in a custom-made box containing a 90 mm petri dish filled with a layer of 1 % agarose in H_2O (arena). Behavioral responses of 10-15 L3 larvae were simultaneously digitally recorded in darkness using a webcam (Logitech HD Pro Webcam C920). The IR blocking filter of the webcam was removed. The arena was illuminated with infrared LEDs. A sine wave tone at a frequency of 900 Hz was generated by a digital encoder (http://www.wavtones.com/functiongenerator.php; the sound protocol (1 sec stimulus, 5 sec break; 10 cycles) was implemented using GarageBand 10.0.2 (Apple Inc, USA) and exported into a digital sound file. The sound file was then played using a computer-connected loudspeaker, which was placed next to the arena inside the box. A digital sound pressure level-measuring device (Voltcraft SL-100; Conrad Electronics, Germany) was used to adjust the sound pressure levels to 60, 70, 80 and 90 dB SPL, respectively, directly at the arena inside the box. Video recordings were blinded and shuffled, and the startle responses were evaluated. A larva was scored as responsive when exhibiting startle behavior including pausing, turning and/or backward locomotion, in response to the sound stimulation. The numbers of (A) startled and (B) all animals present in the field of view at a given sound stimulus were counted. Subsequently the fraction of responsive larvae (A/B) was calculated for every sound event. Each genotype at every sound pressure level (60, 70, 80, 90 dB) was scored at least 10 times, and the startle response score was expressed as the mean of all response fractions ± SEM (Scholz et al., 2015).

10.7.2. Larval locomotion paradigm

Wandering third instar larvae, raised at 25 °C were positioned in a petri dish (90 mm in diameter) filled with 1 % agarose. The crawling paths for each genotype were video recorded for 0.5-2 min using a digital camera (*Part I*; EOS 60D, Canon; *Part II*, Logitech HD webcam). The movies were used to track the crawling path length of single larvae, which were subsequently digitalized and manually or digitally measured using ImageJ (rsbweb.nih.gov/ij/; wrMTrck plugin (J.S. Pedersen, http://www.phage.dk/plugins/wrmtrck.html) for ImageJ, NIH).

10.8. Electrophysiological analysis

Electrophysiological measurements for *Part I* of this thesis were performed by Nadine Ehmann.

Two electrode voltage clamp (TEVC) recordings (Axoclamp 900A amplifier, Molecular Devices) were performed on muscle 6, segments A2 and A3 in late third instar male *Drosophila* larvae essentially as previously described (Ljaschenko et al., 2012). All measurements were obtained at room temperature in HL-3 with the following composition: NaCl 70 mM, KCl 5 mM, $MgCl_2$ 20 mM, $NHCO_3$ 10 mM, trehalose 5 mM, sucrose 115 mM, HEPES 5 mM, $CaCl_2$ 1.5- or 1 mM, pH adjusted to 7.2. Recordings were accomplished using intracellular electrodes with resistances of 10-20 MΩ, filled with 3M KCl. For analysis, only cells with an initial membrane potential of at least - 50 mV and a membrane resistance of ≥ 4 MΩ were considered. During recordings, cells were clamped at a holding potential of - 80 mV (minis) or - 60 mV (eEPSCs). To evoke synaptic currents, nerves were stimulated through a suction electrode (diameter ~ 15 µm) with 300 µs pulses, typically at 10 V (Grass S88 stimulator and isolation unit SIU5, Astro-Med). Signals were low-pass filtered with 10 kHz and analyzed using Clampfit 10.2 (Molecular Devices). Paired-pulse recordings were performed with inter-stimulus intervals of (in ms): 10, 30, 100, 300, 1000. Between recordings cells were afforded 10 sec of rest. For analysis 10 traces per interval were averaged. The amplitude of the second response in 10 ms inter-pulse recordings was measured from the peak to the point of interception with the extrapolated first response.

10.9. Data analysis

Unless stated otherwise, the non-parametrical Mann-Whitney rank sum test was used for statistical analysis (Sigma Plot 12.5, Software Inc., San Jose, USA; Prism 5, GraphPad Software, La Jolla, USA). Data are reported as mean ± SEM, n indicates the sample number and p denotes the level of significance (*$p \leq 0.05$, **$p \leq 0.01$, and ***$p \leq 0.001$).

11. Supplemental information

Part I

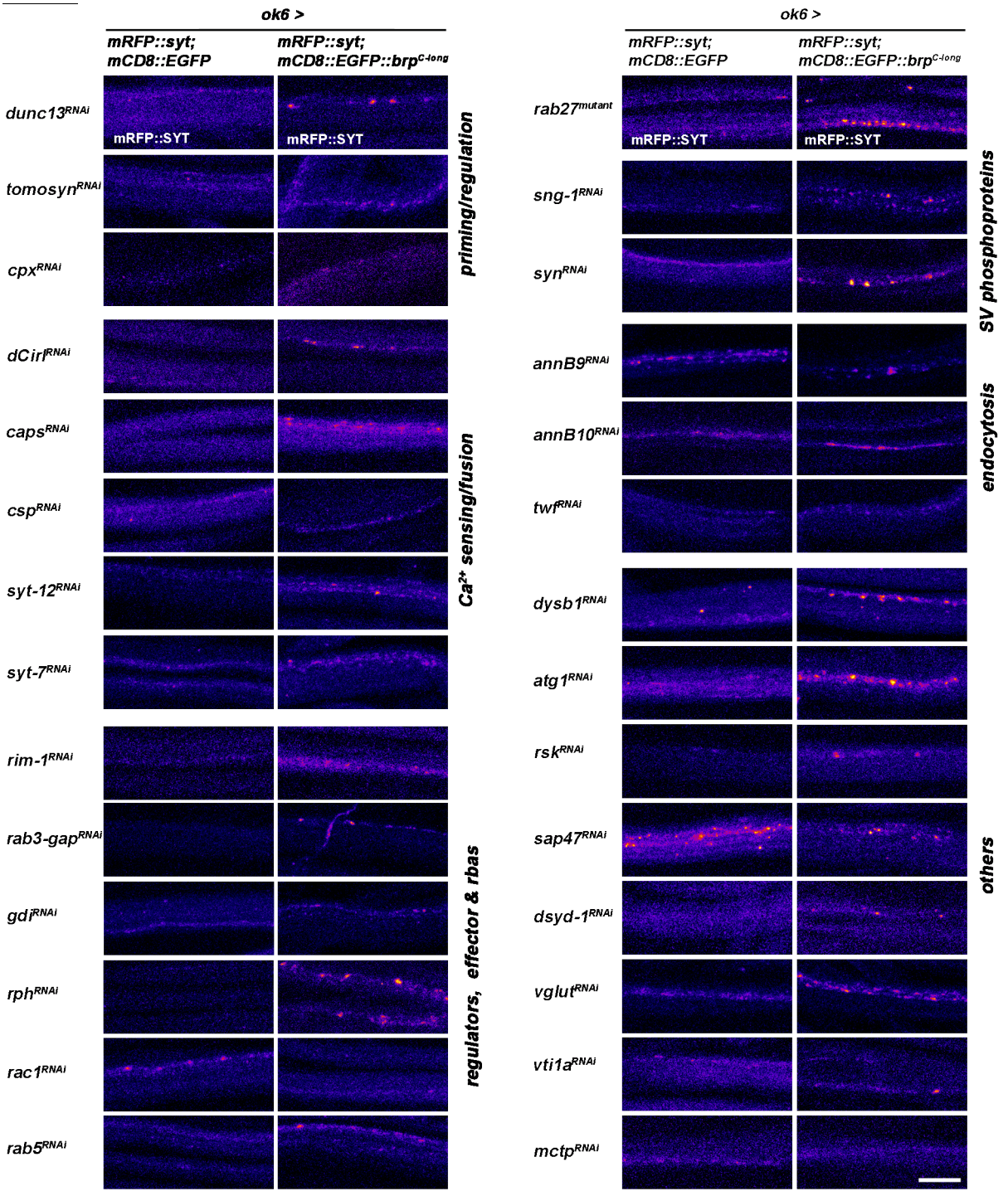

Suppl. Figure 1. Overview of KURZSCHLUSS screening results. Shown are axonal mRFP::SYT profiles of chemically fixed control and *brp*$^{C\text{-}long}$ expressing larvae that were motoneuronally depleted of gene *x*. This screen identified putative binding partners of BRP. Tested genes are represented in groups according to their proposed function or in others. Scale bar 10 µm.

Suppl. Figure 2. Sequence alignment of BRP bait variants. Alignment of BRP$^{C\text{-}tip}$ (17 residues), BRP$^{C\text{-}medium}$ (294 residues) and BRP$^{C\text{-}long}$ (862 residues) depicts high incidence of glutamines within BRP$^{C\text{-}medium}$ (pink overlay). Frequently, these glutamine motifs coincide with regions predicted to form coils (indicated by grey curved line, predicted by EMBOSS garnier). ClustalW Alignment (Cost matrix: BLOSUM, open gap cost 10, gap extend cost: 0.1).

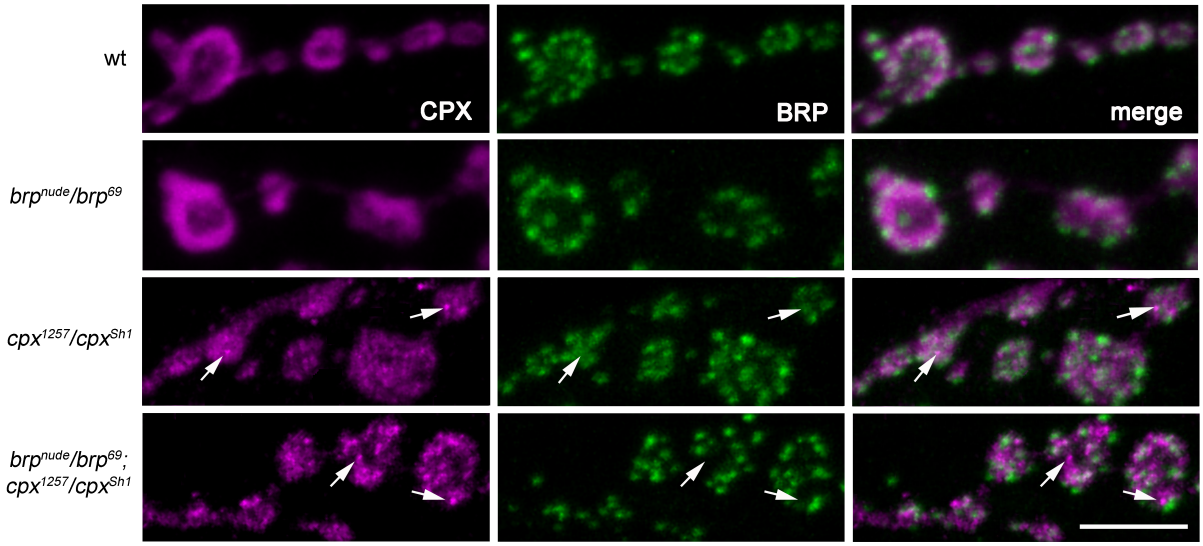

Suppl. Figure 3. AZs are not occupied by CPX accumulations. Uniform distribution of CPX throughout NMJ of wild-type and *brp*^{nude} was abolished in single *cpx*^{1257} (Iyer et al., 2013) and *brp*^{nude}*; cpx*^{1257} double mutants. Importantly and consistent with a previous report CPX clusters do not localized to AZs (Buhl et al., 2013). CPX signal in *cpx*^{1257} single and double mutants was significantly reduced compared to control and *brp*^{nude}. Therefore, laser settings were adjusted to enable proper CPX residence in all genotypes. Scale bar = 5 µm.

Suppl. Table 1. List of genes tested in the KURZSCHLUSS screen. Suppl. Fig. 1 shows corresponding confocal images. 27 different genes involved in different steps of the exo-endocytosis cycle were tested. In addition, the interaction of BRP with *rab27* was examined using *rab27* null mutant (*rab27*^{GAL4KO}; Chan et al., 2011)

Functional involvement	Symbol	Protein name	Off-target	Chromosome location	VDRC stock#/Reference
Priming/regulation	*dunc-13*	dunc-13	0	2	v33606
	tomosyn	tomosyn	0	3	v43629
	cpx	complexin	0	3	v21477
Fusion/Ca^{2+} sensing	*dCirl*	Ca^{2+}-independent receptor of latrotoxin	110	2	v29969
	dCAPS	CAPS	0	2	v25291
	csp	Cysteine string protein			v103201
	syt-12	Synaptotagmin-12	0	2	v10617
	syt-7	Synaptotagmin-7	0	3	v24988
Regulators, Effectors & Rabs	*rim-1*	Rab3-interacting molecule	0	2	v39384
	rab3-GAP	rab3 GTPase binding protein	0	3	v27824
	gdi	GDP dissociation inhibitor	1	3	v26537
	rph	Rabphilin	15	2	v52438
	rac-1		1	1	v49247
	rab5	Rab3-binding protein 5	3	2	v34094
	rab27	Rab27	mutant	1	*Chan et al., 2011*
SV phosphoproteins	*sng-1*	Synaptogyrin	0	3	v8784
	syn	Synapsin	0	2	v110606
endocytosis	*AnnB9*	AnnexinB9	2	2	v27493
	AnnB10	AnnexinB10	0	2	v36107
	twf	Twinfilin	0	2	v25817
others	*dysb*	Dysbindin	0	2	v34354
	atg-1	Autophagy-specific gene 1	0	2	v16133
	rsk	Ribosomal S6 kinase	14	3	v5702
	sap47	Synapse-associated proteine 47 kDa	0	2	v35445
	dsyd-1	Sunday driver-1	0	2	v35346
	dvglut	Vesicular glutamat transporter	0	3	v2574
	vti1a	Vesicle transport through interaction with t-SNAREs homolog 1A	0	3	v45726
	Mctp	Multiple-C2-domain TM proteins	0	3	v10061

Suppl. Table 2. Statistics of crawling distance measurements. Values represent the mean ± SEM; grey values indicate significance compared to control, black values indicate significance between experimental groups.

Genotype	Crawling distance [cm/min]	n	*P*
Related to Figure 11B			
w^{1118};;;	7.5 ± .30	25	-
w^{1118}; brp^{nude}/brp^{69};;	6.0 ± 1.5	25	.0002
w^{1118}; UAS-$mbrp^{C\text{-}tip}$/+;;	8.7 ± .57	18	.0002
w^{1118}; ok6-GAL4/+;;	7.3 ± .29	20	.0007
w^{1118}; ok6-GAL4/UAS-$mbrp^{C\text{-}tip}$;;	5.4 ± .35	21	-
w^{1118} vglut/+;;;	7.7 ± .30	19	-
w^{1118} vglut/+; UAS-$mbrp^{C\text{-}tip}$;;	4.8 ± .24	28	< .0001
w^{1118} vglut/+; UAS-CFP;;	7.2 ± .31	20	.2011
Related to Figure 12			
w^{1118};;;	7.3 ± .22	40	-
w^{1118}; brp^{nude}/brp^{69};;	5.6 ± .14	45	< .0001
w^{1118}; UAS-$brp^{C\text{-}tip}$/+;;	6.9 ± .24	27	-
w^{1118} elav-GAL4;;;	6.8 ± .31	25	-
w^{1118} elav-GAL4; UAS-$brp^{C\text{-}tip}$/+;;	5.9 ± .19	19	.0492 .0097
w^{1118} vglut-GAL4;;;	7.4 ± .32	22	-
w^{1118} vglut-GAL4; UAS-$brp^{C\text{-}tip}$/+;;	4.8 ± .24	28	< .0001 < .0001
w^{1118};; cha-GAL4;	6.1 ± .27	15	-
w^{1118};; cha-GAL4/UAS-$brp^{C\text{-}tip}$;;	4.5 ± .27	15	.0004 < .0001
w^{1118};; vgat-GAL4;	6.7 ± .22	19	-
w^{1118};; vgat-GAL4/UAS-$brp^{C\text{-}tip}$;;	5.6 ± .30	17	.0078 .0028
Related to Figure 20A			
w^{1118};;;	7.7 ± .40	21	-
w^{1118}; brp^{nude}/brp^{69};;	5.8 ± .30	22	.0008 .0004
w^{*};; cpx^{1257}/cpx^{Sh1};	4.1 ± .14	25	<.0001 .4920
w^{1118}; brp^{nude}/brp^{69}; cpx^{1257}/cpx^{Sh1};	4.3 ± .20	19	<.0001
Related to Figure 21			
w^{1118};;;	7.1 ± .25	36	-
w^{1118}; brp^{nude}/+;;	8.24 ± .28	31	.0039 <.0001
w^{*};; cpx^{Sh1}/+;	6.75 ± .27	37	.3343 .0012
w^{1118}; brp^{nude}/+; cpx^{Sh1}/+;	5.03 ± .37	27	.0001
w^{1118}; brp^{69}/+;;	7.92 ± .29	30	.0035 <.0001
w^{*};; cpx^{1257}/+;	7.39 ± .32	29	.7766 .0034

w^{1118}; brp^{69}/+; cpx^{1257}/+;	5.58 ± .37	30	.0062
w^{1118}; brp^{69}/+;;	7.92 ± .29	30	.0062
w^{*};; cpx^{Sh1}/+;	6.75 ± .27	37	.7962
w^{1118}; brp^{69}/+; cpx^{Sh1}/+;	6.76 ± .18	26	.3960
w^{1118}; brp^{nude}/+;;	8.24 ± .28	31	.6453
w^{*};; cpx^{1257}/+;	7.39 ± .32	29	.3274
w^{1118}; brp^{nude}/+; cpx^{1257}/+;	7.72 ± .44	22	.1299

Suppl. Table 3. Quantification of paired-pulse ratios (PPR) of *ok6-GAL4>mBRP*$^{C\text{-}tip}$ animals and respective controls. Top entry served as control. *P* values are shown in brackets and were generated using t-test (indicated in black) or Mann-Whitney U test (indicated in grey). Data are presented as mean ± SEM. Related to Fig. 11C.

Genotype	**PPR**				
Related to Figure 23B					
	10ms	**30ms**	**100ms**	**300ms**	**1000ms**
w^{1118};*ok6-GAL4/+;;* *(n = 12)*	0.94 ± 0.03	0.98 ± 0.02	0.95 ± 0.02	0.92 ± 0.01	0.95 ± 0.01
w^{1118}; brp^{nude}, *ok6-GAL4* /brp^{69};; *(n = 12)*	0.82 ± 0.01 (.0009)	0.89 ± 0.02 (.0038)	0.87 ± 0.01 (.0003)	0.87 ± 0.01 (.0004)	0.91 ± 0.01 (.0004)
w^{1118}; *ok6-GAL4 > UAS-mbrp*$^{C\text{-}tip}$;; *(n = 12)*	0.84 ± 0.04 (.0689)	0.93 ± 0.02 (.0351)	0.90 ± 0.02 (.0120)	0.90 ± 0.01 (.3123)	0.93 ± 0.01 (.2145)

Suppl. Table 4. Quantification of survival rates. Values represent the mean ± SEM; grey values indicate significance compared to control, black values indicate significance between experimental groups. Related to Figure 20C.

Genotype	**Survival rate [days]**	**n**	***P***
w^{1118};;;	22.4 ± 1.87	15	-
w^{1118}; brp^{nude}/brp^{69};;	5.3 ± 0.62	22	<.0001 .0601
w^{*};; cpx^{1257}/cpx^{Sh1};	12.7 ± 1.53	13	.0038 <.0001
w^{1118}; brp^{nude}/brp^{69}; cpx^{1257}/cpx^{Sh1};	3.9 ± 0.32	20	<.0001

Suppl. Table 5. Quantification of KURZSCHLUSS in wt, *cpx*$^{v21477(RNAi)}$ and *cpx*^{1257} mutant background. Values represent the mean ± SEM. Related to Figure 19B.

Genotype	SYT mean intensity axon/NMJ [a.u.]	n	*P*
w^{1118};ok6-GAL4, mRFP::SYT/+;no brp;	.59 ± .04	17	-
w^{1118};ok6-GAL4, mRFP::SYT/+;brp^{C}-long/+;	.78 ± .06	15	.0267
w^{1118};ok6-GAL4, mRFP::SYT/+;brp$^{C\text{-}long}$/ mbrp$^{C\text{-}tip}$;	.59 ± .08	16	.0302
w^{1118};ok6-GAL4, mRFP::SYT/+;no brp/cpx^{v21477};	.31 ± .02	22	-
w^{1118};ok6-GAL4, mRFP::SYT/+; brp$^{C\text{-}long}$/cpx^{v21477} ;	.31 ± .03	22	.6221
w^{1118};ok6-GAL4, mRFP::SYT/+; cpx^{1257}/cpx^{Sh1}	.06 ± .07	13	-
w^{1118};ok6-GAL4, mRFP::SYT/+;brp$^{C\text{-}long}$, cpx^{1257}/cpx^{Sh1}	.44 ± .044	21	.1108

Suppl. Table 6. Quantification of SV numbers at the T-bars of NMJ synapses. Values represent the mean ± SEM.

Genotype	SV number/T-bar	n	*P*
Related to Figure 22C			
w^{1118};;;	8.70 ± .23	232	-
w^{1118}; brp^{nude}/brp^{69};;	6.58 ± .26	168	<.0001 .2696
w*;; cpx^{1257}/cpx^{Sh1};	6.95 ± .20	259	<.0001 .0107
w^{1118}; brp^{nude}/brp^{69}; cpx^{1257}/cpx^{Sh1};	6.27 ± .28	152	<.0001

Related to Figure 22B									
[nm]	**50-100**	*P*	**100-150**	*P*	**150-200**	*P*	**200-250**	*P*	n
	6.0 ± .19	-	8.14 ± .28	-	8.93 ± .43	-	11.76 ± .54	-	58
	3.40 ± .22	<.0001 .8933	5.36 ± .26	<.0001 .8407	6.92 ± .29	.0004 .1143	10.62 ± .48	.0700 .5105	42
	4.52 ± .22	<.0001 .0034	5.80 ± .20	<.0001 .1553	6.91 ± .27	.0001 .1052	10.64 ± .43	.0732 .4081	65
	3.50 ± .22	<.0001	5.24 ± .27	<.0001	6.24 ± .37	<.0001	10.11 ± .60	.0325	38

Suppl. Table 7. Analysis of electrophysiological recordings obtained from *cpx*^{1257} single and *brp*^{nude}; *cpx*^{1257} double mutants. Each top entry served as control. Data are presented as mean ± SEM.

Genotype	PPR				
Related to Figure 23B					
	10ms	**30ms**	**100ms**	**300ms**	**1000ms**
w^{1118};;; *(n = 15)*	1.35 ± 0.09	1.24 ± 0.06	1.09 ± 0.04	1.03 ± 0.02	0.98 ± 0.01
w^{1118}; *brp*-^{nude}/*brp*^{69};; *(n = 14)*	0.94 ± 0.04 (P = .0004)	1.07 ± 0.03 (P = .0056)	0.97 ± 0.02 (P = .0094)	0.95 ± 0.01 (P = .0024)	0.93 ± 0.01 (P = .0246)
w*;; *cpx*^{1257}/*cpx*^{Sh1}; *(n = 14)*	± 0.04 (P = .0010)	1.04 ± 0.04 (P = .0021)	0.97 ± 0.03 (P = .0121)	0.91 ± 0.01 (P ≤ .0001)	0.93 ± 0.01 (P = .0056)
w^{1118}; *brp*^{nude}/*brp*^{69}; *cpx*^{1257}/*cpx*^{Sh1}; *(n = 14)*	0.72 ± 0.02 (P ≤ .0001)	0.79 ± 0.02 (P ≤ .0001)	0.8 ± 0.01 (P ≤ .0001)	0.79 ± 0.01 (P ≤ .0001)	0.88 ± 0.01 (P ≤ .0001)
P values (compared to control: *w*^{1118}) are given in brackets.					
	Related to Figure 23C		Related to Figure 23E		
	eEPSC amplitude (-nA)	***P* value**	**Mini frequency (Hz)**	***P* value**	
w^{1118};;; *(n = 15)*	53.17 ± 5.26		1.11 ± 0.18		
w^{1118}; *brp*-^{nude}/*brp*^{69};; *(n = 14)*	57.88 ± 3.73	.1112	0.83 ± 0.05	.445	
w*;; *cpx*^{1257}/*cpx*^{Sh1}; *(n = 14)*	54.62 ± 3.24	.1832	62.6 ± 5.91	≤ .001	
w^{1118}; *brp*^{nude}/*brp*^{69}; *cpx*^{1257}/*cpx*^{Sh1}; *(n = 14)*	67.20 ± 3.35	.0037	23.19 ± 2.52	≤ .001 ≤ .001	
P values grey: compared to control, black: comparison between experimental genotypes.					

Part II

Suppl. Table 8. Statistics of crawling distance measurements. Colors mark independent experimental data sets. Each top entry served as control. Values represent the mean ± SEM.

Genotype	Crawling distance [cm/min]	n	*P*
Related to Figure 33B			
w^{1118};; *P{ pTL161* w^{+}*};*	6.2 ± 0.4	19	-
w^{1118}; *dCirl*^{KO} w^{+};;	4.5 ± 0.4	18	.0052
w^{*}; *+/Df(2R)Exel8047;;*	5.9 ± 0.3	11	-
w^{*}; *dCirl*^{KO}*/Df(2R)Exel8047;;*	3.7 ±.0.5	14	.0006
w^{*}; *dCirl*^{Rescue}*/Df(2R)Exel8047;;*	6.1 ± 0.6	11	.718
w^{*}; *dCirl*^{Flag}*/Df(2R)Exel8047;;*	5.0 ± 0.5	12	.207
w^{*}; *dCirl*^{RFP}*/Df(2R)Exel8047;;*	5.4 ± 0.4	12	.356
Related to Figure 38C			
w^{1118};;;	6.8 ± 0.3	19	-
w^{1118}; *dCirl*^{KO} w^{+};;	3.7 ± 0.2	21	<.0001
w^{1118}; *dCirl*^{KO}*; +/20xUAS-dCirl;*	4.8 ± 0.3	18	<.0001
w^{1118}; *dCirl*^{KO}*; iav-GAL4/+;*	4.4 ± 0.1	22	-
w^{1118}; *dCirl*^{KO}*; iav-GAL4/20xUAS-dCirl;*	6.0 ± 0.4	16	.0005
Related to Figure 42			
w^{1118};;;	6.6 ± 0.5	19	<.0001
w^{1118}; *dCirl*^{KO} w^{-};;	4.2 ± 0.3	26	-
w^{*}; eys^{BG02208};;	4.9 ± 0.3	26	.002
w^{1118}; *dCirl*^{KO}, eys^{BG0220};;	5.5 ± 0.3	26	.151 .0023
w^{*}; *nompC*^{f00642};;	5.1 ± 0.4	17	.023
w^{*}; *dCirl*^{KO}, *nompC*^{f00642};;	3.8 ± 0.3	20	.313 .0100
w^{*};; *nan*^{36a};	3.3 ± 0.3	22	.029
w^{1118};*dCirl*^{KO}; *nan*^{36a};	4.2 ± 0.1	22	.893 .0183
w^{1118}; *dCirl*^{KO}*; iav-GAL4/+*	5.1 ± 0.3	17	-
w^{1118}; *dCirl*^{KO}*; iav-GAL4/UAS-nompC::GFP*	6.0 ± 0.3	25	<.001
w^{1118}; *dCirl*^{KO}*; +/UAS-nompC::GFP*	4.7 ± 0.2	21	.17
dCirl^{KO}*; iav-GAL4/UAS-iav::GFP*	7.5 ± 0.4	18	<.0001
dCirl^{KO}*; +/UAS-iav::GFP*	6.0 ± 0.2	24	-

Suppl. Table 9. Statistics of morphometric measurements. Values represent the mean ± SEM of absolute measurements. Related to Figure 36E.

	w^{1118};; P{ pTL161 w^{+}};	*w^{1118}; $dCirl^{KO}$ w^{+};;*	*P*
AZ number ± SEM	544 ± 52	515 ± 67	.735
AZ size ± SEM [µm^2]	0.50 ± 0.02	0.57 ± 0.04	.145
GluRIID field number ± SEM	441 ± 64	346 ± 47	.260
GluRIID field size ± SEM [µm^2]	0.80 ± 0.06	0.74 ± 0.06	.445
n	12	10	
NMJ size ± SEM [µm^2]	624 ± 30	704 ± 43	.125
n	21	18	

Suppl. Table 10. Startle response score upon stimulation with a 900 Hz tone. Colors mark independent experimental data sets. Top entry served as control. All values represent the mean ± SEM. Related to Figure 41.

Genotype	**Startle response score at 60 dB (n) [*P*]**	**70 dB (n) [*P*]**	**80 dB (n) [*P*]**	**90 dB (n) [*P*]**
w^{*}; +/Df(2R)Exel8047;;	.17 ± .03 (20) -	.57 ± .06 (20) -	.90 ± .03 (10) -	.99 ± .01 (10) -
w^{*}; $dCir^{KO}$/Df(2R)Exel8047;;	.07 ± .01 (20) [.005]	.19 ± .02 (20) [<.0001]	.52 ± .06 (20) [<.0001]	.91 ± .02 (20) [.013]
w^{*}; $dCirl^{Recue}$/Df(2R)Exel8047;;	.15 ± .04 (10) [.050]	.52 ± .02 (10) [.611]	.83 ± .04 (10) [.220]	.98 ± .01 (10) [.543]
w^{1118};;;	.29 ± .03 (20) -	.58 ± .03 (20) -	.87 ± .03 (20) -	.99 ± .01 (20) -
w^{1118}; $dCirl^{KO}$ w^{-};;	.10 ± .03 (20) [<.0001]	.18 ± .03 (20) [<.0001]	.60 ± .04 (20) [<.0001]	.87 ± .02 (20) [<.0001]

12. References

Adams MD, **Celniker SE**, **Holt RA** et al. The genome sequence of *Drosophila melanogaster*. *Science* 287: 2185–2195, 2000.

Alabi AA, **Tsien RW**. Synaptic vesicle pools and dynamics. *Cold Spring Harb Perspect Biol* 4: a013680, 2012.

Albert JT, **Nadrowski B**, **Göpfert MC**. Mechanical signatures of transducer gating in the *Drosophila* ear. *Current Biology* 17: 1000–1006, 2007.

Allen Mouse Brain Atlas. Allen Institute for Brain Science, 2009. (http:// mouse.brain-map.org).

Araç D, **Boucard AA**, **Bolliger MF**, **Nguyen J**, **Soltis SM**, **Südhof TC**, **Brunger AT**. A novel evolutionarily conserved domain of cell-adhesion GPCRs mediates autoproteolysis. *EMBO J* 31: 1364–1378, 2012.

Arcos-Burgos M, **Jain M**, **Acosta MT**, **Shively S**, **Stanescu H**, **Wallis D**, **Domene S**, **Velez JI**, **Karkera JD**, **Balog J**, **Berg K**, **Kleta R**, **Gahl WA**, **Roessler E**, **Long R**, **Lie J**, **Pineda D**, **Londono AC**, **Palacio JD**, **Arbelaez A**, **Lopera F**, **Elia J**, **Hakonarson H**, **Johansson S**, **Knappskog PM**, **Haavik J**, **Ribases M**, **Cormand B**, **Bayes M**, **Casas M**, **Ramos-Quiroga JA**, **Hervas A**, **Maher BS**, **Faraone SV**, **Seitz C**, **Freitag CM**, **Palmason H**, **Meyer J**, **Romanos M**, **Walitza S**, **Hemminger U**, **Warnke A**, **Romanos J**, **Renner T**, **Jacob C**, **Lesch K-P**, **Swanson J**, **Vortmeyer A**, **Bailey-Wilson JE**, **Castellanos FX**, **Muenke M**. A common variant of the latrophilin 3 gene, *LPHN3*, confers susceptibility to ADHD and predicts effectiveness of stimulant medication. *Mol Psychiatry* 15: 1053–1066, 2010.

Atwood HL, **Govind CK**, **Wu CF**. Differential ultrastructure of synaptic terminals on ventral longitudinal abdominal muscles in *Drosophila* larvae. *Journal of neurobiology* 24: 1008–1024, 1993.

Auld VJ, **Fetter RD**, **Broadie K**, **Goodman CS**. Gliotactin, a novel transmembrane protein on peripheral glia, is required to form the blood-nerve barrier in *Drosophila*. *Cell* 81: 757–767, 1995.

Aust G. Adhesion-GPCRS in tumorigenesis. *Adv Exp Med Biol* 706: 109–120, 2010.

Avery L, **Wasserman S**. Ordering gene function: the interpretation of epistasis in regulatory hierarchies. *Trends Genet.* 8: 312–316, 1992.

Bae B-I, **Tietjen I**, **Atabay KD**, **Evrony GD**, **Johnson MB**, **Asare E**, **Wang PP**, **Murayama AY**, **Im K**, **Lisgo SN**, **Overman L**, **Šestan N**, **Chang BS**, **Barkovich AJ**, **Grant PE**, **Topçu M**, **Politsky J**, **Okano H**, **Piao X**, **Walsh CA**. Evolutionarily dynamic alternative splicing of GPR56 regulates regional cerebral cortical patterning. *Science* 343: 764–768, 2014.

Baker KE, **Parker R**. Nonsense-mediated mRNA decay: terminating erroneous gene expression. *Curr Opin Cell Biol* 16: 293–299, 2004.

Banerjee S, **Pillai AM**, **Paik R**, **Li J**, **Bhat MA**. Axonal ensheathment and septate junction formation in the peripheral nervous system of *Drosophila*. *J Neurosci* 26: 3319–3329, 2006.

Barnett DWD, **Liu JJ**, **Misler SS**. Single-cell measurements of quantal secretion induced by α-latrotoxin from rat adrenal chromaffin cells: dependence on extracellular Ca^{2+}. *Pflugers Arch.* 432: 1039–1046, 1996.

Bate M. The embryonic development of larval muscles in *Drosophila*. *Development* 110: 791–804, 1990.

Benayoun BA, **Caburet S**, **Dipietromaria A**, **Bailly-Bechet M**, **Batista F**, **Fellous M**, **Vaiman D**, **Veitia RA**. The identification and characterization of a FOXL2 response element provides insights into the pathogenesis of mutant alleles. *Hum Mol Genet* 17: 3118–3127, 2008.

Betz A, **Thakur P**, **Junge HJ**, **Ashery U**, **Rhee JS**, **Scheuss V**, **Rosenmund C**, **Rettig J**, **Brose N**. Functional interaction of the active zone proteins Munc13-1 and RIM1 in synaptic vesicle priming. *NEURON* 30: 183–196, 2001.

Birks R, **MacIntosh FC**. ACETYLCHOLINE METABOLISM OF A SYMPATHETIC GANGLION. *Biochem. Cell Biol.* 39: 787–827, 1961.

Bjarnadóttir TK, **Fredriksson R**, **Höglund PJ**, **Gloriam DE**, **Lagerström MC**, **Schiöth HB**. The human and mouse repertoire of the adhesion family of G-protein-coupled receptors. *Genomics* 84: 23–33, 2004.

Bjarnadóttir TK, **Geirardsdóttir K**, **Ingemansson M**, **Mirza MAI**, **Fredriksson R**, **Schiöth HB**. Identification of novel splice variants of Adhesion G protein-coupled receptors. *Gene* 387: 38–48, 2007.

Bloom FE, **Aghajanian GK**. Fine structural and cytochemical analysis of the staining of synaptic junctions with phosphotungstic acid. *J. Ultrastruct. Res.* 22: 361–375, 1968.

Bockaert J, **Pin JP**. Molecular tinkering of G protein-coupled receptors: an evolutionary success. *Embo J* 18: 1723–1729, 1999.

Bodmer R, **Jan YN**. Morphological-Differentiation of the Embryonic Peripheral Neurons in *Drosophila*. *Rouxs Archives of Developmental Biology* 196: 69–77, 1987.

Bohnekamp J, **Schöneberg T**. Cell adhesion receptor GPR133 couples to G_s protein. *J Biol Chem* 286: 41912–41916, 2011.

Bommert K, **Charlton MP**, **DeBello WM**, **Chin GJ**, **Betz H**, **Augustine GJ**. Inhibition of neurotransmitter release by C2-domain peptides implicates synaptotagmin in exocytosis. *Nature* 363: 163–165, 1993.

Bonifacino JS, **Glick BS**. The Mechanisms of Vesicle Budding and Fusion. *Cell* 116: 153–166, 2004.

Boucard AA, **Ko J**, **Südhof TC**. High affinity neurexin binding to cell adhesion G-protein-coupled receptor CIRL1/latrophilin-1 produces an intercellular adhesion complex. *J Biol Chem* 287: 9399–9413, 2012.

Bracher A, **Kadlec J**, **Betz H**, **Weissenhorn W**. X-ray structure of a neuronal complexin-SNARE complex from squid. *J Biol Chem* 277: 26517–26523, 2002.

Brand AH, **Perrimon N**. Targeted gene expression as a means of altering cell fates and generating dominant phenotypes. *Development* 118: 401–415, 1993.

Bray SJ. Notch signalling: a simple pathway becomes complex. *Nature Reviews Molecular Cell Biology* 7: 678–689, 2006.

Bridges JP, **Ludwig M-G**, **Mueller M**, **Kinzel B**, **Sato A**, **Xu Y**, **Whitsett JA**, **Ikegami M**. Orphan G protein-coupled receptor GPR116 regulates pulmonary surfactant pool size. *Am. J. Respir. Cell Mol. Biol.* 49: 348–357, 2013.

Brose N, **Hofmann K**, **Hata Y**, **Südhof TC**. Mammalian homologues of *Caenorhabditis elegans unc-13* gene define novel family of C2-domain proteins. *J Biol Chem* 270: 25273–25280, 1995.

Brose N. For better or for worse: complexins regulate SNARE function and vesicle fusion. *Traffic* 9: 1403–1413, 2008.

Budnik V, **Koh YH**, **Guan B**, **Hartmann B**, **Hough C**, **Woods D**, **Gorczyca M**. Regulation of synapse structure and function by the *Drosophila* tumor suppressor gene dlg. *NEURON* 17: 627–640, 1996.

Buhl LK, **Jorquera RA**, **Akbergenova Y**, **Huntwork-Rodriguez S**, **Volfson D**, **Littleton JT**. Differential regulation of evoked and spontaneous neurotransmitter release by C-terminal modifications of complexin. *Molecular and Cellular Neuroscience* 52: 161–172, 2013.

Bykhovskaia M, **Jagota A**, **Gonzalez A**, **Vasin A**, **Littleton JT**. Interaction of the complexin accessory helix with the C-terminus of the SNARE complex: molecular-dynamics model of the fusion clamp. *Biophys J* 105: 679–690, 2013.

Caldwell JC, **Miller MM**, **Wing S**, **Soll DR**, **Eberl DF**. Dynamic analysis of larval locomotion in *Drosophila* chordotonal organ mutants. *Proc Natl Acad Sci USA* 100: 16053–16058, 2003.

Capogna M, **Volynski KE**, **Emptage NJ**, **Ushkaryov YA**. The α-latrotoxin mutant LTXN4C enhances spontaneous and evoked transmitter release in CA3 pyramidal neurons. *J Neurosci* 23: 4044–4053, 2003.

Carreira-Barbosa F, **Kajita M**, **Kajita M**, **Morel V**, **Wada H**, **Okamoto H**, **Martinez Arias A**, **Fujita Y**, **Wilson SW**, **Tada M**. Flamingo regulates epiboly and convergence/extension movements through cell cohesive and signalling functions during zebrafish gastrulation. *Development* 136: 383–392, 2009.

Chachisvilis M, **Zhang Y-L**, **Frangos JA**. G protein-coupled receptors sense fluid shear stress in endothelial cells. *Proc Natl Acad Sci USA* 103: 15463–15468, 2006.

Chalfie M. Neurosensory mechanotransduction. *Nature Reviews Molecular Cell Biology* 10: 44–52, 2009.

Chan C-C, **Scoggin S**, **Wang D**, **Cherry S**, **Dembo T**, **Ben Greenberg**, **Jin EJ**, **Kuey C**, **Lopez A**, **Mehta SQ**, **Perkins TJ**, **Brankatschk M**, **Rothenfluh A**, **Buszczak M**, **Hiesinger PR**. Systematic Discovery of Rab GTPases with Synaptic Functions in *Drosophila*. *Current Biology* 21: 1704–1715, 2011.

Chang G-W, **Stacey M**, **Kwakkenbos MJ**, **Hamann J**, **Gordon S**, **Lin H-H**. Proteolytic cleavage of the EMR2 receptor requires both the extracellular stalk and the GPS motif. *FEBS Lett* 547: 145–150, 2003.

Chaudhry FA, **Reimer RJ**, **Bellocchio EE**, **Danbolt NC**, **Osen KK**, **Edwards RH**, **Storm-Mathisen J**. The vesicular GABA transporter, VGAT, localizes to synaptic vesicles in sets of glycinergic as well as GABAergic neurons. *J Neurosci* 18: 9733–9750, 1998.

Chen W-S, **Antic D**, **Matis M**, **Logan CY**, **Povelones M**, **Anderson GA**, **Nusse R**, **Axelrod JD**. Asymmetric homotypic interactions of the atypical cadherin flamingo mediate intercellular polarity signaling. *Cell* 133: 1093–1105, 2008.

Chen X, **Tomchick DR**, **Kovrigin E**, **Araç D**, **Machius M**, **Südhof TC**, **Rizo J**. Three-dimensional structure of the complexin/SNARE complex. *NEURON* 33: 397–409, 2002.

Cheng LE, **Song W**, **Looger LL**, **Jan LY**, **Jan YN**. The Role of the TRP Channel NompC in *Drosophila* Larval and Adult Locomotion. *NEURON* 67: 373–380, 2010.

Cho RW, **Kümmel D**, **Li F**, **Baguley SW**, **Coleman J**, **Rothman JE**, **Littleton JT**. Genetic analysis of the Complexin trans-clamping model for cross-linking SNARE complexes *in vivo*. *Proc Natl Acad Sci USA* 111: 10317–10322, 2014.

Cho RW, **Song Y**, **Littleton JT**. Comparative analysis of *Drosophila* and mammalian complexins as fusion clamps and facilitators of neurotransmitter release. *Molecular and Cellular Neuroscience* 45: 389–397, 2010.

Chung YD, **Zhu J**, **Han Y**, **Kernan MJ**. *nompA* encodes a PNS-specific, ZP domain protein required to connect mechanosensory dendrites to sensory structures. *NEURON* 29: 415–428, 2001.

Clapham DE, **Runnels LW**, **Strübing C**. The TRP ion channel family. *Nature Reviews Neuroscience* 2: 387–396, 2001.

Clark AG, **Eisen MB**, **Smith DR**, **Bergman CM**, **Oliver B**, **Markow TA**, **Kaufman TC**, **Kellis M**, **Gelbart W**, **Iyer VN**, **Pollard DA**, **Sackton TB**, **Larracuente AM**, **Singh ND**, **Abad JP**, **Abt DN**, **Adryan B**, **Aguade M**, **Akashi H**, **Anderson WW**, **Aquadro CF**, **Ardell DH**, **Arguello R**, **Artieri CG**, **Barbash DA**, **Barker D**, **Barsanti P**, **Batterham P**, **Batzoglou S**, **Begun D**, **Bhutkar A**, **Blanco E**, **Bosak SA**, **Bradley RK**, **Brand AD**, **Brent MR**, **Brooks AN**, **Brown RH**, **Butlin RK**, **Caggese C**, **Calvi BR**, **Bernardo De Carvalho A**, **Caspi A**, **Castrezana S**, **Celniker SE**, **Chang JL**, **Chapple C**, **Chatterji S**, **Chinwalla A**, **Civetta A**, **Clifton SW**, **Comeron JM**, **Costello JC**, **Coyne JA**, **Daub J**, **David RG**, **Delcher AL**, **Delehaunty K**, **Do CB**, **Ebling H**, **Edwards K**, **Eickbush T**, **Evans JD**, **Filipski A**, **Findeiß S**, **Freyhult E**, **Fulton L**, **Fulton R**, **Garcia ACL**, **Gardiner A**, **Garfield DA**, **Garvin BE**, **Gibson G**, **Gilbert D**, **Gnerre S**, **Godfrey J**, **Good R**, **Gotea V**, **Gravely B**, **Greenberg AJ**, **Griffiths-Jones S**, **Gross S**, **Guigo R**, **Gustafson EA**, **Haerty W**, **Hahn MW**, **Halligan DL**, **Halpern AL**, **Halter GM**, **Han MV**, **Heger A**, **Hillier L**, **Hinrichs AS**,

Holmes I, **Hoskins RA**, **Hubisz MJ** et al. Evolution of genes and genomes on the *Drosophila* phylogeny. *Nature* 450: 203–218, 2007.

Clarke S. Protein isoprenylation and methylation at carboxyl-terminal cysteine residues. *Annual review of biochemistry* 61: 355–386, 1992.

Colbert HA, **Smith TL**, **Bargmann CI**. OSM-9, a novel protein with structural similarity to channels, is required for olfaction, mechanosensation, and olfactory adaptation in *Caenorhabditis elegans*. *J Neurosci* 17: 8259–8269, 1997.

Cold Spring Harb Protoc, *Drosophila* Ringer's Solution, doi:10.1101/pdb.rec10919, 2007.

Connolly JB, **Roberts IJ**, **Armstrong JD**, **Kaiser K**, **Forte M**, **Tully T**, **OKANE CJ**. Associative learning disrupted by impaired G_s signaling in *Drosophila* mushroom bodies. *Science* 274: 2104–2107, 1996.

Corey DP, **Hudspeth AJ**. Response latency of vertebrate hair cells. *Biophys J* 26: 499–506, 1979.

Cork SM, **Van Meir EG**. Emerging roles for the BAI1 protein family in the regulation of phagocytosis, synaptogenesis, neurovasculature, and tumor development. *J. Mol. Med.* 89: 743–752, 2011.

Couteaux R, **Pécot-Dechavassine M**. Synaptic vesicles and pouches at the level of "active zones" of the neuromuscular junction. *C.R. Hebd. Seances Acad. Sci., Ser. D, Sci. Nat.* 271: 2346–2349, 1970.

Curtin JA, **Quint E**, **Tsipouri V**, **Arkell RM**, **Cattanach B**, **Copp AJ**, **Henderson DJ**, **Spurr N**, **Stanier P**, **Fisher EM**, **Nolan PM**, **Steel KP**, **Brown SDM**, **Gray IC**, **Murdoch JN**. Mutation of *Celsr1* disrupts planar polarity of inner ear hair cells and causes severe neural tube defects in the mouse. *Current Biology* 13: 1129–1133, 2003.

Daniels RW, **Collins CA**, **Gelfand MV**, **Dant J**, **Brooks ES**, **Krantz DE**, **DiAntonio A**. Increased expression of the *Drosophila* vesicular glutamate transporter leads to excess glutamate release and a compensatory decrease in quantal content. *Journal of Neuroscience* 24: 10466–10474, 2004.

Daniels RW, **Gelfand MV**, **Collins CA**, **DiAntonio A**. Visualizing glutamatergic cell bodies and synapses in *Drosophila* larval and adult CNS. *J. Comp. Neurol.* 508: 131–152, 2008.

Davletov BA, **Shamotienko OG**, **Lelianova VG**, **Grishin EV**, **Ushkaryov YA**. Isolation and biochemical characterization of a Ca^{2+}-independent α-latrotoxin-binding protein. *J Biol Chem* 271: 23239–23245, 1996.

De Potter WP, **Partoens P**, **Schoups A**, **Llona I**, **Coen EP**. Noradrenergic neurons release both noradrenaline and neuropeptide Y from a single pool: the large dense cored vesicles. *Synapse* 25: 44–55, 1997.

Dean C, **Dresbach T**. Neuroligins and neurexins: linking cell adhesion, synapse formation and cognitive function. *Trends in Neurosciences* 29: 21–29, 2006.

Dedman A, **Sharif-Naeini R**, **Folgering JHA**, **Duprat F**, **Patel A**, **Honoré E**. The mechano-

gated K_{2P} channel TREK-1. *Eur Biophys J* 38: 293–303, 2009.

Deguchi-Tawarada M, **Inoue E**, **Takao-Rikitsu E**, **Inoue M**, **Kitajima I**, **Ohtsuka T**, **Takai Y**. Active zone protein CAST is a component of conventional and ribbon synapses in mouse retina. *J. Comp. Neurol.* 495: 480–496, 2006.

Deken SL, **Vincent R**, **Hadwiger G**, **Liu Q**, **Wang Z-W**, **Nonet ML**. Redundant localization mechanisms of RIM and ELKS in *Caenorhabditis elegans*. *Journal of Neuroscience* 25: 5975–5983, 2005.

Del Castillo JJ, **Katz BB**. Changes in end-plate activity produced by presynaptic polarization. *The Journal of Physiology* 124: 586–604, 1954a.

Del Castillo JJ, **Katz BB**. Quantal components of the end-plate potential. *The Journal of Physiology* 124: 560–573, 1954.

Del Castillo JJ, **Katz BB**. Statistical factors involved in neuromuscular facilitation and depression. *The Journal of Physiology* 124: 574–585, 1954b.

Delgado R, **Maureira C**, **Oliva C**, **Kidokoro Y**, **Labarca P**. Size of vesicle pools, rates of mobilization, and recycling at neuromuscular synapses of a *Drosophila* mutant, shibire. *NEURON* 28: 941–953, 2000.

Deng L, **Kaeser P**, **Xu W**, **Südhof T**. RIM Proteins Activate Vesicle Priming by Reversing Autoinhibitory Homodimerization of Munc13. *NEURON* 69: 317–331, 2011.

Dhara M, **Yarzagaray A**, **Schwarz Y**, **Dutta S**, **Grabner C**, **Moghadam PK**, **Bost A**, **Dobson CM**. The structural basis of protein folding and its links with human disease. *Philos. Trans. R. Soc. Lond., B, Biol. Sci.* 356: 133–145, 2001.

Dhara M, **Yarzagaray A**, **Schwarz Y**, **Dutta S**, **Grabner C**, **Moghadam PK**, **Bost A**, **Schirra C**, **Rettig J**, **Reim K**, **Brose N**, **Mohrmann R**, **Bruns D**. Complexin synchronizes primed vesicle exocytosis and regulates fusion pore dynamics. *J Cell Biol* 204: 1123–1140, 2014.

DiAntonio A, **Burgess RW**, **Chin AC**, **Deitcher DL**, **Scheller RH**, **Schwarz TL**. Identification and characterization of *Drosophila* genes for synaptic vesicle proteins. *J Neurosci* 13: 4924–4935, 1993.

DiAntonio A, **Parfitt KD**, **Schwarz TL**. Synaptic transmission persists in synaptotagmin mutants of *Drosophila*. *Cell* 73: 1281–1290, 1993.

DiAntonio A, **Petersen SA**, **Heckmann M**, **Goodman CS**. Glutamate receptor expression regulates quantal size and quantal content at the *Drosophila* neuromuscular junction. *Journal of Neuroscience* 19: 3023–3032, 1999.

DiAntonio A, **Schwarz TL**. The effect on synaptic physiology of synaptotagmin mutations in *Drosophila*. *NEURON* 12: 909–920, 1994.

Dick O, **tom Dieck S**, **Altrock WD**, **Ammermüller J**, **Weiler R**, **Garner CC**, **Gundelfinger ED**, **Brandstätter JH**. The presynaptic active zone protein bassoon is essential for photoreceptor ribbon synapse formation in the retina. *NEURON* 37: 775–786, 2003.

Dietzl G, **Chen D**, **Schnorrer F**, **Su K-C**, **Barinova Y**, **Fellner M**, **Gasser B**, **Kinsey K**, **Oppel S**, **Scheiblauer S**, **Couto A**, **Marra V**, **Keleman K**, **Dickson BJ**. A genome-wide transgenic RNAi library for conditional gene inactivation in *Drosophila*. *Nature* 448: 151–156, 2007.

Dobson CM. The structural basis of protein folding and its links with human disease. *Philos. Trans. R. Soc. Lond., B, Biol. Sci.* 356: 133–145, 2001.

Domené S, **Stanescu H**, **Wallis D**, **Tinloy B**, **Pineda DE**, **Kleta R**, **Arcos-Burgos M**, **Roessler E**, **Muenke M**. Screening of human *LPHN3* for variants with a potential impact on ADHD susceptibility. *Am J Med Genet B Neuropsychiatr Genet* 156: 11–18, 2010.

Dubruille R, **Laurençon A**, **Vandaele C**, **Shishido E**, **Coulon-Bublex M**, **Swoboda P**, **Couble P**, **Kernan M**, **Durand B**. *Drosophila* regulatory factor X is necessary for ciliated sensory neuron differentiation. *Development* 129: 5487–5498, 2002.

Dulubova I, **Lou X**, **Lu J**, **Huryeva I**, **Alam A**, **Schneggenburger R**, **Südhof TC**, **Rizo J**. A Munc13/RIM/Rab3 tripartite complex: from priming to plasticity? *Embo J* 24: 2839–2850, 2005.

Eberl DF, **Boekhoff-Falk G**. Development of Johnston's organ in *Drosophila*. *Int. J. Dev. Biol.* 51: 679–687, 2007.

Eberl DF, **Hardy RW**, **Kernan MJ**. Genetically similar transduction mechanisms for touch and hearing in *Drosophila*. *J Neurosci* 20: 5981–5988, 2000.

Eberl DF. Feeling the vibes: chordotonal mechanisms in insect hearing. *Current Opinion in Neurobiology* 9: 389–393, 1999.

Effertz T, **Nadrowski B**, **Piepenbrock D**, **Albert JT**, **Göpfert MC**. Direct gating and mechanical integrity of *Drosophila* auditory transducers require TRPN1. *Nature Publishing Group* 15: 1198–1200, 2012.

Eggermann E, **Bucurenciu I**, **Goswami SP**, **Jonas P**. Nanodomain coupling between Ca^{2+} channels and sensors of exocytosis at fast mammalian synapses. *Nature Reviews Neuroscience* 13: 7–21, 2012.

Ehmann N, **van de Linde S**, **Alon A**, **Ljaschenko D**, **Keung XZ**, **Holm T**, **Rings A**, **DiAntonio A**, **Hallermann S**, **Ashery U**, **Heckmann M**, **Sauer M**, **Kittel RJ**. Quantitative super-resolution imaging of Bruchpilot distinguishes active zone states. *Nat Commun* 5: 4650, 2014.

Elmqvist D, **Quastel DM**. A quantitative study of end-plate potentials in isolated human muscle. *The Journal of Physiology* 178: 505–529, 1965.

Fernandez J, **Dittman J**. The Role of Complexin in Neurotransmitter Release. *Ethnicity & Disease* 19: S13–S14, 2009.

Emery P, **Strubin M**, **Hofmann K**, **Bucher P**, **Mach B**, **Reith W**. A consensus motif in the RFX DNA binding domain and binding domain mutants with altered specificity. *Molecular and Cellular Biology* 16: 4486–4494, 1996.

Feeney CJ, **Karunanithi S**, **Pearce J**, **Govind CK**, **Atwood HL**. Motor nerve terminals on

abdominal muscles in larval flesh flies, *Sarcophaga bullata*: comparisons with *Drosophila*. *J. Comp. Neurol.* 402: 197–209, 1998.

Fei H, Chow DM, Chen A, Romero-Calderon R, Ong WS, Ackerson LC, Maidment NT, Simpson JH , Frye MA, Krantz DE. Mutation of the *Drosophila* vesicular GABA transporter disrupts visual figure detection. *Journal of Experimental Biology* 213: 1717–1730, 2010.

Feinberg EH, **Vanhoven MK**, **Bendesky A**, **Wang G**, **Fetter RD**, **Shen K**, **Bargmann CI**. GFP Reconstitution Across Synaptic Partners (GRASP) defines cell contacts and synapses in living nervous systems. *NEURON* 57: 353–363, 2008.

Feng Z, **Koirala S**, **Ko C-P**. Synapse-glia interactions at the vertebrate neuromuscular junction. *Neuroscientist* 11: 503–513, 2005.

Ferguson SS. Evolving concepts in G protein-coupled receptor endocytosis: the role in receptor desensitization and signaling. *Pharmacol Rev* 53: 1–24, 2001.

Fernandez J, **Dittman J**. The Role of Complexin in Neurotransmitter Release. *Ethnicity & Disease* 19: S13–S14, 2009.

Fernández-Busnadiego R, **Schrod N**, **Kochovski Z**, **Asano S**, **Vanhecke D**, **Baumeister W**, **Lucic V**. Insights into the molecular organization of the neuron by cryo-electron tomography. *J Electron Microsc (Tokyo)* 60 Suppl 1: S137–48, 2011.

Fernández-Busnadiego R, **Zuber B**, **Maurer UE**, **Cyrklaff M**, **Baumeister W**, **Lucic V**. Quantitative analysis of the native presynaptic cytomatrix by cryoelectron tomography. *J Cell Biol* 188: 145–156, 2010.

Ferreira A, **Rapoport M**. The synapsins: beyond the regulation of neurotransmitter release. *Cell. Mol. Life Sci.* 59: 589–595, 2002.

Fettiplace R, **Hackney CM**. The sensory and motor roles of auditory hair cells. *Nature Reviews Neuroscience* 7: 19–29, 2006.

Fire A, **Xu S**, **Montgomery MK**, **Kostas SA**, **Driver SE**, **Mello CC**. Potent and specific genetic interference by double-stranded RNA in *Caenorhabditis elegans*. *Nature* 391: 806–811, 1998.

Fischer R. Diploma thesis. Location and function of the latrophilin homolog *dCirl* in *Drosophila melanogaster*. Julius-Maximilians-Universität Würzburg, Würzburg, Deutschland. 2011.

Fiumara F, **Fioriti L**, **Kandel ER**, **Hendrickson WA**. Essential Role of Coiled Coils for Aggregation and Activity of Q/N-Rich Prions and PolyQ Proteins. *Cell* 143: 1121–1135, 2010.

Forsythe ID, **Tsujimoto T**, **Barnes-Davies M**, **Cuttle MF**, **Takahashi T**. Inactivation of presynaptic calcium current contributes to synaptic depression at a fast central synapse. *NEURON* 20: 797–807, 1998.

Fouquet W, **Owald D**, **Wichmann C**, **Mertel S**, **Depner H**, **Dyba M**, **Hallermann S**, **Kittel RJ**, **Eimer S**, **Sigrist SJ**. Maturation of active zone assembly by *Drosophila* Bruchpilot. 186:

129–145, 2009.

Fredj NB, **Burrone J**. A resting pool of vesicles is responsible for spontaneous vesicle fusion at the synapse. *Nature Publishing Group* 12: 751–758, 2009.

Fredriksson R, **Lagerström MC**, **Lundin L-G**, **Schiöth HB**. The G-protein-coupled receptors in the human genome form five main families. Phylogenetic analysis, paralogon groups, and fingerprints. *Mol Pharmacol* 63: 1256–1272, 2003.

Freeman M. Reiterative use of the EGF receptor triggers differentiation of all cell types in the *Drosophila* eye. *Cell* 87: 651–660, 1996.

Freeman MR, **Doherty J**. Glial cell biology in *Drosophila* and vertebrates. *Trends in Neurosciences* 29: 82–90, 2006.

Freeman W, **Morton AJ**. Differential messenger RNA expression of complexins in mouse brain. *Brain Res Bull* 63: 33–44, 2004.

Fujisawa K, **Wrana JL**, **Culotti JG**. The slit receptor EVA-1 coactivates a SAX-3/Robo mediated guidance signal in *C. elegans*. *Science* 317: 1934–1938, 2007.

Fuller MT, **Regan CL**, **Green LL**, **Robertson B**, **Deuring R**, **Hays TS**. Interacting genes identify interacting proteins involved in microtubule function in *Drosophila*. *Cell Motil Cytoskeleton* 14: 128–135, 1989.

Gainetdinov RR, **Premont RT**, **Bohn LM**, **Lefkowitz RJ**, **Caron MG**. Desensitization of G protein-coupled receptors and neuronal functions. *Annual review of neuroscience* 27: 107–144, 2004.

Gehring J., Dissertation. Functional analysis of the latrophilin homolog *dCirl* in *Drosophila melanogaster*. Julius-Maximilians-Universität Würzburg, Würzburg, Deutschland. 2014.

Geiger JR, **Jonas P**. Dynamic control of presynaptic Ca^{2+} inflow by fast-inactivating K^{+} channels in hippocampal mossy fiber boutons. *Neuron* 28: 927–939, 2000.

Geppert M, **Archer B**, **Südhof T**. Synaptotagmin II. A novel differentially distributed form of synaptotagmin. *J Biol Chem* 266: 13548–13552, 1991.

Geppert M, **Goda Y**, **Hammer RE**, **Li C**, **Rosahl TW**, **Stevens CF**, **Südhof TC**. Synaptotagmin I: a major Ca^{2+} sensor for transmitter release at a central synapse. *Cell* 79: 717–727, 1994.

Giannakouros T, **Nikolakaki E**, **Mylonis I**, **Georgatsou E**. Serine-arginine protein kinases: a small protein kinase family with a large cellular presence. *FEBS J.* 278: 570–586, 2011.

Gilestro GF, **Tononi G**, **Cirelli C**. Widespread changes in synaptic markers as a function of sleep and wakefulness in *Drosophila*. *Science* 324: 109–112, 2009.

Giraudo CG, **Eng WS**, **Melia TJ**, **Rothman JE**. A clamping mechanism involved in SNARE-dependent exocytosis. *Science* 313: 676–680, 2006.

Giraudo CG, **Garcia-Diaz A**, **Eng WS**, **Chen Y**, **Hendrickson WA**, **Melia TJ**, **Rothman**

JE. Alternative zippering as an on-off switch for SNARE-mediated fusion. *Science* 323: 512–516, 2009.

Glowatzki E, **Fuchs PA**. Transmitter release at the hair cell ribbon synapse. *Nature Neuroscience* 5: 147–154, 2002.

Goldstein AYN, **Wang X**, **Schwarz TL**. Axonal transport and the delivery of pre-synaptic components. *Current Opinion in Neurobiology* 18: 495–503, 2008.

Gong WJ, **Golic KG**. Ends-out, or replacement, gene targeting in *Drosophila*. *Proc Natl Acad Sci USA* 100: 2556–2561, 2003.

Gong Z, **Son W**, **Chung YD**, **Kim J**, **Shin DW**, **McClung CA**, **Lee Y**, **Lee HW**, **Chang D-J**, **Kaang B-K**, **Cho H**, **Oh U**, **Hirsh J**, **Kernan MJ**, **Kim C**. Two interdependent TRPV channel subunits, Inactive and Nanchung, mediate hearing in *Drosophila*. *Journal of Neuroscience* 24: 9059–9066, 2004.

Göpfert MC, **Albert JT**, **Nadrowski B**, **Kamikouchi A**. Specification of auditory sensitivity by *Drosophila* TRP channels. *Nature Neuroscience* 9: 999–1000, 2006.

Göpfert MC, **Robert D**. Motion generation by *Drosophila* mechanosensory neurons. *Proc Natl Acad Sci U S A* 100: 5514–5519, 2003.

Górska-Andrzejak J, **Makuch R**, **Stefan J**, **Görlich A**, **Semik D**, **Pyza E**. Circadian expression of the presynaptic active zone protein bruchpilot in the lamina of *Drosophila melanogaster*. *Dev Neurobiol* 73: 14–26, 2013.

Grace CRR, **Perrin MH**, **DiGruccio MR**, **Miller CL**, **Rivier JE**, **Vale WW**, **Riek R**. NMR structure and peptide hormone binding site of the first extracellular domain of a type B1 G protein-coupled receptor. *Proc Natl Acad Sci USA* 101: 12836–12841, 2004.

Graf ER, **Daniels RW**, **Burgess RW**, **Schwarz TL**, **DiAntonio A**. Rab3 Dynamically Controls Protein Composition at Active Zones. *NEURON* 64: 663–677, 2009.

Graf ER, **Valakh V**, **Wright CM**, **Wu C**, **Liu Z**, **Zhang YQ**, **DiAntonio A**. RIM Promotes Calcium Channel Accumulation at Active Zones of the *Drosophila* Neuromuscular Junction. *Journal of Neuroscience* 32: 16586–16596, 2012.

Gratz SJ, **Wildonger J**, **Harrison MM**, **O'Connor-Giles KM**. CRISPR/Cas9-mediated genome engineering and the promise of designer flies on demand. *Fly (Austin)* 7: 249–255, 2013.

Gray EG, **Young JZ**. Electron microscopy of synaptic structure of octopus brain. *J Cell Biol* 21: 87–103, 1964.

Gray JX, **Haino M**, **Roth MJ**, **Maguire JE**, **Jensen PN**, **Yarme A**, **Stetler-Stevenson MA**, **Siebenlist U**, **Kelly K**. CD97 is a processed, seven-transmembrane, heterodimeric receptor associated with inflammation. *J Immunol* 157: 5438–5447, 1996.

Groemer TW, **Klingauf J**. Synaptic vesicles recycling spontaneously and during activity belong to the same vesicle pool. *Nature Neuroscience* 10: 145–147, 2007.

Groffen AJ, **Martens S**, **Díez Arazola R**, **Cornelisse LN**, **Lozovaya N**, **de Jong APH**, **Goriounova NA**, **Habets RLP**, **Takai Y**, **Borst JG**, **Brose N**, **McMahon HT**, **Verhage M**. Doc2b is a high-affinity Ca^{2+} sensor for spontaneous neurotransmitter release. *Science* 327: 1614–1618, 2010.

Groth A, **Fish M**, **Nusse R**, **Calos M**. Construction of transgenic *Drosophila* by using the site-specific integrase from phage φC31. *Genetics* 166: 1775, 2004.

Grünert U, **Gnatzy W**. K^+ and Ca^{2+} in the receptor lymph of arthropod cuticular mechanoreceptors. *CORD Conference Proceedings* 161: 329–333, 1987.

Gu CX, **Juranka PF**, **Morris CE**. Stretch-Activation and Stretch-Inactivation of Shaker-IR, a Voltage-Gated K^+ Channel. *Biophys J*. 80: 2678–2693, 2001.

Gutiérrez R, **Heinemann U**. Kindling induces transient fast inhibition in the dentate gyrus-CA3 projection. *Eur. J. Neurosci.* 13: 1371–1379, 2001.

Hall DH, **Hedgecock EM**. Kinesin-related gene *unc-104* is required for axonal transport of synaptic vesicles in *C. elegans*. *Cell* 65: 837-847, 1991.

Hallam SJ, **Goncharov A**, **McEwen J**, **Baran R**, **Jin Y**. SYD-1, a presynaptic protein with PDZ, C2 and rhoGAP-like domains, specifies axon identity in *C. elegans*. *Nature Neuroscience* 5: 1137–1146, 2002.

Hallermann S, **Heckmann M**, **Kittel RJ**. Mechanisms of short-term plasticity at neuromuscular active zones of *Drosophila*. *HFSP Journal* 4: 72–84, 2010a.

Hallermann S, **Kittel RJ**, **Wichmann C**, **Weyhersmüller A**, **Fouquet W**, **Mertel S**, **Owald D**, **Eimer S**, **Depner H**, **Schwarzel M**, **Sigrist SJ**, **Heckmann M**. Naked Dense Bodies Provoke Depression. *Journal of Neuroscience* 30: 14340–14345, 2010b.

Hallermann S, **Silver RA**. Sustaining rapid vesicular release at active zones: potential roles for vesicle tethering. *Trends in Neurosciences* 36: 185–194, 2013.

Hamann J, **Stortelers C**, **Kiss-Toth E**, **Vogel B**, **Eichler W**, **van Lier RA**. Characterization of the CD55 (DAF)-binding site on the seven-span transmembrane receptor CD97. *Eur. J. Immunol.* 28: 1701–1707, 1998.

Hamann J, **Vogel B**, **van Schijndel GM**, **van Lier RA**. The seven-span transmembrane receptor CD97 has a cellular ligand (CD55, DAF). *J Exp Med* 184: 1185–1189, 1996.

Han C, **Jan LY**, **Jan YN**. Enhancer-driven membrane markers for analysis of nonautonomous mechanisms reveal neuron-glia interactions in *Drosophila*. *Proc Natl Acad Sci USA* 108: 9673–9678, 2011.

Han Y, **Kaeser PS**, **Südhof TC**, **Schneggenburger R**. RIM Determines Ca^{2+} Channel Density and Vesicle Docking at the Presynaptic Active Zone. *NEURON* 69: 304–316, 2011.

Harlow ML, **Ress D**, **Stoschek A**, **Marshall RM**, **McMahan UJ**. The architecture of active zone material at the frog's neuromuscular junction. *Nature* 409: 479–484, 2001.

Hartenstein V. Atlas of *Drosophila* development. Cold Spring Harbor Laboratory Press,

1993.

Hartenstein V. Development of *Drosophila* larval sensory organs: spatiotemporal pattern of sensory neurones, peripheral axonal pathways and sensilla differentiation. *Development* 102: 869-886, 1988.

Hays TS, **Deuring R**, **Robertson B**, **Prout M**, **Fuller MT**. Interacting proteins identified by genetic interactions: a missense mutation in α-tubulin fails to complement alleles of the testis-specific β-tubulin gene of *Drosophila melanogaster*. *Molecular and Cellular Biology* 9: 875–884, 1989.

Heckmann M, **Dudel J**. Desensitization and resensitization kinetics of glutamate receptor channels from *Drosophila* larval muscle. *Biophys J* 72: 2160–2169, 1997.

Heidelberger R, **Thoreson WB**, **Witkovsky P**. Synaptic transmission at retinal ribbon synapses. *Prog Retin Eye Res* 24: 682–720, 2005.

Heinze S, **Homberg U**. Maplike representation of celestial E-vector orientations in the brain of an insect. *Science* 315: 995–997, 2007.

Heuser JE, **Reese TS**. Evidence for recycling of synaptic vesicle membrane during transmitter release at the frog neuromuscular junction. *J Cell Biol* 57: 315–344, 1973.

Hibino H, **Pironkova R**, **Onwumere O**, **Vologodskaia M**, **Hudspeth AJ**, **Lesage F**. RIM binding proteins (RBPs) couple Rab3-interacting molecules (RIMs) to voltage-gated Ca^{2+}-channels. *NEURON* 34: 411–423, 2002.

Hida Y, **Ohtsuka T**. CAST and ELKS proteins: structural and functional determinants of the presynaptic active zone. *Journal of Biochemistry* 148: 131–137, 2010.

Hilfiker S, **Pieribone VA**, **Czernik AJ**, **Kao HT**, **Augustine GJ**, **Greengard P**. Synapsins as regulators of neurotransmitter release. *Philos. Trans. R. Soc. Lond., B, Biol. Sci.* 354: 269–279, 1999.

Hirokawa N. Cross-linker system between neurofilaments, microtubules, and membranous organelles in frog axons revealed by the quick-freeze, deep-etching method. *J Cell Biol* 94: 129–142, 1982.

Hirokawa N. Kinesin and Dynein Superfamily Proteins and the Mechanism of Organelle Transport. *Science* 279: 519–526, 1998.

Hoang B, **Chiba A**. Single-cell analysis of *Drosophila* larval neuromuscular synapses. *Dev Biol* 229: 55–70, 2001.

Hobson RJ, **Liu Q**, **Watanabe S**, **Jrgensen EM**. Complexin Maintains Vesicles in the Primed State in *C. elegans*. *Current Biology* 21: 106–113, 2011.

Hochreiter-Hufford AE, **Lee CS**, **Kinchen JM**, **Sokolowski JD**, **Arandjelovic S**, **Call JA**, **Klibanov AL**, **Yan Z**, **Mandell JW**, **Ravichandran KS**. Phosphatidylserine receptor BAI1 and apoptotic cells as new promoters of myoblast fusion. *Nature* 497: 263–267, 2013.

Hofbauer A. Eine Bibliothek monoklonaler Antikörper gegen das Gehirn von *Drosophila*

melanogaster. Habilitation thesis. Julius-Maximilians-Universität Würzburg, Würzburg, Deutschland. 1991.

Hökfelt T. Neuropeptides in perspective: the last ten years. *Neuron* 7: 867–879, 1991.

Hosoi N, **Holt M**, **Sakaba T**. Calcium dependence of exo- and endocytotic coupling at a glutamatergic synapse. *NEURON* 63: 216–229, 2009.

Hough CD, **Woods DF**, **Park S**, **Bryant PJ**. Organizing a functional junctional complex requires specific domains of the *Drosophila* MAGUK Discs large. *Genes Dev* 11: 3242–3253, 1997.

Howard J, **Bechstedt S**. Hypothesis: a helix of ankyrin repeats of the NOMPC-TRP ion channel is the gating spring of mechanoreceptors. *Current Biology* 14: R224–6, 2004.

Howard J, **Hudspeth AJ**. Compliance of the hair bundle associated with gating of mechanoelectrical transduction channels in the bullfrog's saccular hair cell. *NEURON* 1: 189–199, 1988.

Hu C-D, **Chinenov Y**, **Kerppola TK**. Visualization of interactions among bZIP and Rel family proteins in living cells using bimolecular fluorescence complementation. *Mol. Cell* 9: 789–798, 2002.

Huang J, **Zhou W**, **Watson AM**, **Jan YN**, **Hong Y**. Efficient ends-out gene targeting in *Drosophila*. *Genetics* 180: 703–707, 2008.

Huang YS, **Chiang NY**, **Hu CH**, **Hsiao CC**, **Cheng KF**, **Tsai WP**, **Yona S**, **Stacey M**, **Gordon S**, **Chang GW**, **Lin HH**. Activation of Myeloid Cell-Specific Adhesion Class G Protein-Coupled Receptor EMR2 via Ligation-Induced Translocation and Interaction of Receptor Subunits in Lipid Raft Microdomains. *Molecular and Cellular Biology* 32: 1408–1420, 2012.

Hughes CL, **Thomas JB**. A sensory feedback circuit coordinates muscle activity in *Drosophila*. *Molecular and Cellular Neuroscience* 35: 383–396, 2007.

Huntwork S, **Littleton JT**. A complexin fusion clamp regulates spontaneous neurotransmitter release and synaptic growth. *Nature Neuroscience* 10: 1235–1237, 2007.

Hurd DD, **Saxton WM**. Kinesin mutations cause motor neuron disease phenotypes by disrupting fast axonal transport in *Drosophila*. *Genetics* 144: 1075–1085, 1996.

Husain N, **Pellikka M**, **Hong H**, **Klimentova T**, **Choe K-M**, **Clandinin TR**, **Tepass U**. The agrin/perlecan-related protein Eyes Shut is essential for epithelial lumen formation in the *Drosophila* retina. *Developmental Cell* 11: 483–493, 2006.

Ichtchenko KK, **Bittner MAM**, **Krasnoperov VV**, **Little ARA**, **Chepurny OO**, **Holz RWR**, **Petrenko AGA**. A novel ubiquitously expressed α-latrotoxin receptor is a member of the CIRL family of G-protein-coupled receptors. *J Biol Chem* 274: 5491–5498, 1999.

Ichtchenko KK, **Khvotchev MM**, **Kiyatkin NN**, **Simpson LL**, **Sugita SS**, **Südhof TCT**. α-latrotoxin action probed with recombinant toxin: receptors recruit α-latrotoxin but do not transduce an exocytotic signal. *Embo J* 17: 6188–6199, 1998.

Imig C, **Min S-W**, **Krinner S**, **Arancillo M**, **Rosenmund C**, **Südhof TC**, **Rhee J**, **Brose N**, **Cooper BH**. The morphological and molecular nature of synaptic vesicle priming at presynaptic active zones. *NEURON* 84: 416–431, 2014.

Ingber D. Integrins as mechanochemical transducers. *Curr Opin Cell Biol*. 3: 841-848, 1991.

Ishizuka T, **Saisu H**, **Odani S**, **Abe T**. Synaphin: a protein associated with the docking/fusion complex in presynaptic terminals. *Biochemical and Biophysical Research Communications* 213: 1107–1114, 1995.

Ito K, **Suzuki K**, **Estes P**, **Ramaswami M**, **Yamamoto D**, **Strausfeld NJ**. The organization of extrinsic neurons and their implications in the functional roles of the mushroom bodies in *Drosophila melanogaster* Meigen. *Learn. Mem.* 5: 52–77, 1998.

Iyer J, **Wahlmark CJ**, **Kuser-Ahnert GA**, **Kawasaki F**. Molecular mechanisms of COMPLEXIN fusion clamp function in synaptic exocytosis revealed in a new *Drosophila* mutant. *Molecular and Cellular Neuroscience* 56: 244–254, 2013.

Jackman SL, **Choi S-Y**, **Thoreson WB**, **Rabl K**, **Bartoletti TM**, **Kramer RH**. Role of the synaptic ribbon in transmitting the cone light response. *Nature Publishing Group* 12: 303–310, 2009.

Jahn R, **Fasshauer D**. Molecular machines governing exocytosis of synaptic vesicles. *Nature* 490: 201–207, 2012.

Jahn R, **Lang T**, **Südhof T**. Membrane fusion. *Cell* 112: 519–533, 2003.

Jaspars LH, **Vos W**, **Aust G**, **van Lier RA**, **Hamann J**. Tissue distribution of the human CD97 EGF-TM7 receptor. *Tissue Antigens* 57: 325–331, 2001.

Jennings BH. *Drosophila* – a versatile model in biology & medicine. *Materials Today* 14: 190–195, 2011.

Jiao W, **Masich S**, **Franzén O**, **Shupliakov O**. Two pools of vesicles associated with the presynaptic cytosolic projection in *Drosophila* neuromuscular junctions. *J. Struct. Biol.* 172: 389–394, 2010.

Jin Z, **Tietjen I**, **Bu L**, **Liu-Yesucevitz L**, **Gaur SK**, **Walsh CA**, **Piao X**. Disease-associated mutations affect GPR56 protein trafficking and cell surface expression. *Hum Mol Genet* 16: 1972–1985, 2007.

Johnson E III, **Fetter R**, **Davis G**, **Ziv N**. Negative regulation of active zone assembly by a newly identified SR protein kinase. *PLoS Biol* 7: e1000193, 2009.

Jorquera RA, **Huntwork-Rodriguez S**, **Akbergenova Y**, **Cho RW**, **Littleton JT**. Complexin Controls Spontaneous and Evoked Neurotransmitter Release by Regulating the Timing and Properties of Synaptotagmin Activity. *Journal of Neuroscience* 32: 18234–18245, 2012.

Kaeser PS, **Deng L**, **Chávez AE**, **Liu X**, **Castillo PE**, **Südhof TC**. ELKS2α/CAST deletion selectively increases neurotransmitter release at inhibitory synapses. *NEURON* 64: 227–239,

2009.

Kaeser PS. Pushing synaptic vesicles over the RIM. *Cell Logist* 1: 106–110, 2011.

Kaeser-Woo YJ, **Yang X**, **Südhof TC**. C-terminal complexin sequence is selectively required for clamping and priming but not for Ca^{2+} triggering of synaptic exocytosis. *Journal of Neuroscience* 32: 2877–2885, 2012.

Kamikouchi A, **Shimada T**, **Ito K**. Comprehensive classification of the auditory sensory projections in the brain of the fruit fly *Drosophila melanogaster*. *J. Comp. Neurol.* 499: 317–356, 2006.

Karpus ON, **Veninga H**, **Hoek RM**, **Flierman D**, **van Buul JD**, **Vandenakker CC**, **vanBavel E**, **Medof ME**, **van Lier RAW**, **Reedquist KA**, **Hamann J**. Shear stress-dependent downregulation of the adhesion-G protein-coupled receptor CD97 on circulating leukocytes upon contact with its ligand CD55. *J Immunol* 190: 3740–3748, 2013.

Kaufmann N, **DeProto J**, **Ranjan R**, **Wan H**, **Van Vactor D**. *Drosophila* Liprin-α and the Receptor Phosphatase Dlar Control Synapse Morphogenesis. *NEURON* 34: 27–38, 2002.

Kaur B, **Brat DJ**, **Devi NS**, **Van Meir EG**. Vasculostatin, a proteolytic fragment of brain angiogenesis inhibitor 1, is an antiangiogenic and antitumorigenic factor. *Oncogene* 24: 3632–3642, 2005.

Kee HJ, **Koh JT**, **Kim M-Y**, **Ahn KY**, **Kim JK**, **Bae CS**, **Park SS**, **Kim KK**. Expression of brain-specific angiogenesis inhibitor 2 (BAI2) in normal and ischemic brain: involvement of BAI2 in the ischemia-induced brain angiogenesis. *J. Cereb. Blood Flow Metab.* 22: 1054–1067, 2002.

Keil TA. Functional morphology of insect mechanoreceptors. *Microsc Res Tech* 39: 506–531, 1997.

Kernan M, **Cowan D**, **Zuker C**. Genetic dissection of mechanosensory transduction: mechanoreception-defective mutations of *Drosophila*. *NEURON* 12: 1195–1206, 1994.

Kernan MJ. Mechanotransduction and auditory transduction in *Drosophila*. *Pflugers Arch.* 454: 703–720, 2007.

Khorana HG. Rhodopsin, photoreceptor of the rod cell. An emerging pattern for structure and function. *J Biol Chem* 267: 1–4, 1992.

Kim J, **Chung YD**, **Park D-Y**, **Choi S**, **Shin DW**, **Soh H**, **Lee HW**, **Son W**, **Yim J**, **Park C-S**, **Kernan MJ**, **Kim C**. A TRPV family ion channel required for hearing in *Drosophila*. *Nature* 424: 81–84, 2003.

Karhunen T, **Vilim FS**, **Alexeeva V**, **Weiss KR**, **Church PJ**. Targeting of peptidergic vesicles in cotransmitting terminals. *Journal of Neuroscience* 21: –RC127, 2001.

Kim SE, **Coste B**, **Chadha A**, **Cook B**, **Patapoutian A**. The role of *Drosophila* Piezo in mechanical nociception. *Nature* 483: 209–212, 2012.

Kimura H, **Usui T**, **Tsubouchi A**, **Uemura T**. Potential dual molecular interaction of the

Drosophila 7-pass transmembrane cadherin Flamingo in dendritic morphogenesis. *J Cell Sci* 119: 1118–1129, 2006.

Kittel RJ, **Hallermann S**, **Thomsen S**, **Wichmann C**, **Sigrist SJ**, **Heckmann M**. Active zone assembly and synaptic release. *Biochem Soc Trans* 34: 939–941, 2006a.

Kittel RJ, **Wichmann C**, **Rasse TM**, **Fouquet W**, **Schmidt M**, **Schmid A**, **Wagh DA**, **Pawlu C**, **Kellner RR**, **Willig KI**, **Hell SW**, **Buchner E**, **Heckmann M**, **Sigrist SJ**. Bruchpilot promotes active zone assembly, Ca^{2+} channel clustering, and vesicle release. *Science* 312: 1051–1054, 2006b.

Kiyonaka S, **Wakamori M**, **Miki T**, **Uriu Y**, **Nonaka M**, **Bito H**, **Beedle AM**, **Mori E**, **Hara Y**, **De Waard M**, **Kanagawa M**, **Itakura M**, **Takahashi M**, **Campbell KP**, **Mori Y**. RIM1 confers sustained activity and neurotransmitter vesicle anchoring to presynaptic Ca^{2+} channels. *Nature Neuroscience* 10: 691–701, 2007.

Ko J, **Na M**, **Kim S**, **Lee J-R**, **Kim E**. Interaction of the ERC family of RIM-binding proteins with the liprin-α family of multidomain proteins. *J Biol Chem* 278: 42377–42385, 2003.

Kobilka BK, **Deupi X**. Conformational complexity of G-protein-coupled receptors. *Trends Pharmacol Sci* 28: 397–406, 2007.

Koh T-W, **Bellen HJ**. Synaptotagmin I, a Ca^{2+} sensor for neurotransmitter release. *Trends in Neurosciences* 26: 413–422, 2003.

Kokona B, **Rosenthal ZP**, **Fairman R**. Role of the coiled-coil structural motif in polyglutamine aggregation. *Biochemistry* 53: 6738–6746, 2014.

Krasnoperov V, **Bittner MA**, **Holz RW**, **Chepurny O**, **Petrenko AG**. Structural Requirements for α-Latrotoxin Binding and α-Latrotoxin-stimulated Secretion: A study with calcium-independent receptor of α-latrotoxin (*Cirl*) deletion mutants. *Journal of Biological Chemistry* 274: 3590–3596, 1999.

Krasnoperov V, **Bittner MA**, **Mo W**, **Buryanovsky L**, **Neubert TA**, **Holz RW**, **Ichtchenko K**, **Petrenko AG**. Protein-tyrosine Phosphatase-ς Is a Novel Member of the Functional Family of α-Latrotoxin Receptors. *Journal of Biological Chem.* 277: 35887–35895, 2002.

Krasnoperov V, **Deyev IE**, **Serova OV**, **Xu C**, **Lu Y**, **Buryanovsky L**, **Gabibov AG**, **Neubert TA**, **Petrenko AG**. Dissociation of the subunits of the calcium-independent receptor of α-latrotoxin as a result of two-step proteolysis. *Biochemistry* 48: 3230–3238, 2009.

Krasnoperov V. Post-translational Proteolytic Processing of the Calcium-independent Receptor of α-Latrotoxin (CIRL), a Natural Chimera of the Cell Adhesion Protein and the G Protein-coupled Receptor. ROLE OF THE G PROTEIN-COUPLED RECEPTOR PROTEOLYSIS SITE (GPS) MOTIF. *Journal of Biological Chemistry* 277: 46518–46526, 2002.

Krasnoperov VG, **Beavis R**, **Chepurny OG**, **Little AR**, **Plotnikov AN**, **Petrenko AG**. The calcium-independent receptor of α-latrotoxin is not a neurexin. *Biochemical and Biophysical Research Communications* 227: 868–875, 1996.

Krasnoperov VG, **Bittner MA**, **Beavis R**, **Kuang YN**, **Salnikow KV**, **Chepurny OG**, **Little AR**, **Plotnikov AN**, **Wu DQ**, **Holz RW**, **Petrenko AG**. α-latrotoxin stimulates exocytosis by the interaction with a neuronal G-protein-coupled receptor. *NEURON* 18: 925–937, 1997.

Krishnakumar SS, **Radoff DT**, **Kümmel D**, **Giraudo CG**, **Li F**, **Khandan L**, **Baguley SW**, **Coleman J**, **Reinisch KM**, **Pincet F**, **Rothman JE**. A conformational switch in complexin is required for synaptotagmin to trigger synaptic fusion. *Nat Struct Mol Biol* 18: 934–940, 2011.

Kümmel D, **Krishnakumar SS**, **Radoff DT**, **Li F**, **Giraudo CG**, **Pincet F**, **Rothman JE**, **Reinisch KM**. *Nat Struct Mol Biol* 18: 927–933, 2011.

Kuromi H, **Kidokoro Y**. Tetanic stimulation recruits vesicles from reserve pool via a cAMP-mediated process in *Drosophila* synapses. *NEURON* 27: 133–143, 2000.

Lacy SE, **Bönnemann CG**, **Buzney EA**, **Kunkel LM**. Identification of FLRT1, FLRT2, and FLRT3: a novel family of transmembrane leucine-rich repeat proteins. *Genomics* 62: 417–426, 1999.

Lagerström MC, **Schiöth HB**. Structural diversity of G protein-coupled receptors and significance for drug discovery. *Nat Rev Drug Discov* 7: 339–357, 2008.
Lahey T, **Gorczyca M**, **Jia X-X**, **Budnik V**. The *Drosophila* tumor suppressor genedlgis required for normal synaptic bouton structure. *NEURON* 13: 823–835, 1994.

Lai S-L, **Lee T**. Genetic mosaic with dual binary transcriptional systems in *Drosophila*. *Nature Neuroscience* 9: 703–709, 2006.

Landis DMD. Membrane and cytoplasmic structure at synaptic junctions in the mammalian central nervous system. *J. Elec. Microsc. Tech.* 10: 129–151, 1988.

Lang JJ, **Ushkaryov YY**, **Grasso AA**, **Wollheim CBC**. Ca^{2+}-independent insulin exocytosis induced by α-latrotoxin requires latrophilin, a G protein-coupled receptor. *EMBO J* 17: 648–657, 1998.

Lange M, **Norton W**, **Coolen M**, **Chaminade M**, **Merker S**, **Proft F**, **Schmitt A**, **Vernier P**, **Lesch K-P**, **Bally-Cuif L**. The ADHD-susceptibility gene *lphn3.1* modulates dopaminergic neuron formation and locomotor activity during zebrafish development. *Mol Psychiatry* 17: 946–954, 2012.

Langenhan T, **Aust G**, **Hamann J**. Sticky Signaling-Adhesion Class G Protein-Coupled Receptors Take the Stage. *Science Signaling* 6: –re3, 2013.

Langenhan T, **Prömel S**, **Mestek L**, **Esmaeili B**, **Waller-Evans H**, **Hennig C**, **Kohara Y**, **Avery L**, **Vakonakis I**, **Schnabel R**, **Russ AP**. Latrophilin Signaling Links Anterior-Posterior Tissue Polarity and Oriented Cell Divisions in the *C. elegans* Embryo. *Developmental Cell* 17: 494–504, 2009.

Laurençon A, **Dubruille R**, **Efimenko E**, **Grenier G**, **Bissett R**, **Cortier E**, **Rolland V**, **Swoboda P**, **Durand B**. Identification of novel regulatory factor X (RFX) target genes by comparative genomics in *Drosophila* species. *Genome Biol* 8: R195, 2007.

Lee J, **Littleton JT**. Transmembrane tethering of synaptotagmin to synaptic vesicles controls multiple modes of neurotransmitter release. *Proc Natl Acad Sci USA* 112: 3793–3798, 2015.

Lee JS, **Ho W-K**, **Neher E**, **Lee S-H**. Superpriming of synaptic vesicles after their recruitment to the readily releasable pool. *Proceedings of the National Academy of Sciences* 110: 15079–15084, 2013.

Lee T, **Luo L**. Mosaic analysis with a repressible cell marker for studies of gene function in neuronal morphogenesis. *NEURON* 22: 451–461, 1999.

Lehnert BP, **Baker AE**, **Gaudry Q**, **Chiang A-S**, **Wilson RI**. Distinct roles of TRP channels in auditory transduction and amplification in *Drosophila*. *NEURON* 77: 115–128, 2013.

Lenzi D, **Gersdorff von H**. Structure suggests function: the case for synaptic ribbons as exocytotic nanomachines. *Bioessays* 23: 831–840, 2001.

Levine A, **Bashan-Ahrend A**, **Budai-Hadrian O**, **Gartenberg D**, **Menasherow S**, **Wides R**. odd Oz: A novel *Drosophila* pair rule gene. *Cell* 77: 587–598, 1994.

Li A, **Tian X**, **Sung S-W**, **Somlo S**. Identification of two novel polycystic kidney disease-1-like genes in human and mouse genomes. *Genomics* 81: 596–608, 2003.

Liang X, **Madrid J**, **Gärtner R**, **Verbavatz J-M**, **Schiklenk C**, **Wilsch-Bräuninger M**, **Bogdanova A**, **Stenger F**, **Voigt A**, **Howard J**. A NOMPC-dependent membrane-microtubule connector is a candidate for the gating spring in fly mechanoreceptors. *Curr. Biol.* 23: 755–763, 2013.

Liebscher I, **Schön J**, **Petersen SC**, **Fischer L**, **Auerbach N**, **Demberg LM**, **Mogha A**, **Cöster M**, **Simon K-U**, **Rothemund S**, **Monk KR**, **Schöneberg T**. A Tethered Agonist within the Ectodomain Activates the Adhesion G Protein-Coupled Receptors GPR126 and GPR133. *Cell Rep* 9: 2018–2026, 2014.

Liedert A, **Kaspar D**, **Blakytny R**, **Claes L**, **Ignatius A**. Signal transduction pathways involved in mechanotransduction in bone cells. *Biochemical and Biophysical Research Communications* 349: 1–5, 2006.

Lin H-H, **Chang G-W**, **Davies JQ**, **Stacey M**, **Harris J**, **Gordon S**. Autocatalytic cleavage of the EMR2 receptor occurs at a conserved G protein-coupled receptor proteolytic site motif. *J Biol Chem* 279: 31823–31832, 2004.

Lipstein N, **Sakaba T**, **Cooper BH**, **Lin K-H**, **Strenzke N**, **Ashery U**, **Rhee J-S**, **Taschenberger H**, **Neher E**, **Brose N**. Dynamic Control of Synaptic Vesicle Replenishment and Short-Term Plasticity by Ca^{2+}-Calmodulin-Munc13-1 Signaling. *NEURON* 79: 82–96, 2013.

Lise M-F, **El-Husseini A**. The neuroligin and neurexin families: from structure to function at the synapse. *Cell. Mol. Life Sci.* 63: 1833–1849, 2006.

Littleton JT, **Bellen HJ**, **Perin MS**. Expression of synaptotagmin in *Drosophila* reveals transport and localization of synaptic vesicles to the synapse. *Development* 118: 1077–1088, 1993a.

Littleton JT, **Stern M**, **Perin M**, **Bellen HJ**. Calcium dependence of neurotransmitter release and rate of spontaneous vesicle fusions are altered in *Drosophila* synaptotagmin mutants. *Proc Natl Acad Sci USA* 91: 10888–10892, 1994.

Littleton JT, **Stern M**, **Schulze K**, **Perin M**, **Bellen HJ**. Mutational analysis of *Drosophila* synaptotagmin demonstrates its essential role in Ca^{2+}-activated neurotransmitter release. *Cell* 74: 1125–1134, 1993b.

Liu C, **Bickford LS**, **Held RG**, **Nyitrai H**, **Südhof TC**, **Kaeser PS**. The active zone protein family ELKS supports Ca^{2+} influx at nerve terminals of inhibitory hippocampal neurons. *J Neurosci* 34: 12289–12303, 2014.

Liu KSY, **Siebert M**, **Mertel S**, **Knoche E**, **Wegener S**, **Wichmann C**, **Matkovic T**, **Muhammad K**, **Depner H**, **Mettke C**, **Bückers J**, **Hell SW**, **Müller M**, **Davis GW**, **Schmitz D**, **Sigrist SJ**. RIM-Binding Protein, a Central Part of the Active Zone, Is Essential for Neurotransmitter Release. *Science* 334: 1565–1569, 2011.

Liu L, **Li Y**, **Wang R**, **Yin C**, **Dong Q**, **Hing H**, **Kim C**, **Welsh MJ**. *Drosophila* hygrosensation requires the TRP channels water witch and nanchung. *Nature* 450: 294–U14, 2007.

Liu M, **Parker RM**, **Darby K**, **Eyre HJ**, **Copeland NG**, **Crawford J**, **Gilbert DJ**, **Sutherland GR**, **Jenkins NA**, **Herzog H**. GPR56, a novel secretin-like human G-protein-coupled receptor gene. *Genomics* 55: 296–305, 1999.

Ljaschenko D, **Ehmann N**, **Kittel RJ**. Hebbian plasticity guides maturation of glutamate receptor fields *in vivo*. *CellReports* 3: 1407–1413, 2013.

Lloyd TE, **Verstreken P**, **Ostrin EJ**, **Phillippi A**, **Lichtarge O**, **Bellen HJ**. A genome-wide search for synaptic vesicle cycle proteins in *Drosophila*. *NEURON* 26: 45–50, 2000.

López-Muñoz F, **Boya J**, **Alamo C**. Neuron theory, the cornerstone of neuroscience, on the centenary of the Nobel Prize award to Santiago Ramón y Cajal. *Brain Res Bull* 70: 391–405, 2006.

Lu J, **Machius M**, **Dulubova I**, **Dai H**, **Südhof TC**, **Tomchick DR**, **Rizo J**. Structural basis for a Munc13-1 homodimer to Munc13-1/RIM heterodimer switch. *PLoS Biol* 4: e192–e192, 2006.

Lum AM, **Wang BB**, **Beck-Engeser GB**, **Li L**, **Channa N**, **Wabl M**. Orphan receptor GPR110, an oncogene overexpressed in lung and prostate cancer. *BMC Cancer* 10: 40, 2010.

Macao B, **Johansson DGA**, **Hansson GC**, **Härd T**. Autoproteolysis coupled to protein folding in the SEA domain of the membrane-bound MUC1 mucin. *Nat Struct Mol Biol* 13: 71–76, 2006.

Mackler JMJ, **Drummond JAJ**, **Loewen CAC**, **Robinson IMI**, **Reist NEN**. The C(2)B Ca^{2+}-binding motif of synaptotagmin is required for synaptic transmission *in vivo*. *Nature* 418: 340–344, 2002.

Maerker T, **van Wijk E**, **Overlack N**, **Kersten FFJ**, **McGee J**, **Goldmann T**, **Sehn E**, **Roepman R**, **Walsh EJ**, **Kremer H**, **Wolfrum U**. A novel Usher protein network at the periciliary reloading point between molecular transport machineries in vertebrate photoreceptor cells. *Hum Mol Genet* 17: 71–86, 2007.

Magleby KL. Short-term changes in synaptic efficacy. In: Synaptic Function (Edelman GM, Gall WE, Cowan WM, eds), pp 21-56. New York: John Wiley & Sons, 1987.

Markstein M, **Pitsouli C**, **Villalta C**, **Celniker SE**, **Perrimon N**. Exploiting position effects and the gypsy retrovirus insulator to engineer precisely expressed transgenes. *Nat Genet* 40: 476–483, 2008.

Marrus SB, **DiAntonio A**. Preferential Localization of Glutamate Receptors Opposite Sites of High Presynaptic Release. *Current Biology* 14: 924–931, 2004.

Marshall CJ. Protein prenylation: a mediator of protein-protein interactions. *Science* 259: 1865–1866, 1993.

Martin JA, **Hu Z**, **Fenz KM**, **Fernandez J**, **Dittman JS**. Complexin Has Opposite Effects on Two Modes of Synaptic Vesicle Fusion. *Current Biology* 21: 97–105, 2011.

Martinac B. Mechanosensitive channels in prokaryotes. *Cell. Physiol. Biochem.* 11: 61–76, 2001.

Matkovic T, **Siebert M**, **Knoche E**, **Depner H**, **Mertel S**, **Owald D**, **Schmidt M**, **Thomas U**, **Sickmann A**, **Kamin D**, **Hell SW**, **Bürger J**, **Hollmann C**, **Mielke T**, **Wichmann C**, **Sigrist SJ**. The Bruchpilot cytomatrix determines the size of the readily releasable pool of synaptic vesicles. *J Cell Biol* 202: 667–683, 2013.

Matsui H, **Ohnishi J**, **Takahashi T**. Proteolytic activation of tissue-type plasminogen activator by the culture media of mouse cancer cells. *Zool. Sci.* 15: 499–505, 1998.

Matsushita H, **Lelianova VG**, **Ushkaryov YA**. The latrophilin family: multiply spliced G protein-coupled receptors with differential tissue distribution. *FEBS Lett* 443: 348–352, 1999.

Matteoli M, **Haimann C**, **Torri-Tarelli F**, **Polak JM**, **Ceccarelli B**, **De Camilli P**. Differential effect of α-latrotoxin on exocytosis from small synaptic vesicles and from large dense-core vesicles containing calcitonin gene-related peptide at the frog neuromuscular junction. *Proc Natl Acad Sci USA* 85: 7366–7370, 1988.

Matthew WD, **Tsavaler L**, **Reichardt LF**. Identification of a synaptic vesicle-specific membrane protein with a wide distribution in neuronal and neurosecretory tissue. *J Cell Biol* 91: 257–269, 1981.

Matthews G, **Fuchs P**. The diverse roles of ribbon synapses in sensory neurotransmission. *Nature Reviews Neuroscience* 11: 812–822, 2010.

Maximov A, **Tang J**, **Yang X**, **Pang ZP**, **Südhof TC**. Complexin controls the force transfer from SNARE complexes to membranes in fusion. *Science* 323: 516–521, 2009.

McGee J, **Goodyear RJ**, **McMillan DR**, **Stauffer EA**, **Holt JR**, **Locke KG**, **Birch DG**, **Legan PK**, **White PC**, **Walsh EJ**, **Richardson GP**. The very large G-protein-coupled receptor VLGR1: a component of the ankle link complex required for the normal development of auditory hair bundles. *J Neurosci* 26: 6543–6553, 2006.

McIntire SL, **Reimer RJ**, **Schuske K**, **Edwards RH**, **Jorgensen EM**. Identification and characterization of the vesicular GABA transporter. *Nature* 389: 870–876, 1997.

McMahon HT, **Missler M**, **Li C**, **Südhof TC**. Complexins: cytosolic proteins that regulate SNAP receptor function. *Cell* 83: 111–119, 1995.

McMillan DR, **Kayes-Wandover KM**, **Richardson JA**, **White PC**. Very large G protein-coupled receptor-1, the largest known cell surface protein, is highly expressed in the developing central nervous system. *J Biol Chem* 277: 785–792, 2002.

Mee CJ, **Tomlinson SR**, **Perestenko PV**, **De Pomerai D**, **Duce IR**, **Usherwood PNR**, **Bell DR**. Latrophilin is required for toxicity of black widow spider venom in *Caenorhabditis elegans*. *Biochem. J.* 378: 185–191, 2004.

Meinertzhagen IA, **Govind CK**, **Stewart BA**, **Carter JM**, **Atwood HL**. Regulated spacing of synapses and presynaptic active zones at larval neuromuscular junctions in different genotypes of the flies *Drosophila* and *Sarcophaga*. *J. Comp. Neurol.* 393: 482–492, 1998.

Mendoza-Topaz C, **Urra F**, **Barria R**, **Albornoz V**, **Ugalde D**, **Thomas U**, **Gundelfinger ED**, **Delgado R**, **Kukuljan M**, **Sanxaridis PD**, **Tsunoda S**, **Ceriani MF**, **Budnik V**, **Sierralta J**. DLGS97/SAP97 Is Developmentally Upregulated and Is Required for Complex Adult Behaviors and Synapse Morphology and Function. *Journal of Neuroscience* 28: 304–314, 2008.

Michaely P, **Tomchick DR**, **Machius M**, **Anderson RGW**. Crystal structure of a 12 ANK repeat stack from human ankyrinR. *Embo J* 21: 6387–6396, 2002.

Mikoshiba K, **Fukuda M**, **Moreira JE**, **Lewis FM**, **Sugimori M**, **Niinobe M**, **Llinás R**. Role of the C2A domain of synaptotagmin in transmitter release as determined by specific antibody injection into the squid giant synapse preterminal. *Proc Natl Acad Sci USA* 92: 10703–10707, 1995.

Miller KE, **DeProto J**, **Kaufmann N**, **Patel BN**, **Duckworth A**, **Van Vactor D**. Direct Observation Demonstrates that Liprin-α Is Required for Trafficking of Synaptic Vesicles. *Current Biology* 15: 684–689, 2005.

Mills JD, **Kavanagh T**, **Kim WS**, **Chen BJ**, **Kawahara Y**, **Halliday GM**, **Janitz M**. Unique transcriptome patterns of the white and grey matter corroborate structural and functional heterogeneity in the human frontal lobe. *PloS one* 8: e78480–e78480, 2013.

Miskiewicz K, **Jose LE**, **Bento-Abreu A**, **Fislage M**, **Taes I**, **Kasprowicz J**, **Swerts J**, **Sigrist S**, **Versées W**, **Robberecht W**, **Verstreken P**. ELP3 controls active zone morphology by acetylating the ELKS family member Bruchpilot. *NEURON* 72: 776–788, 2011.

Miskiewicz K, **Jose LE**, **Yeshaw WM**, **Valadas JS**, **Swerts J**, **Munck S**, **Feiguin F**, **Dermaut B**, **Verstreken P**. HDAC6 Is a Bruchpilot Deacetylasethat Facilitates Neurotransmitter Release. *Cell Rep*, 2014; doi: 10.1016/j.celrep.2014.05.051.

Monk KR, **Naylor SG**, **Glenn TD**, **Mercurio S**, **Perlin JR**, **Dominguez C**, **Moens CB**, **Talbot WS**. A G protein-coupled receptor is essential for Schwann cells to initiate myelination. *Science* 325: 1402–1405, 2009.

Mori K, **Kanemura Y**, **Fujikawa H**, **Nakano A**, **Ikemoto H**, **Ozaki I**, **Matsumoto T**, **Tamura K**, **Yokota M**, **Arita N**. Brain-specific angiogenesis inhibitor 1 (BAI1) is expressed in human cerebral neuronal cells. *Neuroscience Research* 43: 69–74, 2002.

Morris RL, **Hollenbeck PJ**. Axonal transport of mitochondria along microtubules and F-actin in living vertebrate neurons. *J Cell Biol* 131: 1315–1326, 1995.

Müller M, **Liu KSY**, **Sigrist SJ**, **Davis GW**. RIM Controls Homeostatic Plasticity through Modulation of the Readily-Releasable Vesicle Pool. *Journal of Neuroscience* 32: 16574–16585, 2012.

Murthy VN, **Sejnowski TJ**, **Stevens CF**. Heterogeneous release properties of visualized individual hippocampal synapses. *NEURON* 18: 599–612, 1997.

Nadrowski B, **Albert JT**, **Göpfert MC**. Transducer-based force generation explains active process in *Drosophila* hearing. *Current Biology* 18: 1365–1372, 2008.

Nauli SM, **Kawanabe Y**, **Kaminski JJ**, **Pearce WJ**, **Ingber DE**, **Zhou J**. Endothelial cilia are fluid shear sensors that regulate calcium signaling and nitric oxide production through *polycystin-1*. *Circulation* 117: 1161–1171, 2008.

Neher E, **Sakaba T**. Multiple roles of calcium ions in the regulation of neurotransmitter release. *NEURON* 59: 861–872, 2008.

Neher E. Vesicle pools and Ca^{2+} microdomains: new tools for understanding their roles in neurotransmitter release. *NEURON* 20: 389–399, 1998.

Neuser K, **Triphan T**, **Mronz M**, **Poeck B**, **Strauss R**. Analysis of a spatial orientation memory in *Drosophila*. *Nature* 453: 1244–1247, 2008.

Newton FG, **Lage zur PI**, **Karak S**, **Moore DJ**, **Göpfert MC**, **Jarman AP**. Forkhead transcription factor Fd3F cooperates with Rfx to regulate a gene expression program for mechanosensory cilia specialization. *Developmental Cell* 22: 1221–1233, 2012.

Nieratschker V, **Schubert A**, **Jauch M**, **Bock N**, **Bucher D**, **Dippacher S**, **Krohne G**, **Asan E**, **Buchner S**, **Buchner E**. Bruchpilot in ribbon-like axonal agglomerates, behavioral defects, and early death in SRPK79D kinase mutants of *Drosophila*. *PLoS Genet* 5: e1000700, 2009.

Nishimura T, **Honda H**, **Takeichi M**. Planar cell polarity links axes of spatial dynamics in neural-tube closure. *Cell* 149: 1084–1097, 2012.

Nonet ML, **Grundahl K**, **Meyer BJ**, **Rand JB**. Synaptic function is impaired but not eliminated in *C. elegans* mutants lacking synaptotagmin. *Cell* 73: 1291–1305, 1993.

Nordström KJV, **Lagerström MC**, **Wallér LMJ**, **Fredriksson R**, **Schiöth HB**. The Secretin GPCRs descended from the family of Adhesion GPCRs. *Mol. Biol. Evol.* 26: 71–84, 2009.

O'Orlova EV, **Ushkaryov YA**, **Rahman MA**, **Gowen B**, **Volynski KE**, **Ashton AC**, **Manser C**, **van Heel M**. Structure of α-latrotoxin oligomers reveals that divalent cation-dependent tetramers form membrane pores. *Nat. Struct Biol.* 7: 48–53, 2000.

O'Sullivan ML, **de Wit J**, **Savas JN**, **Comoletti D**, **Otto-Hitt S**, **Yates JRI**, **Ghosh A**. FLRT Proteins Are Endogenous Latrophilin Ligands and Regulate Excitatory Synapse Development. *NEURON* 73: 903–910, 2012.

O'Sullivan ML, **Martini F**, **Daake von S**, **Comoletti D**, **Ghosh A**. LPHN3, a presynaptic adhesion-GPCR implicated in ADHD, regulates the strength of neocortical layer 2/3 synaptic input to layer 5. *Neural Dev* 9: –7, 2014.

Ohtsuka T. Cast: a novel protein of the cytomatrix at the active zone of synapses that forms a ternary complex with RIM1 and munc13-1. *J Cell Biol* 158: 577–590, 2002.

Okada Y, **Yamazaki H**, **Sekine-Aizawa Y**, **Hirokawa N**. The neuron-specific kinesin superfamily protein KIF1A is a unique monomeric motor for anterograde axonal transport of synaptic vesicle precursors. *Cell* 81: 769-780, 1995.

Okajima D, **Kudo G**, **Yokota H**. Brain-specific angiogenesis inhibitor 2 (BAI2) may be activated by proteolytic processing. *J. Recept. Signal Transduct. Res.* 30: 143–153, 2010.

Orlova EV, **Ushkaryov YA**, **Rahman MA**, **Gowen B**, **Volynski KE**, **Ashton AC**, **Manser C**, **van Heel M**. Structure of α-latrotoxin oligomers reveals that divalent cation-dependent tetramers form membrane pores. *Nat. Struct Biol.* 7: 48–53, 2000.

Ormö M, **Cubitt AB**, **Kallio K**, **Gross LA**, **Tsien RY**, **Remington SJ**. Crystal Structure of the Aequorea victoria Green Fluorescent Protein. *Science* 273: 1392–1395, 1996.

Ozeki Y, **Matsui T**, **Suzuki M**, **Titani K**. Amino acid sequence and molecular characterization of a D-galactoside-specific lectin purified from sea urchin (*Anthocidaris crassispina*) eggs. *Biochemistry* 30: 2391–2394, 1991.

Paavola KJ, **Sidik H**, **Zuchero JB**, **Eckart M**, **Talbot WS**. Type IV collagen is an activating ligand for the adhesion G protein-coupled receptor GPR126. *Science Signaling* 7: ra76–ra76, 2014.

Paavola KJ, **Stephenson JR**, **Ritter SL**, **Alter SP**, **Hall RA**. The N Terminus of the Adhesion G Protein-coupled Receptor GPR56 Controls Receptor Signaling Activity. *J Biol Chem* 286: 28914–28921, 2011.

Pabst S, **Margittai M**, **Vainius D**, **Langen R**, **Jahn R**, **Fasshauer D**. Rapid and selective binding to the synaptic SNARE complex suggests a modulatory role of complexins in neuroexocytosis. *J Biol Chem* 277: 7838–7848, 2002.

Pabst S. Selective Interaction of Complexin with the Neuronal SNARE Complex. DETERMINATION OF THE BINDING REGIONS. *Journal of Biological Chemistry* 275: 19808–19818, 2000.

Pack-Chung E, **Kurshan P**, **Dickman D**, **Schwarz T**. A *Drosophila* kinesin required for synaptic bouton formation and synaptic vesicle transport. *Nature Neuroscience* 10: 980–989, 2007.

Paddock BE, **Striegel AR**, **Hui E**, **Chapman ER**, **Reist NE**. Ca^{2+}-dependent, phospholipid-binding residues of synaptotagmin are critical for excitation-secretion coupling *in vivo*. *Journal of Neuroscience* 28: 7458–7466, 2008.

Paddock BE, **Wang Z**, **Biela LM**, **Chen K**, **Getzy MD**, **Striegel A**, **Richmond JE**, **Chapman ER**, **Featherstone DE**, **Reist NE**. Membrane penetration by synaptotagmin is required for coupling calcium binding to vesicle fusion *in vivo*. *Journal of Neuroscience* 31: 2248–2257, 2011.

Pangršič T, **Lasarow L**, **Reuter K**, **Takago H**, **Schwander M**, **Riedel D**, **Frank T**, **Tarantino LM**, **Bailey JS**, **Strenzke N**, **Brose N**, **Müller U**, **Reisinger E**, **Moser T**. Hearing requi-

res otoferlin-dependent efficient replenishment of synaptic vesicles in hair cells. *Nature Publishing Group* 13: 869–876, 2010.

Park D, **Ravichandran KS**. Emerging roles of brain-specific angiogenesis inhibitor 1. *Adv Exp Med Biol* 706: 167–178, 2010.

Parry DAD, **Fraser RDB**, **Squire JM**. Fifty years of coiled-coils and α-helical bundles: a close relationship between sequence and structure. *J. Struct. Biol.* 163: 258–269, 2008.

Parthier C, **Kleinschmidt M**, **Neumann P**, **Rudolph R**, **Manhart S**, **Schlenzig D**, **Fanghänel J**, **Rahfeld J-U**, **Demuth H-U**, **Stubbs MT**. Crystal structure of the incretin-bound extracellular domain of a G protein-coupled receptor. *Proc Natl Acad Sci USA* 104: 13942–13947, 2007.

Patel M, **Lehrman E**, **Poon V**, **Crump J**, **Zhen M**, **Bargmann C**, **Shen K**. Hierarchical assembly of presynaptic components in defined *C. elegans* synapses. *Nature Neuroscience* 9: 1488–1498, 2006.

Patra C, **van Amerongen MJ**, **Ghosh S**, **Ricciardi F**, **Sajjad A**, **Novoyatleva T**, **Mogha A**, **Monk KR**, **Mühlfeld C**, **Engel FB**. Organ-specific function of adhesion G protein-coupled receptor GPR126 is domain-dependent. *Proc Natl Acad Sci USA* 110: 16898–16903, 2014.

Paul MM, **Pauli M**, **Ehmann N**, **Hallermann S**, **Sauer M**, **Kittel RJ**, **Heckmann M**. Bruchpilot and Synaptotagmin collaborate to drive rapid glutamate release and active zone differentiation. *Front Cell Neurosci* 9: 29, 2015.

Peled ES, **Isacoff EY**. Optical quantal analysis of synaptic transmission in wild-type and *rab3*-mutant *Drosophila* motor axons. *Nature Publishing Group* 14: 519–526, 2011.

Peled ES, **Newman ZL**, **Isacoff EY**. Evoked and spontaneous transmission favored by distinct sets of synapses. *Curr. Biol.* 24: 484–493, 2014.

Perin MS, **Brose N**, **Jahn R**, **Südhof TC**. Domain structure of synaptotagmin (p65). *J Biol Chem* 266: 623–629, 1991.

Petersen SA, **Fetter RD**, **Noordermeer JN**, **Goodman CS**, **DiAntonio A**. Genetic analysis of glutamate receptors in *Drosophila* reveals a retrograde signal regulating presynaptic transmitter release. *NEURON* 19: 1237–1248, 1997.

Petersen SC, **Luo R**, **Liebscher I**, **Giera S**, **Jeong S-J**, **Mogha A**, **Ghidinelli M**, **Feltri ML**, **Schöneberg T**, **Piao X**, **Monk KR**. The Adhesion GPCR GPR126 Has Distinct, Domain-Dependent Functions in Schwann Cell Development Mediated by Interaction with Laminin-211. *NEURON* 85: 755–769, 2015.

Petrenko AG, **Kovalenko VA**, **Shamotienko OG**, **Surkova IN**, **Tarasyuk TA**, **Ushkaryov YuA**, **Grishin EV**. Isolation and properties of the α-latrotoxin receptor. *Embo J* 9: 2023–2027, 1990.

Pfeiffer BD, **Ngo T-TB**, **Hibbard KL**, **Murphy C**, **Jenett A**, **Truman JW**, **Rubin GM**. Refinement of tools for targeted gene expression in *Drosophila*. *Genetics* 186: 735–755, 2010.

Pfenninger K, **Akert K**, **Moor H**, **Sandri C**. The fine structure of freeze-fractured presynaptic membranes. *J. Neurocytol.* 1: 129–149, 1972.

Phillips GR, **Huang JK**, **Wang Y**, **Tanaka H**, **Shapiro L**, **Zhang W**, **Shan W-S**, **Arndt K**, **Frank M**, **Gordon RE**, **Gawinowicz MA**, **Zhao Y**, **Colman DR**. The Presynaptic Particle Web:Ultrastructure, Composition, Dissolution, and Reconstitution. *NEURON* 32: 63–77, 2001.

Piao X, **Hill RS**, **Bodell A**, **Chang BS**, **Basel-Vanagaite L**, **Straussberg R**, **Dobyns WB**, **Qasrawi B**, **Winter RM**, **Innes AM**, **Voit T**, **Ross ME**, **Michaud JL**, **Déscarie J-C**, **Barkovich AJ**, **Walsh CA**. G protein-coupled receptor-dependent development of human frontal cortex. *Science* 303: 2033–2036, 2004.

Piasecki BP, **Burghoorn J**, **Swoboda P**. Regulatory Factor X (RFX)-mediated transcriptional rewiring of ciliary genes in animals. *Proc Natl Acad Sci USA* 107: 12969–12974, 2010.

Pierce KL, **Premont RT**, **Lefkowitz RJ**. Seven-transmembrane receptors. *Nature Reviews Molecular Cell Biology* 3: 639–650, 2002.

Poeck B, **Triphan T**, **Neuser K**, **Strauss R**. Locomotor control by the central complex in *Drosophila* - An analysis of the tay bridge mutant. *Dev Neurobiol* 68: 1046–1058, 2007.

Ponting CP, **Hofmann K**, **Bork P**. A latrophilin/CL-1-like GPS domain in polycystin-1. *Current Biology* 9: R585–R588, 1999.

Potter CJ, **Tasic B**, **Russler EV**, **Liang L**, **Luo L**. The Q System: A Repressible Binary System for Transgene Expression, Lineage Tracing, and Mosaic Analysis. *Cell* 141: 536–548, 2010.

Prömel S, **Frickenhaus M**, **Hughes S**, **Mestek L**, **Staunton D**, **Woollard A**, **Vakonakis I**, **Schöneberg T**, **Schnabel R**, **Russ AP**, **Langenhan T**. The GPS motif is a molecular switch for bimodal activities of adhesion class G protein-coupled receptors. *Cell Rep* 2: 321–331, 2012.

Prömel S, **Langenhan T**, **Araç D**. Matching structure with function: the GAIN domain of adhesion-GPCR and PKD1-like proteins. *Trends Pharmacol Sci* 34: 470–478, 2013.

Qian F, **Boletta A**, **Bhunia AK**, **Xu H**, **Liu L**, **Ahrabi AK**, **Watnick TJ**, **Zhou F**, **Germino GG**. Cleavage of polycystin-1 requires the receptor for egg jelly domain and is disrupted by human autosomal-dominant polycystic kidney disease 1-associated mutations. *Proc Natl Acad Sci USA* 99: 16981–16986, 2002.

Qin G. Four Different Subunits Are Essential for Expressing the Synaptic Glutamate Receptor at Neuromuscular Junctions of *Drosophila*. *Journal of Neuroscience* 25: 3209–3218, 2005.

Ramirez DMO, **Khvotchev M**, **Trauterman B**, **Kavalali ET**. Vti1a Identifies a Vesicle Pool that Preferentially Recycles at Rest and Maintains Spontaneous Neurotransmission. *NEURON* 73: 121–134, 2012.

Reim K, **Mansour M**, **Varoqueaux F**, **McMahon HT**, **Südhof TC**, **Brose N**, **Rosenmund C**. Complexins regulate a late step in Ca^{2+}-dependent neurotransmitter release. *Cell* 104: 71–81, 2001.

Reim K. Structurally and functionally unique complexins at retinal ribbon synapses. *J Cell Biol* 169: 669–680, 2005.

Reiners J. Scaffold protein harmonin (USH1C) provides molecular links between Usher syndrome type 1 and type 2. *Hum Mol Genet* 14: 3933–3943, 2005.

Renn SCP, **Armstrong JD**, **Yang M**, **Wang Z**, **Tian X**, **Kaiser K**, **Taghert PH**. Genetic Analysis of the *Drosophila* Ellipsoid Body Neuropil: Organization and Development of the Central Complex.

Rizzoli SO, **Betz WJ**. Synaptic vesicle pools. *Nature Reviews Neuroscience* 6: 57–69, 2005.

Roos J, **Hummel T**, **Ng N**, **Klämbt C**, **Davis GW**. *Drosophila* Futsch Regulates Synaptic Microtubule Organization and Is Necessary for Synaptic Growth. *NEURON* 26: 371–382, 2000.

Rosenmund C, **Sigler A**, **Augustin I**, **Reim K**, **Brose N**, **Rhee J-S**. Differential control of vesicle priming and short-term plasticity by Munc13 isoforms. *NEURON* 33: 411–424, 2002.

Rosenmund C. Molecular mechanisms of active zone function. *Current Opinion in Neurobiology* 13: 509–519, 2003.

Rubin GM, **Spradling AC**. Genetic transformation of *Drosophila* with transposable element vectors. *Science* 218: 348–353, 1982.

Rubin GM. A *Drosophila* Complementary DNA Resource. *Science* 287: 2222–2224, 2000.

Ruiz-Cañada C, **Budnik V**. Introduction on the use of the *Drosophila* embryonic/larval neuromuscular junction as a model system to study synapse development and function, and a brief summary of pathfinding and target recognition. *Int. Rev. Neurobiol.* 75: 1–31, 2006.

Salvaterra PM, **Kitamoto T**. *Drosophila* cholinergic neurons and processes visualized with Gal4/UAS-GFP. *Brain Res. Gene Expr. Patterns* 1: 73–82, 2001.

Sanyal S. Genomic mapping and expression patterns of *C380*, *OK6* and *D42* enhancer trap lines in the larval nervous system of *Drosophila*. *Gene Expression Patterns* 9: 371–380, 2009.

Sara Y, **Virmani T**, **Deák F**, **Liu X**, **Kavalali ET**. An isolated pool of vesicles recycles at rest and drives spontaneous neurotransmission. *NEURON* 45: 563–573, 2005.

Schaub JR, **Lu X**, **Doneske B**, **Shin Y-K**, **McNew JA**. Hemifusion arrest by complexin is relieved by Ca^{2+}-synaptotagmin I. *Nature Publishing Group* 13: 748–750, 2006.

Scheer H, **Madeddu L**, **Dozio N**, **Gatti G**, **Vicentini LM**, **Meldolesi J**. α-latrotoxin of black widow spider venom: an interesting neurotoxin and a tool for investigating the process of neurotransmitter release. *J Physiol (Paris)* 79: 216–221, 1984.

Schirra C, **Rettig J**, **Reim K**, **Brose N**, **Mohrmann R**, **Bruns D**. Complexin synchronizes primed vesicle exocytosis and regulates fusion pore dynamics. *J Cell Biol* 204: 1123–1140, 2014.

Schneggenburger R, **Meyer AC**, **Neher E**. Released fraction and total size of a pool of im-

mediately available transmitter quanta at a calyx synapse. *NEURON* 23: 399–409, 1999.

Schneider I. Cell lines derived from late embryonic stages of *Drosophila* melanogaster. *J Embryol Exp Morphol* 27: 353–365, 1972.

Schnitzler MMY, **Storch U**, **Meibers S**, **Nurwakagari P**, **Breit A**, **Essin K**, **Gollasch M**, **Gudermann T**. G_q-coupled receptors as mechanosensors mediating myogenic vasoconstriction. *Embo J* 27: 3092–3103, 2008.

Schoch S, **Castillo PE**, **Jo T**, **Mukherjee K**, **Geppert M**, **Wang Y**, **Schmitz F**, **Malenka RC**, **Südhof TC**. RIM1α forms a protein scaffold for regulating neurotransmitter release at the active zone. *Nature* 415: 321–326, 2002.

Scholz N, **Gehring J**, **Guan C**, **Ljaschenko D**, **Fischer R**, **Lakshmanan V**, **Kittel RJ**, **Langenhan T**. The Adhesion GPCR Latrophilin/CIRL Shapes Mechanosensation. *Cell Rep* (April 29, 2015). doi: 10.1016/j.celrep.2015.04.008.

Seiler F, **Malsam J**, **Krause JM**, **Söllner TH**. A role of complexin-lipid interactions in membrane fusion. *FEBS Lett* 583: 2343–2348, 2009.

Sepp KJ, **Schulte J**, **Auld VJ**. Developmental dynamics of peripheral glia in *Drosophila* melanogaster. *Glia* 30: 122–133, 2000.

Serra-Pagès C, **Kedersha NL**, **Fazikas L**, **Medley Q**, **Debant A**, **Streuli M**. The LAR transmembrane protein tyrosine phosphatase and a coiled-coil LAR-interacting protein colocalize at focal adhesions. *Embo J* 14: 2827–2838, 1995.

Shao L, **Shuai Y**, **Wang J**, **Feng S**, **Lu B**, **Li Z**, **Zhao Y**, **Wang L**, **Zhong Y**. Schizophrenia susceptibility gene *dysbindin* regulates glutamatergic and dopaminergic functions via distinctive mechanisms in *Drosophila*. *Proc Natl Acad Sci USA* 108: 18831–18836, 2011.

Shima Y, **Copeland NG**, **Gilbert DJ**, **Jenkins NA**, **Chisaka O**, **Takeichi M**, **Uemura T**. Differential expression of the seven-pass transmembrane cadherin genes *Celsr1-3* and distribution of the Celsr2 protein during mouse development. *Dev. Dyn.* 223: 321–332, 2002.

Shima Y, **Kengaku M**, **Hirano T**, **Takeichi M**, **Uemura T**. Regulation of dendritic maintenance and growth by a mammalian 7-pass transmembrane cadherin. *Developmental Cell* 7: 205–216, 2004.

Shin J-B, **Adams D**, **Paukert M**, **Siba M**, **Sidi S**, **Levin M**, **Gillespie PG**, **Gründer S**. *Xenopus* TRPN1 (NOMPC) localizes to microtubule-based cilia in epithelial cells, including inner-ear hair cells. *Proc Natl Acad Sci USA* 102: 12572–12577, 2005.

Shiratsuchi T, **Nishimori H**, **Ichise H**, **Nakamura Y**, **Tokino T**. Cloning and characterization of *BAI2* and *BAI3*, novel genes homologous to brain-specific angiogenesis inhibitor 1 (BAI1). *Cytogenet. Cell Genet.* 79: 103–108, 1997.

Sidi S. NompC TRP Channel Required for Vertebrate Sensory Hair Cell Mechanotransduction. *Science* 301: 96–99, 2003.

Siksou LA, **Triller A**, **Marty S**. Ultrastructural organization of presynaptic terminals. *Current Opinion in Neurobiology* 21: 261–268, 2011.

Silva J-P, **Lelianova V**, **Hopkins C**, **Volynski KE**, **Ushkaryov Y**. Functional cross-interaction of the fragments produced by the cleavage of distinct adhesion G-protein-coupled receptors. *J Biol Chem* 284: 6495–6506, 2009.

Silva J-P, **Lelianova VG**, **Ermolyuk YS**, **Vysokov N**, **Hitchen PG**, **Berninghausen O**, **Rahman MA**, **Zangrandi A**, **Fidalgo S**, **Tonevitsky AG**, **Dell A**, **Volynski KE**, **Ushkaryov YA**. Latrophilin 1 and its endogenous ligand Lasso/teneurin-2 form a high-affinity transsynaptic receptor pair with signaling capabilities. *Proc Natl Acad Sci USA* 108: 12113–12118, 2011.

Silva J-P, **Ushkaryov YA**. The latrophilins, "split-personality" receptors. *Adv Exp Med Biol* 706: 59–75, 2010.

Silva MC, **Fox S**, **Beam M**, **Thakkar H**, **Amaral MD**, **Morimoto RI**. A genetic screening strategy identifies novel regulators of the proteostasis network. *PLoS Genet* 7: e1002438, 2011b.

Snellman J, **Mehta B**, **Babai N**, **Bartoletti TM**, **Akmentin W**, **Francis A**, **Matthews G**, **Thoreson W**, **Zenisek D**. Acute destruction of the synaptic ribbon reveals a role for the ribbon in vesicle priming. *Nature Neuroscience* 14: 1135–1141, 2011.

Snyder DA, **Rivers AM**, **Yokoe H**, **Menco B**, **Anholt R**. Olfactomedin - Purification, Characterization, and Localization of a Novel Olfactory Glycoprotein. *Biochemistry* 30: 9143–9153, 1991.

Söllner T, **Bennett MK**, **Whiteheart SW**, **Scheller RH**, **Rothman JE**. A protein assembly-disassembly pathway *in vitro* that may correspond to sequential steps of synaptic vesicle docking, activation, and fusion. *Cell* 75: 409–418, 1993.

Song WW, **Onishi MM**, **Jan LYL**, **Jan YNY**. Peripheral multidendritic sensory neurons are necessary for rhythmic locomotion behavior in *Drosophila* larvae. *Proc Natl Acad Sci USA* 104: 5199–5204, 2007.

Stacey M, **Chang G-W**, **Davies JQ**, **Kwakkenbos MJ**, **Sanderson RD**, **Hamann J**, **Gordon S**, **Lin H-H**. The epidermal growth factor-like domains of the human EMR2 receptor mediate cell attachment through chondroitin sulfate glycosaminoglycans. *Blood* 102: 2916–2924, 2003.

Stanley EF. The calcium channel and the organization of the presynaptic transmitter release face. *Trends in Neurosciences* 20: 404–409, 1996.

Stearns T, **Botstein D**. Unlinked noncomplementation: isolation of new conditional-lethal mutations in each of the *tubulin* genes of *Saccharomyces cerevisiae*. *Genetics* 119: 249–260, 1988.

Steimel A, **Wong L**, **Najarro EH**, **Ackley BD**, **Garriga G**, **Hutter H**. The Flamingo ortholog FMI-1 controls pioneer-dependent navigation of follower axons in *C. elegans*. *Development* 137: 3663–3673, 2010.

Sterling P, **Matthews G**. Structure and function of ribbon synapses. *Trends in Neurosciences*.

Stevens CF, **Williams JH**. Discharge of the readily releasable pool with action potentials at hippocampal synapses. *J Neurophysiol* 98: 3221–3229, 2007.

Stewart BA, **Atwood HL**, **Renger JJ**, **Wang J**. Improved stability of *Drosophila* larval neuromuscular preparations in haemolymph-like physiological solutions. *Journal of Comp. Physiology* 175: 179-191, 1994.

Stewart BA, **Schuster CM**, **Goodman CS**, **Atwood HL**. Homeostasis of synaptic transmission in *Drosophila* with genetically altered nerve terminal morphology. *J Neurosci* 16: 3877–3886, 1996.

Stigloher C, **Zhan H**, **Zhen M**, **Richmond J**, **Bessereau J-L**. The presynaptic dense projection of the *Caenorhabditis elegans* cholinergic neuromuscular junction localizes synaptic vesicles at the active zone through SYD-2/liprin and UNC-10/RIM-dependent interactions. *J Neurosci* 31: 4388–4396, 2011.

Stoveken HM, **Hajduczok AG**, **Xu L**, **Tall GG**. Adhesion G protein-coupled receptors are activated by exposure of a cryptic tethered agonist. *Proc Natl Acad Sci USA* 112, no. 19: 6194-6199; doi: 10.1073/pnas.1421785112, 2015.

Strokes N, **Piao X**. Adhesion-GPCRs in the CNS. *Adv Exp Med Biol* 706: 87–97, 2010.

Südhof TC, **Rothman JE**. Membrane fusion: grappling with SNARE and SM proteins. *Science* 323: 474–477, 2009.

Südhof TC. Neuroligins and neurexins link synaptic function to cognitive disease. *Nature* 455: 903–911, 2008.

Südhof TC. Neurotransmitter Release: The Last Millisecond in the Life of a Synaptic Vesicle. *NEURON* 80: 675–690, 2013.

Südhof TC. The Presynaptic Active Zone. *NEURON* 75: 11–25, 2012.

Südhof TC. THE SYNAPTIC VESICLE CYCLE. *Annual review of neuroscience* 27: 509–547, 2004.

Südhof TC. α-Latrotoxin and its receptors: neurexins and CIRL/latrophilins. *Annual review of neuroscience* 24: 933–962, 2001.

Sugie A, **Hakeda-Suzuki S**, **Suzuki E**, **Silies M**, **Shimozono M**, **Möhl C**, **Suzuki T**, **Tavosanis G**. Molecular Remodeling of the Presynaptic Active Zone of *Drosophila* Photoreceptors via Activity-Dependent Feedback. *Neuron* 86: 711–725, 2015.

Sugita S, **Ichtchenko K**, **Khvotchev M**, **Südhof TC**. α-Latrotoxin receptor CIRL/latrophilin 1 (CL1) defines an unusual family of ubiquitous G-protein-linked receptors. G-protein coupling not required for triggering exocytosis. *J Biol Chem* 273: 32715–32724, 1998.

Sun Y, **Liu L**, **Ben-Shahar Y**, **Jacobs JS**, **Eberl DF**, **Welsh MJ**. TRPA channels distinguish gravity sensing from hearing in Johnston's organ. *Proc Natl Acad Sci USA* 106: 13606–13611, 2009.

Suster ML, **Bate M**. Embryonic assembly of a central pattern generator without sensory in-

put. *Nature* 416: 174–178, 2002.

Sutton RB, **Fasshauer D**, **Jahn R**, **Brunger AT**. Crystal structure of a SNARE complex involved in synaptic exocytosis at 2.4 A resolution. *Nature* 395: 347–353, 1998.

Swoboda P, **Adler HT**, **Thomas JH**. The RFX-type transcription factor DAF-19 regulates sensory neuron cilium formation in *C. elegans*. *Mol. Cell* 5: 411–421, 2000.

Szule JA, **Harlow ML**, **Jung JH**, **De-Miguel FF**, **Marshall RM**, **McMahan UJ**. Regulation of synaptic vesicle docking by different classes of macromolecules in active zone material. *PloS one* 7: e33333, 2012.

Takahashi S, **Yamamoto H**, **Matsuda Z**, **Ogawa M**, **Yagyu K**, **Taniguchi T**, **Miyata T**, **Kaba H**, **Higuchi T**, **Okutani F**. Identification of two highly homologous presynaptic proteins distinctly localized at the dendritic and somatic synapses. *FEBS Lett* 368: 455–460, 1995.

Takamori S, **Holt M**, **Stenius K**, **Lemke EA**, **Grønborg M**, **Riedel D**, **Urlaub H**, **Schenck S**, **Brügger B**, **Ringler P**, **Müller SA**, **Rammner B**, **Gräter F**, **Hub JS**, **De Groot BL**, **Mieskes G**, **Moriyama Y**, **Klingauf J**, **Grubmüller H**, **Heuser J**, **Wieland F**, **Jahn R**. Molecular anatomy of a trafficking organelle. *Cell* 127: 831–846, 2006.

Takamori S, **Rhee JS**, **Rosenmund C**, **Jahn R**. Identification of a vesicular glutamate transporter that defines a glutamatergic phenotype in neurons. *Nature* 407: 189–194, 2000.

Takao-Rikitsu E. Physical and functional interaction of the active zone proteins, CAST, RIM1, and Bassoon, in neurotransmitter release. *J Cell Biol* 164: 301–311, 2004.

Tang J, **Maximov A**, **Shin O-H**, **Dai H**, **Rizo J**, **Südhof TC**. A complexin/synaptotagmin 1 switch controls fast synaptic vesicle exocytosis. *Cell* 126: 1175–1187, 2006.

Taru H, **Jin Y**. The Liprin homology domain is essential for the homomeric interaction of SYD-2/Liprin-α protein in presynaptic assembly. *Journal of Neuroscience* 31: 16261–16268, 2011.

Thakur AK, **Jayaraman M**, **Mishra R**, **Thakur M**, **Chellgren VM**, **Byeon I-JL**, **Anjum DH**, **Kodali R**, **Creamer TP**, **Conway JF**, **Gronenborn AM**, **Wetzel R**. Polyglutamine disruption of the *huntingtin* exon 1 N terminus triggers a complex aggregation mechanism. *Nat Struct Mol Biol* 16: 380–389, 2009.

Thomas U, **Kim E**, **Kuhlendahl S**, **Koh Y-H**, **Gundelfinger ED**, **Sheng M**, **Garner CC**, **Budnik V**. Synaptic Clustering of the Cell Adhesion Molecule Fasciclin II by Discs-Large and its Role in the Regulation of Presynaptic Structure. *NEURON* 19: 787–799, 1997.

Thorpe HM, **Smith MC**. *In vitro* site-specific integration of bacteriophage DNA catalyzed by a recombinase of the resolvase/invertase family. *Proc Natl Acad Sci USA* 95: 5505–5510, 1998.

Thorpe HM, **Wilson SE**, **Smith MC**. Control of directionality in the site-specific recombination system of the *Streptomyces* phage phiC31. *Mol. Microbiol.* 38: 232–241, 2000.

Tinevez J-Y, **Jülicher F**, **Martin P**. Unifying the various incarnations of active hair-bundle

motility by the vertebrate hair cell. *Biophys J* 93: 4053–4067, 2007.

Titlow JS, **Rice J**, **Majeed ZR**, **Holsopple E**, **Biecker S**, **Cooper RL**. Anatomical and genotype-specific mechanosensory responses in *Drosophila melanogaster* larvae. *Neuroscience Research* 83: 54–63, 2014.

Tobaben S, **Südhof TC**, **Stahl B**. Genetic analysis of α-latrotoxin receptors reveals functional interdependence of CIRL/latrophilin 1 and neurexin 1α. *J Biol Chem* 277: 6359–6365, 2002.

tom Dieck S, **Brandstätter JH**. Ribbon synapses of the retina. *Cell Tissue Res.* 326: 339–346, 2006.

tom Dieck S, **Specht D**, **Strenzke N**, **Hida Y**, **Krishnamoorthy V**, **Schmidt K-F**, **Inoue E**, **Ishizaki H**, **Tanaka-Okamoto M**, **Miyoshi J**, **Hagiwara A**, **Brandstätter JH**, **Löwel S**, **Gollisch T**, **Ohtsuka T**, **Moser T**. Deletion of the presynaptic scaffold CAST reduces active zone size in rod photoreceptors and impairs visual processing. *J. Neurosci.* 32: 12192–12203, 2012.

Tomarev SI, **Nakaya N**. Olfactomedin domain-containing proteins: possible mechanisms of action and functions in normal development and pathology. *Mol Neurobiol* 40: 122–138, 2009.

Tracey WD, **Wilson RI**, **Laurent G**, **Benzer S**. *painless*, a *Drosophila* gene essential for nociception. *Cell* 113: 261–273, 2003.

Truman JW. Metamorphosis of the central nervous system of *Drosophila*. *Journal of neurobiology* 21: 1072–1084, 1990.

Tucker RP, **Chiquet-Ehrismann R**. Teneurins: a conserved family of transmembrane proteins involved in intercellular signaling during development. *Dev Biol* 290: 237–245, 2006.

Tymiak AA, **Norman JA**, **Bolgar M**, **DiDonato GC**, **Lee H**, **Parker WL**, **Lo LC**, **Berova N**, **Nakanishi K**, **Haber E**. Physicochemical characterization of a ouabain isomer isolated from bovine hypothalamus. *Proc Natl Acad Sci USA* 90: 8189–8193, 1993.

Umbach JA, **Grasso A**, **Zurcher SD**, **Kornblum HI**, **Mastrogiacomo A**, **Gundersen CB**. Electrical and optical monitoring of α-latrotoxin action at *Drosophila* neuromuscular junctions. *Neuroscience* 87: 913–924, 1998.

Ushkaryov YA, **Petrenko AG**, **Geppert M**, **Südhof TC**. Neurexins: synaptic cell surface proteins related to the α-latrotoxin receptor and laminin. *Science* 257: 50–56, 1992.

Usui T, **Shima Y**, **Shimada Y**, **Hirano S**, **Burgess RW**, **Schwarz TL**, **Takeichi M**, **Uemura T**. Flamingo, a Seven-Pass Transmembrane Cadherin, Regulates Planar Cell Polarity under the Control of Frizzled. *Cell* 98: 585–595, 1999.

Vakonakis I, **Langenhan T**, **PrOmel S**, **Russ A**, **Campbell ID**. Solution structure and sugar-binding mechanism of mouse latrophilin-1 RBL: a 7TM receptor-attached lectin-like domain. *Structure* 16: 944–953, 2008.

Vay L, **Gu C**, **McNaughton PA**. The thermo-TRP ion channel family: properties and

therapeutic implications. *Br J Pharmacol* 165: 787–801, 2011.

Volynski K, **Silva J**, **Lelianova V**, **Rahman M**, **Hopkins C**, **Ushkaryov Y**. Latrophilin fragments behave as independent proteins that associate and signal on binding of LTXN4C. *Embo J* 23: 4423–4433, 2004.

von Gersdorff H. Synaptic ribbons: versatile signal transducers. *NEURON* 29: 7–10, 2001.

Vrljic M, **Strop P**, **Ernst JA**, **Sutton RB**, **Chu S**, **Brunger AT**. Molecular mechanism of the synaptotagmin-SNARE interaction in Ca^{2+}-triggered vesicle fusion. *Nat Struct Mol Biol* 17: 325–331, 2010.

Wagh DA, **Rasse TM**, **Asan E**, **Hofbauer A**, **Schwenkert I**, **Dürrbeck H**, **Buchner S**, **Dabauvalle M-C**, **Schmidt M**, **Qin G**, **Wichmann C**, **Kittel R**, **Sigrist SJ**, **Buchner E**. Bruchpilot, a protein with homology to ELKS/CAST, is required for structural integrity and function of synaptic active zones in *Drosophila*. *NEURON* 49: 833–844, 2006.

Walker MC, **Ruiz A**, **Kullmann DM**. Monosynaptic GABAergic signaling from dentate to CA3 with a pharmacological and physiological profile typical of mossy fiber synapses. *NEURON* 29: 703–715, 2001.

Walker RG, **Willingham AT**, **Zuker CS**. A *Drosophila* mechanosensory transduction channel. *Science* 287: 2229–2234, 2000.

Waller-Evans H, **Prömel S**, **Langenhan T**, **Dixon J**, **Zahn D**, **Colledge WH**, **Doran J**, **Carlton MBL**, **Davies B**, **Aparicio SAJR**, **Grosse J**, **Russ AP**. The orphan adhesion-GPCR GPR126 is required for embryonic development in the mouse. *PloS one* 5: e14047, 2010.

Walter AM, **Groffen AJ**, **Sørensen JB**, **Verhage M**. Multiple Ca^{2+} sensors in secretion: teammates, competitors or autocrats? *Trends in Neurosciences* 34: 487–497, 2011.

Wandel E, **Saalbach A**, **Sittig D**, **Gebhardt C**, **Aust G**. Thy-1 (CD90) is an interacting partner for CD97 on activated endothelial cells. *J Immunol* 188: 1442–1450, 2012.

Wang JW, **Sylwester AW**, **Reed D**, **Wu DA**, **Soll DR**, **Wu CF**. Morphometric description of the wandering behavior in *Drosophila* larvae: aberrant locomotion in Na^+ and K^+ channel mutants revealed by computer-assisted motion analysis. *J Neurogenet* 11: 231–254, 1997.

Wang Y, **Liu X**, **Biederer T**, **Südhof TC**. A family of RIM-binding proteins regulated by alternative splicing: Implications for the genesis of synaptic active zones. *Proc Natl Acad Sci USA* 99: 14464–14469, 2002.

Wang Y, **Okamoto M**, **Schmitz F**, **Hofmann K**, **Südhof TC**. RIM is a putative Rab3 effector in regulating synaptic-vesicle fusion. *Nature* 388: 593–598, 1997.

Wang Y, **Sugita S**, **Südhof TC**. The RIM/NIM family of neuronal C2 domain proteins. Interactions with Rab3 and a new class of Src homology 3 domain proteins. *J Biol Chem* 275: 20033–20044, 2000.

Weigmann K, **Klapper R**, **Strasser T**, **Rickert C**, **Technau G**, **Jäckle H**, **Janning W**, **Klämbt C**. An evolutionary approach reveals a high protein-coding capacity of the human genome. *Trends Genet.* 19: 310–311, 2003.

Weston MD, **Luijendijk MWJ**, **Humphrey KD**, **Möller C**, **Kimberling WJ**. Mutations in the VLGR1 gene implicate G-protein signaling in the pathogenesis of Usher syndrome type II. *Am. J. Hum. Genet.* 74: 357–366, 2004.

Wetzel R. Physical chemistry of polyglutamine: intriguing tales of a monotonous sequence. *Journal of Molecular Biology* 421: 466–490, 2012.

White JP, **Wrann CD**, **Rao RR**, **Nair SK**, **Jedrychowski MP**, **You JS**, **Martinez-Redondo V**, **Gygi SP**, **Ruas JL**, **Hornberger TA**, **Wu Z**, **Glass DJ**, **Piao X**, **Spiegelman BM**. G protein-coupled receptor 56 regulates mechanical overload-induced muscle hypertrophy. *Proc Natl Acad Sci USA* 111, no. 44: 15756-15761, doi: 10.1073/pnas.1417898111, 2014.

Winter C, **Tom Dieck S**, **Boeckers TM**, **Bockmann J**, **Kämpf U**, **Sanmartí-Vila L**, **Langnaese K**, **Altrock W**, **Stumm M**, **Soyke A**, **Wieacker P**, **Garner CC**, **Gundelfinger ED**. The presynaptic cytomatrix protein Bassoon: sequence and chromosomal localization of the human BSN gene. *Genomics* 57: 389–397, 1999.

Woods DF, **Bryant PJ**. The *discs-large* tumor suppressor gene of *Drosophila* encodes a guanylate kinase homolog localized at septate junctions. *Cell* 66: 451–464, 1991.

Wragg RT, **Snead D**, **Dong Y**, **Ramlall TF**, **Menon I**, **Bai J**, **Eliezer D**, **Dittman JS**. Synaptic Vesicles Position Complexin to Block Spontaneous Fusion. *NEURON* 77: 323–334, 2013.

Wu Z, **Sweeney LB**, **Ayoob JC**, **Chak K**, **Andreone BJ**, **Ohyama T**, **Kerr R**, **Luo L**, **Zlatic Kolodkin AL**. A Combinatorial Semaphorin Code Instructs the Initial Steps of Sensory Circuit Assembly in the *Drosophila* CNS. *NEURON* 70: 281–298, 2011.

Xue M, **Craig TK**, **Xu J**, **Chao H-T**, **Rizo J**, **Rosenmund C**. Binding of the complexin N terminus to the SNARE complex potentiates synaptic-vesicle fusogenicity. *Nat Struct Mol Biol* 17: 568–575, 2010.

Xue M, **Lin YQ**, **Pan H**, **Reim K**, **Deng H**, **Bellen HJ**, **Rosenmund C**. Tilting the Balance between Facilitatory and Inhibitory Functions of Mammalian and *Drosophila* Complexins Orchestrates Synaptic Vesicle Exocytosis. *NEURON* 64: 367–380, 2009.

Xue M, **Reim K**, **Chen X**, **Chao H-T**, **Deng H**, **Rizo J**, **Brose N**, **Rosenmund C**. Distinct domains of complexin I differentially regulate neurotransmitter release. *Nature Publishing Group* 14: 949–958, 2007.

Yamada KM, **Spooner BS**, **Wessells NK**. Ultrastructure and function of growth cones and axons of cultured nerve cells. *J Cell Biol* 49: 614–635, 1971.

Yamada M, **Saisu H**, **Ishizuka T**, **Takahashi H**, **Abe T**. Immunohistochemical distribution of the two isoforms of synaphin/complexin involved in neurotransmitter release: localization at the distinct central nervous system regions and synaptic types. *Neuroscience* 93: 7–18, 1999.

Yan Z, **Zhang W**, **He Y**, **Gorczyca D**, **Xiang Y**, **Cheng LE**, **Meltzer S**, **Jan LY**, **Jan YN**. *Drosophila* NOMPC is a mechanotransduction subunit for gentle touch sensation. *Nature* 493: 221–225, 2013.

Yang L, **Chen G**, **Mohanty S**, **Scott G**, **Fazal F**, **Rahman A**, **Begum S**, **Hynes RO**, **Xu L**. GPR56 Regulates VEGF production and angiogenesis during melanoma progression. *Cancer Res.* 71: 5558–5568, 2011.

Yang L, **Xu L**. GPR56 in cancer progression: current status and future perspective. *Future Oncol* 8: 431–440, 2012.

Yao J, **Gaffaney JD**, **Kwon SE**, **Chapman ER**. Doc2 is a Ca^{2+} sensor required for asynchronous neurotransmitter release. *Cell* 147: 666–677, 2011.

Yao KM, **White K**. Neural specificity of elav expression: defining a *Drosophila* promoter for directing expression to the nervous system. *J Neurochem* 63: 41–51, 1994.

Yook KJK, **Proulx SRS**, **Jorgensen EME**. Rules of nonallelic noncomplementation at the synapse in *Caenorhabditis elegans*. *Genetics* 158: 209–220, 2001.

Yoon T-Y, **Lu X**, **Diao J**, **Lee S-M**, **Ha T**, **Shin Y-K**. Complexin and Ca^{2+} stimulate SNARE-mediated membrane fusion. *Nature Publishing Group* 15: 707–713, 2008.

Young JM, **Armstrong JD**. Structure of the adult central complex in *Drosophila*: organization of distinct neuronal subsets. *J. Comp. Neurol.* 518: 1500–1524, 2009.

Zahler AM, **Lane WS**, **Stolk JA**, **Roth MB**. SR proteins: a conserved family of pre-mRNA splicing factors. *Genes Dev* 6: 837–847, 1992.

Zalewska M, **Siara M**, **Sajewicz W**. G protein-coupled receptors: abnormalities in signal transmission, disease states and pharmacotherapy. *Acta Pol Pharm* 71: 229–243, 2014.

Zander J-F, **Münster-Wandowski A**, **Brunk I**, **Pahner I**, **Gómez-Lira G**, **Heinemann U**, **Gutiérrez R**, **Laube G**, **Ahnert-Hilger G**. Synaptic and vesicular coexistence of VGLUT and VGAT in selected excitatory and inhibitory synapses. *Journal of Neuroscience* 30: 7634–7645, 2010.

Zars T, **Fischer M**, **Schulz R**, **Heisenberg M**. Localization of a short-term memory in *Drosophila*. *Science* 288: 672–675, 2000.

Zhai RG. The Architecture of the Active Zone in the Presynaptic Nerve Terminal. *Physiology* 19: 262–270, 2004.

Zhang FL, **Casey PJ**. Protein prenylation: molecular mechanisms and functional consequences. *Annual review of biochemistry* 65: 241–269, 1996.

Zhang W, **Yan Z**, **Jan LY**, **Jan YN**. Sound response mediated by the TRP channels NOMPC, NANCHUNG, and INACTIVE in chordotonal organs of *Drosophila* larvae. *Proc Natl Acad Sci USA* 110: 13612–13617, 2013.

Zhen M, **Jin Y**. The liprin protein SYD-2 regulates the differentiation of presynaptic termini in *C. elegans*. *Nature* 401: 371–375, 1999.

Zhong L, **Hwang RY**, **Tracey WD**. Pickpocket is a DEG/ENaC protein required for mechanical nociception in *Drosophila* larvae. *Curr. Biol.* 20: 429–434, 2010.

Zou Y, **Akazawa H**, **Qin Y**, **Sano M**, **Takano H**, **Minamino T**, **Makita N**, **Iwanaga K**, **Zhu W**, **Kudoh S**, **Toko H**, **Tamura K**, **Kihara M**, **Nagai T**, **Fukamizu A**, **Umemura S**, **Iiri T**, **Fujita T**, **Komuro I**. Mechanical stress activates angiotensin II type-1 receptor without the involvement of angiotensin II. *Nat. Cell Biol.* 6: 499–506, 2004.

Zucker RS, **Regehr WG**. Short-term synaptic plasticity. *Physiology* 64: 355–405, 2002.

13. Figures and tables

Part I

Part II

14. Abbreviations

aa	amino acid
ag	*Anopheles gambia*
aGPCR	Adhesion-class of G-protein coupled receptor
AH	accessory helix
AT_1	Angiotensin II-type 1
attB	attachment bacteria
attP	attachment plasmid
AZ	active zone
BAI	Brain-specific angiogenesis inhibitor
bd	bipolar dendrite neurons
BFPP	Bilateral frontoparietal polymicrogyria
BiFC	Bimolecular fluorescence complementation
bp	base pair
BRP	Bruchpilot
BSN	Bassoon
CAAX	C: cysteine, A: aliphatic residue, X: any amino acid
CAC	Cacaphony
CAST	Cytomatrix of the active zone-associated structural protein
CC	coiled-coil
cd	ciliary dilation
CD8	Cluster of differentiation 8
cDNA	complementary DNA
ce	*Caenorhabditis elegans*
CFP	cyan fluorescent protein
CH	central helix
cha	choline acetyltransferase
cho	chordotonal organ
ci	*Ciona intestinalis*
CIRL	Ca^{2+} independent receptor of latrotoxin

CNS	central nervous system
CPG	central pattern generator
CPX	Complexin
CRISPR	Clustered Regularly Interspaced Short Palindromic Repeats
CTD	C-terminal domain
CTF	C-terminal fragment
da	dendritic arborization
da	dendritic arborization neurons
dB	decibel
DLM	Dorsal Longitudinal Muscle
DLG	Discs-large
dm	*Drosophila melanogaster*
DNA	Deoxyribonucleic acid
*d*STORM	*direct* stochastic optical reconstruction microscopy
DYSB	Dysbindin
ECD	extracellular domain
eEPSC	evoked excitatory postsynaptic current
EM	electron microscope
ERG	electroretinogram
es	external sense organs
EYS	eyes shut/spacemaker
FASII	Fascilin II
Fd3F	Forkhead box transcription factor
FLRT	Fibronectin
FMI	Flamingo/Starry night
FRET	fluorescence resonance energy transfer
GABA	γ-aminobutyric acid
GAIN	GPCR auto-proteolysis inducing domain
GFP	green fluorescent protein
GluRIID	Glutamate receptor IID
GPCR	G-protein couple receptor
GPS	G-protein couple receptor proteolytic site

h	*human*
HEPES	4-(2-hydroxyethyl)-1-piperazineethanesulfonic acid
HL-3	Hemolymph-like saline solution
hm	*Hirudo medicinalis*
HRM	hormone binding domain
HRP	Horseradish peroxidase
IAV	Inactive
IMAC	Immaculate connections
IR	inverted-repeat
IRS	interrhabdomeral space
kDa	kilo Dalton
KIF	Kinesin superfamily protein
Lasso	LHN1-associated synaptic surface organizer
LDCV	large dense-core vesicles
lp	*Loligo pealei*
LPHN	lectin-like latrophilins
mBRP	mobile Bruchpilot
md	multidendritic sensory cells
mM	millimolar
mRFP	monomeric red fluorescent protein
mRNA	messenger RNA
NAN	Nanchung
NGS	normal goat serum
nj	*Narke japonica*
nm	nanometer
NMD	non-sense mediated decay
NMJ	neuromuscular junction
NMR	Nuclear Magnetic Resonance
NOMPC	No mechanoreceptor potential
NSF	*N*-ethylmaleimide-sensitive fusion protein
NTD	N-terminal domain
NTF	N-terminal fragment
OLF	olfactomedin

ORF	open reading frame
PBS	phosphate buffered saline
PCR	polymerase chain reaction
PFA	paraformaldehyde
PKD	Polycystic kidney disease
PNS	peripheral nervous system
polyQ	poly-glutamine
PTP	Protein-tyrosine phosphatase σ
PTPRF	LAR-type receptor phosphotyrosine phosphatase
$Rab3^{rup}$	Running unapposed
RBL	Rhamnose-binding lectin-like domain
RIM	Rab-3-interacting molecule
RIM-BP	Rab-interacting molecule- binding protein
RNAi	RNA-interference
RP	reserve pool
RRP	readily releasable pool
SNAP-25	Soluble *N*-ethylmaleimide-sensitive factor attachment protein 25
SNARE complex	Soluble N-ethylmaleimide-sensitive- factor attachment receptor complex
SNb/SNd	segmental nerve b/d
SPL	Sound Pressure Level
STEM	Scanning Transmission Electron Microscope
SSR	subsynaptic reticulum
SV	synaptic vesicle
SYB	Synaptobrevin
SYN	Synapsin
SYT	Synaptotagmin
SYX	Synatxin
t-SNARE	target-SNARE
td	tracheal dendrite
TM	transmambrane
TRPV	Transient receptor potential vanilloid channels

UAS	upstream activating sequence
UTR	untranslated region
v-SNARE	vesicle-SNARE
VGAT	Vesicular GABA transporter
VGLUT	Vesicular glutamate transporter
VLGR1	Very large G-protein couples receptor-1
VNC	Ventral nerve cord
xl	*Xenopus laevis*
α-LTX	alpha-latrotoxin

15. Appendix

15.1. Publications

Nicole Scholz[*], Jennifer Gehring[*], Chonglin Guan[*], Dmitrij Ljaschenko, Robin Fischer, Vetrivel Lakshmanan, Robert J. Kittel, Tobias Langenhan, (2015). The Adhesion-GPCR Latrophilin/CIRL shapes mechanosensation. *Cell Reports 11,* 1-9.

Ines Liebscher, Brian Ackley, Demet Arac¸, Donna M. Ariestanti, Gabriela Aust, Byoung-il Bae, Bigyan R. Bista, James P. Bridges, Joseph G. Duman, Felix B. Engel, Stefanie Giera, Andre´ M. Goffinet, Randy A. Hall, Jörg Hamann, **Nicole Hartmann**, Hsi-Hsien Lin, Mingyao Liu, Rong Luo, Amit Mogha, Kelly R. Monk, Miriam C. Peeters, Simone Prömel, Susanne Ressl, Helgi B. Schiöth, Severine M. Sigoillot, Helen Song, William S. Talbot, Gregory G. Tall, James P. White, Uwe Wolfrum, Lei Xu, and Xianhua Piao (2014). New functions and signaling mechanisms for the class of adhesion G protein–coupled receptors. *Ann. N.Y. Acad. Sci.* 1333, 43-64.

[*]Equal contribution

15.2. *Curriculum Vitae*